CORA Cork Open Research Archive
Cartlann Taighde Oscailte Chorcaí

Title	Advanced polymer membrane development in pervaporation dehydration and lateral flow diagnostics
Authors	Flynn, Eoin J.
Publication date	2013
Original Citation	Flynn, E. J. 2013. Advanced polymer membrane development in pervaporation dehydration and lateral flow diagnostics. PhD Thesis, University College Cork.
Type of publication	Doctoral thesis
Rights	© 2013, Eoin J. Flynn. - http://creativecommons.org/licenses/by-nc-nd/3.0/
Download date	2026-11-06 04:15:26
Item downloaded from	https://hdl.handle.net/10468/1288

UCC
University College Cork, Ireland
Coláiste na hOllscoile Corcaigh

Advanced Polymer Membrane Development in Pervaporation Dehydration and Lateral Flow Diagnostics

Eoin Flynn B.Sc. (Hons), PGDip. Sc.

Chemistry Department, University College Cork, Cork, Ireland

Environmental Research Institute, University College Cork, Lee Road, Cork, Ireland



Thesis presented to the national university of Ireland

for the degree of Doctor of Philosophy

June 2013

Work carried out under the supervision of

Prof. Michael A. Morris

Table of Contents

Table of Contents **1**

List of Figures **8**

List of Tables **14**

List of Abbreviations **17**

General Abbreviations 17

Section 1.2 Abbreviations 17

Declaration **19**

Acknowledgements **20**

List of Published Material **23**

Abstract **24**

1. Introduction **26**

1.1. Membrane Processes: Pervaporation, Lateral Flow 30

1.1.1. Pervaporation 30

Azeotropes 31

Industry Overview 33

1.1.2 Lateral Flow Diagnostics 34

Industry Overview 35

1.2 Membrane Transport Theory 36

1.2.1 Solution-Diffusion 37

Proof of Solution-Diffusion Theory 38

1.2.2 Lateral-Flow Theory 43

1.3 Membrane Structure & Formation 45
1.3.1 Pervaporation Membrane Categorisation 46
Polymeric membranes 46
Inorganic Membranes 48
Mixed Matrix Membranes (MMMs) 49
1.3.2 Pervaporation Membrane Formation 49
Support 49
Selective Layer Casting 49
1.3.3 Pervaporation Membranes: Structural Effects & Anomalies 50
Skin Layers 50
Plasticization 50
Crosslinking 51
Polymer Hydrophilicity/Hydrophobicity 51
Glass Transition Temperature 52
Membrane Polymer Matrix Relaxation 53
1.4 Lateral-Flow Membrane Structure and Formation 54
1.4.1 Lateral-Flow Membrane Categorisation 54
Cellulose Nitrate 54
1.4.2 Lateral-Flow Membrane Formation 55
Support 55
Phase Inversion: Formation of Pore Structure 55
Cloud Point 58
1.4.3 Lateral-Flow Membrane: Structural Effects and Anomalies 58
Skin layers 58
Demixing Front & Surface Tension 59
Macrovoids 60
Nodules 61

1.5 Summary 62

References: Chapter 1 64

2. Experimental 74

2.1 Membrane Preparation 74

2.1.1 Materials 74

Pervaporation Materials 74

Lateral Flow Materials 74

2.1.2 Pervaporation Membrane Polymer Solutions 75

Pristine Polymer Solutions 75

Polymer Blend Solutions 75

Mixed Matrix Membrane Solutions 76

2.1.3 Lateral Flow Membrane Polymer Solutions 77

Calculating Weight Percentages 79

2.1.4 Membrane Casting 80

Pervaporation Membrane Casting 81

Lateral-flow Membrane Casting 83

2.2 Membrane Testing 84

2.2.1 Pervaporation Membrane Testing 84

Pervaporation Procedure 87

Pervaporation Membrane Flux and Selectivity Calculations: 90

2.2.2 Lateral-flow Membrane Testing 90

2.3 Membrane Characterisation 91

2.3.1 Scanning Electron Microscopy 91

2.3.2 Flexibility Testing 91

2.3.3 X-Ray Diffraction 92

2.3.4 Fourier Transform Infrared Spectroscopy 92
2.3.5 Differential Scanning Calorimetry/Thermogravimetric Analysis92
2.3.6 Mercury Porosimetry 93
2.3.7 Atomic Force Microscopy 93
2.3.8 Contact Angle Measurement 93
References: Chapter 2 94

3 Pervaporation Membrane Development 97
Abstract 97
3.1 Introduction 98
3.2 Experimental 99
3.3 Results and Discussion 99
3.3.1 Unsupported Pristine Membrane 99
3.3.2 Supported Pristine Membranes 101
3.3.3 Polymer Blend Membranes 104
3.3.4 Polymer Blend Membrane Utilising Glycerol 107
3.4 Conclusion 109
3.5 Summary 111
References: Chapter 3 112
4 Lateral-flow Membrane Development 115
Abstract 115
4.1 Introduction 116
4.2 Experimental 117
4.3 Results and Discussion 117
4.4 Conclusion 132
4.5 Summary 134
References: Chapter 4 135

5 Advanced Pervaporation Membranes: Control of Skin Layer 138

Abstract.....138

5.1 Introduction.....139

5.2 Experimental.....141

5.3 Results and Discussion.....141

5.3.1 DSC.....141

5.3.2 XRD:.....141

5.3.3 SEM:.....146

5.3.4 Pervaporation Results.....150

5.4 Conclusions.....153

5.5 Summary.....155

References: Chapter 5.....156

6 Advanced Lateral Flow Membranes: Control of Pore Structure 159

Abstract.....159

6.1 Introduction.....160

6.2 Experimental.....161

6.2.1 Membrane Preparation.....161

6.2.2 Lateral Flow Testing.....162

6.3 Results and Discussion.....163

6.3.1 EtOH Content.....163

6.3.2 SEM.....163

6.3.3 XRD.....167

6.3.4 Mercury Porosimetry.....168

6.3.5 Lateral-Flow Rate.....169

6.3.6 Discussion.....170

6.4 Conclusion: 173
6.5 Summary....174
References: Chapter 6....175

7 Pervaporation Mixed Matrix Membranes 179
Abstract....179
7.1 Introduction....180
7.2 Experimental....182
7.2.1 Materials 182
7.2.2 Membrane preparation....182
7.2.3 Pervaporation 183
7.2.4 Characterization....183
7.3 Results and Discussion: 183
7.3.1 Characterisation....183
7.3.2 Membrane Absorption 186
7.3.3 Pervaporation 188
7.3.4 Discussion 191
7.4 Conclusion 193
7.5 Summary....195
References: Chapter 7....196

8 Closing Remarks & Future Work 202
Appendices 207
A. Chapter 3 Supporting Information....208
A.1 Pristine Unsupported Membrane Data....208
A.2 Pristine Supported Membrane Data....209
A.3 Blend Membrane Data 209

A.4 Blend Membranes Utilising Glycerol Data 210
A.5 Flexibility Data 211
A.6 Absorption Data 211
B. Chapter 4 Supporting Information 212
B.1 SEM 212
B.2 Flexibility Testing 215
B.3 XRD 216
B.4 AFM 216
B.4.1 2 mm Melinex 217
B.4.1 4 mm Melinex 218
B.5 Contact Angle Measurements 219
C. Chapter 5 Supporting Information 221
C.1 Membrane Selective Layer Data 221
C.2 Pervaporation Data: 222
D. Chapter 6 Supporting Information 223
D.1 XRD 223
D.2 Flow Rate Data 223
D.3 SEM 224
D.4 Flexibility 224
E. Chapter 7 Supporting Information 225
E.1 Absorption Data 225
E.2 Flexibility Data 225

List of Figures

Chapter 1:

Figure 1.0: Membrane technologies timeline.....27
Figure 1.1: Pervaporation process 30
Figure 1.2: Mechanism of lateral flow diagnostic strip 34
Figure 1.3: Molecular level view of intermolecular forces acting on a molecule at the surface of a liquid compared to those in the interior..... 43
Figure 1.4: Flow of liquid up a narrow tube by capillary action and representation of flow through tortuous pore structure of a membrane by same mechanism 44
Figure 1.5: isotropic vs anisotropic membrane structures in porous and non-porous membranes..... 45
Figure 1.6: Sodium alginate 46
Figure 1.7: Poly(vinyl alcohol)..... 47
Figure 1.8: Supported pervaporation membrane structure..... 49
Figure 1.9: Solvent evaporation and polymer density in thick vs thin pervaporation membrane 50
Figure 1.10: Cellulose nitrate 54
Figure 1.11: Cellulose..... 55
Figure 1.12: Phase inversion in polymer solution 57
Figure 1.13: Binodal and spinodal in phase diagram 57
Figure 1.14: Soluto-capillary convection macrovoid formation 61

Chapter 2:

Figure 2.1: K202 Control Coater..... 81
Figure 2.2: Close wound (A) and spirally wound (B) coating bars..... 81
Figure 2.3: Glass plate and support fabric prepared for casting..... 82
Figure 2.4: K202 Control Coater diagram with casting bar and membrane support in place 82
Figure 2.5: Mbraun GP 2202 PB single piece moulded glovebox and technical drawings 84
Figure 2.6: Sulzer Chemtech Laboratory 6" Test Cell (detailed on following 3 pages) 86

Figure 2.7: Diagram of feed chamber of pervaporation unit (details in text; see figure 2.6 for full pervaporation unit diagram) 87
Figure 2.8: Diagram of the membrane cell of pervaporation unit (details in text; see figure 2.6 for full pervaporation unit diagram) 88
Figure 2.9: Diagram of feed pump and peripherals of pervaporation unit (details in text; see figure 2.6 for full pervaporation unit diagram) 89

Chapter 3:

Figure 3.1: Flux (3.1A) & selectivity (3.1B) vs. time for unsupported & supported pristine pervaporation membranes. Flux (3.1C) and selectivity (3.1D) figures for polymer blend pervaporation membranes. Flux figures given on linear scales, selectivities given on logarithmic scales. 100
Figure 3.2: SEM surface images of pristine supported 5wt% NaAlg pervaporation membrane showing cracks in membrane selective layer. 102
Figure 3.3: SEM image of early PVA membrane with PAN support layer delaminating from fabric support 102
Figure 3.4: SEM images of supported polymer blend membranes: A, C and E show cross sections of 7:3, 9:1 and 4:1 NaAlg:PVA blends respectively while G and I show cross sections of 4:1 and 9:1 NaAlg:PVA blends utilising glyercol respectively. B, D and F show exposed surface images of 7:3, 9:1 and 4:1 NaAlg:PVA blends respectively while H and J show surface images of 4:1 and 9:1 NaAlg:PVA blends utilising glyercol respectively. 105
Figure 3.5: Plot of membrane flexibility where r = radius of cylinder (see section 2.3.2). 1/r utilised to facilitate understanding of data; unsupported PVA most flexible membrane therefore, highest on graph. 107

Chapter 4:

Figure 4.1: SEM images of membranes produced from lacquers of 17 wt% CN dissolved in 100 % acetone. Images A, B and C show cross section, cross-section close-up and surface images respectively of the air dried membrane. Images D, E and F show cross section, cross-section close-up and surface images respectively of the oven dried membrane. 119

Figure 4.2: SEM images of membranes produced from lacquers of 17 wt% CN dissolved in 85 wt%:15 wt% acetone:water solvent mix and air dried. Images A and B show surface and cross section images respectively of the membrane produced from a lacquer not brought to cloud point. Images C and D show surface and cross section images respectively of the membrane produced from a lacquer brought to cloud point. 120

Figure 4.3: SEM images of membranes produced from lacquers of 17 wt% CN dissolved in 90 wt%:10 wt% acetone:water solvent mix and air dried. Images A and B show surface and cross section images respectively of the membrane produced from a lacquer *not* brought to cloud point. Images C and D show surface and cross section images respectively of the membrane produced from a lacquer brought to *cloud point*. 123

Figure 4.4: SEM images of membranes produced from lacquers of 17 wt% CN dissolved in 95 wt%:5 wt% acetone:water solvent mix. Images A, B and C show air surface, backing surface and cross section images respectively of the air dried membrane produced from a lacquer *not* brought to cloud point. Images D, E and F show cross air surface, backing surface and cross section images respectively of the air dried membrane produced from a lacquer brought to *cloud point*. 124

Figure 4.5: XRD profile of the cellulose nitrate polymer before incorporation into lacquer. Shows a sharp diffraction feature at approximately 45 $^{o}2\theta$ (15,000 counts s-1), a broad feature around 22 $^{o}2\theta$ (11,000 counts s-1). Broad feature typical of cellulose compounds. Also a relatively sharp diffraction feature around 12 $^{o}2\theta$ (5,700 counts s-1). 126

Figure 4.6: XRD profile of BasMemBCP shows no sharp diffraction features. Broad feature typical of cellulose compounds observed around 22 $^{o}2\theta$ (2,200 counts s^{-1}). 126

Figure 4.7: XRD profile of BasMemDCP. Sharp diffraction feature at around 45 o2θ, but this feature – unlike in the raw material – is of a lower intensity (5,500 counts s-1) than the broad feature around 22 o2θ. 127

Figure 4.8: Plot of membrane flexibility where r = radius of cylinder (see section 2.3.2). 1/r utilised to facilitate understanding of data; unsupported PVA most flexible membrane therefore, highest on graph. 128

Chapter 5:

Figure 5.1: Schematic of a diffusion profile across a pervaporation membrane.... 140
Figure 5.2: Upper image: DSC curve for the 4:1 ratio NaAlg:PVA selective membrane. Lower image: XRD curves for same membrane with additional glycerol; upper curve contains 5 g glycerol; lower curve contains 4 g (bottom)..... 143
Figure 5.3: (A) XRD profiles of 60 um films with and without glycerol addition. (B) XRD profiles of membrane films (with PVA and glycerol) as a function of cast thickness as described in figure. 144
Figure 5.4: SEM images of membranes prepared: Left are cross-sectional images and right are top-down images. Thicknesses are shown in image. Magnifications as shown. 148
Figure 5.5: SEM images of membranes prepared: Left are cross-sectional images and right are top-down images. Thicknesses are shown in image. Magnifications as shown. 149
Figure 5.6: Plots of pervaporation performance indicators versus time. A and B are flux and C and D are selectivity. Various films were studied; the cast thickness is indicated in the figure. Estimated errors in measurements are around 5% of value. 151
Figure 5.7: Plots of flux (A and B) and selectivity (C and D) against measured (A and C) and cast (B and D) thickness. Estimated errors in measurements are around 5 % of value..... 152

Chapter 6:

Figure 6.1: Plot of non-solvent (water) required to reach cloud point versus ethanol content in casting solution at cloud point..... 163
Figure 6.2: SEM images of the lateral flow membranes MesoACP – MesoCCP and BasMemBCP (lettering follows sample labels see table 6.1). Images with the (i) labels show membrane cross sectional morphology while those with label (ii) show membrane surface morphology 165
Figure 6.3: XRD profiles of MesoDCP and BasMemBCP (to see images superimposed see appendix D, section D.1, figure D.1)..... 167
Figure 6.4: MesoDCP and BasMemBCP porosimetry. As labelled in diagram. ... 169

Figure 6.5: Lateral flow rate against the ethanol content for each of the membranes prepared here (for tabulated data see appendix D, section D.2, table D.1)..... 170

Chapter 7:

Figure 7.1: A) mesoporous silica particles SEM image B) TEM image of pores resulting from modified Stöber process..... 183
Figure 7.2: A) surface image of 15 wt% silica loaded PVA membrane B) surface image of 10 wt% silica loaded PVA membrane..... 185
Figure 7.3: Images A, B, C and D show surface of pervaporation membranes with 0 wt%, 5 wt%, 10 wt% and 15 wt% silica loading respectively. Images E,F and G show cross section images of 0 wt%, 10 wt% and 15 wt% silica loaded membranes respectively..... 186
Figure 7.4: Membrane absorption vs. time; shows absorption of a solution of 50 wt% EtOH and 50 wt% water into selective membrane over time. Maxima represent point at which membrane becomes dissolute, i.e. loses membrane form and so becomes unusable. (See appendix E, table E.1 for tabulated data) 187
Figure 7.5: A: Selectivity vs. time for membranes of particle loading from 0 wt% to 15 wt% silica loading. B: Flux vs. time for membranes of particle loading from 0 wt% to 15 wt% silica loading. C: Average flux of membrane vs. membrane silica loading. D: Average selectivity of membrane vs. membrane silica loading..... 190

Appendices A-E:

Figure B.1: SEM images of a lateral flow membrane after treatment with surfactant SDBS at 100 µm (image A) and 50 µm (image B) 212
Figure B.2: SEM images of *Melinex* 100 % polyester backing material; surface in contact with membrane (image A) and cross section (image B)..... 212
Figure B.3: SEM images of of Millipore HiFlow 120 lateral flow membrane; air surface (image A), blet surface (image B) and cross section (image C)..... 213
Figure B.4: SEM images of CN raw material at 200 µm (A), 100 µm (B), 50 µm (C) and 20 µm (D). 214
Figure B.5: Skin formation at membrane support interface..... 214

Figure B.6: SEM images of linear pore patterns at membrane support interface: Image A shows patterns in a membrane brought to cloud point with only acetone and water in the solvent mix. Image B shows patterns in a membrane cast from the same lacquer but *not* brought to cloud point 215
Figure B.7: XRD profile of BasMemD..... 216
Figure B.8: AFM images of topography of three randomly chosen 10x10 µm sections of 2 mm thick Melinex film 217
Figure B.9: AFM images of topography of three randomly chosen 10x10 µm sections of 4 mm thick Melinex film 218
Figure B.10: Typical contact angle of water droplet on Melinex surface (specific image: 4 mm Melinex sample B)..... 220
Figure B.11: Typical contact angle of acetone droplet on Melinex surface (specific image: 4 mm Melinex)..... 220
Figure D.1: XRD profiles of MesoDCP and BasMemBCP..... 223
Figure D.2: SEM images of a lateral flow membrane after treatment with surfactant SDBS at 100 µm (image A) and 50 µm (image B) 224

List of Tables

Chapter 2:

Table 2.1: Polymer blend solutions 76

Table 2.2: Pervaporation membrane casting solution compositions 77

Table 2.3: Basic Membrane Casting Solutions 78

Table 2.4: Meso-solvent (ethanol) containing membranes 78

Table 2.5: wt% for components of glycerol and butanol casting solutions. Abbreviations: Mem. (membrane), CN (cellulose nitrate), ace. (acetone), EtOH (ethanol), gly. (glycerol), but. (butanol). Cloud Point (water added to reach cloud point 79

Chapter 4:

Table 4.1: Tabulated data showing the water content of the lacquers (casting solutions) of the basic lateral flow membranes (see chapter 2, section 2.1.3, table 2.3 for precise composition of lacquers) produced from lacquers at both cloud point and not. The exact water content required to reach cloud point in the lacquer is shown as is the water content of membranes not cast from lacquers at cloud point (definition of lacquer cloud point given in chapter 2, section 2.1.3). Also shown is the presence of a skin layer in the final membrane and flow rate, if any..... 118

Chapter 6:

Table 6.1: Casting solution composition before/after cloud point 162

Chapter 7:

Table 7.1: Tabulated flux, selectivity, feed and permeate purity, and contact angle data for membranes at different wt% silica particle loadings 189

Appendices A-E:

Table A.1: Pervaporation performance of unsupported pristine NaAlg membrane cast from 2 wt% solution of NaAlg in water. Cast at 400 µm thickness 208

Table A.2: Pervaporation performance of unsupported pristine PVA membrane cast from 10 wt% solution of PVA in water. Cast at 150 µm thickness..... 208
Table A.3: Pervaporation performance of supported pristine NaAlg membrane cast from 5 wt% solution of NaAlg in water. Cast at 100 µm thickness..... 209
Table A.4: Pervaporation performance of supported pristine PVA membrane cast from 10 wt% solution of PVA in water. Cast at 100 µm thickness..... 209
Table A.5: Pervaporation performance of supported pristine PVA membrane cast from 10 wt% solution of PVA in water. Cast at 100 µm thickness..... 209
Table A.6: Pervaporation performance of supported 4:1 NaAlg:PVA blend membrane cast from 5 wt% solution of polymer blend in water. Cast at 100 µm thickness..... 210
Table A.7: Pervaporation performance of supported 7:3 NaAlg:PVA blend membrane cast from 5 wt% solution of polymer blend in water. Cast at 100 µm thickness..... 210
Table A.8: Pervaporation performance of supported 9:1 NaAlg:PVA blend membrane cast from solution of 5 g polymer blend + 5 g glycerol in 90 g water. Cast at 100 µm thickness..... 210
Table A.9: Pervaporation performance of supported 4:1 NaAlg:PVA blend membrane cast from solution of 5 g polymer blend + 5 g glycerol in 90 g water. Cast at 100 µm thickness..... 211
Table A.10: Results of flexibility tests (method outlined in chapter 2, section 2.3.2) 211
Table A.11: Absorption data in solution of 50 wt% water/50 wt% ethanol for supported polymer blend membranes (designated by PVA:NaAlg ratio). Points at which mass data end represent points at which membranes dissolve..... 211
Table B.1: Flexibility testing data of lateral flow membranes including industrial standard..... 215
Table B.2: Contact angle data..... 219
Table C.1: Summary of SEM quantification and observations (P = partial, WD = well developed; describe nature of the skin layer at surface)..... 221
Table C.2: Thickness and flexibility data..... 221
Table C.3: Flux, selectivity and permeate water content figures for NaAlg based membranes at 60 ^{o}C operating temperature and 90 wt% ethanol feed solution..... 222

Table D.1: Lateral flow rates and ethanol content 223
Table D.2: Flexibility testing data of lateral flow membranes 224
Table E.1: Absorption data in solution of 50 wt% water/50 wt% ethanol for MMMs. Tabulated data of figure 7.4 (see chapter 7). Points at which mass data end represent points at which membranes dissolve 225
Table E.2: Results of flexibility tests (method outlined in chapter 2, section 2.3.2) 225

List of Abbreviations

General Abbreviations

- **Ace.** – Acetone
- **AFM** – Atomic Force Microscopy
- **CN** – Cellulose Nitrate
- **CP** – Cloud Point
- **CRISP** – Cryo-Rupture Imaging Sample Preparation
- **DIPS** – Diffusion Induced Phase Separation
- **DMSO** – DiMethylSulphOxide
- **DSC** – Differential Scanning Calorimetry
- **EtOH** – Ethanol
- **Gly.** – Glycerol
- **IIPS** – Immersion Induced Phase Separation
- **Meso-sol.** – Meso-solvent
- **MMM** – Mixed Matrix Membrane
- **NaAlg** – Sodium Alginate
- **NG** – Nucleation & Growth
- **Non-sol.** – Non solvent
- **PAN** – Poly(AcryloNitrile)
- **PET** – Poly(EthyleneTerephthalate)
- **PTFE** – Poly(TetraFluoroEthylene)
- **PVA** – Poly(VinylAlcohol)
- **RIPS** – Reaction Induced Phase Separation
- **SD** – Spinodal Decomposition
- **SDBS** – Sodium Dodecyl BenzeneSulphate
- **Sel**. - Selectivity
- **SEM** – Scanning Electron Microscopy
- **Sol**. – Solvent
- **SOP** – Standard Operating Procedure
- **TEM** – Transmission Electron Microscopy
- **T_g –** Glass transition temperature
- **TGA –** ThermoGravimetric Analysis
- **TIPS –** Thermally Induced Phase Separation
- **VIPS** – Vapour Induced Phase Separation
- **XRD** – X-Ray Diffraction

Section 1.2 Abbreviations

- **A –** Area of membrane
- **c –** Concentration
- **D –** Diffusion coefficient
- **f (subscript) -** Feed
- **G (superscript) –** Gas phase
- **g** – Local gravitational field strength
- **h –** Height of columnar glass vessel

- **i –** Component of feed (water)
- **J –** Flux
- **j –** Component of feed (ethanol)
- **K –** Sorption Coefficient
- **L –** Coefficient of proportionality (links chemical potential to flux)
- **L (superscript) –** Liquid phase
- **m –** Molecular weight
- **p –** Partial pressure
- **n –** Mole fraction
- **p (subscript) –** Permeate
- **R –** Universal gas constant
- **r -** Radius
- **T –** Temperature
- **W –** Mass of permeate
- **x –** Water/ethanol in feed
- **y –** Water/ethanol in permeate
- **γ –** Activity coefficient
- **θ –** Contact angle
- **ρ –** Density
- **μ -** Chemical potential

Declaration

I, Eoin Flynn, certify that this is my own work and I have not obtained a degree in this university or elsewhere on the basis of this PhD thesis

_____

Eoin Flynn

Acknowledgements

Looking back on the duration of this PhD and my academic career before it, I must admit that there is an element of luck to my life. I am very fortunate to have been born in Ireland at a time when I could obtain a third level education for relatively little expense. In addition to being plainly lucky, I have also had a great number of people throughout my life who have helped, encouraged, advised and guided me. Most likely, more people than I am capable of remembering. Reflecting on all of that, I realise I am privileged more than most could ever hope for. I have endeavoured to thank everyone I can think of. If you read these acknowledgements and feel that I have somehow forgotten you I am profoundly sorry…

Thanks must go to my family: To my parents - Bernadette Flynn and Sean Flynn - who have always provided for me and put me through the academic process that has led to this PhD. To my grandparents - Mary Flynn and John Flynn - who have doted on me and encouraged me as long as I can remember and who seem absurdly proud of me without, to my mind, my having to do a whole lot to earn it. Though their pride pales in significance when compared to my mother's beaming adoration of me. I never know how to react to it Mam, but I'm glad I'm something you can be proud of. To my sisters - Sarah Flynn and Aoife Flynn - both of whom have never ceased to make me feel like an over-achiever with their admiration of their big brother; thank you. Special thanks must go to my father who, once upon a time, heavily suggested - though never demanded - that I should choose a college career in science and not one in English, as was my wish. A lack of maturity didn't let me see the wisdom in it then, but looking back; there are few moments in my life that I can highlight and state so unequivocally that *that* was a turning point. Without it I really and truly would not be able to submit this thesis. Thank you.

To those that I had the pleasure to work and socialise with during the PhD, past and present, from labs 115 and 343 of the Kane Building in UCC's chemistry dept., from the ERI, Tyndall and the CRAC lab, and the new guys from Limerick - Atul, Atul "eile", Barbara, Cian, Colm O'Mahony, Dave, Eoin Wilson, Eoin McGillicuddy, Gil, Ian, JV, Keith, Michael, Olan, Pete, Raj, Sven, Riosín, Sankar, Shelly, Sibu, Subhajit, Tandra and Tim; those directly involved in my work from the same laboratories - Aoife Burke, Séamus Ó Riada, Donal Creedon; from CIT (who

kindly lent us the pervaporation unit) – Grainne Byrne and Cilian Ó'Súilleabháin; from Glantreo Ltd. – John Hanrahan, Joseph Tobin and Jennifer Coakley; and from Milipore – Mike Mansfield, Kami Beyzavi and Niamh Curran; those who made significant contributions to my published material - Parvaneh Mokarian, Léa Brothier, and Thomas Fitzgerald. Thank you to all of you. You made my PhD a pleasure. An extra special thank you must go to Sheena O'Driscoll who, on the day I got my underwhelming degree results, consoled me and advised me that I go and talk to Prof. Mick Morris before I completely despaired. That was some very sound advice. Thank you.

To the administrative staff in UCC - Pat, Mattie, Donnacha, Terry, Mick, Tony, Johnny, Noel, Chrissy, Trevor, Rose - thank you.

To the lecturers who weren't my direct supervisors but were happy to give me advice and tips whenever I sought it - Justin Holmes, Dave Otway, Jeremy Glennon and John Wenger - thank you. You'd be surprised how important some of those tips turned out to be.

To Jovanna's parents - Harry Mittelstadt and Marion Arndt – who were every bit as encouraging as my own parents throughout my PhD and before it. Thank you.

To the people I am lucky to be able to call friends as well as colleagues - Colm O'Regan, Colm "eile" McManamon, John Hayes, John O'Connell, Joseph Tobin, Kamil Rahme, Mark Armstrong, Paul Delaney and Tom Fitzgerald. You are some of the best people I've ever met (spare me the abuse when you read this, please!). I could write another thesis on all the reasons I have to thank you lot. But this inadequate paragraph will have to suffice. Thank you, really and truly.

The two people who did more than any others to help me in this PhD are my professor, Mick Morris, and Donal Keane, who was leading my project at the beginning. Mick, you gave me an opportunity to do a PhD when I didn't think I'd ever be able to and you've stuck your neck out for me, encouraged me and offered me advice many times since. You even managed to prevent me panicking when I thought all was lost while trying to get my first publication. I can never thank you enough for all that. Donal, I've no doubt you'll be far too humble to admit that you did a lot for me. I can assure you, you did. You showed me the ropes when I was starting the PhD; how to assimilate literature effectively, how to manage my

laboratory, how to objectively assess my results and generally how to be a better scientist, and on top of all that you contributed more to my publications than anyone bar myself. To both of you – Mick and Donal – you have my utmost respect and thanks.

Finally to Jovanna; you've been with me throughout my PhD and since long before that. You've never failed to raise my spirits at the worst times and you've been the source of many of the best times. You've even got your name on one of my papers through your help with my research. Despite my usual verbosity, for once, I don't have adequate words. You've been integral to my PhD and to my life. I know you won't think so, but, as much as anyone else - perhaps more - I could not have done this without you. Thank you.

List of Published Material

Unusual trend of increasing selectivity and decreasing flux with decreasing thickness in pervaporation separation of ethanol/water mixtures using sodium alginate blend membranes

Eoin J. Flynn, Donal A. Keane, Justin D. Holmes, Michael A. Morris

Journal of Colloid and Interface Science, Volume 370, Issue 1, March 2012, Pages 176–182

Control of Pore Structure Formation in Cellulose Nitrate Polymer Membranes

Eoin J. Flynn, Jovanna Arndt, Léa Brothier, Michael A. Morris

Advances in Chemical Science Volume 2 Issue. 2, June 2013, Pages 9-18

Pervaporation performance enhancement through the incorporation of mesoporous silica spheres into PVA membranes

Eoin J. Flynn , Donal A. Keane, Parvaneh M. Tabari, Michael A. Morris

Separation and Purification Technology, Volume 118, October 2013, Pages 73–80

Preparation of supported hydrophilic polymeric and mixed matrix membranes for dehydration of ethanol by pervaporation

Donal A. Keane, Eoin J. Flynn , Michael A. Morris

Final Report for the Environmental Protection Agency STRIVE project: 2007-FS-ET-13-S5, January 2010, ISBN: 978-1-84095-347-3

Abstract

The work in this thesis concerns the advanced development of polymeric membranes of two types; *pervaporation* and *lateral-flow*. The former produced from a solution casting method and the latter from a phase separation. All membranes were produced from casting *lacquers*.

Early research centred on the development of viable membranes. This led to a supported polymer blend pervaporation membrane. Selective layer: plasticized 4:1 mass ratio sodium-alginate:poly(vinyl-alcohol) polymer blend. Using this membrane, pervaporation separation of ethanol/water mixtures was carefully monitored as a function of film thickness and time. Contrary to literature expectations, these films showed increased selectivity and decreased flux as film thickness was reduced. It is argued that morphology and structure of the polymer blend changes with thickness and that these changes define membrane efficiency.

Mixed matrix membrane development was done using spherical, discreet, size-monodisperse mesoporous silica particles of 1.8 - 2µm diameter, with pore diameters of ~1.8 nm were incorporated into a poly(vinyl alcohol) [PVA] matrix. Inclusion of silica benefitted pervaporation performance for the dehydration of ethanol, improving flux and selectivity throughout in all but the highest silica content samples.

Early lateral-flow membrane research produced a membrane from a basic lacquer composition required for phase inversion; polymer, solvent and non-solvent. Results showed that bringing lacquers to cloud point benefits both the pore structure and skin layers of the membranes. Advancement of this work showed that incorporation of ethanol as a *meso-solvent* into the lacquer effectively enhances membrane pore structure resulting in an improvement in lateral flow rates of the final membranes.

This project details the formation mechanics of pervaporation and lateral-flow membranes and how these can be controlled. The principle methods of control can be applied to the formation of any other flat sheet polymer membranes, opening many avenues of future membrane research and industrial application.

Chapter 1

Introduction

1. Introduction

Membranes have obtained a place of prominence within worldwide chemical technologies in the past four decades due to the ever increasing diversity of separations they can perform; separation of gaseous mixtures into constituent gases; filtration of particulates from solutions; efficient separation of closely boiling liquids from one another, to name a few. There is a broad range of processes in which such separations can be utilized, from the largest industrial scale in pharmaceutical, chemical and food science processes, down to the smallest personal and domestic scale in water filters, pregnancy tests, and medical diagnoses.

It is this versatility of function that has seen membranes grow from origins in the 18th century into the global membrane industries seen today. Frenchman Abbé Jean-Antoine Nollet is accredited with the first recorded observations of membranes. He noted the permeability of a sealed pig bladder filled with wine and placed in a barrel of water as early as 1748.[1] By the early 19th century another Frenchman, Henri Dutrochet, coined the term "osmosis" to describe the spontaneous flow of liquid across a permeable barrier[2]. In the mid-19th century German scientist, Adolf Fick, produced the first synthetic membrane from *collodion* (cellulose nitrate) and defined *Fick's Law of Diffusion*[3]. By the late 19th century the culmination of three decades work by Polish chemist Moritz Traube [4] and German botanist Wilhelm Pfeffer[5] – producing and testing numerous membranes – resulted in data which was used by Dutch scientist Jacobus van't Hoff in 1887 to develop the *van't Hoff equation*[6]. In the early 20th century further advances in membrane studies were made that would lead to early industrialization. German scientist, Philip Adolf Kober, identified, described and named *pervaporation* in cellulose nitrate bags, in 1917[7]. By the 1930's the first commercial membranes were in production; cellulose nitrate membranes used for microfiltration. By the end of the Second World War membranes had been implemented by the U.S. Army for water filtration; research into which was conducted by Millipore. Soon after, Dutch scientist W. J. Wolf demonstrated in 1945 the first artificial kidneys for medical use: dialysis.

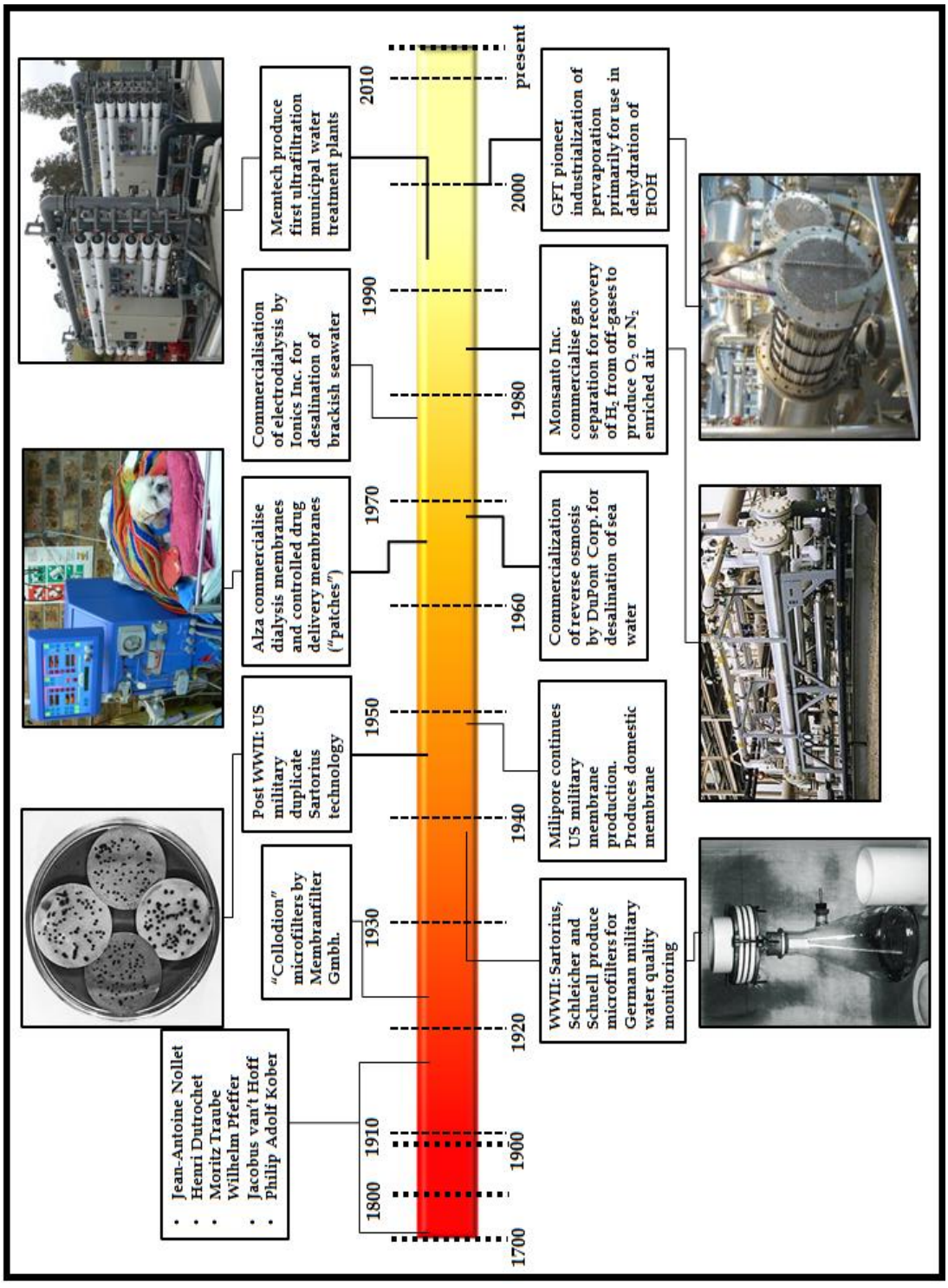


Figure 1.0: Membrane technology timeline

By the mid-point of the 20th century membranes had become fully industrialized and from the 1960's onwards the greatest advances in membrane technologies were made; commercialisation of dialysis in medicine and controlled drug delivery through membranes by Alza. This led to the development of microfiltration, ultrafiltration, reverse osmosis and electrodialysis during the 1970's. The final two decades of the 20th century saw the development of gas separation and pervaporation membrane technologies and the establishment of the current membrane industry. The 21st century has seen further advances in membrane technologies, particularly focussed on the areas of pervaporation and gas separation. As the industry currently stands there are four established industrial membrane types; microfiltration, ultrafiltration, reverse osmosis and electrodialysis; and two developing industrial membrane processes; gas separation and pervaporation. All other membrane technologies, such as facilitated transport though liquid membranes, are still at research and development levels.

The vast majority of membranes used are composed of organic polymers and are produced as thin films cast from polymer solutions (although production methods have been developed to produce membranes of different structure to increase membrane surface area, such as spirally wound and columnar membranes). However, there are differences in precisely how these thin polymer films are formed from solution. The simplest formulations involve the production of dense polymer membranes - such as pervaporation and ion-exchange membranes - from a method known as *solution casting:* Polymer solution is cast either onto a supporting substrate/reinforcing framework, or is unsupported, and the solvent subsequently evaporates from the cast solution which dries to form the thin film that will be the membrane. By comparison, the formation of reverse osmosis and ultrafiltration membranes is relatively complex: The process, known as the *Loeb-Sourirajan method* [8] still involves casting a polymer solution onto a support and allowing the solvent to evaporate to form the membrane but, while this process occurs a *phase separation* process is occurring simultaneously: A polymer lean liquid phase and a polymer rich liquid phase form and separate within the drying casting solution to create a porous structure in the final membrane. An adapted form of this process is used to form gas separation membranes, while yet another adaptation of the process

known as *vapour induced phase separation* is used to form microfiltration membranes.

Common features of these formation processes are the initial solution casting and the evaporation of solvent from the cast solution. All the membranes researched in this work were produced by casting polymer solutions as thin polymer films. A significant part of this thesis will show how control of the evaporation of solvents from those cast polymer solutions provides a core means of manipulating the internal structures and performance of the final membranes.

Two membrane types from the six dominant industrial membrane technologies outlined above were chosen for study; pervaporation membranes and lateral flow membranes (a type of microfiltration membrane); membranes with formation processes from opposite ends of the scale of complexity. Pervaporation membranes represent a simple formation process, namely the *solution casting* process, wherein the entirety of formation is defined by evaporation of solvent from the cast polymer solution, allowing the formation to be profoundly manipulated to affect the final membrane characteristics. Lateral flow membranes by comparison, represent a highly complex formation process in which the evaporation of solvent from the membrane casting solution occurs simultaneously with complicated *phase inversion* mechanisms to yield the final membrane, making manipulation of the formation difficult.

These two membrane technologies, pervaporation and lateral-flow, are among these least studied of all membranes; pervaporation being a relative newcomer to the established membrane industries and lateral flow being long established industrially but relatively poorly understood. The work herein aims to show how control of their formation processes can enhance membrane performance. It will center on the production of hydrophilic pervaporation membranes for the dehydration of ethanol and on the production of porous cellulose nitrate microporous membranes for lateral flow diagnostic strips.

1.1. Membrane Processes: Pervaporation, Lateral Flow

Membranes are produced to perform specific separations in industrial processes, analyses, diagnostics, etc. How a membrane performs its intended task is the best test of its efficacy. For this reason, a comprehensive knowledge of any process in which a membrane will be utilized is required for a full understanding of a membrane's functionality. What follows is an outline of the pervaporation process into which pervaporation membranes are incorporated and an outline of the function of lateral flow diagnostic strips of which lateral flow membranes are the fundamental components.

1.1.1. Pervaporation

Pervaporation – meaning permeation and evaporation – is a separation process which permits the selective removal of one or more components from a multi-component liquid. This separation is achieved by passing the multi-component liquid over a polymeric membrane, of appropriate composition, that preferentially allows the permeation of certain components in the liquid. The driving force of this permeation is the use of a partial vacuum so that the permeate is removed as a vapour. Maintenance of a lower vapour pressure on the permeate side of the membrane than on the feed side induces transport of feed components through the membrane polymeric matrix by solution diffusion[9–13]. This is shown in figure 1.1 below.

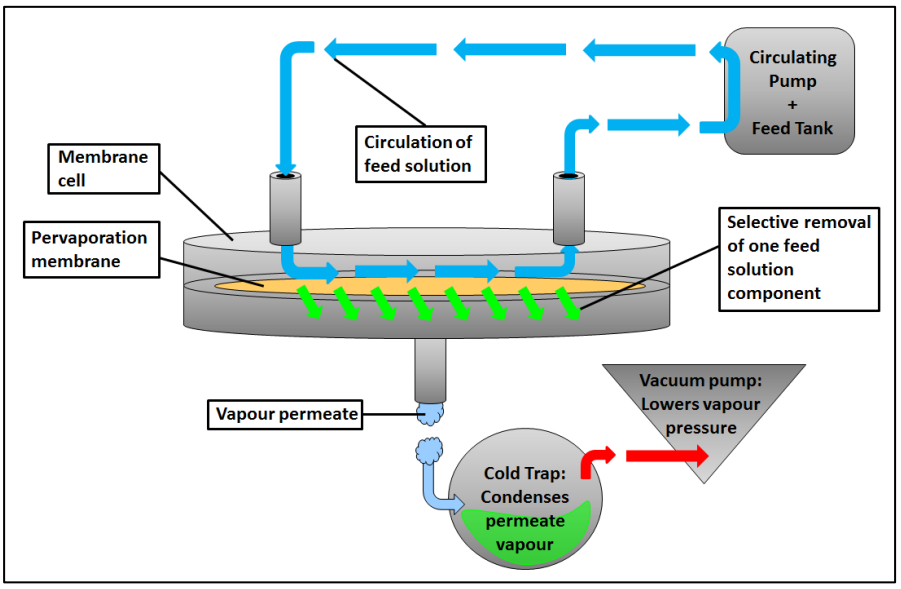


Figure 1.1: Pervaporation process

The current primary use of pervaporation is in the separation of *azeotropic solutions* in solvent dehydration and solvent-solvent separation. Traditionally *azeotropic distillation* has been the preferred method of achieving such separations, but this method requires the use of entrainer compounds (benzene, cyclohexane, etc). These chemicals remain in the separated liquids in trace amounts after separation and contaminate whatever processes and/or ecosystems they find their way in to afterwards. Entrainers are usually environmentally malign and with modern environmental regulations placed on industry, the use of this means of separating azeotropic solutions is not a feasible long term option. Another traditionally favoured method of separating azeotropic solutions is *pressure swing distillation* which does not utilize any harmful and/or contaminating entrainer compounds but does require high pressures and temperatures rendering the process both expensive and potentially dangerous. Pervaporation by comparison, is a clean process requiring no entrainers, operates at safe temperatures and pressures, and is relatively inexpensive[11].

Pervaporation is potentially most important in rendering ethanol suitable for use as a biofuel. Ethanol can only be used as a fuel in internal combustion engines at purities higher than 99% otherwise *knocking* occurs causing damage to the engine pistons. Since ethanol forms an azeotrope with water at 95.63 wt% ethanol to 4.37 wt% water, the only clean means of achieving a purity high enough for use as a fuel is through pervaporation.

Azeotropes

An azeotrope is loosely defined as a binary (or ternary) liquid solution which, at a certain critical composition, cannot be separated into its constituent liquids by conventional distillation. Distillation results in vapours which upon condensation will gradually approach the azeotrope limit. Once the azeotrope has been reached, any further distillations will result in a vapour, and subsequent condensate, with the composition of the azeotrope of the solution.

Azeotropes can be either homogenous or heterogeneous depending on the miscibility of the constituent liquids of the solution[14].

Azeotropes are defined as positive or negative: A positive azeotrope will have a boiling point lower than the pure boiling points of its constituents. A negative azeotrope will have a boiling point higher than the pure boiling points of its

constituents. A positive azeotrope may also be referred to as a *minimum boiling mixture* or a *pressure maximum azeotrope*. Likewise, a negative azeotrope may also be referred to as a *maximum boiling mixture* or a *pressure minimum azeotrope*[15], [16].

In terms of molar constituents, azeotropes differ from compounds in that the molar ratios of their constituents cannot be expressed as small integers.

The positive and negative terminology refers to the deviation of an azeotrope from ideal solution behaviour as defined by *Raoult's Law*. It is this law by which we accurately define an azeotrope. Azeotropic solutions are *always* non-ideal solutions.

Raoult's Law expresses the vapour pressure of an ideal solution (i.e. a solution in which the solute is non-volatile and so does not contribute to the vapour pressure above the solution) as:

$$P_{soln} = \chi_{solvent} P^{o}_{solvent} \qquad \textbf{1(i)}$$

Where P_{soln} is the vapour pressure of the solution, $\chi_{solvent}$ is the mole fraction of the solvent in the solution and $P^{o}_{solvent}$ is the vapour pressure of the pure solvent[17]. However in non-ideal solutions, where both constituents are volatile and so contribute to the vapour pressure above the solution an adjustment to the above equation must be made. Otherwise the figure obtained at the end will be greater or lesser than the actual vapour pressure of a non-ideal solution. Let us take the example of a solution of ethanol and water, where both are volatile solvents in solution:

$$P_{Total} = P_{EtOH} + P_{Water} = \chi_{EtOH} P^{o}_{EtOH} + \chi_{Water} P^{o}_{Water} \qquad \textbf{1(ii)}$$

P_{Total} is the total vapour pressure of the solution containing ethanol and water, χ_{EtOH} and χ_{Water} are the molar fractions of ethanol and water in solution respectively, P^{o}_{EtOH} and P^{o}_{Water} are the vapour pressures of pure ethanol and pure water respectively, and P_{EtOH} and P_{Water} are the partial vapour pressures of ethanol and water respectively contributing to the vapour pressure above the solution[18]. The figure obtained from this equation will differ from that obtained from equation 1(i). If we are dealing with an azeotropic solution and there is a negative deviation

from equation 1(i) by equation 1(ii) then it is a negative azeotrope. If the deviation from equation 1(i) by equation 1(ii) is positive then it is a positive azeotrope[19].

The reason for the difference in vapour pressures and the deviation from ideal behaviour and Raoult's law is due to the interactions between molecules of the constituents of a solution; *van der Waals forces* and *hydrogen bonding*. For example, in a liquid solution containing liquid A and liquid B, nearly ideal behaviour is approached when the A-A, B-B and A-B interactions are energetically similar. However, if the molecules of A and B have a special affinity for one another, i.e. they require less energy to interact than the energy required for A molecules to interact with A or for B molecules to interact with B, then the molecules will have a greater tendency to remain in the liquid solution rather than move into the vapour phase which creates the vapour pressure[18], [20]. Thus, the solution will have a lower vapour pressure than that predicted by Raoult's law and so have a negative deviation. Similarly, if the molecules of liquid A have a special affinity for others of their own type (equally for molecules of B) then they well have a tendency to enter the vapour phase, resulting in an increase in vapour pressure over what is predicted by Raoult's law, thus having a positive deviation[18], [20], [21].

Taking, once again, the example of a solution of ethanol and water; the hydrogen bonding interactions between water molecules results in the water molecules having a greater attraction for one another than the attraction between ethanol molecules, or the attraction between ethanol and water molecules. This results in a positive deviation from Raoult's law and ideal behaviour as described above.

From all of the above, it can be said that the solutions of ethanol and water used in the pervaporation experiments of this work are homogenous, positive azeotropes. The solution-diffusion process is the reason that azeotropes can be broken by pervaporation membranes. This process is explained in section 1.1.2.

Industry Overview

The first industrial patents on pervaporation were registered by the German company Gesellschaft fur Trenntechnik (GFT) Co. in 1982, after which, research into pervaporation began to become more widespread. GFT's membrane utilized a hydrophilic poly(vinyl alcohol) (PVA) membrane on a fabric support. This

membrane makeup exhibited high-abrasion resistance, elongation, tensile strength, and flexibility, with excellent water perm-selective properties [11].

Research since GFT's success has yielded many more polymers which can be effectively utilized for pervaporation through novel manipulation of the polymers via, polymer blending, organic-inorganic hybridization and cross-linking among others methods[22–31]. This has meant that pervaporation has developed a high potential for a wide range of separations, however its most common use remains the production of anhydrous ethanol.

Much research has gone into improving the process of purifying ethanol through separation. This means making membranes that are more selective and have greater flux. There is a trade-off that must be made between *flux* and *selectivity*; as selectivity is increased, flux decreases. Efforts have gone into minimising this trade off as much as possible. However where polymers have been found to be both selective and exhibit high flux, mechanical and thermal stability have become problems. For example, sodium alginate and chitosan are naturally occurring polysaccharides which have been found to exhibit outstanding flux and selectivity but are mechanically and thermally weak[11], [32]. Other polymers have been found to have similar properties but also similar faults; sodium alginate seems to be the most promising of all of these and has been researched extensively for the purpose of ethanol dehydration. This is discussed in greater detail in section 1.3.

1.1.2 Lateral Flow Diagnostics

Cellulose nitrate (CN) lateral flow membranes are a type of microporous flat sheet membrane used as a material in diagnostic and filtration applications. Lateral-flow refers to the transport of the solution to be filtered and/or analysed through the membrane as described in section 1.2.1. This movement is driven by capillary flow through the porous membrane polymer network. Membranes are typically surface functionalised to retain certain compounds – in the case of filtration – or, to react to certain target

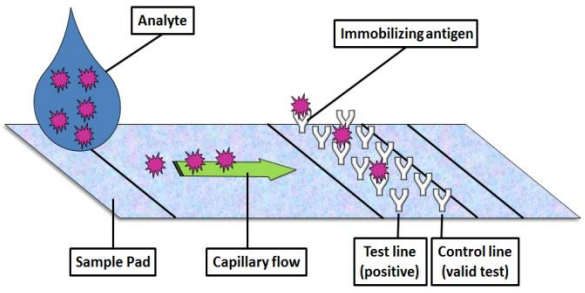


Figure 1.2: Mechanism of lateral flow diagnostic strip

analytes, usually in the form of a colour change – in the case of diagnostic strips (see figure 1.2).

Industry Overview

The nineteen fifties saw the establishment of industrial CN membrane processes. Initial uses for such microporous membranes were filtration applications that were based on the membranes' ability to retain microorganisms and particles from fluids. These characteristics provided opportunities for use in new types of applications based on the identification and quantification of microorganisms [33], [34], protein contaminant removal, and the immobilization of proteins [35]; including blotting techniques [36], enzyme-linked immunosorbent assay (ELISA) testing [37], and lateral-flow immunochromatographic tests [38–42]. In immunodiagnostic tests, proteins are the most common samples applied to a solid membrane surface; therefore, the protein-binding capacity is a critical property of the membrane [43]. Cellulose nitrate membrane filters have also been used for solid phase extraction and determination of trace elements in various media[44–48], where those comprised of materials with a strong affinity for hydrophobic species in water are particularly useful for retaining metal species by filtration[48]. The sensitive and accurate determination of heavy metal ions at trace levels in natural samples, including waters, biological fluids, soils and sediments is a very important part of environmental and public health studies[49–51]. Pre-concentration and separation of the trace analytes on the cellulose nitrate membrane filters addresses the interference effects from sample matrices and inadequate detection limits often associated with other techniques e.g. flame atomic absorption spectrometry (FAAS).

Lateral-flow cellulose nitrate membranes function as a transport medium to carry target analyte and bind it together with the immobilizing antigen on the membrane surface control line. Membrane surface properties and cross-sectional morphology are important parameters in the production of effective immunological assays for diagnostic and healthcare analysis. If the membrane surface and internal layer structure could be controlled precisely, various types of immunological analysis could be performed effectively and accurately[52]. To gain greater control of the internal structure of these membranes requires a greater understanding of the rhealogical factors involved in the membrane composition and of the membrane

internal structures and their formation. Control of membrane structure and properties is the chief aim of this section of the project.

1.2 Membrane Transport Theory

The following is a detailed description of the mechanisms of permeation within membranes. It will be apparent from this that the functionality of pervaporation membranes is far more complex than that of lateral flow. This is in contrast with the membrane formation processes which will be described later; those of lateral flow membranes are far more complex than those of pervaporation membranes.

Membrane separation processes generally are described by two primary theories: *pore-flow,* which describes, in part, the transport mechanism of lateral flow membranes, and *solution-diffusion*, which describes the transport mechanism of pervaporation membranes.

The difference between the solution-diffusion and pore-flow mechanisms is in the relative size and volume of the membrane pores. In membranes with solution diffusion functionality the free volume element (pores) of the membrane are - in effect - spaces between the polymer chains of the membrane which are utterly dependent on the random thermal motion of the polymer chains. The greater the thermal motion the more these pores will appear and disappear in a dynamic manner with the diameter of the pores varying constantly. In addition to this the pores are not necessarily in contact with one another. This lack of permanent, defined pore structure leads to the description of such membranes as *non-porous*. Membranes that function in this manner have pore diameters in the region of 2-5 Å. This is typical of reverse osmosis, gas separation and pervaporation membranes.

In membranes with pore-flow functionality the free volume element is relatively large, of fixed position and volume, and is of networked structure with the pores connected to one another. Membranes that function in this manner have pore diameters of greater than 10Å. This is typical of ultrafiltration, *Knudsen-flow* gas separation, and microfiltration (which includes lateral flow) membranes. Membranes with pore size between 5 Å and 10 Å are known as *intermediate* membranes. This is the domain of nanofiltration membranes and is only mentioned for posterity.

1.2.1 Solution-Diffusion

Diffusion is a process by which matter is transported from one part of a system to another by a concentration gradient. If a concentration gradient of permeate molecules is formed in a membrane medium, statistics show that a net transport of matter will occur from the high concentration region to the low concentration region. This was first described by *Fick's law of diffusion* [3]:

$$J_i = -D_i \left(dc_i/dx\right) \qquad \textbf{1(iii)}$$

Where J_i is the rate of transfer (flux) of component ***i*** (g cm^{-2} s^{-1}), dc_i/dx is the concentration gradient of ***i*** across the membrane, and D_i is the *diffusion coefficient* (cm^2 s^{-1}). The negative sign in equation 1(iii) indicates the direction of diffusion; down the concentration gradient. From the earlier description, it is known that the solution diffusion occurs through randomly fluctuating, (in both diameter and position) not necessarily networked pores in the polymer matrix of a membrane. As such, diffusion is a slow process. Thus, speed is achieved in separations with membranes that function through the use of very thin membranes and high concentration gradients across them. The pressure, temperature and composition of fluids on either side of a membrane determine the concentration of the diffusing species at the membrane surface in equilibrium with the fluid and so affect the concentration gradient[53]. The pervaporation process is driven by a vapour pressure difference across a membrane between the relatively high vapour pressure of the feed liquid and the low vapour pressure of the permeate vapour.

Solution-diffusion in pervaporation can best be described if one looks at an individual molecule. Once a solution has dissolved into the non-porous polymer matrix of a pervaporation membrane, individual molecules occupy the fluctuating free volume holes (pores). These molecules can then diffuse through the membrane by moving from one free volume hole to another. This movement is permitted by the thermal motion of the polymer chains.

The advent of powerful computers has allowed these statistical fluctuations in the volumes between polymer chains to be calculated[9]. Smit *et al*[54] simulated the diffusion of a single carbon dioxide molecule through a polyimide matrix. They showed that for the first 100 ps the carbon dioxide molecule "bounced" around in the free volume hole in which it had been placed, never

moving more than 5 Å, i.e. the diameter of the free volume hole. After 100 ps however, a random thermal movement of the polymer chains allowed sufficient space for the carbon dioxide molecule to shift approximately 10 Å to an adjacent free volume hole, where it remained until another random movement of the polymer chains allowed it to move further.

The free volume holes of a membrane's polymeric matrix will only allow the passage of molecules small enough to pass through the holes. In the case of sodium alginate used in pervaporation membranes in the dehydration of ethanol, the free volumes formed in the polymer matrix are, on average, only large enough to allow the passage of water molecules, while the holes are too small for ethanol molecules to pass through, making it ideal for ethanol dehydration[32]. Flux is also governed by these free volume holes; the larger and more numerous the holes, the more feed solution can pass through a membrane. However, larger the holes get, i.e. the greater the membrane free volume, the less selective a membrane becomes. This is the trade-off that must be made between flux and selectivity and provides the much of the impetus for our pervaporation research.

Proof of Solution-Diffusion Theory

*Much of the following section is adapted from the book "*Membrane Technology and Applications*" by Richard W. Baker*[55].

A mathematical description of diffusion in membranes is based in thermodynamics, on the proposition that pressure, temperature, concentration and electrical potential are interrelated and the overall driving force of a permeant is the gradient in its chemical potential. Thus, the flux, J_i, of a component ***i,*** is described by equation 1(iv):

$$J_i = -L_i \left(d\mu_i / dx\right) \qquad \textbf{1(iv)}$$

where $\left(d\mu_i / dx\right)$ is the chemical potential gradient of ***i*** and L_i is a coefficient of proportionality linking chemical potential driving force to flux. In pervaporation, the driving force is dictated by concentration and pressure, as such, chemical potential, μ_i, can be expressed as in equation 1(v):

$$d\mu_i = RTd\ln(\gamma_i n_i) + \upsilon_i dp \qquad \textbf{1(v)}$$

where γ_i is the activity coefficient (mol/mol) linking mole fraction with activity of i, p is pressure, n_i is the mole fraction (mol/mol) of i, and v_i is the molar volume of i.

In incompressible phases such as liquids or a solid membrane - the scenario encountered at the feed side of a pervaporation membrane - molar volume does not change with pressure and so equation 1(v) can be rewritten as equation 1(vi):

$$\mu_i = \mu_i^o + RTln(\gamma_i n_i) + v_i(p - p_{isat}) \quad \textbf{1(vi)}$$

where μ_i^o is the chemical potential of pure i at reference pressure p_i^o, where the reference pressure is defined as the saturation vapour pressure of i, p_{isat}.

In compressible phases, i.e. gases - the scenario encountered at the permeate side of a pervaporation membrane - molar volume *does* change with pressure and so equation 1(v) can be rewritten as equation 1(vii):

$$\mu_i = \mu_i^o + RT\ ln(\gamma_i n_i) + RT\ ln(p/p_{isat}) \quad \textbf{1(vii)}$$

Several assumptions must be made for any permeation model, including for pervaporation:

- Fluids on either side of a membrane are in equilibrium with the membrane surface with which they are in contact.
- Rates of adsorption and desorption of permeant molecules are higher than the rate of diffusion of permeant molecules through the membrane (hence *concentration polarization*)
- When pressure is applied across a dense membrane, pressure throughout the membrane is constant at the highest value (therefore pressure within a membrane is constant and chemical potential across a membrane is only expressed as a concentration gradient)

In the solution-diffusion model, the pressure within the membrane is constant at the high-pressure value (in the case of pervaporation the vapour pressure of the feed side of the membrane, p_f), and the gradient in chemical potential across the membrane is expressed as a smooth gradient in solvent activity ($\gamma_i n_i$). The flow that occurs down this gradient is expressed by equation 1(v), but because no pressure gradient exists within the membrane, equation 1(iv) can be rewritten by combining equations 1(iv) and 1(v). Assuming γ_i is constant, this gives equation 1(viii):

$$J_i = -(RTL_i / n_i).(dn_i/dx) \quad \textbf{1(viii)}$$

Using the term to express concentration of component ***i,*** c_i, rather than the more cumbersome mole fraction used above, equation 1(viii) can be rewritten as equation 1(ix):

$$J_i = -(RTL_i / c_i).(dc_i/dx) \qquad \textbf{1(ix)}$$

Since c_i (g/cm^3) can be expressed in terms of molar fraction of ***i***, n_i, molar density, ρ, and molecular weight of ***i***, m_i as shown in equation 1(x):

$$c_i = m_i \rho n_i \qquad \textbf{1(x)}$$

and since equation 1(ix) has the same form as Fick's law of diffusion (equation 1(iii), (RTL_i / c_i) can be replaced by the diffusion coefficient D_i to give equation 1(iii):

$$J_i = -D_i (dc_i / dx) \qquad \textbf{1(iii)}$$

From this, by integrating over the thickness of the membrane, we can obtain equation 1(xi):

$$J_i = \{D_i(c_{i\,f\,(m)} - c_{i\,p\,(m)})\}/l \qquad \textbf{1(xi)}$$

where ***l*** is the thickness of the membrane, the subscript ***m*** designates "…of the membrane", the subscript ***f*** designates the feed side and the subscript ***p*** designates the permeate side.

Recalling the assumption made above, that fluids on either side of a membrane are in equilibrium with the membrane surface with which they are in contact, it can then be said that the chemical potential of a component ***i*** of a fluid is equal to its chemical potential at the membrane surface with which it makes contact. Taking the example of a pervaporation membrane, we can use this assumption to first express this equilibrium at the feed side of the membrane as equation 1(xii):

$$\mu_{if} = \mu_{if(m)} \qquad \textbf{1(xii)}$$

which using equation 1(vi) for incompressible liquids becomes equation 1(xiii):

$$\mu_i^o + RTln(\gamma_{if}^L n_{if}) + v_{if}(p_f - p_{isat}) = \mu_i^o + RTln(\gamma_{if(m)} n_{if(m)}) + v_{if(m)}(p_f - p_{isat}) \qquad \textbf{1(xiii)}$$

where the superscript ***L*** designates liquid phase (rather than ***G*** which designates gas phase). Equation 1(xiii) which becomes equation 1(xiv):

$$RTln(\gamma_{if}^L n_{if}) = RTln(\gamma_{if(m)} n_{if(m)}) \qquad \textbf{1(xiv)}$$

and thus to equation 1(xv):

$$n_{if(m)} = (\gamma_{if}^{L} / \gamma_{if(m)}).\ N_{if} \qquad \textbf{1(xv)}$$

Using equation 1(x), equation 1(xv) becomes equation 1(xvi):

$$c_{if(m)} = (\gamma_{if}^{L} / \gamma_{if(m)}).\ C_{if} \qquad \textbf{1(xvi)}$$

and from equation 1(xvi), one can define a sorption coefficient of component ***i*** in liquid phase as in equation 1(xvii):

$$K_i^{L} = (\gamma_{if}^{L} / \gamma_{if(m)}) = c_{if(m)} / c_{if} \qquad \textbf{1(xvii)}$$

Therefore, the concentration of permeant ***i***, at the feed side of the membrane is defined as the sorption coefficient times the concentration of ***i*** in the feed solution:

$$c_{if(m)} = K_i^{L}.\ c_{if} \qquad \textbf{1(xviii)}$$

If one were to take the example of a dialysis membrane in which both sides of the membrane are in contact with an incompressible liquid, then the above equations would be applied to both sides - feed and permeate - to yield two concentration figures (one for each side of the membrane) which could be substituted into equation 1(xi) to all cancel conveniently leaving us with an expression describing permeation in a dialysis membrane. In the case of pervaporation however, one side of the membrane is in contact with a liquid feed, which is described in equations 1(xii) - 1(xviii) above, while the other side of the membrane is in contact with a gaseous permeate vapour and must be described using equations 1(vii) – 1(x), which is used to describe chemical potential in compressible gases, as follows:

Equation 1(xix) equates the chemical potential of component ***i*** in the permeate vapour with the chemical potential of component ***i*** at the membrane surface it contacts:

$$\mu_{ip} = \mu_{ip(m)} \qquad \textbf{1(xix)}$$

which using equation 1(vii) for compressible gases becomes equation 1(xx):

$$\mu_i^{o} + RTln(\gamma_{ip}^{G} n_{ip}) + RT\ ln(p_p / p_{isat}) = \mu_i^{o} + RTln(\gamma_{ip(m)} n_{ip(m)}) + \upsilon_{ip(m)}(p_p - p_{isat}) \qquad \textbf{1(xx)}$$

This rearranges to give equation 1(xxi):

$$n_{ip(m)} = (\gamma_{ip}^{G} / \gamma_{ip(m)}).(\ p_p / p_{isat}).n_{ip}.exp[\{-\upsilon_{ip(m)}(p_p - p_{isat})\}/RT] \qquad \textbf{1(xxi)}$$

Since the exponent term in equation 1(xxi) is close to unity, it becomes:

$$n_{i_{p(m)}} = (\gamma_{i_p}{}^{G} / \gamma_{i_{p(m)}}).n_{i_p} .(p_p / p_{i_{sat}}) \qquad \textbf{1(xxii)}$$

And since the term $n_{i_p} .p_p$ is equivalent to the partial pressure of i in the permeate vapour it can be written as p_{i_p} to give equation 1(xxiii):

$$n_{i_{p(m)}} = (\gamma_{i_p}{}^{G} / \gamma_{i_{p(m)}}). (p_{i_p} / p_{i_{sat}}) \qquad \textbf{1(xxiii)}$$

Using equation 1(x), equation 1(xxiii) becomes equation 1(xxiv):

$$c_{i_{p(m)}} = m_i \rho_m .(\gamma_{i_p}{}^{G} p_{i_p} / \gamma_{i_{p(m)}} p_{i_{sat}}) = K_i{}^{G} p_{i_p} \qquad \textbf{1(xxiv)}$$

which gives us a figure for the gas phase sorption coefficient of i in terms of the concentration of component i at the membrane surface in contact with the permeate vapour.

If one were to take the example of a gas separation membrane in which both sides of the membrane are in contact with a compressible gas, then the above equations would be applied to both sides - feed and permeate - to yield two concentration figures which could be substituted into equation 1(xi) to all cancel conveniently leaving us with an expression describing permeation in a gas separation membrane.

We now have an expression for the concentration of the permeating component, i, at each surface of the pervaporation membrane. By substituting equations 1(xviii) and 1(xxiv) into equation 1(xi) we obtain an equation for pervaporation membrane flux, as shown in equation 1(xxv):

$$J_i = \{D_i(K_i^{L} c_{i_f} - K_i^{G} p_{i_p})\}/l \qquad \textbf{1(xxv)}$$

There is now a problem however: The equation above contains a sorption coefficient in the liquid phase and another in the gas phase. They must be interconverted. This is done by making another assumption in the theory, specific to pervaporation, in addition to those already made in the general theory above: A hypothetical vapor in equilibrium with the feed solution. This vapor–liquid equilibrium can then be written:

$$\mu_i^{o} + RT\ln(\gamma_i^{L} n_i^{L}) + v_i(p_i - p_{i_{sat}}) = \mu_i^{o} + RT\ln(\gamma_i^{G} n_i^{G}) + RT \ln(p_i / p_{i_{sat}}) \qquad \textbf{1(xxvi)}$$

Following the same logic as that used to go from equation 1(xx) to equation 1(xxiii), equation 1(xxvi) becomes:

$$n_i^{L} = \gamma_i^{G} p_i / \gamma_i^{L} p_{i_{sat}} \qquad \textbf{1(xxvii)}$$

Using equation 1(x), this becomes:

$$c_i^L = m_i \rho (\gamma_i^G p_i / \gamma_i^L p_{isat}) \qquad \textbf{1(xxviii)}$$

Which becomes:

$$c_i^L = (K_i^G / K_i^L).m_i \qquad \textbf{1(xxix)}$$

Substituting this into equation 1(xxv) yields:

$$J_i = \{D_i K_i^G (p_{if} - p_{ip})\}/l \qquad \textbf{1(xxx)}$$

wherein p_{if} and p_{ip} are the partial vapour pressures of component i on either side of the membrane.

It should be noted that equation 1(xxix) links the concentration of a sorbed vapor in the liquid phase(c_i^L)with the equilibrium partial pressure of the vapor. This is known as *Henry's law* and is more commonly written as:

$$H_i \,.\, c_i^L = p_i \qquad \textbf{1(xxxi)}$$

Equation 1(xxx) expresses the driving force in pervaporation as the difference in vapour pressure across the membrane, as first described by Katoaka *et al*[56]. This expression has been demonstrated experimentally [57], [58]. The agreement between experiment and theory demonstrated is good evidence for the veracity of the solution-diffusion model.

1.2.2 Lateral-Flow Theory

Mass transport in lateral flow membranes is described by capillary flow, with retention of analyte particles due to capture by Brownian diffusion, membrane pore tortuosity and the incorporation of surface charged groups on the membrane.

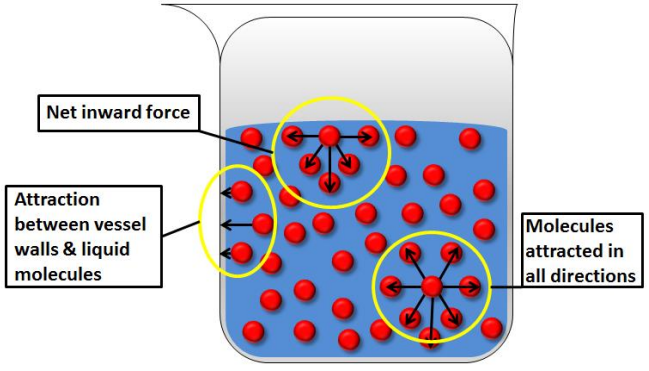


Figure 1.3: Molecular level view of intermolecular forces acting on a molecule at the surface of a liquid compared to those in the interior

Capillary Flow

Capillary flow, or *capillary action,* is determined by the surface tension of a liquid which is in turn dependent on

its viscosity which is ultimately determined by the attractive forces between the molecules of a liquid.

A molecule in a liquid is attracted equally in all directions by the molecules surrounding it, however, for molecules at the liquid surface there can be no attractive forces from above the liquid. This results in a net inward force on the molecules as illustrated in figure 1.3.

The net inward force highlighted above pulls molecules from the surface into the interior of the liquid. This reduces the surface area and causes the molecules at the surface to pack more closely together than those in the bulk solution below. This causes the liquid to behave as though it has a skin. The surface tension of a liquid is the energy required to break this surface skin, represented by, $\boldsymbol{\gamma}$. In addition to this force there is an attraction between the molecules of the liquid and the vessel walls - also highlighted in figure 3. This is a measure of how much a liquid will wet the surface of the vessel and is quantified by contact angle, $\boldsymbol{\theta}$. These two forces can allow us to predict the height, $\boldsymbol{h}$, to which a liquid will rise when contained in a columnar vessel of radius, $\boldsymbol{r}$.

$$\boldsymbol{h = 2\gamma cos\theta / \rho g r} \qquad \textbf{1(xxxi)}$$

where $\boldsymbol{\rho}$ is the density of liquid (mass/volume) and $\boldsymbol{g}$ is local gravitational field strength (force/unit mass).

For a water-filled glass tube in air at standard laboratory conditions, γ = 0.0728 N m^{-1} at 20°C, θ = 20°, ρ is 1000 kg m^{-3}, and g = 9.81 m s^{-2} the height of the water column is: $\boldsymbol{h} \approx (1.48 \times 10^{-5}) / \boldsymbol{r}$. Thus for a 4m diameter glass tube in the laboratory conditions given above, the water would rise only 0.007 mm. However, for a 4 cm diameter tube, the water would rise 0.7 mm, and for a 0.4 mm diameter tube, the water would rise 70 mm. This act of water rising up a narrow tube, or capillary, is known as capillary action. It is by this mechanism that a liquid travels through the tortuous pores of a lateral flow

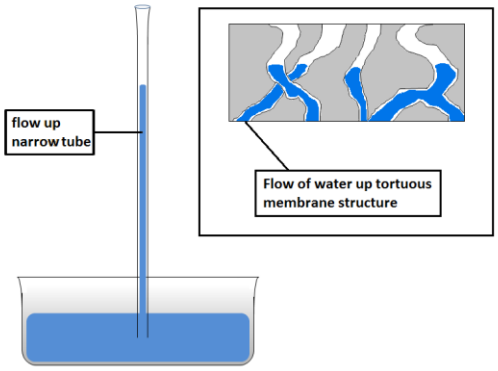


Figure 1.4: Flow of liquid up a narrow tube by capillary action and representation of flow through tortuous pore structure of a membrane by same mechanism

membrane, as illustrated in figure 1.5 below. The overall lateral direction of flow (as distinct from than upward direction) is reliant upon the internal structure of the membrane being isotropic (explained in section 1.3) and tortuous. It is the generation of this internal structure to optimise lateral flow rate, which is the objective of this work.

The means by which a target analyte is retained in the membrane is due to any one, or all of; Brownian diffusion, membrane pore tortuosity and the incorporation of surface charged groups on the membrane. In all three cases particles smaller than the diameter of the pore are captured by adsorption of the particles to the internal surface of the membrane. The membrane pore tortuosity is such that relatively large particles cannot flow along the fluid flow lines through the membrane and so impact with the pore walls and are captured by the specifically functionalized polymer. The retention of smaller particles is due to Brownian diffusion primarily. Relatively small particles are carried along the fluid flow lines in the membrane, but are subject to random Brownian motion[59]. This random motion regularly brings these small particles into contact with pore walls and they are subsequently captured by surface absorption. Finally, many colloidal materials carry a small negative charge; through the incorporation of positively charged surface groups on the membrane, such particles are captured.

In the case of lateral flow cellulose nitrate membranes, target analyte capture is achieved through immobilizing antigen on the membrane surface control line as shown in figure 1.2 above.

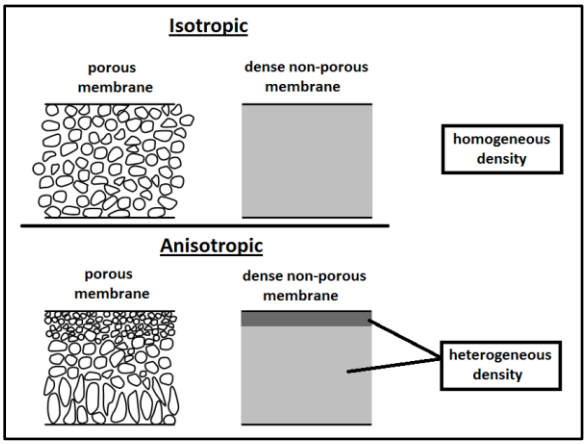


Figure 1.5: isotropic vs anisotropic membrane structures in porous and non-porous membranes

1.3 Membrane Structure & Formation

Membranes fall into two major categories; isotropic (symmetric) and anisotropic (asymmetric)[60]. Isotropic membranes have uniform physical characteristics throughout their structure, while anisotropic do not (see figure 1.5). In the cases of the membranes investigated in this work, they can be produced with either structure. As

was highlighted in the opening of this chapter, membranes are cast as thin films of polymer solutions and then allowed to dry to form the final membrane. The manner of - and the processes that occur during - drying determines the final membrane structure. At the beginning of section 1.2 it was pointed out that the membrane formation processes of lateral flow membranes are far more complex than those of pervaporation membranes. For this reason this section will start by explaining the formation of pervaporation membranes, the manipulation of their internal structures by control of formation processes, outline any structural anomalies that occur and explain the effect on membrane performance caused by structure. The same will then be done for the more complicated lateral flow formations.

1.3.1 Pervaporation Membrane Categorisation

Pervaporation membranes can be divided into three groups based on their material composition: polymeric, inorganic and mixed matrix membranes. All three can be isotropic or anisotropic.

Polymeric membranes

Composed of dense non-porous polymers and polysaccharides such as poly(vinyl alcohol) (PVA), poly(imide) (PI), sodium alginate (NaAlg), chitosan, silicon rubber, etc. Those produced in this project are dense, non-porous, polymeric membranes composed of sodium alginate, or PVA, or some blend of the two.

Sodium Alginate

Sodium alginate (NaAlg) has long been considered one of the most effective materials for producing hydrophilic water selective pervaporation membranes for the dehydration of ethanol. It is a naturally occurring polysaccharide obtained from the cell walls of a class of brown algae known as *phaeophyceae*[61], [62]. With environmental restrictions coming to bear on industry, ecologically benign materials such as NaAlg are preferentially sought for industrial applications; its pervaporation characteristics (high water selectivity with relatively high flux) make it ideal for use

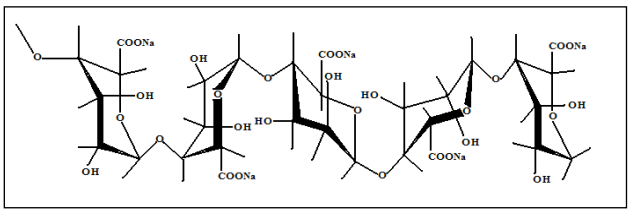


Figure 1.6: Sodium alginate

in pervaporation membranes. However, it is mechanically unstable (Young's modulus: 5551Mpa [63]); and thin membranes cast from solutions of pure NaAlg are brittle and prone to cracking, especially in relatively large diameter membranes like those used in these experiments (membrane diameter: 0.158 m)

Poly(vinyl alcohol)

PVA is the material most commonly used in industrial pervaporation membranes for the dehydration of alcohols. PVA membranes exhibit high tensile strength (Young's Modulus of approximately 1697 Mpa [63]), elongation, high abrasion resistance and flexibility. Its hydrophilic nature means it can be utilized as a pervaporation membrane material but, in comparison with other polymer types it exhibits low water permselecitivty. Only its mechanical durability has made it the mainstay of industrial pervaporation membranes.

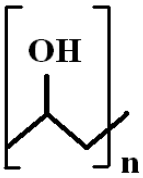


Figure 1.7: Poly(vinyl alcohol)

Polymer Blends

Polymer blend membranes are composed of multiple polymers blended together with the aim of incorporating the desired features of said polymers (high flux, high selectivity, structural and thermal stability) into one membrane while minimizing the undesired features[64].

As was stated above, sodium alginate exhibits high flux and selectivity but is mechanically weak. Polymer blend membranes are potentially a way of producing pervaporation membranes with high flux and selectivity combined with durability. Numerous combinations of materials have been studied with this goal in mind; particularly the use of high selectivity/high flux polysaccharides with durable synthetic polymers; chitosan/polysulfone[65], chitosan/polyacrylic acid[23], chitosan/PVA[24], NaAlg/PVA[25], [63], [66–70], sericin/PVA[22] and NaAlg/hydroxyehtylcellulose[26]. NaAlg/PVA blends will be produced in this project with the aim of creating a membrane which has the flux and selectivity of NaAlg combined with the physical durability of PVA.

Blending changes the properties of the polymers within the blend. A blend will differ from its component polymers in Young's moduli and glass transition temperature as well as flux and selectivity.

Inorganic Membranes

Composed of solid, inorganic, porous materials, these are generally subdivided into two types; ceramic membranes which are formed from silica; and zeolitic membranes which are manufactured from aluminasilicates[71].

Ceramics

Ceramic materials are usually silica based although they can be produced from alumina, titania and zirconia. They are thermally and chemically stable in comparison with polymer membranes, with high melting points and the ability to operate over a wide pH range. Being hard materials they also exhibit good mechanical stability[11].

Chapman *et al*. [11] found that ceramic membranes do not show the same levels of selectivity in pervaporation as polymeric membranes do. This property can be explained by the fact that ceramic membranes contain permanent pores as were described above.

In general pure ceramic membranes are not used for pervaporation. Instead they are used as supports for polymers with inferior mechanical properties[27], [28], [72].

Zeolites

Zeolites are aluminasilicates. They offer a good basis for separation materials due to their highly ordered porous structure. The size of the pores in a zeolite particle can vary depending on type. A range of different zeolite structures exist with different aluminium to silica ratios and pore sizes ranging from 3 Å – 8 Å [71]. The zeolite type used in this project was zeolite A (MCM41). The crystal lattice carries a negative charge which is balanced by positive sodium ions (cations) in the interstices. These cations make the particles very hydrophilic[73].

As with ceramics; membranes comprised of zeolites exhibit good thermal and chemical stability and high flux. They differ from ceramic membranes in that they can exhibit high selectivities. Selectivity as high as 53,989 with a zeolitic membrane using a water/ethanol feed solution has been reported[74].

The high selectivities exhibited by zeolite membranes is due to the molecular sieving effect of their pores.

Mixed Matrix Membranes (MMMs)

Membrane hybrids incorporating materials from both polymeric and inorganic membranes, with the aim of obtaining membranes with the best characteristics of both while eliminating many of the flaws[75]. Those properties exhibited by ceramic and zeolitic particles have led to much research into incorporating them into polymeric membranes to increase flux, selectivity and, thermal and mechanical stability. By incorporating ceramic or zeolitic particles into a polymeric matrix one will reduce the non-porous nature of the polymer[29], [31], [76], [77]. The inherent mechanical, chemical and thermal stability of these particles increases that of polymeric membranes while the inherent brittleness of the ceramic and zeolitic membranes is alleviated by the rubber-like properties of polymeric membranes. Chapter 7 will discuss the formation of these membranes in detail.

1.3.2 Pervaporation Membrane Formation

Support

Pervaporation membranes can be supported or unsupported depending on the membrane requirements. Supports provide increased structural integrity for the selective polymer layer. Our membranes utilize a 100% polyester non-woven fabric material to provide structural support. The details of its construction are outlined in chapter 2.

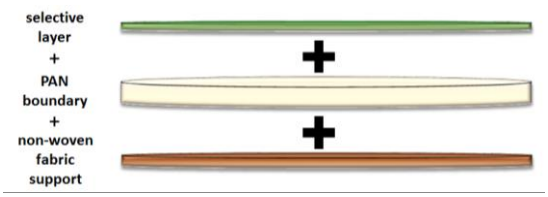


Figure 1.8: Supported pervaporation membrane structure

Selective Layer Casting

The formation of the pervaporation selective layer is through the evaporation of solvent from the cast polymer solution resulting in densification and drying to yield the final membrane, which is much thinner than the casting thickness. The rate of evaporation affects the final structure of the membrane however, rendering it isotropic or anistropic. (See chapters 5 and 6 for details)

1.3.3 Pervaporation Membranes: Structural Effects & Anomalies

Skin Layers

Yiotis *et al* have described how polymer films cast from solution are strongly dependent on evaporation rate[78]. The force of evaporation of the solvent upwards through the drying polymer matrix drags polymer molecules upwards, resulting in a higher density of polymer at the air exposed side of the final membrane.

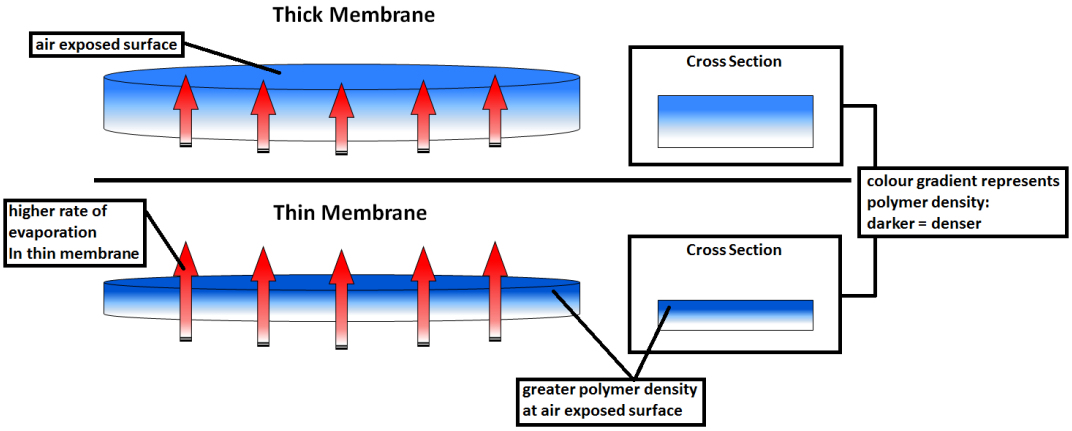


Figure 1.9: Solvent evaporation and polymer density in thick vs thin pervaporation membrane

The rate/force of evaporation is dependent upon the mass and area of the drying membrane: The greater the area per mass of drying membrane the greater the force of evaporation. Since the area of the membrane is fixed then only the mass can be reduced to increase the force of evaporation. This is achieved through thinner castings of the membrane polymer solution. The greater force of evaporation means that over the course of the drying period a greater number of polymer molecules are dragged to the air exposed surface of the thin membrane resulting in a greater polymer density in the polymer matrix at that side of the membrane. This has the effect of forming a denser surface layer, known as a *skin layer* (or *diffuse layer*). In thicker cast membranes the skin layer is thinner while for thinner cast membranes the opposite is true (see figure 1.9 and chapter 5).

Plasticization

Plasticization in a polymer is achieved through an *additive plasticizing agent*; a molecule added to lower glass transition temperature, crystallinity or melting temperature, thereby increasing elasticity[79]. It is believed that this is achieved through the low molecular weight plasticizer's thermal motion increasing the

polymer's free volume, which increases the long-range segmental motion of the polymer molecules (decreasing Young's modulus)[62]. In the case of highly hydrophilic polymers such as NaAlg, during pervaporation water can function as a plasticizing agent as it solvates the membrane and increases polymer chain mobility.

Crosslinking

Crosslinking serves the opposite function of plasticization; where plasticizers increase polymer chain mobility, crosslinking reduces it. This is achieved by increasing the number of bonds (crosslinks) between the chains of a polymer to form a network[62], [79].

Crosslinking can be achieved chemically through the use of additives or thermally by simple heating[68], [80]. This brings about changes in the polymer properties; if previously soluble the polymer will no longer dissolve (except when ionically crosslinked), the glass transition temperature of the polymer is increased and the flexibility of the polymer is reduced (increasing Young's modulus). Many of the properties of crosslinked amorphous polymers resemble those of crystalline polymers because of the strong secondary forces arising from close chain packing in crystalline polymers.

Polymer Hydrophilicity/Hydrophobicity

In this project pervaporation membranes are used for the dehydration of ethanol. This requires that the pervaporation membranes used selectively remove water from the feed. To aid in this membranes can be produced from polymers which have an affinity for water, i.e. hydrophilic polymers.

The hydrophilicity of a polymer is determined by the functional groups of the polymer backbone. Hydrophilicity is due to polarity in a molecule. The more polar a functional group the more readily it can hydrogen bond with water molecules. In the case of NaAlg, it is the $–COO^-Na^+$ functional group which makes the polymer hydrophilic and therefore useful for the dehydration of ethanol. The negative charge on the oxygen which is stabilised by the sodium counter-ion creates a highly polarized –COONa functional group which readily hydrogen bonds with water molecules: Added to this are the numerous –OH functional groups on the polymer

backbone which are also polar and form hydrogen bonds. This renders NaAlg a highly hydrophilic polymer[32].

However, the more hydrophilic a polymer the more water soluble it is. As more water is absorbed into a membrane from the feed the membrane swells, which reduces flux, and eventually the membrane begins to dissolve. There are ways of reducing this without adversely affecting a membrane's affinity for water: One way is through cross linking, however, in the case of sodium alginate which has a Young's modulus of 5551 Mpa, this results in the polymer becoming too brittle to use as a membrane material. The solution is to blend the membrane with a less hydrophilic and more durable polymer such as PVA, as described in section 1.3.1.

Another problem brought about by water solubility is that water – by solvating a hydrophilic membrane – effectively plasticizes the polymer and reduces the glass transition temperature of the polymer as it is absorbed into the membrane[52]. Reduction of the glass transition temperature can result in a phase change across the membrane during pervaporation. This can bring about problems with relaxation of polymer chains in the glassy phase of membranes.

Glass Transition Temperature

Polymers typically exist in an amorphous state. Depending on thermal conditions a polymer may exhibit properties of an amorphous glass or those more in common with a rubber. When a polymer in a rubbery state is cooled, its kinetic energy decreases; reducing the mobility of the polymer chains. As the temperature decreases further the motion of the polymer chains becomes restricted to short range vibrations and rotations and the polymer takes on the properties an amorphous glass. The temperature at which this transition occurs is known as the *glass transition temperature* (T_g)[62].

The T_g of a polymer can be changed by plasticization, crosslinking, blending or solvation. In this project the membranes utilized are composed of PVA, NaAlg, or some combination of both: The T_g of NaAlg is reported to be in the region of 119 ^{o}C[26], [68]. When combined with PVA in 4:1 ratio of NaAlg:PVA, according to DSC results, the T_g is lowered to ~96 ^{o}C, (see chapter 5) although literature suggests that it is ~90 ^{O}C[26]. The more permeant absorbed in the membrane the greater the plasticization effect exerted on the polymer chain mobility, resulting in the T_g being

reduced[9]. Since pervaporation works through a mechanism of absorption-diffusion and water is an effective solvent for both sodium alginate and poly(vinyl alcohol), the T_g of the of the polymer blend is further lowered as the water in the feed solution diffuses through the membrane polymer matrix. This lowers the T_g to a point where the higher temperature at the feed side of the membrane is above the T_g meaning the feed side is in a rubbery state while the permeate side of the membrane is at a temperature lower than the T_g and so in a glassy state: It follows that there is also a change in the Young's modulus across the membrane.

This change in state across the membrane from an amorphous rubbery polymer to an amorphous glassy polymer creates a common problem in pervaporation membranes; "relaxation".

Membrane Polymer Matrix Relaxation

According to Yeom *et al*[81], since a glass is not in a state of thermodynamic equilibrium, its physical and mechanical properties change with time as the material attempts to achieve equilibrium through changes in its molecular configuration which can induce the release of the formed stress. The release of this formed stress is known as relaxation, wherein the polymer structure is made denser by the configurational rearrangement of polymer chains. This increased density brings the polymer chains into greater proximity and so there is less polymer chain movement due to entanglement.

The effect of this on the pervaporation performance of a polymer membrane is that the reduced polymer chain movement and the increased polymer density reduces the number and fluctuation of the free volume holes within the polymer matrix. This limits the rate at which molecular diffusion can occur through the membrane; decreasing the permeate flux of the membrane without any gain in selectivity.

As stated above, there is a change in the Young's modulus across the membrane: This ranges from extremely low on the rubbery feed side - meaning that the relaxation process outlined above would occur almost instantly; to extremely high on the glassy permeate side - where relaxation would occur over an almost infinite period due to the lack of mobility of the side groups of the polymer chains. As a result, equilibrium can never be fully achieved and is instead approached asymptotically.

There is typically a gradual loss in flux over time in a pervaporation experiment: As the feed solution circulates over the membrane a single component of that feed is selectively removed. It follows that per unit time there is less of that single component in the feed solution and so less permeate diffuses through the membrane per unit time. However, there is an inverse relationship between flux and selectivity, and as flux gradually decreases with time, selectivity gradually increases. Relaxation effects are distinct from this typical flux loss in that they are evinced by a sudden and significant loss in flux with no corresponding gain in selectivity.

1.4 Lateral-Flow Membrane Structure and Formation

1.4.1 Lateral-Flow Membrane Categorisation

Lateral-flow cellulose nitrate based membranes are microporous membranes, the composition of which is defined by two things primarily; the polymer; cellulose nitrate, which is derived from cellulose; and the structure, which is formed through a polymer phase inversion process. As mentioned previously, the formation of lateral-flow membranes is more complex than that of pervaporation membranes.

Cellulose Nitrate

Cellulose nitrate is prepared from cellulose and nitric acid, usually in the presence of sulphuric acid, although phosphoric or acetic acids may also be used. The degree of nitration varies according to application; cellulose containing 10 – 11 % nitrogen is mainly used for lacquers or plastics, while cellulose containing about 13.5 % is used for explosives. Completely nitrated cellulose contains about 14.14 % nitrogen, [62] and is hydrophobic[82][83].

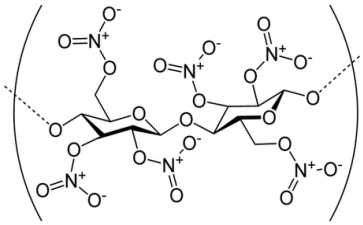


Figure 1.10: Cellulose nitrate

Cellulose, a polysaccharide consisting of a linear chain of several hundred to over ten thousand β(1→4) linked D-glucose units, is the most abundant organic compound on the planet[62], being the structural component of the primary cell wall of plants, many forms of algae and the oomycetes.

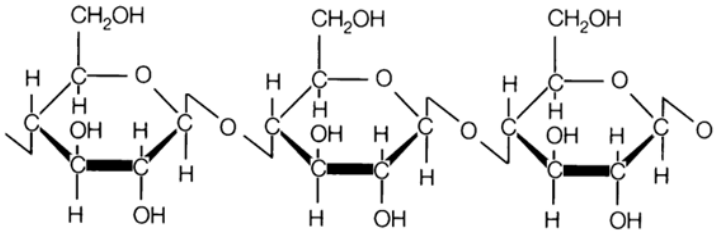


Figure 1.11: Cellulose

Approximately a third of all plant matter is cellulose, averaging about 50 % in typical wood and comprising 85-90 % of cotton. Variability in the cellulose source will produce variability in cellulose nitrate, the density of which can range, as a result, from 1300 to 1400 kg m^{-3}. Achieving consistency in membrane characteristics from batch to batch therefore becomes difficult, which is a primary concern for industrial scale manufacturers.

1.4.2 Lateral-Flow Membrane Formation

Support

Cellulose nitrate lateral flow membranes produced in this project were formed on supports. After formation they could be removed from these supports for analysis. The support material used was a 100 % polyester film (Melinex). This provided physically durable support material for the active membrane layer and polymer solutions were cast directly onto it.

Phase Inversion: Formation of Pore Structure

The internal pore structure of CN lateral-flow membranes is formed through a polymer phase inversion process. During a phase inversion the phases of a liquid-liquid dispersion interchange such that the dispersed phase spontaneously inverts to become the continuous phase and vice versa, under conditions determined by the system properties, volume ratio and energy input[84].

Phase inversion was first identified in 1956 by Rodger *et al*[85]. However, the precise physical processes which drive it have yet to be fully understood. No models which can accurately describe the process have been developed. What has been established is that phase inversion is a sensitive process, affected by many

parameters; solution concentration, viscosity, surface tension, density, temperature, humidity, container geometry, agitation and flow[86].

Phase inversion can be regarded as an instability of the system, the stability of the dispersion being least at the point of phase inversion (*cloud point*), beyond which a spontaneous inversion of the phases of the solution occurs. The way in which a phase inversion is precipitated dictates the morphology of the final structure of our polymer.

Phase inversion mechanisms can generally be subdivided in three main categories depending on the parameters that induce demixing. By changing the temperature at the interface of the polymer solution, heat will be exchanged and demixing can be induced (temperature induced phase separation or TIPS)[87]. The polymer solution can also be subjected to a reaction which causes phase separation (reaction induced phase separation or RIPS)[88]. The most used technique is based on diffusion induced phase separation (DIPS); this method can be subdivided into vapour induced phase separation (VIPS) [89] and immersion phase separation (IIPS). By contacting a polymer solution to a vapour or liquid, diffusional mass exchange will lead to a change in the local composition of the polymer film and demixing can be induced. In this project, all effective CN membranes are formed through VIPS, with atmospheric moisture acting as the non-solvent to precipitate the phase inversion (by comparison, the PAN supports described in section 1.3.2 were prepared by IIPS).

In all cases the phase inversion process is the same. When a polymer solution is in a single phase the polymer is stable in the solvent. The addition of a nonsolvent decreases the thermodynamic stability of the solution as the relative concentration of the solvent decreases. At the critical concentration of nonsolvent, the polymer desolves, the solution becomes thermodynamically unstable, and two liquid phases are formed. The solid polymer rich phase forms the rigid matrix of the membrane while the liquid polymer lean phase forms the pores of the membrane[90], finally the loss of solvent precipitates the membrane morphology[91]. This process is outlined in figure 1.12 below.

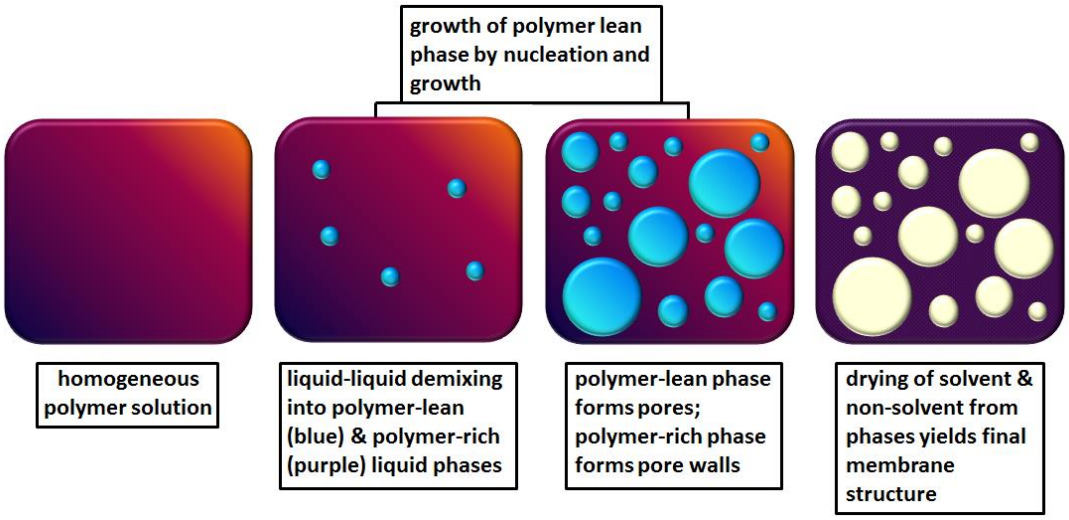


Figure 1.12: Phase inversion in polymer solution

All these factors, *including* the manner of phase inversion, determine the final pore structure of the polymer. The general pore structure of a membrane is defined by two processes; *spinodal decomposition* and *nucleation and growth*[89], [92], [93].

Spinodal Decomposition, Nucleation and Growth

Phase separation is thermodynamically possible in the unstable region of the phase diagram. The unstable region is defined by the spinodal (see figure 1.13). When a system has crossed this region, phase separation occurs spontaneously without the presence of a nucleation step. This process is known as spinodal decomposition (SD)[94]. It is also possible for this process to occur more slowly, where the polymer solution system leaves the thermodynamically stable region and enters the metastable between the spinodal and binodal of the phase diagram. Nucleation and growth (NG) is the expected mechanism here (see figure 1.13). Dispersed nuclei are formed and become stable if the activation energy for nuclei formation is higher than their surface free energy[92].

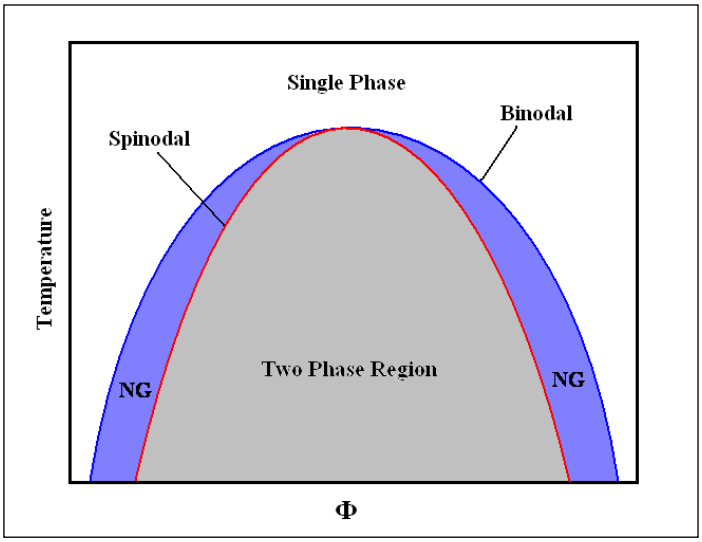


Figure 1.13: Binodal and spinodal in phase diagram

In the case of a polymer solution like those in this project the single phase is the dissolved polymer casting solution while the dual phase consists of a polymer-rich region (comprised of polymer and solvent) and a polymer-lean region (comprised of the non-solvent; water). The nucleation and growth of the polymer-lean phase precipitates the formation of pockets of nonsolvent. These non-solvent globules form the nascent pores of the final membrane structure, while the surrounding polymer-rich phase, upon drying, forms the polymer walls [95].

Cloud Point

The cloud point is defined as temperature/non-solvent concentration at which phase separation occurs for a 1 wt% polymer solution due to the increased turbidity of the system as this temperature/non-solvent concentration is reached[96]. Beyond this point phase separation of the polymer solution occurs.

Despite the rigid definition given above, it has been found through experimentation that the turbidity which defines the cloud point occurs over a range of non-solvent concentration. Turbidity begins in solution but agitation through stirring causes it re-dissolve [85]. While stirring the solution, turbidity will eventually become permanent; beyond this point phase inversion occurs.

The closer to this point one takes a solution the more crystalline it becomes and the more porous is the membrane produced. It also reduces diffuse layer formation, for this reason, polymer solutions were brought to cloud point (taken as the time when turbidity remains in solution for three minutes with stirring) using a burette to add the non-solvent to the solution. For the sake of comparison a non-cloud point solution equivalent was also produced and cast. By adding non-solvent with the burette the original concentration of the non-solvent in the solution is, of course, changed. The final figure for the percentage of non-solvent in the solution must be adjusted accordingly using the titration figure.

1.4.3 Lateral-Flow Membrane: Structural Effects and Anomalies

Skin layers

The mechanism for skin-layer formation in a phase inverting polymer layer is generally the same as that described in section 1.3.3 above, but with one notable exception: In pervaporation membranes there is only a polymer dissolved in solvent

solution and the subsequent drying and solidification of the non-porous membrane; in lateral flow membranes there is not only a polymer dissolved in solvent but also a non-solvent to precipitate phase inversion; the affinity that the solvent and non-solvent have for each other has a significant effect upon the formation of the diffuse layer and therefore on the overall membrane structure.

Young *et al* [95] consider the diffusion ratio of the solvent and non-solvent from the cast polymer solution in membrane formation and assume that the rate of evaporation, i.e. the diffusion, of each from the membrane can be considered as a single value which is a ratio of their respective diffusions:

$$k = \tilde{n}_1/\tilde{n}_2 \qquad \textbf{1(xxxiii)}$$

Where k is the diffusion ratio of solvent to non-solvent and n_1 and n_2 are the diffusion fluxes of solvent and non-solvent respectively. When the solvent and non-solvent have a high affinity for each other k has a low value and when they have a low affinity for each other k has a large value.

The diffuse layer forms in the same manner as that described in pervaporation membranes, once it has formed however, it effects the structure of the porous membrane layer below it: If k is very large then the solvent diffuses rapidly from the membrane; this creates a dense diffuse layer which will increase the barrier to diffusion of solvent from the membrane structure below which creates an asymmetric, anhomogenous membrane structure in the sub-layers. Conversely, if k has a low value then solvent will diffuse more slowly and so the diffuse layer formed will be less dense, presenting less of a barrier to solvent diffusion creating a more symmetrically porous, homogenous membrane structure in the membrane sublayers.

Controlling the affinity that the solvent and non-solvent have for one another is important as skin layers prevent lateral flow of fluids though the pore network of the membrane, rendering them of little value.

Demixing Front & Surface Tension

The force of evaporation of the polymer solvent upwards through the drying polymer matrix drags polymer molecules upwards with it. As the solvent evaporates from the membrane the relative concentration of non-solvent increases in the solution until demixing occurs resulting in phase inversion. This creates a demixing front which

passes down through the membrane from the air exposed surface. At the air exposed surface of the membrane the rate of evaporation is at its highest, resulting in the greatest density of polymer molecules which creates a diffuse or skin layer. The rate of solvent evaporation decreases as the demixing front moves back from the air exposed surface and layers of polymer build up above it[78]. As the polymer solution solidifies there is an increase in surface tension at the demixing front above that of the bulk polymer solution below it. Higher surface tension causes the stretching of pores formed through NG, increasing their size significantly.

Macrovoids

According to Ahmad *et al*[52] *macrovoids* are channel like structures which form within the internal structure of lateral flow membranes if the polymer solution is cast above 800 µm thickness when utilising VIPS. Ahmad *et al*, contradict this in later work where macrovoid formation is observed at under 200 µm cast thickness [97].

The proposed theory for macrovoid formation is that it is due to the diffusion and displacement of solvent and non-solvent in the casting film. Therefore, when the casting film is thin, there are no macrovoids formed in the sublayers of the membrane due to insufficient space to allow the macrovoids to appear between the film surface and bottom. A thicker initial casting film results in the formation of higher numbers of macrovoids by lowering the initial solvent outflow in the sublayers of the membrane [52].

As the polymer solution solidifies there is an increase in surface tension at the demixing front above that of the bulk polymer solution below it. This generates a surface-tension gradient through the polymer solution which generates a surface-tension gradient along the macrovoid/casting solution interface that facilitates macrovoid growth in conjunction with a viscous drag-force that resists macrovoid growth; and a gravitationally induced body force that can either resist or promote MV growth, depending on its orientation[16], [24]. This process is referred to as *solutocapillary convection* [100], [101]. According to Khare *et al*,[98] it causes the macrovoid/casting solution interface to experience motion from the leading edge (low surface tension) to the trailing edge (high surface tension) of the macrovoid. This results in a force on the growing macrovoid that propels it away from the demixing front and into the underlying bulk solution. Continuity of velocity

requirements of the macrovoid/casting solution interface result in the development of convection cells inside the macrovoid. The overall effect is to enhance the mass transfer of non-solvent into the growing macrovoid. This is shown in figure 1.14. Macrovoids, like skin layers, inhibit or retard lateral flow in the membrane, reducing their efficacy.

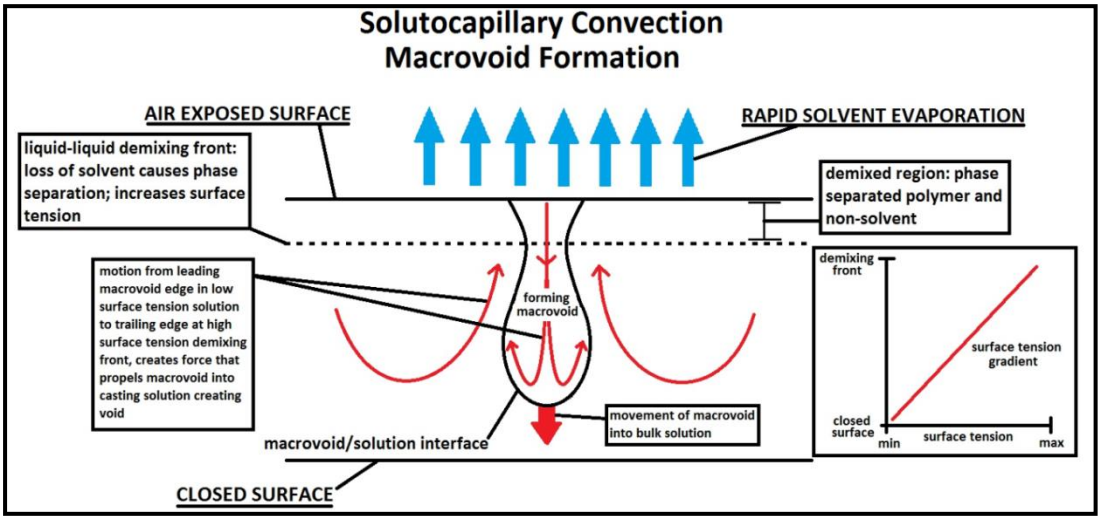


Figure 1.14: Soluto-capillary convection macrovoid formation

Nodules

Within a polymer solution, the onset of crystallinity during drying (known as *nucleation*), can occur. This process can occur randomly throughout the matrix as polymer molecules begin to align (homogeneous nucleation) or at the interface of an impurity (heterogeneous nucleation). Nucleation about an impurity results in a number of semi-crystalline morphologies observed in membranes; *spherulites* - which are aggregates of small hair-like strands called *fibrils*; *epitaxials* - which are defined by one crystalline growth on another [62]. However, while these morphologies *can* occur within a lateral flow membrane matrix they are rare in comparison with another crystalline morphology; *nodules*.

Nodules are spherical morphologies that occur in membranes due to coarsening. Coarsening occurs when the two separated phases in an *instantaneous* phase inversion build up energy at interfacial regions between them, which makes the solution unstable. Stability is regained by dissipating this energy into coarsening; which is the formation of droplets of semi-crystalline polymer at the interfacial regions. From these droplets nodules are formed[102]. The further from

instantaneous (or binodal) the phase inversion is, the less coarsening will occur. Therefore, if the affinity of the solvent for the non-solvent is increased, the phase inversion will proceed more through the spinodal region of nucleation and growth [95] and reduce the degree of coarsening and so the eventual number of nodules. However this effect is offset to a degree by the crystallinity of a polymer solution.

The formation of nodules in phase separating membranes is described by the Ostwald ripening process, wherein two assumptions are made: the area fraction of the dispersed phase is small, and the chemical potential of a coarsening droplet is directly proportional to its curvature. Based on this second assumption, smaller particles with high curvature are unstable, and larger particles tend to grow by dissolution of the smaller particles in an evaporation-condensation mechanism[93], [102].

By the logic stated above it is expected that as the solvent used in the production of our membranes (ethanol/acetone) increases in affinity (by addition of ethanol) for the non-solvent (water), the number of nodules should increase up to a maximum concentration of ethanol. This is because ethanol increases the crystallinity of the solution (as it is not an effective solvent for cellulose nitrate) thus increasing the number of nodules (which are formed from crystalline polymer), while increasing the affinity of the non-solvent (water) for the solvent, which decreases the coarsening effect as the phase separation occurs more through the spinodal region, countering the increase in the crystallinity of the solution: Thus once a point is reached, beyond the maximum nodule formation, where the affinity of the solvent for the non-solvent outweighs the increase in polymer crystallinity, there will be a decrease in the number of nodules formed.

There is no literature evidence to suggest that nodules have any adverse effect on lateral flow performance, however, they do create problems industrially; forming a fine powder on membrane production lines.

1.5 Summary

When producing membranes from thin cast films of polymer solutions, the rate of evaporation of solvent from the drying membrane is the predominant force is defining the membrane structure. In the case of pervaporation membranes, the formation process is relatively simple and the rate of evaporation is the only

significant force determining the final membrane structure. The force of evaporation evinces itself in the formation of skin layers at the membrane surface. The force is dictated by the rate of evaporation which can be controlled through the solvent volatility or the volume:area ratio of the drying membrane. Skin layer density and thickness can be controlled to enhance pervaporation performance.

By comparison, during the formation of lateral flow membranes the rate of evaporation of solvent is not the only significant force present: The phase inversion process has equal gravitas. As with pervaporation membranes the rate of evaporation can lead to the formation of skin layers, and this rate is controlled as described above. The evaporation process occurs separately and concurrently to SD and NG. The higher the rate of solvent evaporation from the system, the greater the surface tension at the demixing front, which has an effect on formed pores; stretching them. This also has an effect if any macrovoids begin to form within the drying membrane, as the increased surface tension contributes to their growth. Skin layers and macrovoids are undesirable in lateral flow membranes as they inhibit and retard the rate of lateral flow.

In summation, controlling the rate of solvent evaporation from drying castings of polymer solutions is of paramount importance in determining the final structure of the membrane to be formed as the membrane structures determine their efficacy in pervaporation - in the case of pervaporation membranes - and as diagnostic materials - in the case of lateral flow membranes.

References: Chapter 1

[1] A. J.-A. Nollet, “Investigations on the Causes for the Ebullition of Liquids,” *Histoire Académie Royale des Sciences, Math. et Phys.*, pp. 57–104, 1752.

[2] R. J. H. Dutrochet, “Nouvelles Observations sur l’Endosmose et l'Exosmose, et sur la cause de ce double phénomène,” *Annales de Chimie et de Physique*, vol. 35, pp. 393–400, 1827.

[3] A. Fick, “Uber Diffusion,” *Annalen der Physik*, vol. 170, no. 1, pp. 59–86, 1855.

[4] M. Traube, “Experimente zur Theorie der Zellenbildung und Endosmose,” *Archiv fúr Anatomie und Physiologie und wissenschaftliche Medizin*, pp. 87–128; 129–165, 1867.

[5] W. Pfeffer, *Osmotische Untersuchungen: Studien zur Zeil-Mechanik*. Engelmann, Leipzig.

[6] J. H. Van’t-Hoff, “Die Rolle des osmotischen Druckes in der Analogie zwischen Lösungen und Gasen,” *Zeitschrift für Physikalische Chemie*, vol. 1, no. 1, pp. 481–508, 1887.

[7] P. A. Kober, “Pervaporation, perstillation and percrystallisation,” *Journal of the American Chemical Society*, vol. April, no. 39, pp. 944–948, 1917.

[8] S. S. Sidney Loeb, “Sea Water Demineralization by Means of an Osmotic Membrane,” in *Saline Water Conversion—II*, American Chemical Society, 1963, pp. 117–132.

[9] R. W. Baker, *Membrane Technology and Applications*, 2nd ed. John Wiley and Sons, Ltd., 2007.

[10] R. Singh, *Hybrid Membrane System for Water Purification*, 1st ed. Elsevier, 2006, p. 291.

[11] P. D. Chapman, T. Oliveira, A. G. Livingston, and K. Li, “Membranes for the dehydration of solvents by pervaporation,” *Journal of Membrane Science*, vol. 318, no. 1–2, pp. 5–37, Jun. 2008.

[12] A. Jonquières, “Industrial state-of-the-art of pervaporation and vapour permeation in the western countries,” *Journal of Membrane Science*, vol. 206, no. 1–2, pp. 87–117, Aug. 2002.

[13] P. Shao and R. Huang, “Polymeric membrane pervaporation,” *Journal of Membrane Science*, vol. 287, no. 2, pp. 162–179, Jan. 2007.

[14] J. Gmehling, J. Menke, J. Krafczyk, and K. Fischer, *Azeotropic Data, 2nd Edition*. 2004.

[15] J. Gmehling, B. Kolbe, M. Kleiber, and J. Rarey, *Chemical Thermodynamics*. 2012, pp. 82–90.

[16] J. Gmehling, J. Menke, J. Krafczyk, and K. Fischer, *Azeotropic Data, 2nd Edition*. 2004.

[17] S. A. Zumdahl and S. A. Zumdahl, "11.4 Vapour Pressures of Solutions," in *Chemistry*, 8th ed., Charles Hartford, 2010, pp. 509–516.

[18] S. A. Zumdahl and S. A. Zumdahl, "11.4 Vapour Pressures of Solutions," in *Chemistry*, 8th ed., Charles Hartford, 2010, pp. 509–516.

[19] J. Gmehling, B. Kolbe, M. Kleiber, and J. Rarey, *Chemical Thermodynamics*. 2012, pp. 82–90.

[20] D. D. Ebbing and S. D. Gammon, "Chapter 12.5: Vapour Pressure of a Solution," in *General chemistry*, 9th ed., Charles Hartford, 2007, pp. 496–500.

[21] D. E. Goldberg, "15.6 Colligative Properties," in *Fundamentals of Chemistry*, 5th Editio., The McGraw-Hill Companies, 2007, pp. 417–419.

[22] M. Gimenes, L. Liu, and X. Feng, "Sericin/poly(vinyl alcohol) blend membranes for pervaporation separation of ethanol/water mixtures," *Journal of Membrane Science*, vol. 295, no. 1–2, pp. 71–79, May 2007.

[23] Jyh-Jeng Shieh and R. Y. M. Huang, "Pervaporation with chitosan membranes II. Blend membranes of chitosan and polyacrylic acid and comparison of homogeneous and composite membrane based on polyelectrolyte complexes of chitosan and polyacrylic acid for the separation of ethanol-water mixture," *Journal of Membrane Science*, vol. 127, no. 2, pp. 185–202, 1997.

[24] B. Li, Z. Xu, F. Alsalhyqusay, and R. Li, "Chitosan-poly (vinyl alcohol)/poly (acrylonitrile) (CS–PVA/PAN) composite pervaporation membranes for the separation of ethanol–water solutions," *Desalination*, vol. 193, no. 1–3, pp. 171–181, May 2006.

[25] M. D. Kurkuri, U. S. Toti, and T. M. Aminabhavi, "Syntheses and characterization of blend membranes of sodium alginate and poly(vinyl alcohol) for the pervaporation separation of water + isopropanol mixtures," *Journal of Applied Polymer Science*, vol. 86, no. 14, pp. 3642–3651, Dec. 2002.

[26] B. Kumarnaidu, M. Sairam, K. Raju, and T. Aminabhavi, "Thermal, viscoelastic, solution and membrane properties of sodium alginate/hydroxyethylcellulose blends," *Carbohydrate Polymers*, vol. 61, no. 1, pp. 52–60, Jul. 2005.

[27] T. Peters, C. Poeth, N. Benes, H. Buijs, F. Vercauteren, and J. Keurentjes, “Ceramic-supported thin PVA pervaporation membranes combining high flux and high selectivity; contradicting the flux-selectivity paradigm,” *Journal of Membrane Science*, vol. 276, no. 1–2, pp. 42–50, May 2006.

[28] Y. Zhu, S. Xia, G. Liu, and W. Jin, “Preparation of ceramic-supported poly(vinyl alcohol)–chitosan composite membranes and their applications in pervaporation dehydration of organic/water mixtures,” *Journal of Membrane Science*, vol. 349, no. 1–2, pp. 341–348, Mar. 2010.

[29] Z. Huang, Y. Shi, R. Wen, Y. Guo, J. Su, and T. Matsuura, “Multilayer poly(vinyl alcohol)–zeolite 4A composite membranes for ethanol dehydration by means of pervaporation,” *Separation and Purification Technology*, vol. 51, no. 2, pp. 126–136, Sep. 2006.

[30] H. Guan, T. Chung, Z. Huang, M. Chng, and S. Kulprathipanja, “Poly(vinyl alcohol) multilayer mixed matrix membranes for the dehydration of ethanol–water mixture,” *Journal of Membrane Science*, vol. 268, no. 2, pp. 113–122, Jan. 2006.

[31] M. Patil, R. Veerapur, S. Patil, C. Madhusoodana, and T. Aminabhavi, “Preparation and characterization of filled matrix membranes of sodium alginate incorporated with aluminum-containing mesoporous silica for pervaporation dehydration of alcohols,” *Separation and Purification Technology*, vol. 54, no. 1, pp. 34–43, Mar. 2007.

[32] R. Y. M. Huang, R. Pal, and G. Y. Moon, “Characteristics of sodium alginate membranes for the pervaporation dehydration of ethanol–water and isopropanol–water mixtures,” *Journal of Membrane Science*, vol. 160, no. 1, pp. 101–113, Jul. 1999.

[33] L. Mocé-Llivina, J. Jofre, X. Méndez, D. Akkelidou, F. Lucena, and G. T. Papageorgiou, “Counting cytopathogenic virus adsorbed to cellulose nitrate membrane filters as a simple method for counting viruses in raw sewage and sewage effluents.,” *Journal of virological methods*, vol. 102, no. 1–2, pp. 83–92, Apr. 2002.

[34] G. T. Papageorgiou, L. Mocé-Llivina, C. G. Christodoulou, F. Lucena, D. Akkelidou, E. Ioannou, and J. Jofre, “A Simple Methodological Approach for Counting and Identifying Culturable Viruses Adsorbed to Cellulose Nitrate Membrane Filters,” *Applied and Environmental Microbiology*, vol. 66, no. 1, pp. 194–198, 2000.

[35] J. D. Czerwinski, S. C. Hovan, and D. P. Mascotti, “Quantitative nonisotopic nitrocellulose filter binding assays: bacterial manganese superoxide dismutase-DNA interactions.,” *Analytical biochemistry*, vol. 336, no. 2, pp. 300–4, Jan. 2005.

[36] M. S. Levy, I. J. Collins, J. T. Tsai, P. a Shamlou, J. M. Ward, and P. Dunnill, “Removal of contaminant nucleic acids by nitrocellulose filtration during

pharmaceutical-grade plasmid DNA processing.," *Journal of biotechnology*, vol. 76, no. 2–3, pp. 197–205, Jan. 2000.

[37] R. Grunow, W. Splettstoesser, S. McDonald, C. Otterbein, T. O'Brien, C. Morgan, J. Aldrich, E. Hofer, E.-J. Finke, and H. Meyer, "Detection of Francisella tularensis in Biological Specimens Using a Capture Enzyme-Linked Immunosorbent Assay, an Immunochromatographic Handheld Assay, and a PCR," *Clinical and Diagnostic Laboratory Immunology*, vol. 7, no. 1, pp. 86–90, 2000.

[38] S. Aidoo, W. K. Ampofo, J. A. M. Brandful, S. V. Nuvor, J. K. Ansah, N. Nii-Trebi, J. S. Barnor, F. Apeagyei, T. Sata, D. Ofori-Adjei, and K. Ishikawa, "Suitability of a Rapid Immunochromatographic Test for Detection of Antibodies to Human Immunodeficiency Virus in Ghana, West Africa," *Journal of Clinical Microbiology*, vol. 39, no. 7, pp. 2572–2575, 2007.

[39] H. Arai, B. Petchclai, K. Khupulsup, T. Kurimura, and K. Takeda, "Evaluation of a Rapid Immunochromatographic Test for Detection of Antibodies to Human Immunodeficiency Virus," *Journal of Clinical Microbiology*, vol. 37, no. 2, pp. 367–370, 1999.

[40] M. Guan, H. Y. Chen, S. H. Foo, Y.-J. Tan, P.-Y. Goh, and S. . Wee, "Recombinant Protein-Based Enzyme-Linked Immunosorbent Assay and Immunochromatographic Tests for Detection of Immunoglobulin G Antibodies to Severe Acute Respiratory Syndrome (SARS) Coronavirus in SARS Patients," *Clinical and Diagnostic Laboratory Immunology*, vol. 11, no. 2, pp. 287–291, 2004.

[41] S. K. Lam and P. L. Devine, "Evaluation of capture ELISA and rapid immunochromatographic test for the determination of IgM and IgG antibodies produced during dengue infection.," *Clinical and diagnostic virology*, vol. 10, no. 1, pp. 75–81, May 1998.

[42] R.-H. Shyu, H.-F. Shyu, H.-W. Liu, and S.-S. Tang, "Colloidal gold-based immunochromatographic assay for detection of ricin.," *Toxicon : official journal of the International Society on Toxinology*, vol. 40, no. 3, pp. 255–8, Mar. 2002.

[43] A. L. Ahmad, S. C. Low, S. R. A. Shukor, and A. Ismail, "Synthesis and Characterization of Polymeric Nitrocellulose Membranes : Influence of Additives and Pore Formers on the Membrane Morphology," *Journal of Applied Polymer Science*, vol. 108, no. 4, pp. 2550–2557, 2008.

[44] U. Divrikli, A. A. Kartal, M. Soylak, and L. Elci, "Preconcentration of Pb(II), Cr(III), Cu(II), Ni(II) and Cd(II) ions in environmental samples by membrane filtration prior to their flame atomic absorption spectrometric determinations.," *Journal of hazardous materials*, vol. 145, no. 3, pp. 459–64, Jul. 2007.

[45] I. Narin, “Enrichment and determinations of nickel(II), cadmium(II), copper(II), cobalt(II) and lead(II) ions in natural waters, table salts, tea and urine samples as pyrrolydine dithiocarbamate chelates by membrane filtration–flame atomic absorption spectrometry co,” *Analytica Chimica Acta*, vol. 493, no. 2, pp. 205–212, Oct. 2003.

[46] T. Shimizu, “Extraction of Trace Amounts of Copper(II) on a Membrane Filter Using 5,10,15,20-Tetraphenyl-21H,23H-porphinetetrasulfonic Acid for the Determination by Solid-Phase Spectrophotometry.,” *Analytical Sciences*, vol. 15, no. 2, pp. 153–157, 1999.

[47] M. Soylak and R. S. Cay, “Separation/preconcentration of silver(I) and lead(II) in environmental samples on cellulose nitrate membrane filter prior to their flame atomic absorption spectrometric determinations.,” *Journal of hazardous materials*, vol. 146, no. 1–2, pp. 142–7, Jul. 2007.

[48] M. Soylak, U. Divrikli, L. Elci, and M. Dogan, “Preconcentration of Cr(III), Co(II), Cu(II), Fe(III) and Pb(II) as calmagite chelates on cellulose nitrate membrane filter prior to their flame atomic absorption spectrometric determinations.,” *Talanta*, vol. 56, no. 3, pp. 565–70, Mar. 2002.

[49] A. Elik, “Heavy Metal Accumulation in Street Dust Samples in Sivas,” *Communications in Soil Science and Plant Analysis*, vol. 34, no. 1&2, pp. 145–156, Feb. 2003.

[50] E. Kendüzler, “Atomic absorption spectrophotometric determination of trace copper in waters, aluminium foil and tea samples after preconcentration with 1-nitroso-2-naphthol-3,6-disulfonic acid on Ambersorb 572,” *Analytica Chimica Acta*, vol. 480, no. 2, pp. 259–266, Mar. 2003.

[51] N. Yunes, S. Moyano, S. Cerutti, J. Gasquez, and L. Martinez, “On-line preconcentration and determination of nickel in natural water samples by flow injection-inductively coupled plasma optical emission spectrometry (FI-ICP-OES),” *Talanta*, vol. 59, no. 5, pp. 943–949, Apr. 2003.

[52] A. L. Ahmad, S. Low, and S. Shukor, “Effects of membrane cast thickness on controlling the macrovoid structure in lateral flow nitrocellulose membrane and determination of its characteristics,” *Scripta Materialia*, vol. 57, no. 8, pp. 743–746, Oct. 2007.

[53] J. G. Wijmans and R. W. Baker, “The solution-diffusion model : a review,” *Journal of Membrane Science*, vol. 107, no. 1–2, pp. 1–21, 1995.

[54] M. Smit, H. V. Mulder, C. A. Smolders, H. Karrenbeld, J. Van Eerden, and D. Feil, “Modelling of the diffusion of carbon dioxide in polyimide matrices by computer simulation,” *Journal of Membrane Science*, vol. 73, no. 2, pp. 247–257, 1992.

[55] R. W. Baker, “Chapter 2: Membrane Trasport Theories,” in *Membrane Technology and Applications*, 2nd ed., John Wiley & Sons Ltd., 2007, pp. 15–42.

[56] T. Kataoka, T. Tsuro, S.-I. Nakao, and S. Kimura, “Membrane Transport Properties of Pervaporation and Vapor Permeation in an Ethanol–Water System Using Polyacrylonitrile and Cellulose Acetate Membranes,” *Journal of Chemical Engineering, Japan*, vol. 326, no. 24, 1991.

[57] F. W. Greenlaw, W. D. Prince, R. A. Shelden, and E. V. Thompson, “Dependence of Diffusive Permeation Rates by Upstream and Downstream Pressures,” *Journal of Membrane Science*, vol. 2, no. 141, 1977.

[58] J. G. Wijmans and R. W. Baker, “A Simple Predictive Treatment of the Permeation Process in Pervaporation,” *Journal of Membrane Science*, vol. 101, no. 79, 1993.

[59] W. B. Russel, “Brownian Motion of Small Particles Suspended in Liquids,” *Annual Review of Fluid Mechanics*, vol. 13, no. 1, pp. 425–455, 1981.

[60] J. M. Coulson and J. F. Richardson, “Chapter 8: Membrane Separation Processes,” in *Coulson an Richardson’s Chemical Engineering: Particle Technology and Separation Processes, vol. 2, 5th ed.*, 5th ed., 2002, p. 437.

[61] L. Barsanti and P. Gualtieri, *Algae: Anatomy, Biochemistry, and Biotechnology*, 1st ed. Taylor & Francis, 2006.

[62] M. P. Stevens, *Polymer Chemistry: An Introduction*, 1st ed. Oxford University Press, Inc., 1999.

[63] R. Russo, M. Malinconico, L. Petti, and G. Romano, “Physical behavior of biodegradable alginate-poly(vinyl alcohol) blend films,” *Journal of Polymer Science Part B: Polymer Physics*, vol. 43, no. 10, pp. 1205–1213, May 2005.

[64] L. A. Utracki, *Polymer Blends Handbook, Vol. 1-2*, vol. 1. Kluwer Academic Publishers, 2002.

[65] X. Feng and R. Y. M. Huang, “Pervaporation with chitosan membranes. I. Separation of water from ethylene glycol by a chitosan/polysulfone composite membrane,” *Journal of Membrane Science*, vol. 116, no. 1, pp. 67–76, 1996.

[66] T. Çaykara and S. Demirci, “Preparation and Characterization of Blend Films of Poly(Vinyl Alcohol) and Sodium Alginate,” *Journal of Macromolecular Science, Part A*, vol. 43, no. 7, pp. 1113–1121, Jul. 2006.

[67] C. K. Yeom and K.-H. Lee, “Characterization of sodium alginate and poly(vinyl alcohol) blend membranes in pervaporation separation,” *Journal of Applied Polymer Science*, vol. 67, no. 5, pp. 949–959, Jan. 1998.

[68] K. Miura, N. Kimura, H. Suzuki, Y. Miyashita, and Y. Nishio, “Thermal and viscoelastic properties of alginate/poly(vinyl alcohol) blends cross-linked with calcium tetraborate,” *Carbohydrate Polymers*, vol. 39, no. 2, pp. 139–144, Jun. 1999.

[69] J. Jegal and K. H. Lee, “Pervaporation separation of water-ethanol mixtures through PVA-Sodium alginate blend membranes,” *Journal of Applied Polymer Science*, vol. 61, no. 2, pp. 389–392, Mar. 2003.

[70] K. Wu, Z. Xu, and Y. Wei, “Sodium alginate-polyvinyl alcohol/polysulfone (SA-PVA/PSF) hollow fiber composite pervaporation membrane for dehydration of ethanol-water solution,” *Journal of Shanghai University (English Edition)*, vol. 12, no. 2, pp. 163–170, May 2008.

[71] R. W. Broach, “Zeolite Types and Structures,” in *Zeolites in Industrial Separation and Catalysis*, Wiley-VCH Verlag GmbH & Co. KGaA, 2010, p. 27.

[72] R. Kreiter, D. Wolfs, C. Engelen, H. Vanveen, and J. Vente, “High-temperature pervaporation performance of ceramic-supported polyimide membranes in the dehydration of alcohols,” *Journal of Membrane Science*, vol. 319, no. 1–2, pp. 126–132, Jul. 2008.

[73] C.-Y. Chen, H.-X. Li, and M. E. Davis, “Studies on mesoporous materials: I. Synthesis and characterization of MCM-41,” *Microporous Materials*, vol. 2, no. 1, pp. 17–26, 1993.

[74] A. Vandenberg, L. Gora, J. Jansen, M. Makkee, and T. Maschmeyer, “Zeolite A membranes synthesized on a UV-irradiated TiO coated metal support: the high pervaporation performance,” *Journal of Membrane Science*, vol. 224, no. 1–2, pp. 29–37, Oct. 2003.

[75] C. Liu and S. Kulprathipanja, “Mixed - Matrix Membranes,” in *Zeolites in Industrial Separation and Catalysis*, 2010, pp. 329–353.

[76] S. Bhat, B. Naidu, G. Shanbhag, S. Halligudi, M. Sairam, and T. Aminabhavi, “Mesoporous molecular sieve (MCM-41)-filled sodium alginate hybrid nanocomposite membranes for pervaporation separation of water – isopropanol mixtures,” *Separation and Purification Technology*, vol. 49, no. 1, pp. 56–63, Apr. 2006.

[77] Z. Huang, H. Guan, W. Tan, X. Qiao, and S. Kulprathipanja, “Pervaporation study of aqueous ethanol solution through zeolite-incorporated multilayer poly(vinyl alcohol) membranes: Effect of zeolites,” *Journal of Membrane Science*, vol. 276, no. 1–2, pp. 260–271, May 2006.

[78] A. G. Yiotis, I. N. Tsimpanogiannis, A. K. Stubos, and Y. C. Yortsos, “Pore-network study of the characteristic periods in the drying of porous materials.,” *Journal of colloid and interface science*, vol. 297, no. 2, pp. 738–48, May 2006.

[79] L. H. Sperling, *Introduction to Physical Polymer Science*, 4th ed. John Wiley & Sons, Inc., 2006.

[80] G. Tillet, B. Boutevin, and B. Ameduri, "Chemical reactions of polymer crosslinking and post-crosslinking at room and medium temperature," *Progress in Polymer Science*, vol. 36, no. 2, pp. 191–217, 2011.

[81] C. K. Yeom, J. G. Jegal, and K. H. Lee, "Characterization of relaxation phenomena and permeation behaviors in sodium alginate membrane during pervaporation separation of ethanol-water mixture," *Journal of Applied Polymer Science*, vol. 62, no. 10, pp. 1561–1576, Dec. 1996.

[82] M. A. Mansfield, "The use of Nitro-Cellulose Membranes in Lateral Flow Assays," in *Forensic Science and Medicine: Drugs of Abuse: Body Fluid Testing*, 1st ed., Humana Press, Inc., 2005.

[83] a. Książczak, A. Radomski, and T. Zielenkiewicz, "Nitrocellulose porosity - thermoporometry," *Journal of Thermal Analysis and Calorimetry*, vol. 74, no. 1, pp. 559–568, 2003.

[84] S. Arirachakaran, K. D. Oglesby, M. S. Malinowsky, O. Shoham, and J. P. Brill, "An Analysis of Oil/Water flow Phenomena in Horizontal Pipes," in *society of Petroleum Engineers, Oklahoma*, 1989.

[85] W. A. Rodger, V. G. Trice, and J. H. Rushton Jr., "The effect of fluid motion on interfacial area of dispersions.," *Chemical Engineering Progress,*, vol. 52, no. 12, pp. 515–520, 1956.

[86] B. Hu, L. Liu, O. Matar, P. Angeli, G. Hewitt, and E. Perezdeortiz, "Investigation of Phase Inversion of Liquid-Liquid Dispersions in Agitated Vessels*," *Tsinghua Science & Technology*, vol. 11, no. 2, pp. 202–206, Apr. 2006.

[87] T. Nishi, T. T. Wang, and T. K. Kwei, "Thermally Induced Phase Separation Behavior of Compatible Polymer Mixtures," *Macromolecules*, vol. 8, no. 2, pp. 227–234, 1974.

[88] T. Inoue, "Reaction induced phase decomposition in polymer blends," *Progress in Polymer Science*, vol. 20, no. 94, pp. 119–153, 1995.

[89] H. Chae Park, K. Yoon Po, K. Hwa Yong, and K. Yong Su, "Membrane formation by water vapor induced phase inversion," *Journal of Membrane Science*, vol. 156, no. 2, pp. 169–178, Apr. 1999.

[90] Y.-S. Kang, H.-J. Kim, Y.-H. Kim, and W.-H. Jo, "The Mechanism of Assymetric Membrane Formation via Phase Inversion," *Polymer Society of Korea*, vol. 12, no. 3, pp. 279–287, 1988.

[91] J. P. Salamone, *Polymeric Materials Encyclopedia*, Vol. 6. CRC Press, 1996.

[92] S. P. Nunes and T. Inoue, “Evidence for Spinodal Decomposition and Nucleation and Growth Mechanisms during Membrane Formation,” *Journal of Membrane Science*, vol. 111, no. 1, pp. 93–103, 1996.

[93] I. Pinnau and W. J. Koros, “A qualitative skin layer formation mechanism for membranes made by dry/wet phase inversion,” *Journal of Polymer Science Part B: Polymer Physics*, vol. 31, no. 4, pp. 419–427, Mar. 1993.

[94] E. P. Favvas and A. Ch. Mitropoulos, “What is Spinodal Decomposition,” *Engineering Science and Technology Reveiw*, vol. 1, no. 1, pp. 25–27, 2008.

[95] T. Young and L. Chen, “Pore formation mechanism of membranes from phase inversion process,” *Desalination*, vol. 103, no. 3, pp. 233–247, Dec. 1995.

[96] K. Holmberg, B. Jonsson, B. Kronberg, and B. Lindman, *Surfactants and Polymers in Aqueous Solutions*, 2nd ed. John Wiley & Sons Ltd., 2002.

[97] A. L. Ahmad, S. C. Low, S. R. Abd Shukor, A. Ismail, and A. R. Sunarti, “Development of lateral flow membranes for immunoassay separation,” *Desalination and Water Treatment*, vol. 5, no. November 2008, pp. 99–105, May 2009.

[98] V. P. Khare, A. R. Greenberg, J. Zartman, W. B. Krantz, and P. Todd, “Macrovoid growth during polymer membrane casting,” *Desalination*, vol. 145, no. 1–3, pp. 17–23, 2002.

[99] M. Pekny, a Greenberg, V. Khare, J. Zartman, W. Krantz, and P. Todd, “Macrovoid pore formation in dry-cast cellulose acetate membranes: buoyancy studies,” *Journal of Membrane Science*, vol. 205, no. 1–2, pp. 11–21, Aug. 2002.

[100] S. S. Shojaie, W. B. Krantz, and A. R. Greenberg, “Dense polymer film and membrane formation via the dry-cast process part II. Model validation and morphological studies,” *Journal of Membrane Science*, vol. 94, no. 1, pp. 281–298, 1994.

[101] S. S. Prakash, L. F. Francis, and L. E. Scriven, “Microstructure evolution in dry–wet cast polysulfone membranes by cryo-SEM: A hypothesis on macrovoid formation,” *Journal of Membrane Science*, vol. 313, no. 1–2, pp. 135–157, Apr. 2008.

[102] C. K. Haas and J. M. Torkelson, “Two-dimensional coarsening and phase separation in thin polymer solution films,” *American physical Society: Physical Review E*, vol. 55, no. 3, pp. 3191–3201, Mar. 1997.

Chapter 2

Experimental Methods

2. Experimental

2.1 Membrane Preparation

The active polymer layers of all membranes in this work were cast from solutions of polymer in an appropriate solvent.

2.1.1 Materials

Pervaporation Materials

Sodium alginate as a crystalline solid, dimethylsulphoxide (DMSO) (0.03% approx.), glycerol (a.k.a glycerine) 85 % and molecular sieve type 4A, a form of zeolite with pore size of 4 Å, were purchased from Sigma-Aldrich Chemie Gmbh, Germany. Poly(vinyl alcohol) (PVA), molecular weight approximately 78,000 g mol^{-1}, was purchased from Polysciences Inc. as a crystalline solid. Poly(acrylo nitrile) (PAN) was obtained from Scientific Polymer Products Inc. as a fine powder and casting solutions were made by dissolving in dimethylsulphoxide. Ethanol (100% HPLC grade) was purchased from Carbon Group, Ringaskiddy, Co. Cork, Ireland. For the production of silica particles, tetraethylorthosilicate (TEOS), hexadecyltrimethylammonium bromide (CTAB), N,N-Dimethyldecylamine (DMDA) $\geq$90 %, ammonium hydroxide solution 28.0–30.0 % (NH4OH) and sodium hydroxide (NaOH) [reagent grade, $\geq$98 %], pellets (anhydrous) were obtained from Sigma-Aldrich Chemie Gmbh, Germany. Methanol was supplied in-house. All chemicals were used without further purification. 120 µm thick nonwoven fabric (CraneCU414), made of 100 % polyester, was supplied by Crane and Company Inc., USA. All 25 cm^2 glass plates were purchased from Water's Glass, Togher, Cork City, Cork, Ireland and Cork Glass Centre, Kinsale Road Business Park, Cork City, Cork, Ireland.

Lateral Flow Materials

Cellulose nitrate (E80), the 50 µm and 100 µm thick 100 % polyester films (Melinex) were provided by Millipore Ireland B.V. Glycerol (a.k.a glycerine) 85 %, 2-butanol (MW 74.12 g mol^{-1}) were obtained from Sigma-Aldrich Chemie Gmbh, Germany. Acetone was supplied in-house. Ethanol (100 % HPLC grade) was purchased from Carbon Group, Ringaskiddy, Co. Cork, Ireland. All chemicals were

used without further purification. All 25 cm^2 glass plates were purchased from Water's Glass, Togher, Cork City, Cork, Ireland and Cork Glass Centre, Kinsale Road Business Park, Cork City, Cork, Ireland.

2.1.2 Pervaporation Membrane Polymer Solutions

Membrane solutions were prepared for three distinct types of selective layer in pervaporation membranes; pristine polymer membranes, polymer blend membranes and mixed matrix membranes. A single solution type was prepared for the PAN support layer.

Pristine Polymer Solutions

Pristine polymer pervaporation membranes were cast from solutions of polymers in appropriate solvents at various weight percentages of polymer.

Sodium Alginate Solutions

The solvent used for NaAlg was deionised water. Solutions were produced at 2.5 wt%, 5 wt% and 6 wt% NaAlg in deionised water. Solutions above 6 wt% NaAlg were too viscous for even dispersion when casting. Only 2 wt% yielded unsupported membranes that could withstand pervaporation conditions for any length of time. Supported membranes were produced from 5 wt% solutions of NaAlg in water.

Poly(vinyl alcohol) Solutions

The solvent used for PVA was deionised water. Solutions were produced at 5 wt%, 7 wt%, 10 wt%, and 12 wt% PVA in deionised water. Solutions below 5 wt% PVA were too fluid for effective casting. Only solutions above 10wt% could be used for casting unsupported membranes.

Pervaporation Membrane Support Solutions

All supports were cast using 7 wt% solutions of poly(acrylonitrile) in dimethylsulphoxide (DMSO) solvent.

Polymer Blend Solutions

Blends of NaAlg and PVA were made from solutions of total mass of 100 g composed of 5 g of polymers, 5 g of plasticizer (glycerol) and 90 g of solvent. The 5 g of polymers was composed of NaAlg and PVA in integer ratios of 9:1, 4:1 and 7:3.

This is shown in table 2.1. These blends were cast at various thicknesses in order to study relaxation and diffuse layer formation effects in pervaporation membranes. These thicknesses were dictated by the limits of the automated casting machine utilised. A description of this machine can be seen below.

Table 2.1: Polymer blend solutions

Polymer Ratio in Blend Solution	NaAlg (g)	PVA (g)	Glycerol (g)	Water (g)
9:1	4.5	0.5	0.0	95.0
9:1 Gly	4.5	0.5	5.0	90.0
4:1	4.0	1.0	0.0	95.0
4:1 Gly	4.0	1.0	5.0	90.0
7:3	3.5	1.5	5.0	90.0

Mixed Matrix Membrane Solutions

Mixed matrix membranes were prepared with two types of silica particles and one type of zeolite particle: zeolite-A, an aluminosilicate particle with a pore size of ~4 Å. Silica particles were produced by the method of Keane *et al.*[1] This yielded two types of mono-disperse mesoporous silica spheres. Both silica types were of approximately 1.5-2 μm in diameter but differed in pore size. In one particle type the pore diameter was ~2 nm while the other particle type had a pore diameter of ~20 nm; a much reduced surface area.

Zeolite-A, large pore silica, and small pore silica particles were incorporated into three polymer types: Pristine PVA, pristine NaAlg and a 4:1 NaAlg:PVA polymer blend. Both the NaAlg and 4:1 NaAlg:PVA polymer blends proved too brittle upon introduction of particles for practical use. In addition to this, the use of pristine PVA proved advantageous. PVA possesses a high strain at fracture[2] allowing for significant particle loadings without overly compromising the mechanical stability of the membrane. (See chapter 7)

PVA solutions were prepared so: X g of particle + 12 g – X g of PVA + 88 g water produced by combination of two initial solutions of 12 g – X g of PVA in 65 g water (soln. 1) + X g particle in 23 g water (soln. 2). Soln. 2 is sonicated to ensure the silica particles are dispersed and discreet within. This is then added to soln. 1. The combined solutions are left to mix before a brief sonication. NaAlg and blend membranes containing particles were prepared similarly but using 5 g rather than 12

g of polymer. Masses of components of final casting solutions listed in table 2.2 below.

Table 2.2: Pervaporation membrane casting solution compositions

Membrane	Polymer			Solvent Water (g)	Particle			Casting Thickness (µm)	Final Membrane
	NaAlg (g)	4:1 NaAlg:PVA Blend (g)	PVA (g)		Small Pore Silica (g)	Large Pore Silica (g)	Zeolite-A (g)		
	4.75	-	-	95	0.25	-	-	100	Tested
	4.50	-	-	95	0.50	-	-	100	**Too brittle for testing**
	4.75	-	-	95	-	0.25	-	100	Tested
	4.50	-	-	95	-	0.50	-	100	**Too brittle for testing**
	4.75	-	-	95	-	-	0.25	100	Tested
	4.50	-	-	95	-	-	0.50	100	**Too brittle for testing**
	-	4.75	-	95	0.25	-	-	100	Tested
	-	4.50	-	95	0.50	-	-	100	**Too brittle for testing**
	-	4.75	-	95	-	0.25	-	100	Tested
	-	4.50	-	95	-	0.50	-	100	**Too brittle for testing**
	-	4.75	-	95	-	-	0.25	100	Tested
	-	4.50	-	95	-	-	0.50	100	**Too brittle for testing**
	-	-	11.40	88	0.60	-	-	100	Tested
	-	-	10.80	88	1.20	-	-	100	Tested
	-	-	10.20	88	1.80	-	-	100	Tested
	-	-	11.40	88	-	0.60	-	100	Tested
	-	-	10.80	88	-	1.20	-	100	Tested
	-	-	11.40	88	-	-	0.60	100	Tested
	-	-	10.80	88	-	-	1.20	100	Tested

2.1.3 Lateral Flow Membrane Polymer Solutions

Lateral-flow membranes were cast from solutions of increasing complexity, beginning with the basic components for phase inversion of polymer solution: solvent, non-solvent and polymer; acetone, water and cellulose nitrate respectively in this instance; shown in table 2.3 below. A *meso-solvent* was then introduced (ethanol) and solutions were produced for casting membranes; shown in table 2.4. Finally, components were added based on knowledge of the casting processes used industrially in an attempt to understand their functions. These components were glycerol and butanol; shown in table 2.5.

For phase inversion to occur effectively casting solutions were required to be brought to cloud point [3][4] (note: cloud point is a misnomer; cloud region is the reality). This was done by the addition of non-solvent (water) up to a point where the cloudiness of the polymer solution was maintained under stirring at 250 rpm at room

temperature (controlled at 24 ^{o}C) for a period of 3 mins. The apparent cloudiness of the solution is caused by nucleation of polymer molecules within.

All casting solutions contained 17 wt% cellulose nitrate as this provided the optimum viscosity for casting. The solvent, meso-solvent and non-solvent were contained in the other 83 wt% of the casting solutions. Thus, if a solution is referred to as containing a 95:5 ratio of solvent to non-solvent, this refers to the ratio of acetone to water in this 83 wt% of the casting solution before being brought to cloud-point.

Table 2.3: Basic Membrane Casting Solutions

Mem.	Initial Phase Inversion Solution			Non-sol. (H_2O) for CP. (g)	Solution Near Cloud Point		
	Poly. (CN) wt%	Sol. (ace) wt%	Non-solvent (water) wt%		Poly. (CN) wt%	Sol. (ace) wt%	Non-solvent (water) wt%
BasMemA	17	83.00	0	0	17	83.00	0
BasMemB	17	78.85	4.15	0	17	78.85	4.15
BasMemC	17	74.70	8.30	0	17	74.70	8.30
BasMemD	17	70.55	12.45	0	17	70.55	12.45
BasMemACP	17	83.00	0	2.76	14.39	70.23	15.38
BasMemBCP	17	78.85	4.15	2.30	15.12	70.14	14.73
BasMemCCP	17	74.70	8.30	2.01	14.73	66.36	18.52
BasMemDCP	17	70.55	12.45	1.77	15.35	63.73	20.92

Table 2.4: Meso-solvent (ethanol) containing membranes

Mem.	Initial Phase Inversion Solution				Non-sol. (H_2O) for CP. (g)	Solution Near Cloud Point			
	Poly. (CN) wt%	Sol. (ace) wt%	Meso-Sol. (EtOH) wt%	Non-solvent (water) wt%		Poly. (CN) wt%	Sol. (ace) wt%	Meso-Sol. (EtOH) wt%	Poly. (CN) wt%
MesoA	17	58.10	20.75	4.15	0	17	58.10	20.75	4.15
MesoB	17	53.95	24.90	4.15	0	17	53.95	24.90	4.15
MesoC	17	49.80	29.05	4.15	0	17	49.80	29.05	4.15
MesoD	17	45.65	33.20	4.15	0	17	45.65	33.20	4.15
MesoE	17	41.50	37.35	4.15	0	17	41.50	37.35	4.15
MesoACP	17	58.10	20.75	4.15	5.30	13.03	44.53	15.90	26.53
MesoBCP	17	53.95	24.90	4.15	5.43	12.89	40.90	18.88	27.33
MesoCCP	17	49.80	29.05	4.15	5.55	12.80	37.50	21.87	27.83
MesoDCP	17	45.65	33.20	4.15	5.94	12.57	33.74	24.54	29.15
MesoECP	17	41.50	37.35	4.15	4.80	13.22	32.27	29.04	25.47

Table 2.5: wt% for components of glycerol and butanol casting solutions. Abbreviations: Mem. (membrane), CN (cellulose nitrate), ace. (acetone), EtOH (ethanol), gly. (glycerol), but. (butanol). Cloud Point (water added to reach cloud point

Mem.	Initial Phase Inversion Solution						Cloud Point (g)
	CN wt%	Ace. Wt%	H_2O wt%	EtOH wt%	Gly. Wt%	But. Wt%	
GlyA	17	45.650	4.15	32.785	0.415	-	6.01
GlyB	17	45.650	4.15	32.619	0.581	-	6.10
GlyC	17	45.650	4.15	32.453	0.747	-	6.19
GlyD	17	45.650	4.15	32.287	0.913	-	6.31
GlyE	17	45.650	4.15	32.121	1.079	-	6.29
GlyF	17	45.650	4.15	31.955	1.245	-	6.27
ButA	17	41.500	4.15	36.935	-	4.15	5.92
ButB	17	74.700	4.15	-	-	4.15	2.12
ButSub	17	45.650	4.15	-	-	33.2	5.39
Mem.	**Solution at Cloud Point**						-
	CN wt%	**Ace. Wt%**	**H_2O wt%**	**EtOH wt%**	**Gly. Wt%**	**But. Wt%**	
GlyA	12.35	33.16	30.38	23.81	0.30	-	-
GlyB	12.30	33.04	30.64	23.60	0.42	-	-
GlyC	12.26	32.91	30.90	23.40	0.54	-	-
GlyD	12.19	32.74	31.26	23.16	0.65	-	-
GlyE	12.21	32.77	31.18	23.06	0.78	-	-
GlyF	12.30	32.81	31.11	22.97	0.90	-	-
ButA	12.40	30.27	30.08	26.94	-	3.03	-
ButB	14.95	65.63	15.79	-	-	3.65	-
ButSub	12.77	34.26	28.05	-	-	24.92	-

Calculating Weight Percentages

Casting solution final weight percentages were recalculated from the initial weight percentages to account for the additional water required to reach solution cloud point. An illustrative example, utilising membrane GlyA (seen in table 2.5 above) follows:

- Initially a solution of 100 g mass is made. This comprises 17 g of CN and 83 g of solvent mixture.
- The solvent mixture is composed of 5 wt% of water, 0.5 wt% glycerol, 55 wt% acetone and 40.5 wt% of ethanol. When these percentages of 83 g are worked out they give masses of 4.15 g water, 0.415 g glycerol, 45.65 g acetone and 32.785 g ethanol.
- This gives an initial solution (before cloud point) of 17 wt% CN, 4.15 wt% water, 0.415 wt% glycerol, 45.65 wt% acetone and 32.785 wt% ethanol.

- A 20 ml sample of this solution is taken and weighed, giving a solution sample of mass 15.951 g.
- To this solution 6.01 g of water are added to bring the solution to cloud point, creating a solution of 21.961 g mass. The weight percentages of the components of this solution must now be worked out.
- Since only water was added, the masses of the other individual component are unchanged, thus they can be worked out using their original weight percentages applied to the mass of the 20 ml solution – 15.951 g. They become:
  - Cellulose nitrate mass in final solution = 15.951 g x 0.17 = 2.712 g
    - Weight percentage in final solution = (2.712 g / 21.961 g) x 100 = 12.35 wt%
  - Acetone mass in final solution = 15.951 g x 0.4565 = 7.282 g
    - Weight percentage in final solution = (7.282 g / 21.961 g) x 100 = 33.16 wt%
  - Ethanol mass in final solution = 15.951 g x 0.32785 = 5.230 g
    - Weight percentage in final solution = (5.230 g / 21.961 g) x 100 = 23.81 wt%
  - Glycerol mass in final solution = 15.951 g x 0.00415 = 0.066 g
    - Weight percentage in final solution = (0.066 g / 21.961 g) x 100 = 0.30 wt%
- Calculating the final weight percentage of water is slightly different, as follows:
  - Water mass in solution before cloud point = 15.951 g x 0.0415 = 0.662 g
  - Water mass in final solution = 0.662 g + 6.010 g = 6.672 g
    - Weight percentage in final solution = (6.672 g / 21.961 g) x 100 = 30.38 wt%

This method of calculating solution weight percentages after solutions were brought to cloud point was applied to all solutions used within this project.

2.1.4 Membrane Casting

Membrane casting, for all membrane types in this project, was done on an automatic film applicator; model K202 Control Coater produced by RK Printcoat Instruments Ltd., UK (see figures 2.1 and 2.2). This unit allows for a fully reproducible casting method. The unit is comprised of:

- A coating area of 325 mm x 250 mm
- A latch mechanism for coating bars with adjustable weights to allow for calibration to different substrate and coating thicknesses

- An electrical drive allowing one to coat at different rates
- Spiral and close wound coating bars (see figure 2.2) to allow one to coat at different thicknesses
- The casting thickness available are limited by the bars to: 6, 12, 24, 40, 50, 60, 80, 100, 150, 200, 300, 400, and,500 µm. One additional bar was manufactured for specialised applications which casts at 570 µm but is not spirally wound.



Figure 2.1: K202 Control Coater

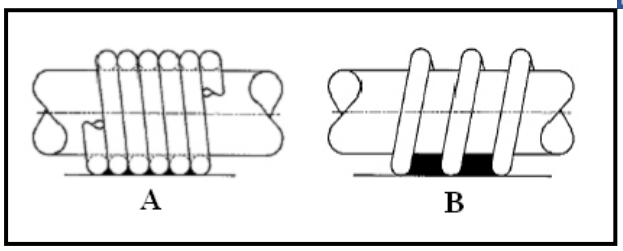


Figure 2.2: Close wound (A) and spirally wound (B) coating bars

Pervaporation Membrane Casting

Unsupported

Only the very earliest membranes were cast using this method: A casting solution is poured onto a circular glass plate approximately 164 mm in diameter and left to dry for 24 h – 72 h depending on thickness. Once dry, an incision is made in the edge of the membrane and peeled back to facilitate easy removal of the membrane from the plate. After removal from the plate, the membrane is cut to fit the pervaporation unit cell.

Supported

The nonwoven polyester support fabric is cut to fit a 25 cm^2 glass plate. One edge of the fabric is taped down with waterproof "Duck" tape. DMSO (approx. 10 mls) is placed beneath the fabric on the glass plate using a dropper. DMSO surface tension

helps adhere the fabric to the glass plate, while a ruler is used to remove air bubbles from beneath to ensure even casting. The opposing side of the fabric is then taped down (see figure 2.3) DMSO is used in this role rather than water as water would cause the casting solution of PAN to phase invert at the support side which would adversely affect the support structure.

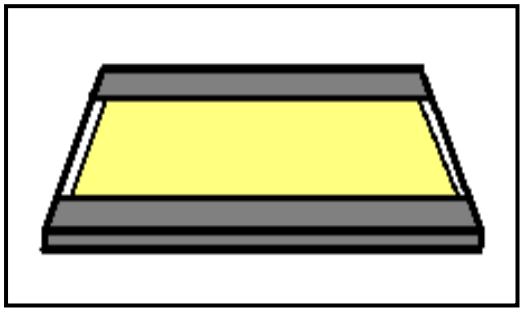


Figure 2.3: Glass plate and support fabric prepared for casting

On to the prepared glass plate and support fabric a solution of 7 wt% PAN in DMSO is cast with the K202 Control Coater using a 150 µm casting bar calibrated to the height of the glass plate and fabric. Once the bar has been clamped in place, a casting speed is set and the solution is cast (see figure 2.4).

Once the PAN support layer is dry the selective layer can then be cast. The K202 Control Coater is recalibrated for the support, a casting bar of desired thickness is chosen and the polymer solution of the selective layer of the pervaporation membrane is cast in the same manner as described above. This layer is then dried in a manner appropriate to the cast solution to produce the final pervaporation membrane. In some cases, where low volatility solvents such as glycerol have been incorporated into the membrane, drying in an oven at a maximum temperature of 40 ^{o}C is necessary.

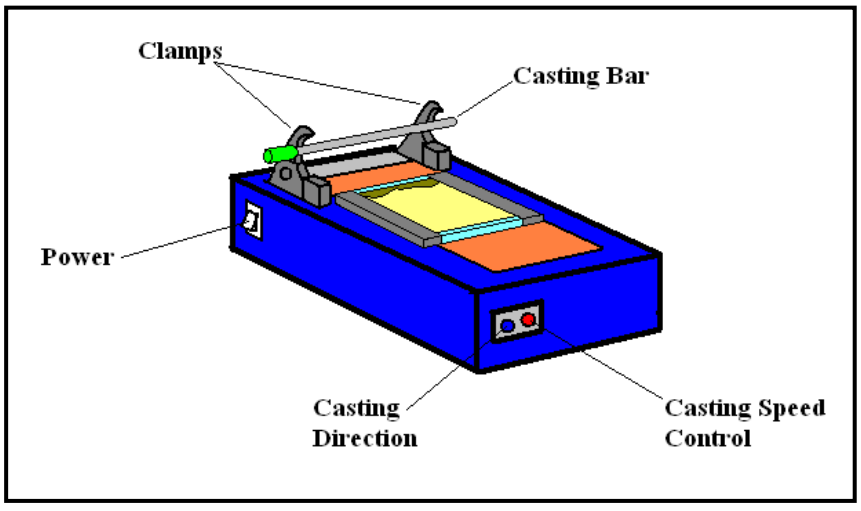


Figure 2.4: K202 Control Coater diagram with casting bar and membrane support in place

Lateral-flow Membrane Casting

Lateral-flow membranes are cast in a similar manner to that described above for pervaporation membranes with the addition of inducing phase inversion before drying to precipitate the final membrane.

The support material - a 100 % polyester film (Melinex) of 100, or 50 µm thickness - is attached to a glass plate as described above, but no DMSO is required to ensure that the film is free of air bubbles. The glass plate with attached Melinex is then placed on the K202 Control Coater, a casting bar of desired thickness is chosen and the unit is calibrated for the support with the casting bar. The casting solution for the lateral flow membrane to be made is then cast on to the Melinex as described in the pervaporation membrane casting procedure above.

Phase inversion of the cast solution must then be induced through VIPS (described in section 1.4.2) by allowing the solution to phase separate in a controlled humidity environment. Humidity is maintained at 35 % inside an Mbraun GP 2202 PB single piece moulded glovebox, supplied by Mbraun UK, Ltd (see figure 2.5). Membranes were left in this environment for a minimum of 12 h to ensure complete phase separation and drying, after which membranes were dried in an oven at 40 ^{o}C to ensure any excess solvent, non-solvent or meso-solvent were removed.

Once cast the membranes must be rendered hydrophilic. This is done by placing the membrane in solutions of 0.1 wt% of SDBS surfactant in deionised water for 20 mins, followed by drying the membrane at room temperature. Subsequent SEM images of surfactant on the membrane surfaces (see appendix B, figure B1.) and bestowment of hydrophilicity upon the membrane confirmed the presence and effect of the surfactant treatment. This form of lateral flow test is an industrial SOP (for the determination of efficacy of flow rate in a given membrane batch) making results directly comparable with the stated flow rates of industrial membranes. The effect of gravity on the flow rate is constant for all membranes so the relative differences in flow between membranes serves to show improvement brought about through changes in membrane structure.

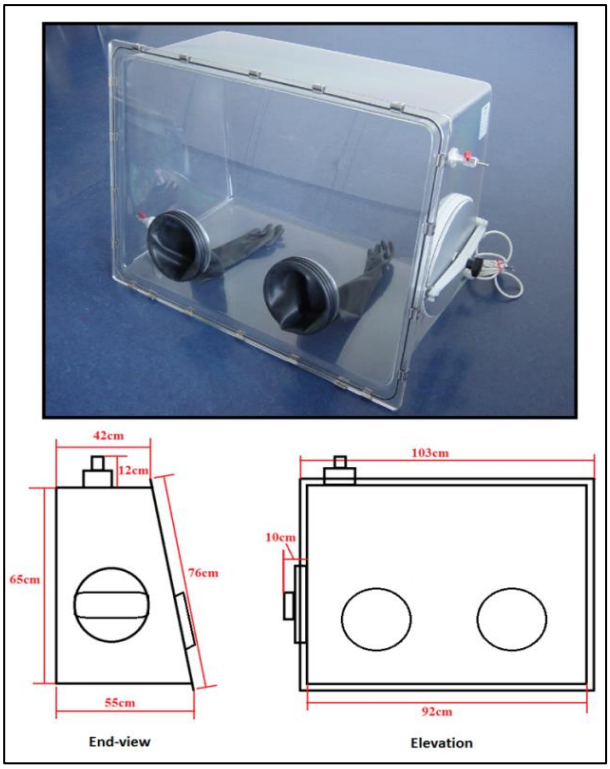


Figure 2.5: Mbraun GP 2202 PB single piece moulded glovebox and technical drawings

2.2 Membrane Testing

As was highlighted in chapter 1, the testing of pervaporation membranes is a far more complex process than the testing of lateral flow membranes. This is reflected in the detailing of the procedures for both below.

2.2.1 Pervaporation Membrane Testing

Pervaporation experiments were conducted using a Sulzer Chemtech Laboratory 6" Test Cell (see figure 2.6 for a schematic diagram), produced by Sulzer Chemtech Gmbh, supplied by Cork Institute of Technology (CIT) where the Irish National Institute for Membrane Technology is based.

Much of the literature cites the use of indigenous pervaporation units. In the interests of reliability and reproducibility the Sulzer unit was chosen over an indigenously produced unit. Despite the proliferation of indigenous units in some published papers, a great number of publications use this unit and exhibit far more reliable data in their papers[5–9].

The laboratory bench test unit is designed for testing of the performance of flat sheet membranes for the removal of minor components from feed mixtures by means

of pervaporation. All parts in contact with the feed mixture are either stainless steel, polytetrafluoroethylene (PTFE), the membrane, or appropriate elastomers. The unit is comprised of

- Heating bath with temperature control and recycling pump.
- Closed feed tank, double jacketed, heated by circulation of the heat transfer liquid from the heating bath through the double jacket.
- Feed pump which circulates the feed from the feed tank through the test cell, over the membrane and back to the tank.
- Circular test cell with inner diameter of 158 mm, in which membrane is contained. Test cell comprised of upper section – with connection for inlet and outlet of feed mixture – and lower section – to which cold trap is connected. During operation, upper and lower sections held together by four clamps. Membrane is supported by a porous steel plate in lower section through which permeating vapours can pass. Seal between feed side and permeate side is achieved by means of an O-ring around circumference of the membrane at the inner wall of bottom section of test cell.
- Permeate condenser (cold trap) with vacuum connection and Dewar vessel for liquid N_2

Typical pervaporation tests were conducted for a minimum of 5 h to allow for equilibration of the membrane within the cell with the feed solution. This took - on average - 1 h, thus data after the first hour of testing was considered truly indicative of a membrane's performance. As such all average selectivity and flux figures given in the subsequent chapters are calculated excluding the first hour of data.

Where membrane mechanical, thermal, or chemical stability caused it to fail before the 5 h minimum test time was reached the membranes were tested for as long as permitted by their physical characteristics. What follows is a detailed outlining of the pervaporation unit operation.

It should be noted that the earliest membranes tested suffered from concentration polarization effects which resulted in falsely positive selectivity results; as such, static mixers were installed in the membrane housing to prevent this effect.

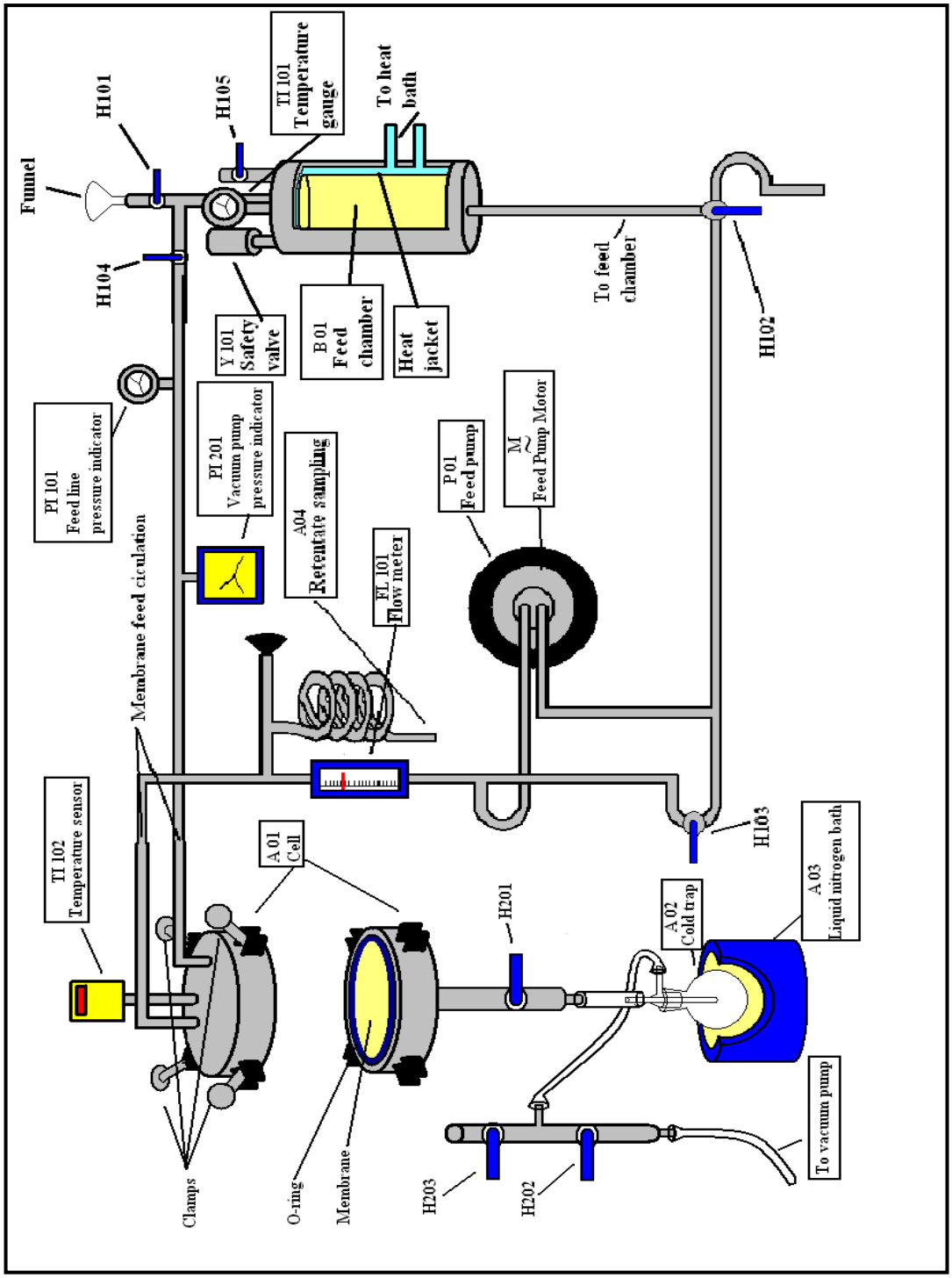


Figure 2.6: Sulzer Chemtech Laboratory 6" Test Cell (detailed on following 3 pages)

Pervaporation Procedure

Start Up

For a pervaporation experiment to be conducted, an appropriate feed solutionis required. Two feeds were used: 74 wt%, and 90 wt% ethanol in water solutions.

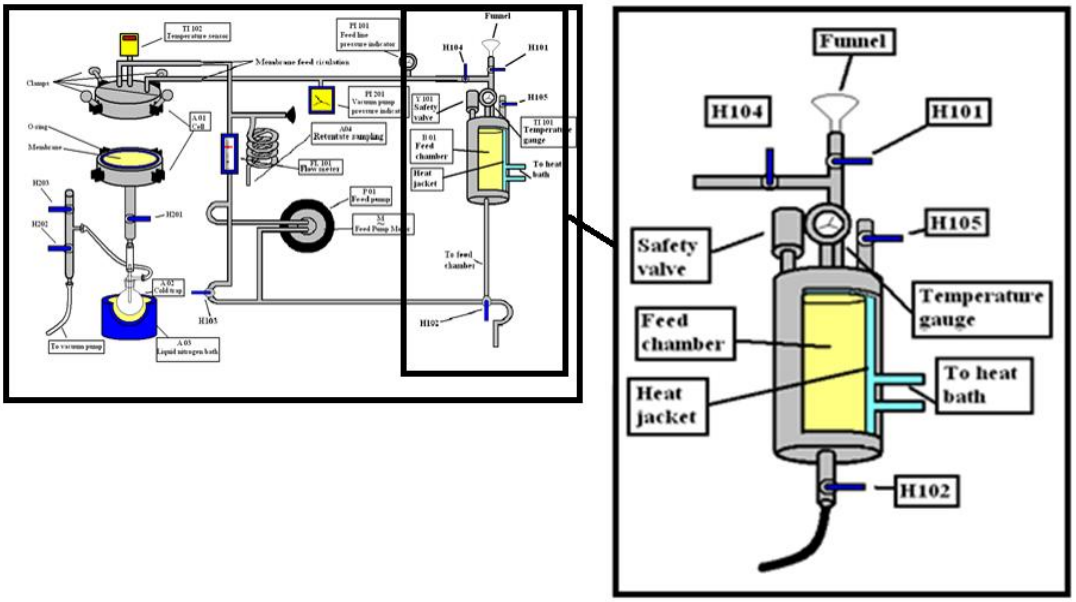


Figure 2.7: Diagram of feed chamber of pervaporation unit (details in text; see figure 2.6 for full pervaporation unit diagram)

From figure 2.7 is can be seen that introduction of feed solution to the feed chamber of the pervaporation unit is done by fully opening valve H101 and closing valve H102. A minimum of 1.5 L of the chosen feed solution is poured in through a funnel into the feed chamber and valves H101 and H105 are closed.

In the event of changing feed solutions the feed chamber can be emptied by opening valve H102 and letting the solution flow out into a storage vessel. In the event of a pressure build up within the unit, a safety valve located above the feed chamber releases pressure above the design threshold. The temperature of the feed solution is controlled by using a heating bath to circulate heated water into the jacket which surrounds the feed chamber internally.

Membrane Installation

Membranes are cut to fit the membrane cell of the pervaporation unit. Upon installation a vacuum must be obtained by sealing the membrane in place with a rubber O-ring. The vacuum is created by using a vacuum pump. As shown in figure

2.8, valves H201 and H202 are closed and valve H203 is opened causing the membrane to flatten. The O-ring is then inserted to create a complete vacuum. If a vacuum of less than 1.0 mbar cannot be created at this stage then the membrane must be considered faulty.

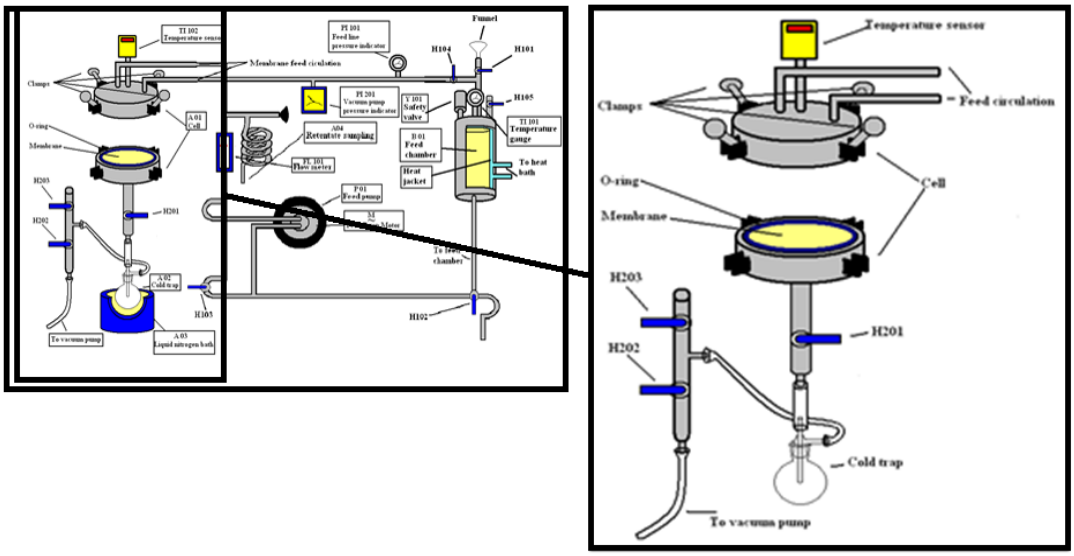


Figure 2.8: Diagram of the membrane cell of pervaporation unit (details in text; see figure 2.6 for full pervaporation unit diagram)

Pervaporation Unit Set-up

The pervaporation experiment itself involves circulating the feed solution over the upper side of the membrane in the cell and collecting permeate on the lower side in a cold trap. The circulation of the feed requires the use of a pump. Once the above procedures have been followed the pervaporation unit can undergo final setup for initiation of an experiment.

Figure 2.9 shows valves H103 and H104 are half opened and valve H102 is fully closed. The heat bath for the feed chamber is switched on and set to 60 ^{0}C (see figure 2.7), liquid nitrogen is used to cool the cold trap (see figure 2.8), and the feed pump is turned on. Once the pump is on valves H103 and H104 can be used to adjust the flow of the feed. The flow rate can be read from the flow meter and should be adjusted to approximately 80 l h^{-1}.

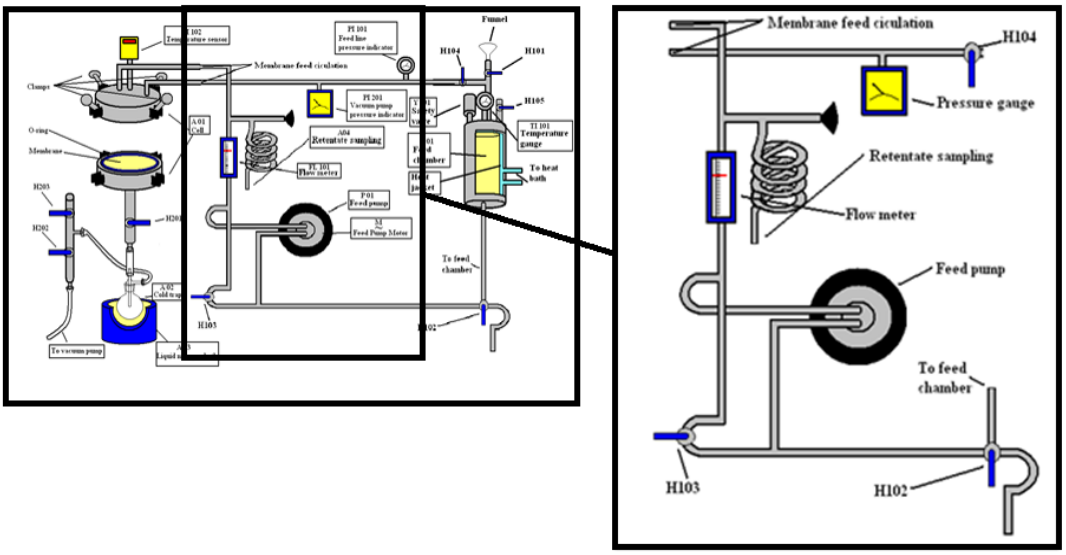


Figure 2.9: Diagram of feed pump and peripherals of pervaporation unit (details in text; see figure 2.6 for full pervaporation unit diagram)

Sampling

Permeate is collected in a cold trap (see figure 2.8). Before installing the cold trap it is weighed. After an hour of collecting permeate the cold trap is removed and replaced with another empty, pre-weighed cold trap. The removed cold trap contains the permeate sample; trap and permeate are weighed and the weight of the empty trap (previously determined) is subtracted to give the weight of the permeate, from which we can determine the flux.

The removal of the cold trap is conducted by closing valves H201 and H202 and opening valve H203 (see figures 2.6 and 2.8). This maintains the vacuum in the unit above H201 and releases the vacuum surrounding the cold trap, allowing for its removal. The replacement cold trap is connected to the appropriate tubes and valve H203 is closed, followed by opening valve H202. Finally valve H201 is opened slowly so that sudden release of vacuum does not disrupt the membrane and/or O-ring position, which would render the experiment a failure.

This procedure of collecting permeate every hour continues for the duration of the pervaporation experiment. Samples are stored after weighing until they reach room temperature, after which they can be characterised in terms of their selectivities.

Pervaporation Membrane Flux and Selectivity Calculations:

Calculation of Membrane Flux

$$J = W/At \qquad \textbf{2(i)}$$

Where J is flux of the membrane in g $m^{-2}h^{-1}$, W is the mass of permeate in grams, A is the area of the membrane in metres squared and t is the time interval between samples in hours.

Calculation of Membrane Selectivity

$$A = (Y_i/Y_j)/(X_i/X_j) \qquad \textbf{2(ii)}$$

Where α is the selectivity of the membrane (a ratio of ratios; no units), Y_i is the weight percentage water in the permeate, X_i is the weight percentage water in the retentate, Y_j is the weight percentage ethanol in the permeate and X_j is the weight percentage ethanol in the retentate.

Calculation of Retentate and Permeate Densities

Ethanol concentration in a sample at a given temperature was calculated by the programme Alcodens (version 2.1. copyright 2003-2009 Katmar Software) from the density readings of the Mettler-Toledo DE40 Density Meter. This is a four place digital density meter for measurement of density, specific gravity, API (petroleum), BRIX (sugar), alcohol or concentration of aqueous solutions, designed for quality control, general lab practice or general manufacturing practice.

2.2.2 Lateral-flow Membrane Testing

Lateral-flow membranes were tested using an industry standard testing method for measuring the rate of lateral capillary flow of fluid through their internal pore network.

Membrane lateral flow speeds determined by testing capillary flow rates of water through the membranes. Membranes were cut into 12 mm x 28 mm strips. A horizontal line was drawn 3 mm from the bottom; a second line was drawn 3mm from the top; giving a region 22 mm in length between: An area of 264 mm^2 or 2.64 cm^2. The membrane strip was then placed vertically in a 2 mm depth of water. The water flow was timed between the two marks and a flow speed determined to give the lateral flow rates. The cellulose nitrate polymer was inherently hydrophobic and

little or no flow was observed. In order to render it hydrophilic and so fit for lateral flow purposes, it was treated with surfactant. This was achieved by placing the membrane in solutions of 0.1 wt% of sodiumdodecylbenzenesulfate (SDBS) surfactant in deionised water for 20 mins, followed by drying the membrane at room temperature. Subsequent SEM images of surfactant on the membrane surfaces (Appendix B, figure B.1) and rendering of hydrophilicity upon the membrane confirmed the presence and effect of the surfactant treatment. This form of lateral flow test is an industrial SOP, making results directly comparable with the stated flow rates of industrial membranes. The effect of gravity on the flow rate is constant for all membranes so the relative differences in flow between membranes serves to show improvement brought about through changes in membrane structure.

2.3 Membrane Characterisation

All characterisation methods were used for membranes of both pervaporation and lateral-flow types unless otherwise stated.

2.3.1 Scanning Electron Microscopy

The morphologies of the cross sections and top surfaces of the membranes were characterised using a Jeol model FEI FP 2031/11 Inspect F field emission scanning electron microscope. All membrane samples were prepared for imaging by Cryo-Rupture Imaging Sample Preparation (CRISP)[10] method, whereby a section of membrane is immersed in liquid nitrogen and subsequently broken to preserve the structural integrity of the cross section, which is typically destroyed by cutting the sample with a blade. All polymer membrane samples required gold-coating to provide a conductive surface to allow imaging. All coatings were approximately 45 nm thick.

2.3.2 Flexibility Testing

A method for testing membrane flexibility was developed by quantifying that of a membrane composed of the most flexible polymer used in the study (PVA). An unsupported PVA membrane can be bound around a cylinder of 2.0 mm radius without suffering any damage to its polymer matrix that reduces pervaporation performance in a discernible way. Such damage is typified by cracks which reduce selectivity and falsely increase flux. Use of a cylinder of any lower radius than this

results in a reduction in pervaporation performance of the membrane. This was used as the standard to which other membranes were compared in order to assess their flexibility, e.g. it was found that a supported pristine sodium alginate membrane could only be bound to a cylinder of minimum radius 42 mm without suffering damage to its polymer matrix that results in a reduction in pervaporation performance. This method was also applied to lateral flow membranes where a loss in lateral flow was the critical factor. The data from this method will be presented as ***r X*** in text, where **r** is radius and **X** is the length of the minimum radius of the cylinder to which a membrane could be bound, in millimetres.

2.3.3 X-Ray Diffraction

Membrane crystallinity was determined by X-ray powder diffraction using a Philips X'Pert MPD Pro diffractometer with Cu Kα radiation 1.540598 Å, utilizing Panalytical X'Pert data collector and X'Pert Highscore. Samples were prepared by attaching membranes to glass microscope slides. Scans were conducted in triplet and the angular range for analysis of all membrane samples was 10 ^{o} to 80 ^{o}.

2.3.4 Fourier Transform Infrared Spectroscopy

FTIR analysis of membranes was conducted using a Thermo Scientific Nickolet 6700 – FTIR. Membrane samples were prepared by grinding membranes up in KBr, the subsequent powder being placed in a press to produce a sample disk, which was then analysed.

2.3.5 Differential Scanning Calorimetry/Thermogravimetric Analysis

Sodium alginate based polymer of pervaporation membranes was tested using a DSC/TGA Q1000 version 9.9 build 303 instrument from TA instruments, with a Mettler Toledo Microgram balance. Analysis was conducted in a temperature range of -40.10 ^{o}C to 397.10 ^{o}C, with a temperature gradient of 20.01 ^{o}C min^{-1}, and conducted under nitrogen at 50 ml min^{-1} flow rate.

2.3.6 Mercury Porosimetry

Porosimetry was conducted on two lateral flow membranes (BasMemBCP and MesoDCP, see above) using a mercury porosimeter model, Micromeritics AutoPore IV 9500 V1.09 by MCA Services UK.

2.3.7 Atomic Force Microscopy

Membrane topographies were characterised using an Atomic Force Microscope (AFM), SPM, Park systems, XE-10, operated in AC (tapping) mode under ambient conditions using silicon microcantilever probe tips with a force constant of 60,000 N m^{-1} and a scanning force of 0.11 nN

2.3.8 Contact Angle Measurement

Membrane surface contact angle tests were conducted utilizing a sessile drop system at 25 ^{o}C (goniometer/optical-subsystem angle measurement limits 15 ^{o} – 165 ^{o}). Samples were ~2.5 cm^2. Droplet size was 10 µl. Each film sample was analysed with three drops.

References: Chapter 2

[1] D. A. Keane, J. P. Hanrahan, M. P. Copley, J. D. Holmes, and M. A. Morris, "A modified Stöber process for the production of mesoporous Sub 2 micron silica microspheres; applications in HPLC," *Journal of Porous Materials*, vol. 17, no. 2, pp. 145–152, Mar. 2009.

[2] R. Russo, M. Malinconico, L. Petti, and G. Romano, "Physical behavior of biodegradable alginate-poly(vinyl alcohol) blend films," *Journal of Polymer Science Part B: Polymer Physics*, vol. 43, no. 10, pp. 1205–1213, May 2005.

[3] H. Sun, S. Liu, B. Ge, L. Xing, and H. Chen, "Cellulose nitrate membrane formation via phase separation induced by penetration of nonsolvent from vapor phase," *Journal of Membrane Science*, vol. 295, no. 1–2, pp. 2–10, May 2007.

[4] P. Van-de-Witte, "Phase separation processes in polymer solutions in relation to membrane formation," *Journal of Membrane Science*, vol. 117, no. 1–2, pp. 1–31, Aug. 1996.

[5] Z. Huang, Y. Shi, R. Wen, Y. Guo, J. Su, and T. Matsuura, "Multilayer poly(vinyl alcohol)–zeolite 4A composite membranes for ethanol dehydration by means of pervaporation," *Separation and Purification Technology*, vol. 51, no. 2, pp. 126–136, Sep. 2006.

[6] Z. Huang, H. Guan, W. Tan, X. Qiao, and S. Kulprathipanja, "Pervaporation study of aqueous ethanol solution through zeolite-incorporated multilayer poly(vinyl alcohol) membranes: Effect of zeolites," *Journal of Membrane Science*, vol. 276, no. 1–2, pp. 260–271, May 2006.

[7] W. F. Guo, T.-S. Chung, and T. Matsuura, "Pervaporation study on the dehydration of aqueous butanol solutions: a comparison of flux vs. permeance, separation factor vs. selectivity," *Journal of Membrane Science*, vol. 245, no. 2, pp. 199–210, 2004.

[8] H.-M. Guan, T.-S. Chung, Z. Huang, M. L. Chang, and S. Kulprathipanja, "Poly(vinyl alcohol) Multilayer Mixed Matrix Membranes for the Dehydration of Ethanol-Water Mixture," *Journal of Membrane Science*, vol. 268, no. 1, pp. 113–122, 2006.

[9] Q. G. Zhang, Q. L. Liu, A. M. Zhu, Y. Xiong, and L. Ren, "Pervaporation performance of quaternized poly(vinyl alcohol) and its crosslinked membranes for the dehydration of ethanol," *Journal of Membrane Science*, vol. 335, no. 1, pp. 68–75, 2009.

[10] E. J. Flynn, D. Keane, J. D. Holmes, and M. A. Morris, "Unusual trend of increasing selectivity and decreasing flux with decreasing thickness in pervaporation separation of ethanol/water mixtures using sodium alginate

blend membranes.," *Journal of Colloid and Interface Science*, vol. 370, no. 1, pp. 176–82, Mar. 2012.

Chapter 3

Pervaporation Membrane Development

3 Pervaporation Membrane Development

Parts of the following are adapted from "*The EPA Strive Report Series no. 50: Preparation of Polymer-Based Membranes for Dehydration of Ethanol by Pervaporation*". ISBN: 978-1-84095-347-3

Abstract

The earliest phases of this research centred on the development of basic viable membranes; attaining a reproducible method of making a supported membrane. This is the method outlined in chapter 2, section 2.1.4. The simplest membranes – membranes of pristine polymers – were first produced unsupported and compared with supported membranes in terms of separation performance. Their pervaporation efficacy was assessed and their chemical, physical and mechanical properties characterised. The surface areas of the membranes utilised in this project are on a par with those of industrial membranes. This scale makes the flexibility of a membrane of paramount importance, unlike in the majority of academic pervaporation research. Results from pristine membranes led to the development of a polymer blend membrane with superior pervaporation performance and durability which was the base composition for all future high-performance pervaporation membranes in the project.

3.1 Introduction

Literature suggests that the optimum membrane for pervaporation separation of water-ethanol solution could be produced from pristine sodium alginate.[1–4] With this in mind, the earliest membranes in the project were unsupported pristine sodium alginate membranes. For comparison, an unsupported pristine PVA membrane was also produced, as PVA is an industrial standard material. The composition of the solutions from which these membranes were cast can be seen in chapter 2 section 2.1.2.

It was immediately apparent that when NaAlg is used in membranes of the area we utilize (0.0177 m^2; the area of a full size industrial reactor membrane), the inherently brittle polysaccharide had a tendency to crack: No great surprise when one considers its reported Young's modulus; 5551 Mpa.[5] Most literature on pervaporation cites use of indigenous membranes of below 5cm diameter (0.0079 m^2 area). At this relatively small scale brittleness is less of an issue. The use of small area membranes gives unrealistic flux figures and can exaggerate concentration polarization effects giving unrepresentative selectivity figures as well as allowing brittle materials to be used for testing. All of this means that any results obtained are incomparable with industrial membranes and so, impractical.

Unsupported pristine pervaporation membranes of PVA and NaAlg were produced. It was found that the weight percentage of NaAlg that will dissolve in water to yield a readily castible solution is limited to below 6 wt%. Above this, solutions were too viscous for even casting of films. However, membranes formed from 6 wt% casting solutions proved too brittle for practical use. Literature studies suggested membranes formed from 3 wt% casting solutions [2] but, as highlighted above, these were on membranes of much smaller area and when scaled up proved unusable. PVA solutions were produced from 10 wt% solutions as solutions below this weight percentage were too fluid for casting.

For comparison, supported pervaporation membranes were produced. Supported NaAlg membranes were produced from 5 wt% solutions of NaAlg in water. The use of a support (support material and production described in chapter 2 sections 2.1.2 and 2.1.4) allowed for higher weight percentage solutions of NaAlg

to be used which, according to literature [6], should increase the membrane selective properties.

The results obtained from the membranes outlined above led to the development of polymer blend membranes. Membranes were cast from 9:1 NaAlg:PVA, 4:1 NaAlg:PVA and 7:3 NaAlg:PVA solutions. The pervaporation performances of these membranes are shown in tables A.5, A.6 and A.7 of Appendix A. The compositions of the solutions from which the blend membranes were cast are outlined in chapter 2, section 2.1.2, table 2.1.

Two more casting solutions of 9:1 NaAlg:PVA and 4:1 NaAlg:PVA with glycerol plasticizer incorporated were produced, the compositions of which are shown in chapter 2, section 2.1.2, table 2.1. Detailed pervaporation performance of these membranes can be seen in tables A.8 and A.9 of Appendix A.

It was expected that the unsupported pristine membranes would exhibit high selectivity figures due to their greater thickness compared to the supported membranes, but that they would have correspondingly low flux. The supported pristine membranes by comparison were expected to exhibit the opposite trend, higher flux and lower selectivity.[7], [8]

It was also expected that the pristine PVA membranes would perform with lower selectivity and higher flux than their pristine NaAlg counterparts, but that the PVA membranes would be more durable.[2], [9–12]

It was hoped that the production of a polymer blend membrane would provide enhanced durability and flux compared to the pristine NaAlg membranes - such as PVA exhibits - while maintaining the NaAlg membranes' reported high selectivities.[12]

3.2 Experimental

See chapter 2 for details on all materials, apparatus and procedures.

3.3 Results and Discussion

3.3.1 Unsupported Pristine Membrane

Figure 3.1 shows the pervaporation performances of all membranes. Flux and selectivity versus time for unsupported and supported pristine (3.1A and 3.1B) and

blend (3.1 C and 3.1D) pervaporation membranes with flux (3.1A and 3.1C) given on a linear scale and selectivity (3.1B and 3.1D) given on a logarithmic scale. The unsupported PVA membrane was cast at 150 µm thickness however the unsupported NaAlg could not form a stable membrane at this thickness and had to be cast at 400 µm to be self-supporting. For comparison; all supported membranes were cast at 100 µm as the support provided stability for thinner castings. The dry thicknesses of the final membranes were considerably less than the casting thickness, typically varying between 2.5 % and 10 % of casting thickness depending on membrane composition and use – or not – of a support (based on cross sectional SEM images in figure 3.4; detailed in chapter 5).

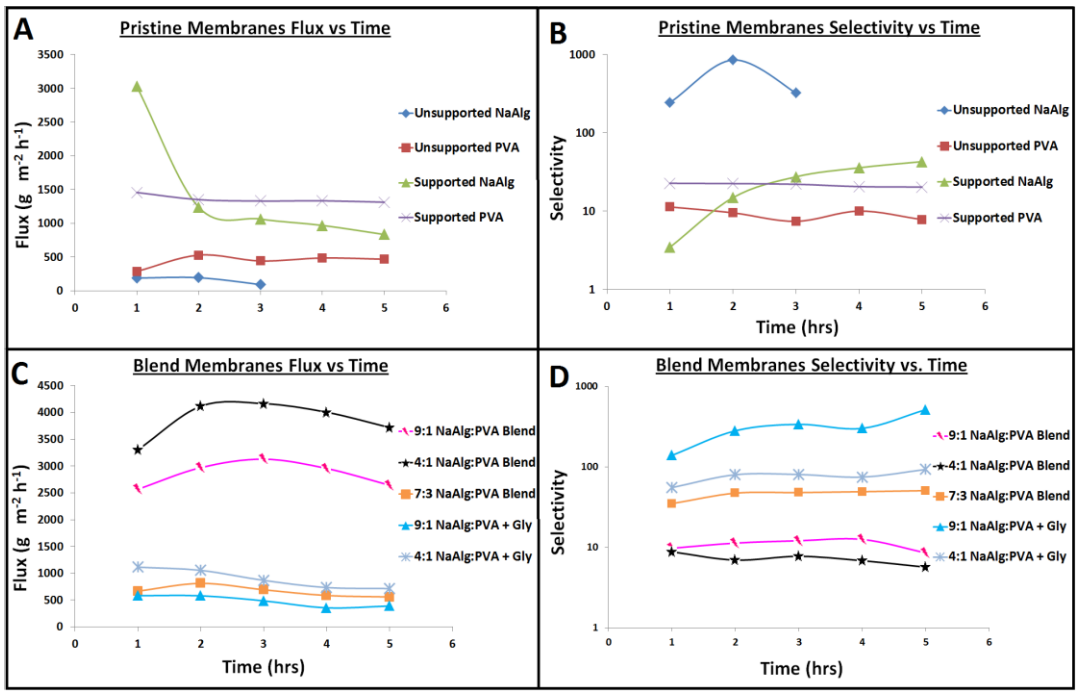


Figure 3.1: Flux (3.1A) & selectivity (3.1B) vs. time for unsupported & supported pristine pervaporation membranes. Flux (3.1C) and selectivity (3.1D) figures for polymer blend pervaporation membranes. Flux figures given on linear scales, selectivities given on logarithmic scales

Starting with the unsupported pristine NaAlg membrane, it can be seen from figures 3.1A and 3.1B that the membrane did not complete the five hours of testing that the other membranes achieved. The reason for the failure is NaAlg's highly hydrophilic nature. This is due to its many polar –OH and $–COO^- Na^+$ groups (see chapter 1 section 1.3.1). NaAlg pervaporation membranes work by absorption diffusion (see chapter 1, section 1.3.3). This requires the absorption of water molecules into the membrane which causes those comprised of NaAlg to become

saturated, resulting in swelling and eventual disintegrating. Using a feed solution with a density of 0.8199 g cm^{-3} (101pprox.. 90 wt% ethanol, 10 wt% water) the membrane did precisely that, resulting in its disintegration and a subsequent significant loss in flux (193.33 g $m^{-2}h^{-1}$ to 91.69 g $m^{-2}h^{-1}$) and selectivity (853.72 to 323.78) figures in the third hour. This is indicative of total membrane failure; confirmed upon removal of the membrane from the pervaporation unit. It was found to have been partially – almost completely – dissolved, rendering it a gel.

By comparison, the unsupported PVA membrane withstood pervaporation testing relatively well. Upon removal it was found the membrane had partially dissolved, though not to the extent that the NaAlg membrane had. The data suggests that while the membrane is more physically durable (withstood 5hrs pervaporation testing compared to NaAlg unsupported membrane; 3hrs) and its performance in terms of flux (avg. flux = 495.64 g $m^{-2}h^{-1}$) is superior to that of the NaAlg membrane (avg. flux = 142.51 g $m^{-2}h^{-1}$) its selectivity is inferior (avg. selectivity of unsupported PVA membrane = 8.76, avg. selectivity excluding first hour of unsupported NaAlg membrane = 588.75).

In terms of tensile strength, both the unsupported membranes, as a result of their relatively great thickness, proved to be quite flexible. From figure 3.5 (section 3.3.5 below) data; the unsupported pristine PVA membrane was bound to a cylinder of 2.0 mm minimum radius (r 2.0) without suffering any loss in pervaporation performance due to damage to its polymer matrix. The unsupported NaAlg membrane was not as flexible, managing only r 6.5, but, as shall be seen below, this represents a high flexibility for a NaAlg membrane. Details of how flexibility is tested and quantified are contained in chapter 2 section 2.3.2. Tabulated data from figure 3.5 contained in table A.10 of appendix A, section A.5.

The conclusion from the above was that in order to prevent total or almost total dissolution of the membrane under pervaporation conditions, a support is required, particularly in the case of NaAlg membranes

3.3.2 Supported Pristine Membranes

The use of a support yielded more physically durable membranes; both supported NaAlg and PVA withstood pervaporation testing for 6 h. In the case of the supported NaAlg there was a drop in selectivity (avg. selectivity = 32.836)

compared with the unsupported membrane (avg. selectivity = 588.75). It should be noted that this average figure is unlikely to be representative of actual membrane efficacy as, given the membrane's 400 µm thickness, it was unlikely to have reached stable condition within the pervaporation unit before critical failure. Additionally, as can be seen from figure 3.2 below, the supported NaAlg membrane contained many fractures after drying. This was due to it being brittle; flexibility only r 42.0 compared to r 6.5 for the unsupported equivalent (see figure 3.5). These fractures allow unselective passage of feed through the membrane, creating a false negative selectivity figure. Note that at such a thickness as that of the unsupported membrane, the flux is reduced to an impractical level (avg. 142.5 g m^{-2} h^{-1}). The selectivity of the supported NaAlg membrane improves as the pervaporation testing proceeds, rising to a maximum of 43.26 in the final hour of testing while the flux is far superior to that of the unsupported NaAlg.

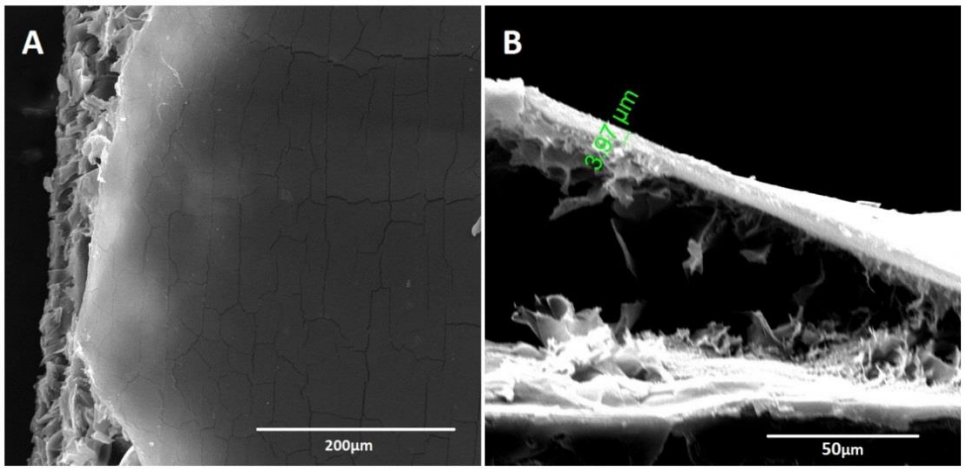


Figure 3.2: SEM surface images of pristine supported 5wt% NaAlg pervaporation membrane showing cracks in membrane selective layer

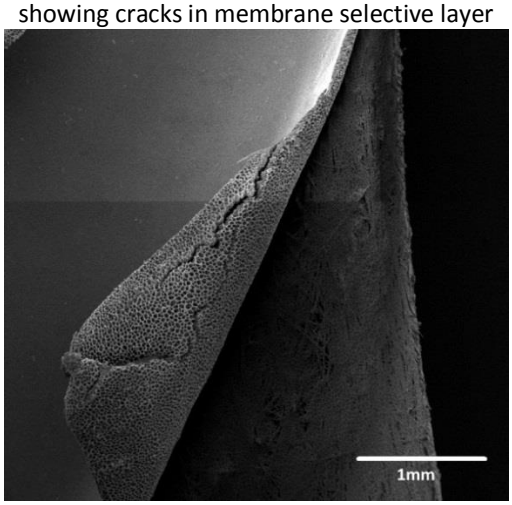


Figure 3.3: SEM image of early PVA membrane with PAN support layer delaminating from fabric support

The PVA membrane showed an increase in selectivity upon inclusion of a support, going from an average selectivity of 8.76 in the unsupported membrane to an average of 21.03 in the supported. This may be due to the increased density of membrane skin layer [13]. Unsupported membranes are necessarily thicker. In these instances the unsupported NaAlg and PVA membranes would have been much thicker (approximately 400 µm when dry) than the supported equivalents (approximately 25 µm when dry for NaAlg and 35 µm for PVA). A thicker membrane provides a greater amount of polymer matrix through which diffusing feed molecules must travel, leading to greater selectivity in theory. However, given the drying processes of thin layers [14], [15] it would be expected that the thinner supported membrane *could* have a greater density in the skin layer. This is due to greater rate of evaporative loss of solvent from the greater exposed surface area upon casting compared with the supported membrane[13]. From this, one might expect to see an increase in selectivity with a decrease in thickness - down to a minimum - below which the sheer quantity of selective material in a thick membrane (such as in an unsupported membrane) would be more efficacious for pervaporation separation. This is the subject of chapter 5 and will be discussed in greater detail then.

As with the NaAlg membranes, there is an increase in flux for the supported PVA membrane over its unsupported counterpart: supported PVA avg. flux = 1331.497 g m^{-2} h^{-1}, unsupported PVA avg. flux = 480.75 g m^{-2} h^{-1}. This is due simply to the polymer layer being thinner which decreases diffusion time scales. This is also the case with the NaAlg membranes.

Regarding flexibility, figure 3.5 shows the supported PVA membrane had r 3.5 flexibility compared to r 2.0 for the unsupported. It should be noted however, that the 3.5mm minimum radius seen here was the point at which the PAN support layer began to suffer damage – adversely affecting pervaporation performance – rather than any damage being suffered to the selective PVA layer (flexibility testing; chapter 2 section 2.3.2).

For the earliest membranes primary analysis was pervaporation testing to establish a base for production of more complex membranes. The SEM images obtained for membranes from this period show significant surface defects typified by the cracks seen in figure 3.2. Such defects allow unselective passage of feed

solution through the polymer matrix which has a negative effect on selectivity figures and gives falsely positive flux figures. Figure 3.3 illustrates the lamellar structure of the supported membranes with a top surface of selective polymer and the PAN layer delaminating from the support fabric.

SEM analysis and pervaporation performance led to the conclusion that the use of pristine polymers produced membranes either too low in selectivity – as in the case of PVA – or physically untenable – as in the case of NaAlg. Thus, investigation into the production of a membrane produced from a blend of PVA and NaAlg was undertaken.

3.3.3 Polymer Blend Membranes

Pervaporation results for membranes produced from blends of NaAlg and PVA can be seen in figure 3.1C and 3.1D, which show flux and selectivity figures respectively. The three which performed best are shown here; polymer blends of 7:3, 4:1 and 9:1 ratios of NaAlg:PVA. Addressing first the 7:3 membrane and the flux data shown in figure 3.1C, it can be seen that it has the lowest flux (avg. = 662.797 g m^{-2} h^{-1}, max. = 811.977 g m^{-2} h^{-1}) and the highest selectivity (avg. = 48.687, max. = 50.638), despite having the highest low-selectivity polymer content of the three. This is counter to what is expected from theory. The 7:3 membrane has a much greater flexibility (r 4.0) than the 4:1 (r 12.5) or 9:1 (r 31.5) as seen from figure 3.5 (flexibility testing; chapter 2 section 2.3.2). This difference in flexibility explains the difference in flux and selectivity between the 7:3 and 9:1 membrane (avg. flux = 2925.156 g m^{-2} h^{-1}, max. flux = 3128.927 g m^{-2} h^{-1}, avg. selectivity = 11.1, max. selectivity = 12.53): The 9:1 membrane was so brittle that fracturing occurred in its selective layer allowing for non-selective passage of feed solution through it. Looking at image C in figure 3.4 one can see that the cross sectional structure of the 9:1 membrane is more porous than either the 7:3 (image A figure 3.4) or the 4:1 (image E figure 3.4) membrane. Porous structures in materials render them brittle[16] which explains the formation of cracks and so the high flux and low selectivity. However, the flux is not as high, nor is the selectivity as low, as the 4:1 membrane (avg. flux = 4001.752 g m^{-2} h^{-1}, max. flux = 4165.989 g m^{-2} h^{-1}, avg. selectivity = 6.787, max. selectivity = 7.729), both of which would be expected from the above analysis. Looking at image E of figure 3.4 it is clear that the cross

sectional structure of the 4:1 membrane is non-porous suggesting a greater flexibility than the 9:1 membrane; which is confirmed from the flexibility figures listed above.

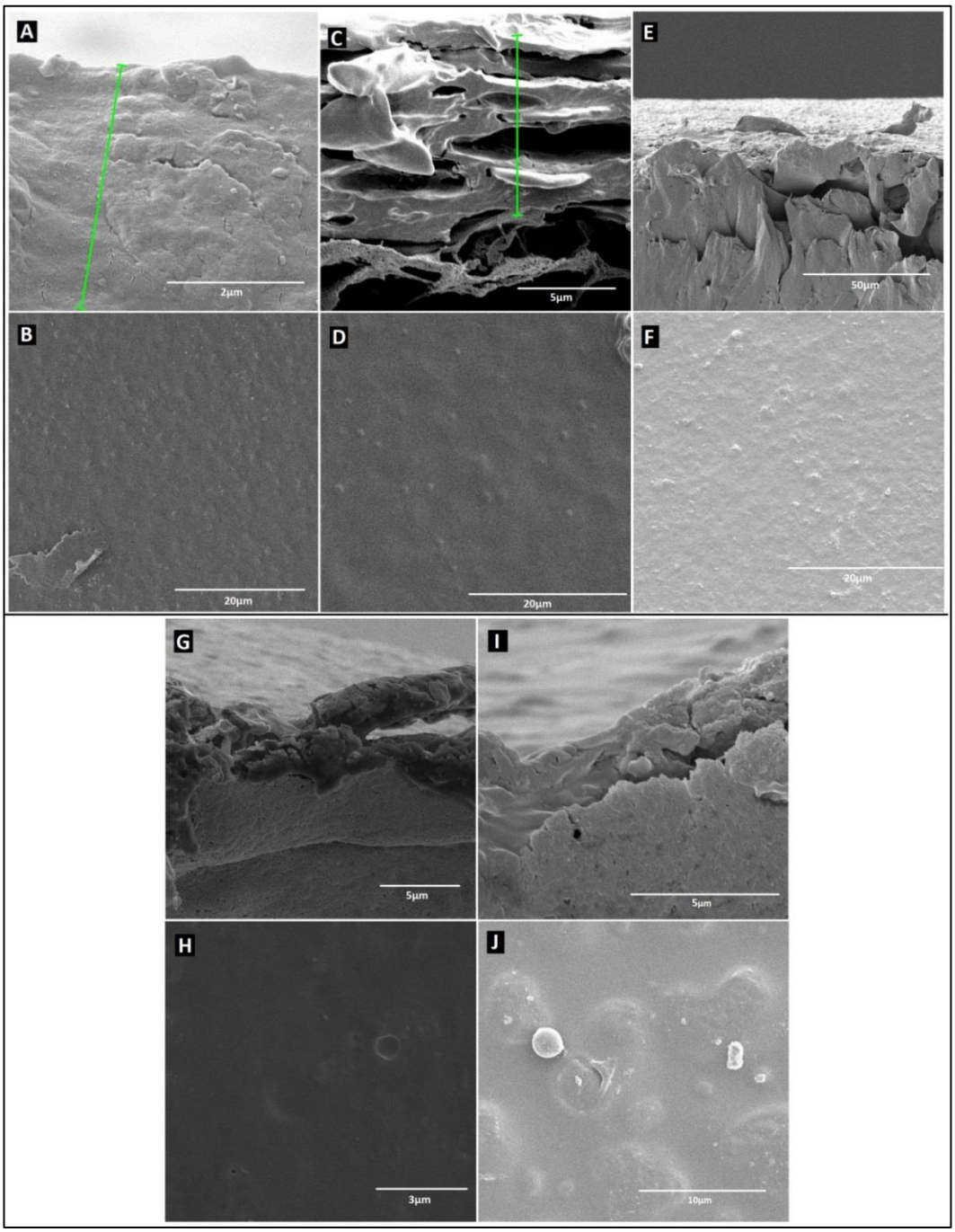


Figure 3.4: SEM images of supported polymer blend membranes: A, C and E show cross sections of 7:3, 9:1 and 4:1 NaAlg:PVA blends respectively while G and I show cross sections of 4:1 and 9:1 NaAlg:PVA blends utilising glyercol respectively. B, D and F show exposed surface images of 7:3, 9:1 and 4:1 NaAlg:PVA blends respectively while H and J show surface images of 4:1 and 9:1 NaAlg:PVA blends utilising glyercol respectively

The explanation for this lies in how the membranes swell in combination with the cracks in their structure caused by their being brittle. The functional groups of NaAlg render it more water selective[1] than PVA but, also cause it to swell more under pervaporation conditions as it is essentially water-soluble, as seen with the pristine unsupported NaAlg membranes above. Thus, the greater the sodium alginate content of a membrane the more it will swell under pervaporation conditions. This can be seen from the absorption data shown in table A.11 (appendix A, section A.6). If a membrane can swell sufficiently it will close up some of the cracks in the selective layer if they are of such a scale to allow this. This is easily observed if one simply takes a cracked supported NaAlg membrane and places it in water. Looking at the data in figure 3.5 it can be seen that the 9:1 membrane (r 31.5) is 2.52 times more brittle (taking r 2.0 as the zero point for the calculation) than the 4:1 membrane (r 12.5) but contains only 1.125 times the NaAlg content of the 4:1 membrane (flexibility testing; chapter 2 section 2.3.2). This means that the 9:1 membrane will suffer larger scale fractures and more extensively than the 4:1 membrane but will not swell by an equivalent margin. Thus, the swelling of the membrane in insufficient to overcome it's fracturing to the same extent as is possible in the 4:1 membrane. Thus, the selectivity figures of the 9:1 membrane are poorer than those of the 4:1 membrane and the flux figures are correspondingly higher explaining the trends observed in the data of figures 3.1C and 3.1D, wherein the 9:1 membrane has lower selectivity and higher flux than the 4:1 membrane while both are inferior to the performance of the 7:3 membrane in terms of flux and selectivity.

The conclusions drawn from this section of data are that while the 7:3 membrane is sufficiently flexible for practical use as a pervaporation membrane, the flux and selectivity figures are not sufficiently high to merit further investigation. The flux and selectivity figures obtained for the higher NaAlg content membranes here - 4:1 and 9:1 - are not representative of the true performance of these membranes as they are too brittle for practical use. Thus, a means of producing a high NaAlg content membrane that has greater flexibility than the 4:1 and 9:1 membranes must be found.

3.3.4 Polymer Blend Membrane Utilising Glycerol

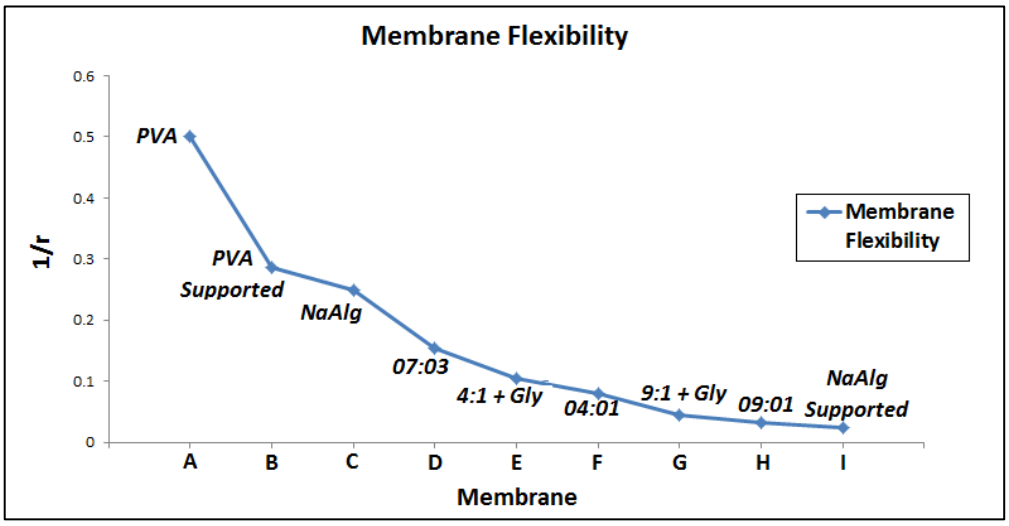


Figure 3.5: Plot of membrane flexibility where r = radius of cylinder (see section 2.3.2). 1/r utilised to facilitate understanding of data; unsupported PVA most flexible membrane therefore, highest on graph

In an effort to increase membrane flexibility without sacrificing selective performance, a plasticizing agent was introduced; namely, glycerol. Glycerol was chosen as it has "poor" solubility in the polymer blends being used. This reduces its plasticizing effect on the final membrane but also, reduces its permanence within the membrane, making it easier to remove by drying afterwards [17]. This is important as a plasticizer with "good" solubility – and so greater permanence – would require higher temperatures to remove, leading to inadvertent crosslinking of the membrane; having the opposite effect desired.

The exact mechanism through which plasticizers work is subject to much speculation, but certain general statements about them can be made: They are small molecules added to soften a polymer by lowering its T_g [17] or reducing its crystallinity or melting temperature[18]. In the case of most plasticizers, hydrogen bonding between polymer chain functional groups and the plasticizing agent is the primary factor in plasticization.[19]

Although the 7:3 membrane showed better pervaporation performance without glycerol, it was expected that if the 4:1 and 9:1 membranes could be rendered more flexible and so more durable through plasticization they would yield superior performance.

Addressing flux first; the data from figure 3.1C shows that 4:1 + gly membrane (*"+ gly"* denotes "with glycerol") (avg. flux = 843.347 g m^{-2} h^{-1}, max. flux = 1054.632 g m^{-2} h^{-1}) achieved greater flux than the 7:3 membrane (avg. = 662.797g m^{-2} h^{-1}, max. = 811.977 g m^{-2} h^{-1}) and the 9:1 + gly membrane (avg. = 343.588 g m^{-2} h^{-1}, max. = 358.279 g m^{-2} h^{-1}). Note that the 9:1+ gly membrane has a lower flux than the 7:3 membrane.

Looking at selectivity (figure 3.1D), the 9:1 + gly membrane (avg. = 358.279, max. = 513.858) and the 4:1 + gly membrane (avg. = 81.919, max. = 92.850) have the highest and second highest selective performance respectively. This confirms the expectation that these blends would offer superior performance upon inclusion of a plasticizer. However whether the plasticizer has affected membrane performance through an increase in polymer chain mobility or an increase in water adsorption capacity is uncertain. Karbowiak *et al*, in a study on *carrageenan* - another water soluble polysaccharide – membranes, have shown how the action of glycerol on diffusion is not through direct plasticization but through enabling of larger amounts of water to be adsorbed to the membrane surface.[20] This is corroborated in other studies [21][22] and suggests that the plasticizing effect on the membranes may be limited to increased flexibility, while the increase in selectivity is due to any glycerol remaining in the membrane. In this instance the major increase in selectivity is primarily due to the lack of cracks in the selective layers of the glycerol utilising membranes, compared to those without it. Future quantification of the increase in selective pervaporation performance of sodium alginate membranes by incorporation of glycerol into their polymer matrices is worthy of investigation.

The increase in membrane durability due to plasticization is quantified by the flexibility data listed in figure 3.5: The 9:1 + gly membrane had r 22.0 flexibility compared to r 31.5 for the 9:1 membrane. The 4:1 + gly membrane had r 9.5 flexibility compared to r 12.5 for the 4:1 membrane. While glycerol increased the flexibility of the 9:1 membrane significantly, r 22.0 for the 9:1 + gly is still a relatively brittle membrane (flexibility testing; chapter 2 section 2.3.2), rendering it somewhat impractical for use, despite its impressive selectivity figures. The 4:1 + gly membrane is relatively flexible and compares favourably with the unsupported NaAlg membrane while having greater flux and selectivity. Its selectivity, while not

as high as that of the 9:1 + gly membrane, is still superior to all others tested and its flux is relatively high for such a selective membrane; despite having the second highest selectivity it does not have the second lowest flux as one might expect (see figures 3.1C, 3.1D and 3.5).

SEM images of the 9:1 + gly (figure 3.4I and 3.4J) and 4:1 + gly (figure 3.4G 3.4H) membranes do not exhibit any significantly different characteristics to the images of the 4:1 membrane. Both however exhibit a denser, non-porous structure than the 9:1 membrane, again indicative of an increase in flexibility. Cross sectional images of both membranes (figure 3.4G = 4:1 + gly and 3.4I = 9:1 + gly) exhibit this dense structure clearly, while the surface images (figure 3.4H = 4:1 + gly and 3.4J = 9:1 + gly) show no surface fractures or defects. Pock-mark-like surface defects are due to solvent pooling and/or trapped air forming bubbles in the drying process.[23]

The combination of flexibility with relatively high selectivity and flux makes the 4:1 + gly membrane ideal for general testing of high performance pervaporation membranes on an industrial scale such as that used in our pervaporator (see chapter 2 section 2.2.1). As such it was adopted as the base membrane for all future high performance pervaporation studies in the project.

3.4 Conclusion

Directly comparing pristine polymers; PVA is more flexible – and therefore more durable – than NaAlg. PVA also exhibits marginally superior flux to that of NaAlg but significantly inferior selectivity.

Regarding supports; they are essential: In order for an unsupported membrane to be self-supporting it must necessarily be relatively thick, which significantly reduces flux. Additionally, in the case of water selective membranes in a water-containing feed, a support is required to prevent gelification and potential dissolution of the membrane under pervaporation conditions. While unsupported membranes are more flexible on account of their greater thickness, their flexibility and therefore durability, is not so significantly greater than a supported equivalent to overcome the substantial loss in flux that must be incurred by utilising them. A support allows for the use of relatively thin selective layers which results in a large gain in flux.

Given the higher surface-area to mass ratio of the selective layer in the supported membrane, the rate of evaporative loss of solvent from the membrane during drying should be increased, rendering the surface skin layer denser, which should, in theory, offset the loss in selectivity compared to the unsupported membrane. This will be investigated in chapter 5.

Regarding polymer blends: In order to obtain a membrane with comparable durability to that of a PVA membrane and pervaporation performance comparable with that of a NaAlg membrane, a polymer blend must be utilised. A polymer blend with enough NaAlg to still have highly selective performance is too brittle for practical use at an industrial scale. Therefore a plasticizer must be used in the membrane production process; in this case; glycerol. The use of glycerol renders the blend membrane durable enough to be used on a large scale while maintaining a far higher performance than the industrial standard pristine PVA membrane. The quantification and precise nature of the effect of plasticizing agents in general, and glycerol specifically in this instance, on the selective performance is still unknown and may be worthy of further investigation.

The overall conclusion to this section is that the polymer blend membrane comprised of four parts NaAlg to one part PVA and utilizing glycerol plasticizing agent and a support is the optimum membrane for high performance pervaporation tests in this project. Though this membrane may not be suitable for mixed matrix membrane tests (explained in chapter 7) it will be suitable for any other membrane tests.

3.5 Summary

Membrane Support Essential

Optimum pervaporation membrane
• Supported
• Selective layer: plasticized polymer blend
  • Blend: 4:1 ratio of NaAlg:PVA
  • Plasticizer: Glycerol

Pristine PVA remains best material for testing particles for MMMs due to superior mechanical properties

References: Chapter 3

[1] R. Y. M. Huang, R. Pal, and G. Y. Moon, "Characteristics of sodium alginate membranes for the pervaporation dehydration of ethanol–water and isopropanol–water mixtures," *Journal of Membrane Science*, vol. 160, no. 1, pp. 101–113, Jul. 1999.

[2] S. Kalyani, B. Smitha, S. Sridhar, and a Krishnaiah, "Pervaporation separation of ethanol–water mixtures through sodium alginate membranes," *Desalination*, vol. 229, no. 1–3, pp. 68–81, Sep. 2008.

[3] C. K. Yeom, "Characterization of permeation behaviors of ethanol-water mixtures through sodium alginate membrane with crosslinking gradient during pervaporation separation," *Journal of Applied Polymer Science*, vol. 69, no. 8, pp. 1607–1619, Aug. 1998.

[4] Y. Shi, X. Wang, and G. Chen, "Pervaporation characteristics and solution-diffusion behaviors through sodium alginate dense membrane," *Journal of Applied Polymer Science*, vol. 61, no. 8, pp. 1387–1394, Aug. 1996.

[5] R. Russo, M. Malinconico, L. Petti, and G. Romano, "Physical behavior of biodegradable alginate-poly(vinyl alcohol) blend films," *Journal of Polymer Science Part B: Polymer Physics*, vol. 43, no. 10, pp. 1205–1213, May 2005.

[6] C. K. Yeom and K.-H. Lee, "Characterization of sodium alginate and poly(vinyl alcohol) blend membranes in pervaporation separation," *Journal of Applied Polymer Science*, vol. 67, no. 5, pp. 949–959, Jan. 1998.

[7] P. D. Chapman, T. Oliveira, A. G. Livingston, and K. Li, "Membranes for the dehydration of solvents by pervaporation," *Journal of Membrane Science*, vol. 318, no. 1–2, pp. 5–37, Jun. 2008.

[8] A. Jonquières, "Industrial state-of-the-art of pervaporation and vapour permeation in the western countries," *Journal of Membrane Science*, vol. 206, no. 1–2, pp. 87–117, Aug. 2002.

[9] J. Jegal, "Pervaporation separation of water-ethanol mixtures through PVA-Sodium alginate blend membranes," *Journal of Applied Polymer Science*, vol. 51, no. 2, pp. 253–392, Mar. 2003.

[10] R. Y. M. Huang and C. K. Yeom, "Pervaporation separation of aqueous mixtures using crosslinked poly(vinyl alcohol)(pva). II. Permeation of ethanol-water mixtures," *Journal of Membrane Science*, vol. 51, no. 3, pp. 273–292, 1990.

[11] J. Chen, J. Huang, J. Li, X. Zhan, and C. Chen, "Mass transport study of PVA membranes for the pervaporation separation of water/ethanol mixtures," *Desalination*, vol. 256, no. 1–3, pp. 148–153, Jun. 2010.

[12] C. K. Yeom, “Characterization of sodium alginate and poly(vinyl alcohol) blend membranes in pervaporation separation,” *Journal of Applied Polymer Science*, vol. 67, no. 5, pp. 949–959, Jan. 1998.

[13] E. J. Flynn, D. Keane, J. D. Holmes, and M. A. Morris, “Unusual trend of increasing selectivity and decreasing flux with decreasing thickness in pervaporation separation of ethanol/water mixtures using sodium alginate blend membranes.,” *Journal of Colloid and Interface Science*, vol. 370, no. 1, pp. 176–82, Mar. 2012.

[14] B. Guerrier, C. Bouchard, C. Allah, C. Bknard, and P. M. Curie-universitc, “Drying Kinetics of Polymer Films,” vol. 44, no. 4, 1998.

[15] A. G. Yiotis, I. N. Tsimpanogiannis, A. K. Stubos, and Y. C. Yortsos, “Pore-network study of the characteristic periods in the drying of porous materials.,” *Journal of colloid and interface science*, vol. 297, no. 2, pp. 738–48, May 2006.

[16] M. S. Widmer and A. G. Mikos, “Chapter II.5 Fabrication of Biodegradable Polymer Scaffolds fo Tissue Engineering,” in *Frontiers in Tissue Engineering*, Elsevier Science Ltd., 1998, pp. 107–116.

[17] M. P, “Chapter 4.10 Additives,” in *Polymer Chemistry: An Introduction*, Oxford University Press, 1999, pp. 121–126.

[18] L. H. Sperling, “Chapter 1.5: Crosslinking, Plasticizers and Fillers,” in *Introduction to Polymer Science*, 4th ed., John Wiley & Sons Ltd., 2006, p. 18.

[19] L. H. Sperling, “Chapter 8.2: Five Regions of Viscoelastic Behaviour,” in *Introduction to Polymer Science*, 4th ed., John Wiley & Sons Ltd., 2006, p. 361.

[20] T. Karbowiak, H. Hervet, L. Léger, D. Champion, F. Debeaufort, and A. Voilley, “Effect of plasticizers (water and glycerol) on the diffusion of a small molecule in iota-carrageenan biopolymer films for edible coating application.,” *Biomacromolecules*, vol. 7, no. 6, pp. 2011–9, Jun. 2006.

[21] N. Gontard, S. Guilbert, and J. Cuq, “Water and Glycerol as Plasticizers Affect Mechanical and Water Vapor Barrier Properties of an Edible Wheat Gluten Film,” *Journal of Food Science*, vol. 58, no. 1, pp. 206–211, 1992.

[22] J.-W. Rhim, “Physical and mechanical properties of water resistant sodium alginate films,” *LWT - Food Science and Technology*, vol. 37, no. 3, pp. 323–330, May 2004.

[23] L. B. S. Seldon L. Dotson, “Hydrodynamic analysis of calenderable PVC and ABS compounds,” *Journal of Vinyl Technology*, vol. 1, no. 2, pp. 76–83, 1995.

Chapter 4

Lateral-Flow Membrane Development

4 Lateral-flow Membrane Development

Abstract

The earliest phases of lateral-flow membrane research centred on the development of basic viable membranes and attaining a reproducible production method. The simplest membranes were produced with the basic polymer solution composition required for phase inversion; polymer, solvent and non-solvent. Membranes were produced from such lacquers at near cloud point and non-cloud point. The resulting membranes were characterised and assessed in terms of their lateral flow performance. Results showed that – as is seen throughout the membrane work in this thesis – control of skin layer formation in conjunction with control of pore structure is essential to the efficacy of lateral flow membranes. Additionally, bringing lacquers to cloud point is shown to have an effect on both the pore structure and skin layers of the membranes.

4.1 Introduction

The industrial processes involved in developing porous lateral flow cellulose nitrate membranes are long established but poorly understood. Manipulation of these processes for the purposes of optimisation is thus, difficult. In recent years increased competition and a consumer demand for high quality, specialised membranes has driven research toward a greater understanding of the membrane formation process i.e. the phase inversion process.

The aim of the work outlined in this chapter was to produce a viable, basic lateral flow membrane, comparable with the industrial standard produced by Millipore[1]. From there it is possible to study both how the membrane forms through the phase inversion process and how that process, and therefore membrane structure/performance, can be controlled. To do this one must manufacture a membrane from the minimum components required for phase inversion.

The fundamentals of phase inversion are detailed in the *Loeb-Sourirajan*[2] method (outlined in chapter 1, section 1.4.2). For the vapour induced phase separation (*VIPS*)[3–5] three components are required; polymer, solvent and non-solvent[5–7]. The solvent and non-solvent used are dictated by the choice of polymer. Since the industrial standard lateral-flow membrane material is cellulose nitrate (CN), that polymer was chosen to conduct this research (see chapter 1 section 1.4.1). This necessitated the use of acetone as the solvent and water as the non-solvent for two reasons: 1) these are highly effective 2) they are what is used industrially[1], [7]. Thus, the casting "lacquer" for these membrane was one composed of CN (polymer), acetone (solvent) and water (non-solvent) in percentages outlined in chapter 2, section 2.1.3, table 2.3. The drying process for these membranes was done at room temperature (controlled at approximately 25 ^{o}C) and in an oven at elevated temperature (approximately 40 ^{o}C).

The resulting membranes were characterized by SEM and XRD, and tested for lateral flow performance (where possible). These results are presented below (supporting information to results contained in appendix B). In order to test the lateral flow rate of a membrane it must be rendered hydrophilic: As was explained in chapter 1, CN membranes are hydrophobic and must be treated with surfactant in order to achieve this and thus allow for lateral flow of water across/through

them[8]. An SDBS surfactant is used; *sodiumdodecylbenzenesulfate* (see chapter 2 section 2.1.4 for details on procedure).

In the earliest stages of this work it was attempted to produce these membranes without any support material by applying the lacquer directly to glass plates. It was subsequently found that it was not possible to remove the membranes from the glass without damaging them to a point where characterization and lateral flow testing was impossible. Therefore, the membranes were produced on backing (from which the membranes could later be removed easily and without suffering any damage). The material used for backing was again chosen to parallel industrial parameters as much as practically possible on the lab scale. The chosen material was a 100% polyester film (Melinex) of 100, or 50 µm thickness which is used by Millipore for the same purpose (see appendix B, figure B.2 for SEM images of backing material). This material and the experimental procedure of its use are described in chapter 2 section 2.1.4.

The final membranes produced were shown to have poor or, no lateral flow when made from this basic composition of polymer, solvent and non-solvent. This was due to the formation of skin layers which inhibit lateral flow[9]. The formation of these layers and means of preventing them, along with all other results from this section are discussed below.

4.2 Experimental

See chapter 2 for details on all materials, apparatus and procedures.

4.3 Results and Discussion

Table 4.1 shows the basic membranes' lacquer water content for casting. Each membrane was cast with a clear lacquer (BasMemX) and at cloud point (BasMemXCP). Lacquers cast at cloud point have a higher water content than their non-cloud point equivalents for reasons outlined in chapter 1, section 1.4.2. Table 4.1 also shows the flow rates – if any – of the membranes studied and whether or not a skin layer is present.

Table 4.1: Tabulated data showing the water content of the lacquers (casting solutions) of the basic lateral flow membranes (see chapter 2, section 2.1.3, table 2.3 for precise composition of lacquers) produced from lacquers at both cloud point and not. The exact water content required to reach cloud point in the lacquer is shown as is the water content of membranes not cast from lacquers at cloud point (definition of lacquer cloud point given in chapter 2, section 2.1.3). Also shown is the presence of a skin layer in the final membrane and flow rate, if any

Membrane	Water Content of Final Lacquer (weight %)	Lacquer Brought to Cloud Point?	Flow Rate ($cm^2 s^{-1}$)	Skin Layer Present?
BasMemA	0	No	-	No
BasMemACP	15.38	Yes	-	-
BasMemB	4.15	No	-	Yes
BasMemBCP	14.73	Yes	0.005	Yes
BasMemC	8.30	No	-	Yes
BasMemCCP	18.52	Yes	0.002	Minimal
BasMemD	12.45	No	-	Yes
BasMemDCP	20.92	Yes	-	Yes

Examining BasMemA which was cast from 100 % acetone to make a lacquer of 83 wt% acetone and 17 wt% CN; it can be seen from table 4.1 that no skin layer data is present for BasMemACP. This is because the lacquer for this membrane proved uncastable. BasMemA by comparison, was readily castable and produced membranes characterized under SEM; shown in figure 4.1 (below). This lacquer underwent phase inversion to produce final membranes at two temperatures; room temperature (approx. 25 ^{o}C) and in an oven at approx. 40 ^{o}C. This was done to ascertain the effect of temperature on the VIPS method used for our membranes given the profound effect that temperature is reported to have on phase inversion[10], [11].

What was found is that while the membranes produced at both temperatures were too dense for lateral flow purposes the one produced at room temperature appears less dense in cross section (figures 4.1A and 4.1B) than that produced at 40 ^{o}C (figures 4.1D and 4.1E). This is apparent from the respective pore sizes of the membranes. The room temperature dried membrane has pore diameters in the region of 0.2-0.4 µm while the oven dried membrane has pores of <0.2 µm in diameter. Looking at the surface images the same thing is observed; no pore structures in the oven dried membrane (suggesting some skin-layer formation, though this is not observed in cross section; it may be very thin and difficult to observe or, it may be of only slightly higher density than the bulk membrane substructure) compared to pores of 2-4 µm diameter on the surface of the room temperature membrane.

It is tempting to attribute the lack of/small pores in the oven-dried membrane to the higher temperature in the oven and the increase in rate of evaporation of solvent from the lacquer [12], [13]. However, given the nucleation and growth mechanism by which VIPS and phase separation are understood to form pore structures [14], it is likely that the lower amount of atmospheric moisture inside the oven also contributes to the more dense membrane structure produced at 40 ^{o}C.

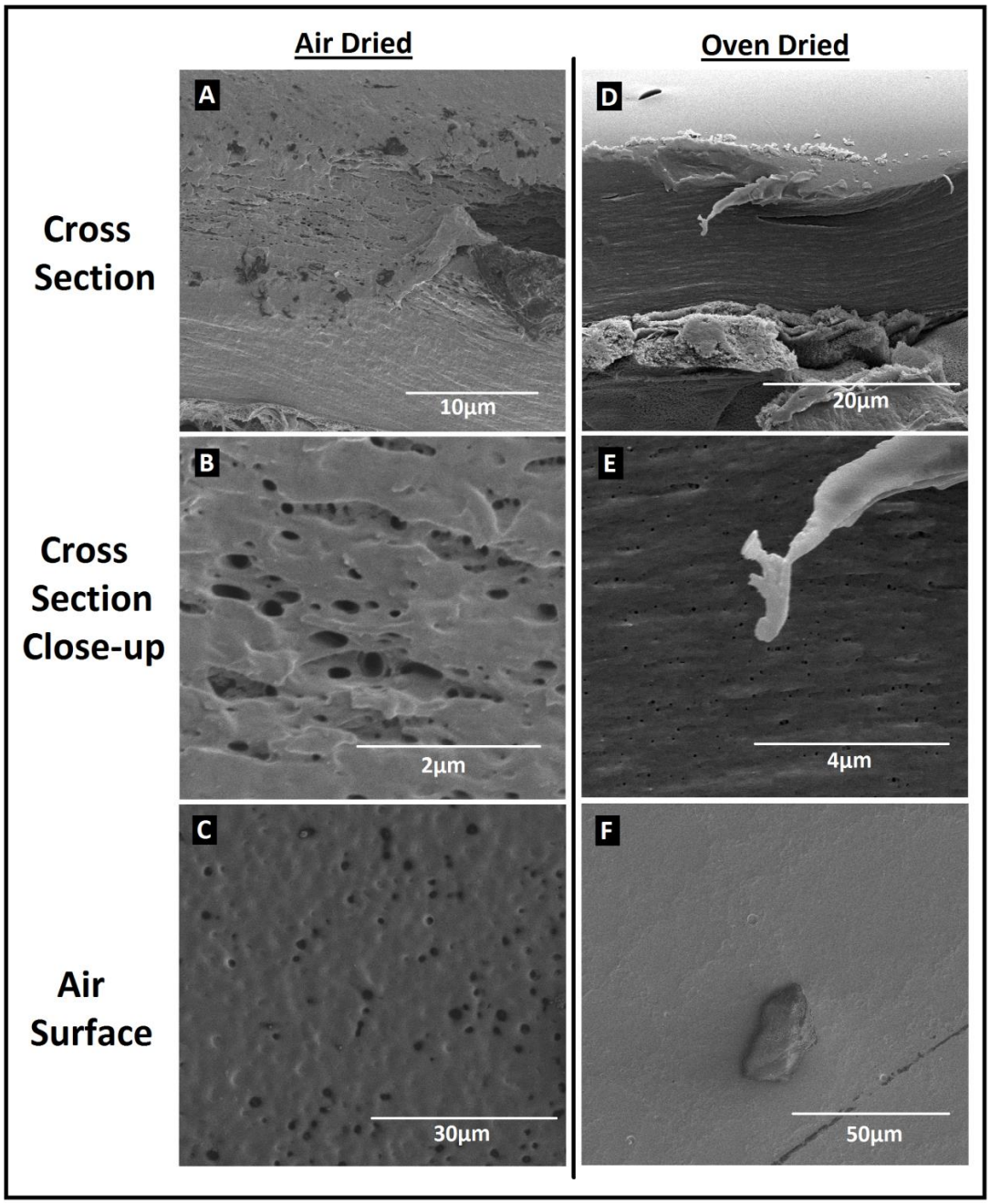


Figure 4.1: SEM images of membranes produced from lacquers of 17 wt% CN dissolved in 100 % acetone. Images A, B and C show cross section, cross-section close-up and surface images respectively of the air dried membrane. Images D, E and F show cross section, cross-section close-up and surface images respectively of the oven dried membrane

Given the respective densities of these membranes, it was concluded that producing membranes at room temperature and humidity was preferable. Considering the potential variability in humidity, future membranes were cast in a controlled humidity environment inside the Mbraun GP 2202 PB single piece moulded glovebox (see chapter 2, section 2.1.4) at 35 % humidity. Neither membrane showed signs of lateral flow when tested.

A series of lacquers were then made in which 50-20 wt% water was used in the solvent mixture with acetone. It was found that greater than 20 wt% water in the mix rendered it ineffective for dissolving CN. Reasons for this are given below.

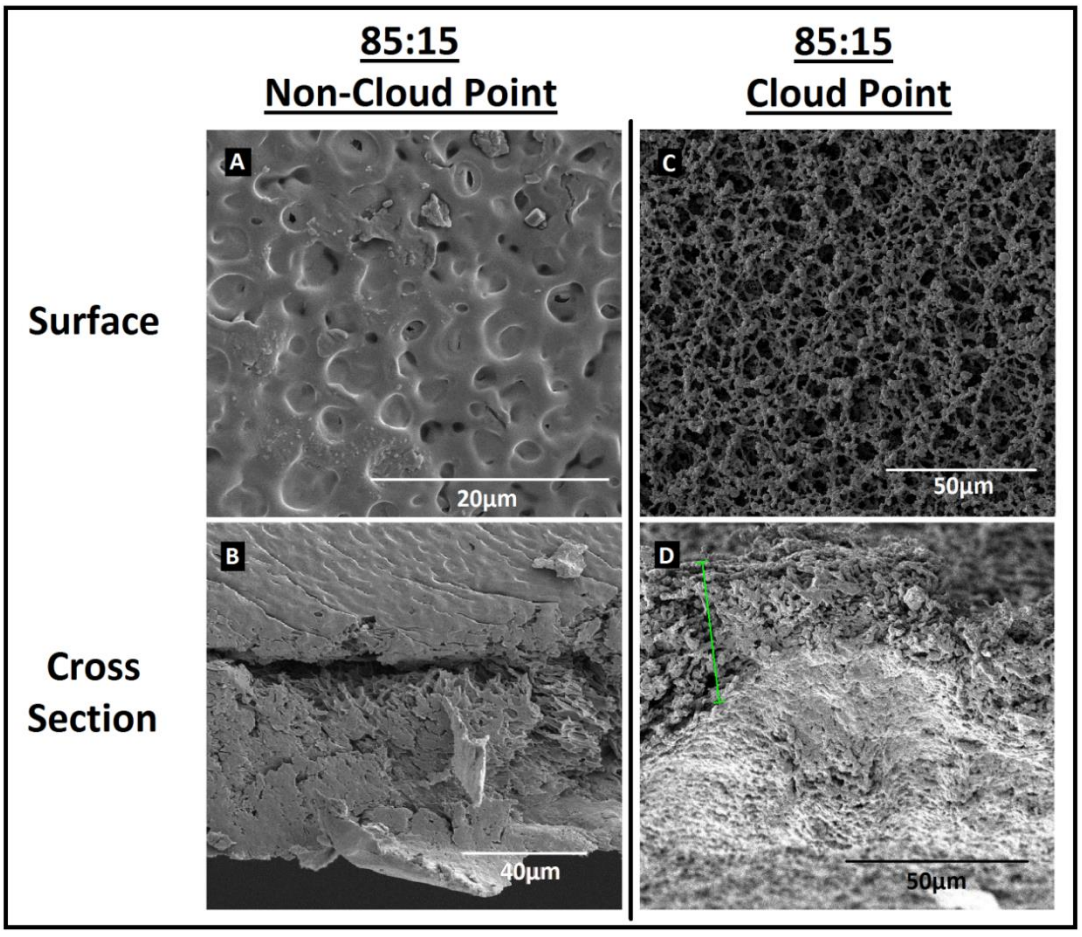


Figure 4.2: SEM images of membranes produced from lacquers of 17 wt% CN dissolved in 85 wt%:15 wt% acetone:water solvent mix and air dried. Images A and B show surface and cross section images respectively of the membrane produced from a lacquer not brought to cloud point. Images C and D show surface and cross section images respectively of the membrane produced from a lacquer brought to cloud point

Chronologically BasMemD and BasMemDCP were then produced. BasMemD contained 85 wt% acetone and 15 wt% water in the solvent mix which was used to dissolve CN. This yielded a lacquer of 17 wt% CN to 70.55 wt% acetone and 12.45 wt% water (see chapter 2 section 2.1.3, table 2.3). BasMemDCP was produced by

taking the aforementioned lacquer and bringing it to cloud point (see chapter 2 section 2.1.3 for details). This resulted in a final lacquer comprising 15.35 wt% CN, 63.73 wt% acetone and 20.92 wt% water (see chapter 2 section 2.1.3, table 2.3 for details on calculations).

SEM images of these membranes are shown in figure 4.2 above and it is immediately apparent that the surface structures of the two membranes differ. The surface of BasMemC (figures 4.2C and 4.2D) is very different to the non-cloud point equivalent (BasMemD; figures 4.2A and 4.2B). The surface image of BasMemD shows the beginnings of pore structures but no open pores in the surface. This is due to the presence of a skin layer which can be seen as a dense region of polymer in the upper part of the cross sectional image (figure 4.2B) separated from the bulk membrane by what appears to be a large macrovoid cavity [11], [15] (although this cavity may simply be the result of the difference in densities of the two regions causing delamination of the skin layer from the membrane bulk). The bulk membrane shows some networked pore structure with pores of approximately 1- 5 µm diameters, however lateral flow testing showed that there was no flow through the membrane despite this; suggesting that the presence of a skin layer inhibits lateral flow.

The structure of BasMemDCP showed a surface (figure 4.2C) that was very open and similar in appearance to equivalent industrial membranes (see appendix B, figure B.3) while the cross section (figure 4.2D) shows a deformed structure which, unlike the industrial equivalents, has great variation in density. This membrane also exhibited no lateral flow upon testing. The lacquer from which it was cast contained over 20 wt% water. This meant that the CN did not dissolve fully in the solvent mixture. The Hildebrand solubility parameters of acetone, and water are 19 and 48$Mpa^{1/2}$ respectively whilst CN is around 22 $Mpa^{1/2}$[16]. Given the relatively similar solubility parameters of acetone and CN and their great difference with that of water, one would expect that as the water content of the solvent mixture increases the solubility of the CN in the solvent mix should decrease, which is what is seen. This yields the fibrous structure seen in the surface and cross sectional images of figure 4.2C and 4.2D. This structure results from the fibrous, raw CN remaining undissolved (see appendix B, figure B.4; in particular figure B.4D).

This is confirmed by examining the XRD profile of the membrane (figure 4.7 below) when compared to that of the raw material (figure 4.5 below) and that of the optimum membrane produced in this series, BasMemBCP (figure 4.6 below). The XRD profile of the raw material – CN (figure 4.5) – shows a sharp diffraction feature at approximately 45 $^{o}2\theta$ of greater intensity (15,000 counts s^{-1}) than the broad feature observed around 22 $^{o}2\theta$ (max. approx.. 11,000 counts s^{-1}). This broad feature is typical of cellulose compounds[17], [18]. There is also a relatively sharp, low intensity (5,700 counts s^{-1}) diffraction feature observed at around 12 $^{o}2\theta$. By comparison, the XRD profile of BasMemBCP (the optimum membrane produced as shown below) shows no sharp diffraction features. The overall signal intensity is reduced and the broad feature typical of cellulose compounds is still observed around 22 $^{o}2\theta$ though with a reduced intensity (max. approx.. 2,200 counts s^{-1}) compared to that observed in the raw material. The lack of sharp features suggests a more amorphous compound with little or no crystalline nature, which would be expected if the polymer is completely dissolved and the membrane produced by the method outlined in chapter 2. The XRD profile of BasMemDCP sits between the two, exhibiting crystalline features of the raw material; most notably a sharp diffraction feature at around 45 $^{o}2\theta$, but this feature – unlike in the raw material – is of a lower intensity (5,500 counts s^{-1}) than the broad feature around 22 $^{o}2\theta$. The general intensity of the signal is higher than that of BasMemBCP but lower than that of the raw material. This suggests that BasMemDCP – which contains 20.92 wt% water (see chapter 2 section 2.1.3, table 2.3 for details on calculations) – is more crystalline than BasMemBCP but less so than the raw material, confirming that the presence of high weight percentage non-solvent – in this instance; water – in the lacquer resulted in raw material – CN – remaining undissolved within it, yielding the membrane structures observed in the SEM images of BasMemDCP (figure 4.2C and 4.2D). Regarding membranes not brought to cloud point; their XRD profiles are similar to that seen for BasMemBCP; no sharp diffraction features and a broad feature, typical of cellulose compounds, observed around 22 $^{o}2\theta$ (see appendix B, figure B.7 for typical XRD profile of BasMemB). This sort of profile is observed for any membrane in which the CN raw material is completely dissolved in the lacquer.

Chronologically BasMemC and BasMemCCP were then produced; BasMemC contained 90 wt% acetone and 10 wt% water in the solvent mix which was used to dissolve CN yielding a lacquer of 17 wt% CN to 74.70 wt% acetone and 8.30 wt% water (see chapter 2 section 2.1.3, table 2.3). BasMemCCP was produced by taking the aforementioned lacquer and bringing it to cloud point (see chapter 2 section 2.1.3 for details). This resulted in a final lacquer comprising 14.73 wt% CN, 66.36 wt% acetone and 18.52 wt% water (see chapter 2 section 2.1.3, table 2.3 for details on calculations).

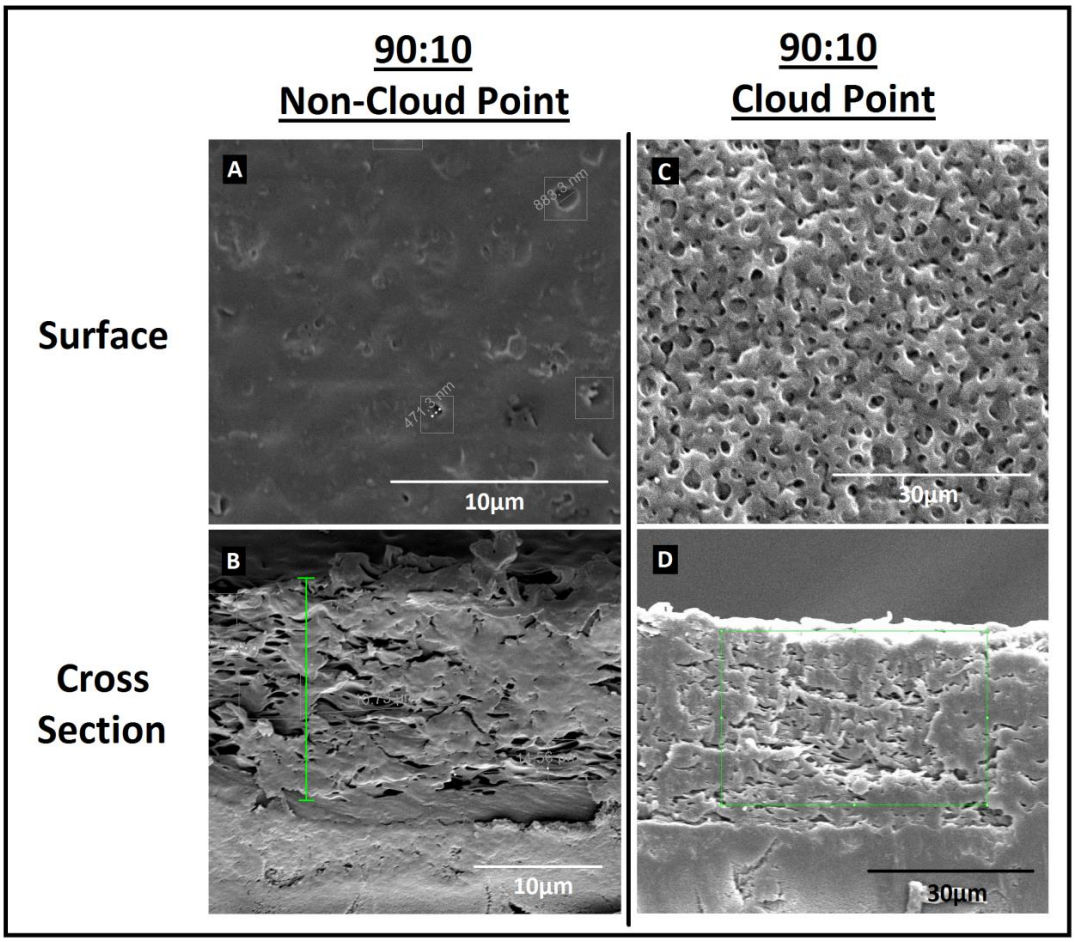


Figure 4.3: SEM images of membranes produced from lacquers of 17 wt% CN dissolved in 90 wt%:10 wt% acetone:water solvent mix and air dried. Images A and B show surface and cross section images respectively of the membrane produced from a lacquer *not* brought to cloud point. Images C and D show surface and cross section images respectively of the membrane produced from a lacquer brought to *cloud point*

Looking first at the surface of the cloud point (BasMemCCP; figure 4.3C) membrane compared non-cloud point membrane (BasMemC; figure 4.3A) it can be seen that there are pores present in the surface of BasMemCCP while there are no open pore structures on the surface of BasMemC. This is evidence of a skin layer on the surface of BasMemC and a lack of one, or a greatly reduced one, on the

surface of BasMemCCP. BasMemC exhibited no lateral flow when tested. The surface pores on BasMemCCP are of 2-3 µm in diameter. In cross section it is difficult to observe any difference between the two membranes.

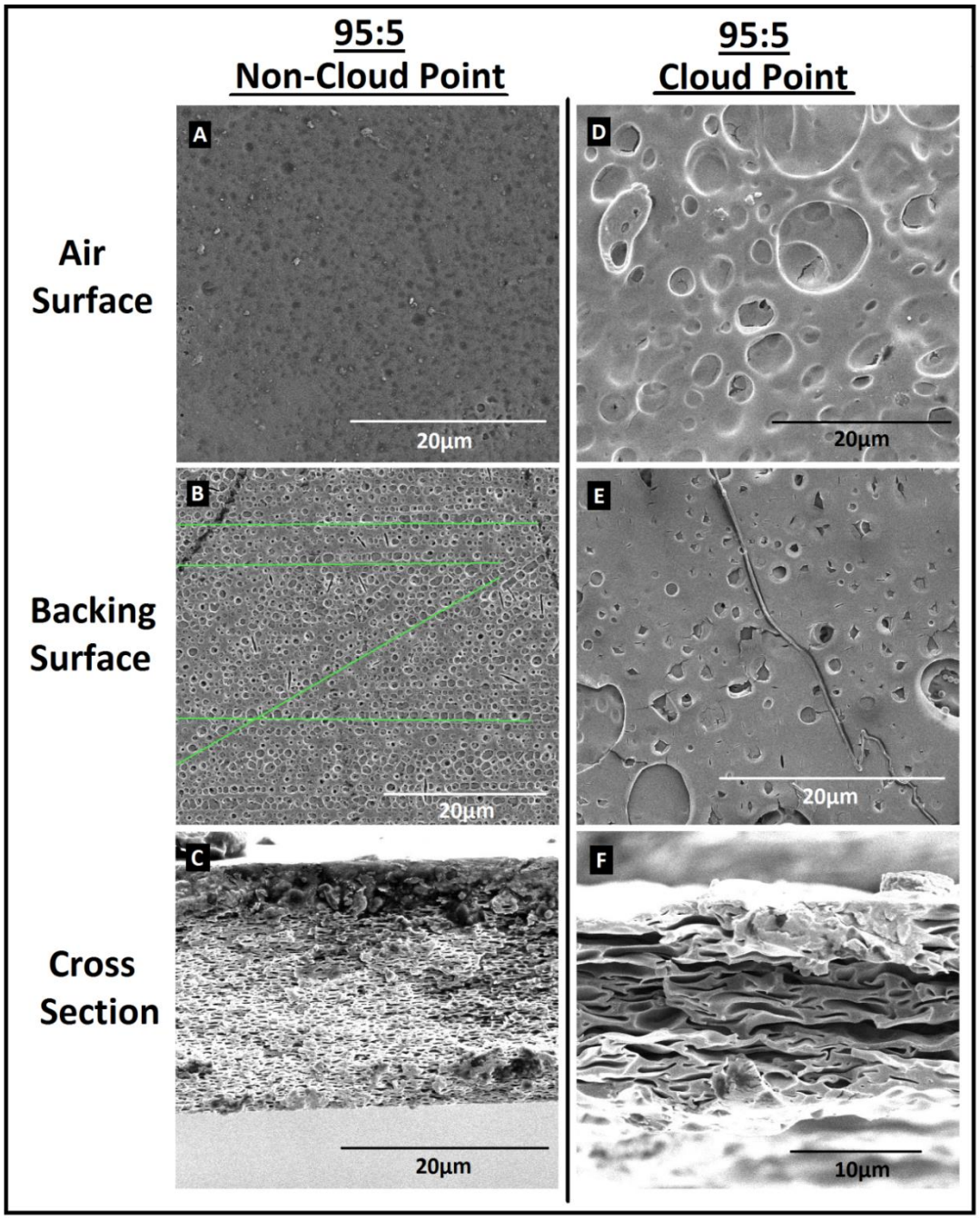


Figure 4.4: SEM images of membranes produced from lacquers of 17 wt% CN dissolved in 95 wt%:5 wt% acetone:water solvent mix. Images A, B and C show air surface, backing surface and cross section images respectively of the air dried membrane produced from a lacquer *not* brought to cloud point. Images D, E and F show cross air surface, backing surface and cross section images respectively of the air dried membrane produced from a lacquer brought to *cloud point*

The bulk membrane structures look broadly similar, however the pores visible in BasMemCCP are slightly larger (2-3 µm in diameter) than those of BasMemCCP

(1-2 µm in diameter). From table 4.1 it should be noted that BasMemCCP is the first to exhibit any lateral flow with a flow rate of 0.002 cm^{-2} s^{-1}. This is dependent on the use of less water in the lacquer than BasMemDCP but more than that used in the lacquer for BasMemA or BasMemACP which effects the formation of skin layers which inhibit lateral flow[9].

BasMemB and BasMemBCP were then produced at room temperature and 35 % humidity. The lacquer for BasMemB was made from a solvent mixture of 95 wt% acetone and 5 wt% water. This mixture was then used to dissolve CN to give a lacquer comprising 17 wt% CN, 4.15 wt% water and 78.85 wt% acetone (see chapter 2 section 2.1.3, table 2.3). BasMemBCP was produced by taking the aforementioned lacquer and bringing it to cloud point (see chapter 2 section 2.1.3 for details). This resulted in a final lacquer comprising 15.12 wt% CN, 70.14 wt% acetone and 14.73 wt% water (see chapter 2 section 2.1.3, table 2.3 for details on calculations).

SEM images of these membranes are shown in figure 4.4 above. Surface images of BasMemB (figure 4.4A) show that a skin layer formed, inhibiting the formation of open pores at the membrane surface: Figure 4.4C confirms this; the cross section showing a distinct layer of greater polymer density at the top of the membrane. By comparison, the surface of BasMemBCP displays larger morphologies (figure 4.4D) than those seen on the surface of BasMemB, however they rarely seem to be open, suggesting – as was the case with BasMemCCP – that there is a skin layer present although it is thinner than that seen in BasMemB. This is confirmed in cross section by figure 4.4F which shows a region of denser polymer at the surface of the membrane. This region is 4-5 µm in thickness in BasMemBCP compared to 7-8 µm thickness in BasMemB. The cross sections of figures 4.4C and 4.4F show that the pore network in the bulk membrane of BasMemB is similar to that seen in BasMemCCP, while the bulk membrane pore network structure of BasMemBCP is far more open than any other membrane observed herein. This structure led to the best lateral flow results obtained from these basic membranes, of 0.005 cm^{-2} s^{-1} flow rate (see table 4.1 above). The shapes of the pores observed in the cross section image of BasMemBCP are oblong, suggesting a collapse of the pore walls, which has been attributed to differences in tensile strength elsewhere[19].

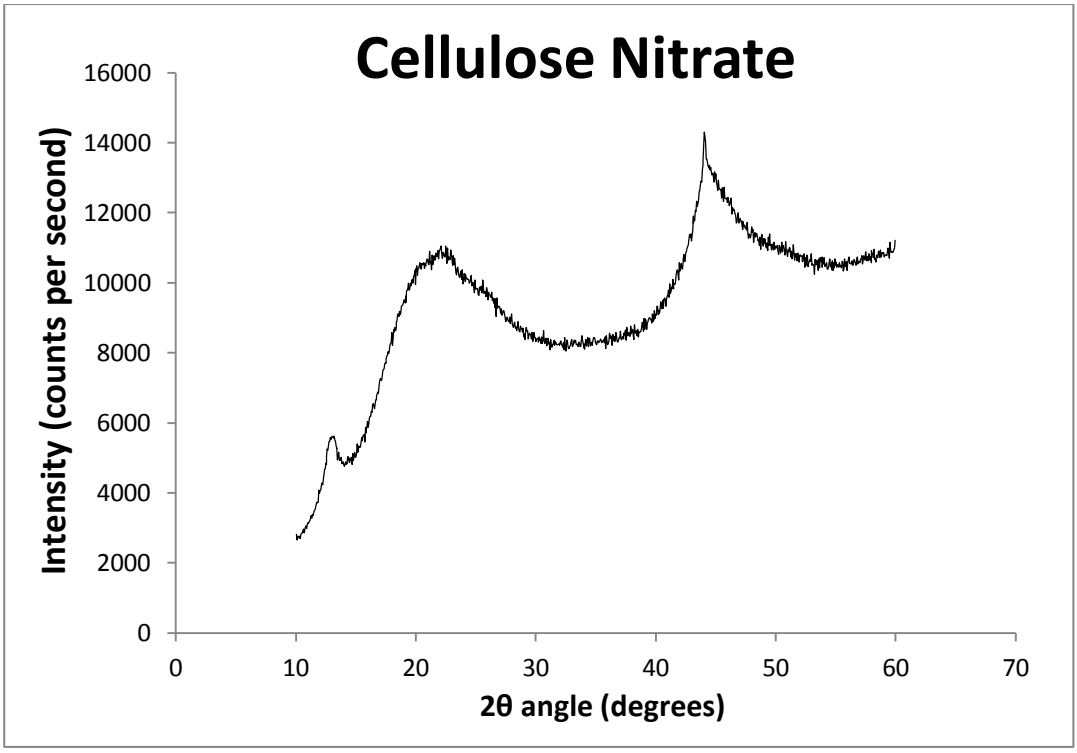


Figure 4.5: XRD profile of the cellulose nitrate polymer before incorporation into lacquer. Shows a sharp diffraction feature at approximately 45 ^{o}2θ (15,000 counts s-1), a broad feature around 22 ^{o}2θ (11,000 counts s-1). Broad feature typical of cellulose compounds. Also a relatively sharp diffraction feature around 12 ^{o}2θ (5,700 counts s-1)

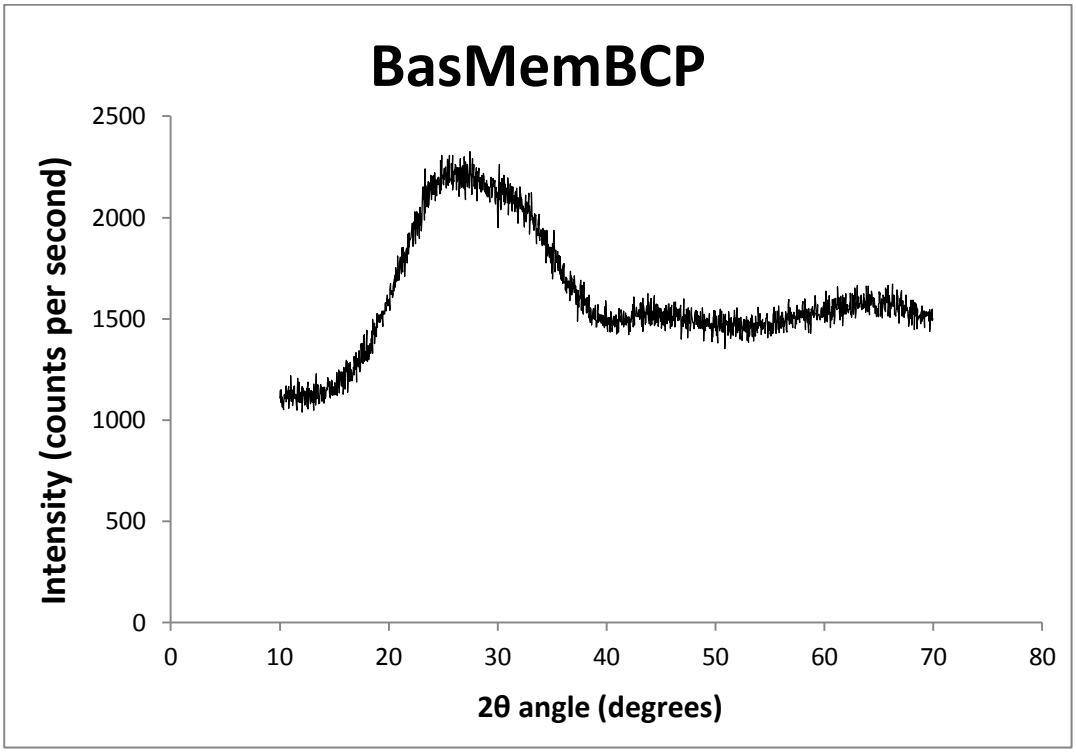


Figure 4.6: XRD profile of BasMemBCP shows no sharp diffraction features. Broad feature typical of cellulose compounds observed around 22 ^{o}2θ (2,200 counts s^{-1})

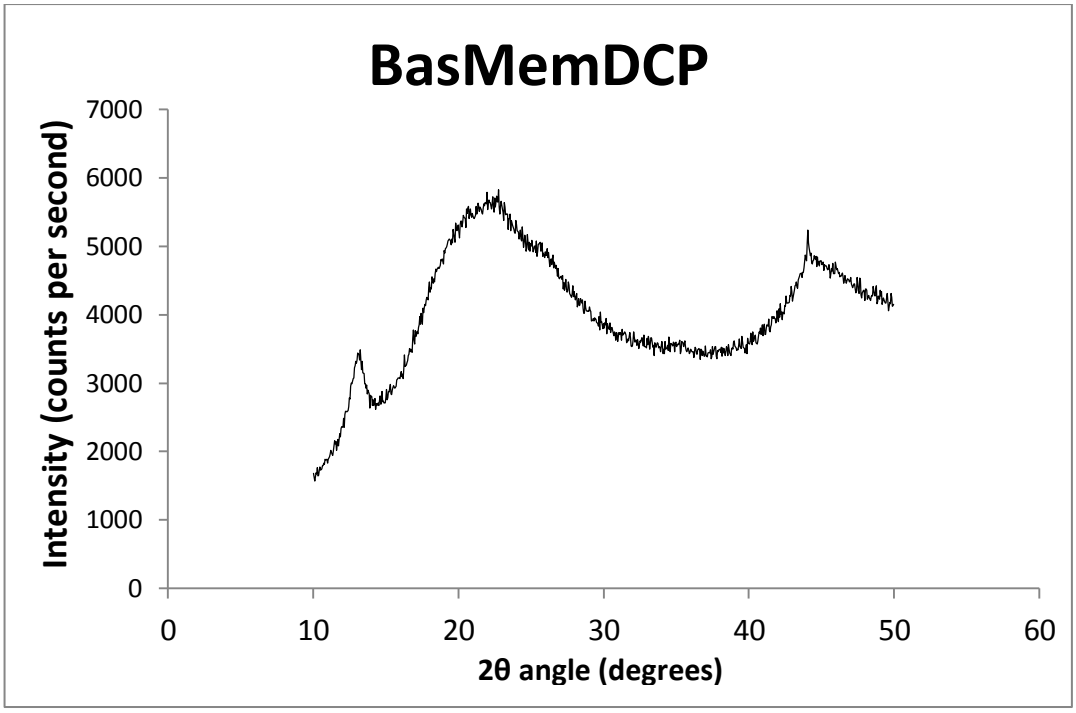


Figure 4.7: XRD profile of BasMemDCP. Sharp diffraction feature at around 45 o2θ, but this feature – unlike in the raw material – is of a lower intensity (5,500 counts s-1) than the broad feature around 22 o2θ

The collapse of the pores may be due to low crystallinity of the membrane making it more malleable. The XRD profile of the membrane (figure 4.6 above) shows a mostly amorphous material with no sharp diffraction features visible and a broad feature observed around 22 ^{o}2θ (max. 127pprox.. 11,000 counts s^{-1}) the only thing of note, suggesting an amorphous material.

The flexibility testing data shows that BasMemBCP is the most flexible of the membranes brought to cloud point with a flexibility of r 3.5 (see figure 4.8 below, and table B.1, appendix B), on a par with the highly flexible supported PVA membranes and unsupported NaAlg membranes seen previously (see chapter 3). This seems to corroborate the idea that the pore structures of the membrane collapsed being more malleable, but looking at the flexibility data again it can be seen that the non-cloud point membranes are all more flexible, so why does one not see this same collapsing of pore structures within? The reason is simple, in the membranes that were not brought to cloud point we see either no pore-formation (BasMemA) or smaller pores (BasMemD and BasMemC) than in BasMemBCP. This means they have thicker pore walls making them more resistant to collapse (flexibility testing; chapter 2 section 2.3.2).

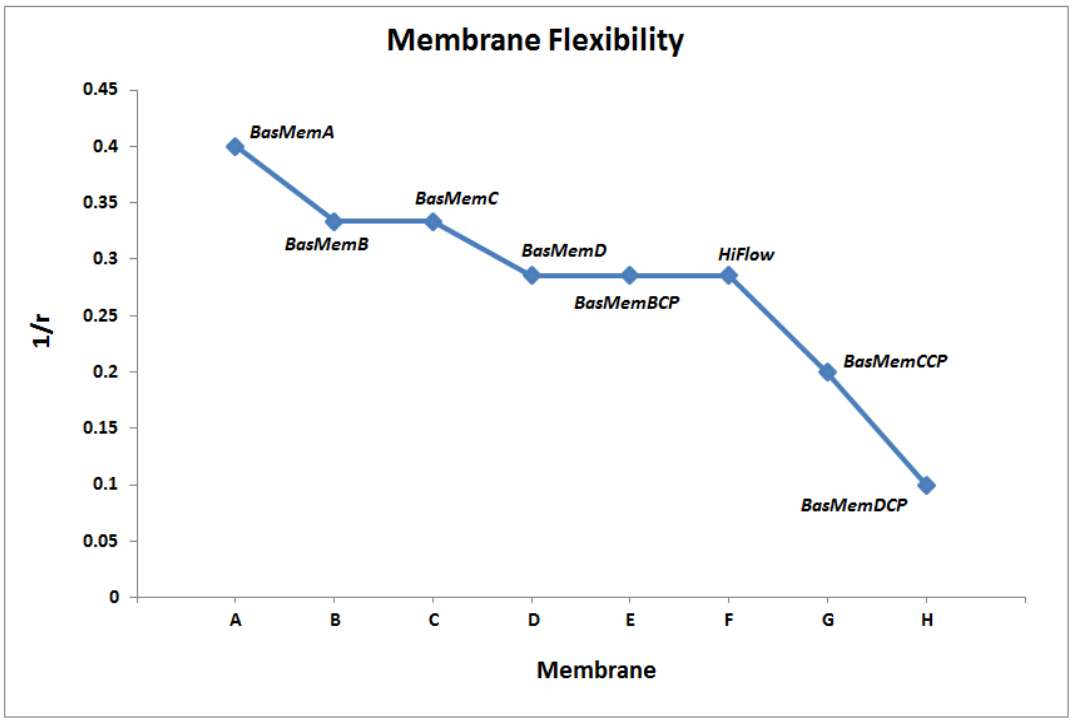


Figure 4.8: Plot of membrane flexibility where r = radius of cylinder (see section 2.3.2). 1/r utilised to facilitate understanding of data; unsupported PVA most flexible membrane therefore, highest on graph

Looking at the rest of the flexibility data it can be seen that the membranes brought to cloud point were all more brittle than those not brought to cloud point. Additionally, the higher the initial lacquer water content before being brought to cloud point the more brittle the membrane, with BasMemDCP being the most brittle/least flexible with a flexibility of r 10.0. BasMemCCP was the next most brittle membrane with flexibility of r 5.0, followed by the industrial membrane; Milipore's HiFlow at r 3.5, the same flexibility as observed for BasMemBCP and BasMemD. BasMemC and BasMemB are the second most flexible membranes both with flexibilities or r 3.0. Finally BasMemA is the most flexible membrane with r 2.5. The XRD profiles of the membranes correlates with the flexibility data in some ways; the most crystalline membrane; BasMemDCP is the least flexible, which is as one would expect[20] (flexibility testing; chapter 2 section 2.3.2).

An unusual morphology was observed in the membranes once Melinex backing was used. It was possible to remove the membranes from the Melinex backing after production to observe the support interface surface. Four significant observations were made; the pores that form at this surface seem to be more open than the corresponding pores at the exposed surface (there is no significant

difference in pore diameter, only in pore volume); there appears to be a skin formed from the flattening of the polymer at the support surface – particularly apparent around the edges of pores (see figure 4.4B above and appendix B, figure B.5); a residue is left behind on the backing material which is made up of the same flattened polymer as observed on the membrane itself (this appears to be part of the same skin layer observed on the underside of the membrane); there are distinct linear patterns visible in the pore distributions (highlighted in figure 4.4B).

Addressing first the linear patterns seen in the membranes; these were only observed in the membranes with acetone content greater than 95 wt% in the solvent mix and were less apparent in membranes brought to cloud point (see appendix B; figure B.6). The reason for them being less apparent is that the skin layer formed at this surface, in the membranes brought to cloud point, maintains its integrity when the membrane is removed from the support (see appendix B, figure B.6B), obscuring the pore structure. The potential reasons for the thicker skin in the cloud point membrane are discussed below. The reason for the formation of linear pore patterns was believed to be connected with the nature of the Melinex backing. Under SEM and AFM analysis the surface images and topographical images respectively show lines in the poly(ethylene terephthalate) (PET) from which Melinex is made. These lines form because of the process by which PET films, like Melinex, are made; extruding and drawing of the polymer[21]. This produces the PET film linearly which results in lines in the material. These are visible under SEM (see appendix B, figure B.2A) and are particularly prominent in SEM cross section (see appendix B, figure B.2B) and can most clearly be seen under AFM (see appendix B, figures B.8 and B.9). It would seem that the lacquer is being channelled along these lines thus forming pores in matching linear distributions during phase inversion.

The greater pore volume at the support side of the membrane is due to the evaporation of solvent from the membrane; the same process which causes skin layer formation at the opposing surface[12], [13]. While the force of solvent evaporation draws polymer molecules upwards, towards the exposed surface, increasing polymer density, decreasing pore volume and creating a skin layer; at the opposite, unexposed, support interface polymer molecules are being drawn *away*, having the opposite effect and increasing pore volume. There is no significant

difference between the pore volume at this surface and that of the bulk membrane due to the effect of the skin layer on evaporation rate once it has formed and the demixing front has moved back through the membrane beyond it (see chapter 1, section 1.4.3)[12].

The flattening of polymer at the support interface and the residue remaining on the support after removal are related, as stated above. Initially the residue was thought to be the result of detached nodules [22] (the occurrence of these morphologies is explained in a later chapter) however upon examination it was found to be the remnants of the thin skin layer formed at this surface. How this layer formed was subject to much speculation: Initially it was thought to be the result of the acetone in the polymer rich phase diffusing through/into the PET support upon liquid-liquid demixing. This would result in a build-up of polymer at the support interface as the acetone content in the polymer rich phase decreased causing the polymer to desolve and create a skin layer.

In order to establish whether acetone would permeate the Melinex, pervaporation tests were conducted using an acetone rich feed solution composed of acetone and water, and Melinex as the membrane. It was found that there was no permeation of the Melinex by acetone *or* water. The conclusion was that diffusion through the membrane was not occurring. Swelling measurements before and after pervaporation was also inconclusive.

Finally, contact angle measurements were obtained (see appendix B, table B.2). These were conducted on both 50 µm and 100 µm thick Melinex. There was no significant difference in the contact angle of water droplets between the two thicknesses of Melinex: The average contact angle on the left side of a droplet for the 2 mm thick Melinex was 77.82^{o} (max. 90.9^{o}, min. 71.3^{o}) while that for the 4 mm Melinex was 80.92^{o} (max. 86.9^{o}, min 74.7^{o}); a 3.1^{o} difference which represents a 1.72% difference between the two (taking 180^{o} to be the max. angle possible) which is not statistically significant. The average contact angle on the right side of a droplet for the 2 mm thick Melinex was 79.41^{o} (max. 89.9^{o}, min. 63.2^{o}) while that for the 4 mm Melinex was 81.71^{o} (max. 89.3^{o}, min. 76.0^{o}); a 2.3^{o} difference which represents a 1.28% difference between the two which is, again, not statistically significant. All the acetone droplet measurements showed that the acetone had a contact angle with the Melinex (regardless of thickness) of less than 15^{o}. This was

below what was measurable by the goniometer but any measurement below 15^{o} is significantly less than that exhibited by the water droplet contact angles (>34.9 % decrease in contact angle over droplet left side contact angle with 2 mm Melinex and >33.0 % decrease over right side. >36.6 % decrease in contact angle over droplet left side contact angle with 4 mm Melinex and >37.1 % decrease over right side). Figures B.10 and B.11 of appendix B show images of a typical water droplet measurement and a typical acetone droplet measurement and the difference between the two is plain to see.

The conclusion here is that the Melinex support is more attractive to acetone than it is hydrophilic. This may result in the formation of a thin layer of the polymer rich phase (which contains the acetone) at the support interface during liquid-liquid demixing with a polymer lean layer above it, which once phase inversion is complete results in the easily detachable thin skin layers observed in SEMs of the support interface of the lateral flow membranes. In membranes not brought to cloud point the acetone content is higher which may result in the formation of a thicker layer, this would explain why the skin layer at this surface appears to have a greater integrity in membranes not brought to cloud point.

Regarding the general properties of lateral flow membranes produced lacquers containing a mix of acetone solvent and water non-solvent; it is certain that bringing the lacquer to cloud-point produces a more porous membrane. Membranes utilising such lacquers develop skin layers at their exposed surface regardless of whether or not the lacquer is brought to cloud point. However, the skin layer in membranes produced from lacquers brought to cloud-point are significantly reduced, which is directly linked to the formation of more open pore networks and thus better lateral flow.

This is due to the higher water content of the membrane lacquers brought to cloud point, which means that the phase inversion process occurs faster, thus the evaporation of solvent from the membrane surface occurs in a smaller timeframe before the demixing front moves back through the membrane, solidifying the skin layer. This has the effect of reducing the skin layer thickness (as it has less time to form) and, since the skin layer is solidified earlier, reducing the evaporation rate of solvent from the bulk membrane below the skin layer, therefore increasing the

timeframe over which phase inversion occurs in the bulk membrane, thus allowing more time for nucleation and growth and so a more open pore network[14].

4.4 Conclusion

Regarding the effect of the Melinex backing on the formation of linear pore patterns; it is highly likely that the linear patterns in the Melinex itself are the source of the linear pore distributions observed at the support interface of the membranes. Future experiments utilising a Melinex film without these lines to produce a lateral flow membrane and observe whether or not the linear pore distributions are present would allow us to confirm this. However, no such film exists to the best of our knowledge, due to the linear extrusion process by which polyethylene terephthalate (PET) films of this type are produced. The pore distributions have no discernible effect on lateral flow performance as they do not occur throughout the bulk membrane but only in the immediate region above the support interface.

Regarding the skin layer formed at the support interface; the evidence showing the greater affinity for acetone than water of the Melinex backing explains this phenomenon in part. Using an impermeable, hydrophilic support would, in theory create a skin layer as well; through the formation of a polymer lean phase layer at the support interface with a corresponding polymer rich phase layer above it, during liquid-liquid demixing. In order to confirm that this is what is occurring, future experiments would be conducted using an impermeable, non-polar support material which would, theoretically, eliminate the skin layers. This would be a costly – though simple – venture but, since the residue left by these skin layers on the support material has been cited as a problem industrially it may be suitable for further investigation.

Regarding the general properties of the lateral flow membranes; it is certain that bringing the casting lacquer to cloud point produces a better lateral-flow membrane. Greater control of the evaporation rate of solvent from the membrane, through the control of the solvent and non-solvent affinities [23] for one another may inhibit the formation of skin layer entirely, thus increasing pore size and the openness of formed pore networks. An increase in the crystallinity of the polymer in the final membrane may inhibit the collapse of the pore network structure as seen

in the membranes above. This is the subject of the investigations outlined in chapter 6.

4.5 Summary

Membrane must be supported • 100µm thick Melinex support material
Casting lacquer must be brought to cloud point
Optimum lacquer composition • 15.12wt% CN • 70.14wt% Ace • 14.73wt% water
Phase inversion - vapour induced phase separation (VIPS)
Lateral flow rate • 0.005cm2 s-1
Skin layer present • Inhibits and retards lateral flow
Lateral flow rate poor compared to industrial standards • Fastest industrial membrane; Milipore HF075   • flow rate: 0.053cm2 s-1
Greater control of evaporation rate of solvent from membrane required in prevent skin layer formation • Control of solvent - non-solvent affinities is key

References: Chapter 4

[1] M. A. Mansfield, “Chapter 6: Nitrocellulose Membranes for Lateral Flow Immunoassays: A Technical Treatise,” in *Lateral Flow Immunoassay*, 2009, pp. 95–115.

[2] S. S. Sidney Loeb, “Sea Water Demineralization by Means of an Osmotic Membrane,” in *Saline Water Conversion—II*, American Chemical Society, 1963, pp. 117–132.

[3] H. Chae Park, K. Yoon Po, K. Hwa Yong, and K. Yong Su, “Membrane formation by water vapor induced phase inversion,” *Journal of Membrane Science*, vol. 156, no. 2, pp. 169–178, Apr. 1999.

[4] O. K. Matar, G. F. Hewitt, and E. S. Ortiz, “Phase Inversion in Liquid-Liquid Dispersions,” *System*, 1989.

[5] H. Sun, S. Liu, B. Ge, L. Xing, and H. Chen, “Cellulose nitrate membrane formation via phase separation induced by penetration of nonsolvent from vapor phase,” *Journal of Membrane Science*, vol. 295, no. 1–2, pp. 2–10, May 2007.

[6] H. Chae, Y. Po, H. Yong, and Y. Soo, “Membrane formation by water vapor induced phase inversion,” *Journal of Membrane Science*, vol. 156, no. 1, pp. 169–178, 1999.

[7] Millipore-Corporation, *Rapid Lateral Flow Test Strips: Considerations for Product Development*. Lit. No. TB500EN00. Bedford, MA., 2002.

[8] K. Jones, “Chapter 7: FUSION 5: A New Platform For Lateral Flow Immunoassay Tests,” in *Lateral Flow Immunoassay*, 2009, pp. 115–131.

[9] C.-C. Ho and A. L. Zydney, “Protein Fouling of Asymmetric and Composite Microfiltration Membranes,” *Industrial & Engineering Chemistry Research*, vol. 40, no. 5, pp. 1412–1421, Mar. 2001.

[10] C. K. Haas and J. M. Torkelson, “Two-dimensional coarsening and phase separation in thin polymer solution films,” *Physical Review E*, vol. 55, no. 3, pp. 3191–3201, 1997.

[11] P. Van De Witte, J. W. A. Van Den Berg, and J. Feijen, “Phase separation processes in polymer solutions in relation to membrane formation,” *Journal of Membrane Science*, vol. 117, pp. 1–31, 1996.

[12] A. G. Yiotis, I. N. Tsimpanogiannis, A. K. Stubos, and Y. C. Yortsos, “Pore-network study of the characteristic periods in the drying of porous materials.,” *Journal of colloid and interface science*, vol. 297, no. 2, pp. 738–48, May 2006.

[13] B. Guerrier, C. Bouchard, C. Allah, C. Bknard, and P. M. Curie-universitc, “Drying Kinetics of Polymer Films,” vol. 44, no. 4, 1998.

[14] S. P. Nunes and T. Inoue, “Evidence for Spinodal Decomposition and Nucleation and Growth Mechanisms during Membrane Formation,” *Journal of Membrane Science*, vol. 111, no. 1, pp. 93–103, 1996.

[15] A. L. Ahmad, S. Low, and S. Shukor, “Effects of membrane cast thickness on controlling the macrovoid structure in lateral flow nitrocellulose membrane and determination of its characteristics,” *Scripta Materialia*, vol. 57, no. 8, pp. 743–746, Oct. 2007.

[16] A. F. M. Barton, *CRC Handbook of Polymer-Liquid Interaction Parameters and Solubility Parameters*. CRC Press, 1990.

[17] S.-J. Kim, A. A. Dwiatmoko, J. W. Choi, Y.-W. Suh, D. J. Suh, and M. Oh, “Cellulose pretreatment with 1-n-butyl-3-methylimidazolium chloride for solid acid-catalyzed hydrolysis.,” *Bioresource technology*, vol. 101, no. 21, pp. 8273–9, Nov. 2010.

[18] P. Bubner, J. Dohr, H. Plank, C. Mayrhofer, and B. Nidetzky, “Cellulases dig deep: in situ observation of the mesoscopic structural dynamics of enzymatic cellulose degradation.,” *The Journal of biological chemistry*, vol. 287, no. 4, pp. 2759–65, Jan. 2012.

[19] G. C. Li, P. Zhang, H. P. Zhang, L. C. Yang, and Y. P. Wu, “A porous polymer electrolyte based on P(VDF-HFP) prepared by a simple phase separation process,” *Electrochemistry Communications*, vol. 10, no. 12, pp. 1883–1885, Dec. 2008.

[20] M. P. Stevens, “Chapter 3: Chemical Structure and Polymer Morphology,” in *Polymer Chemistry: An Introduction*, Oxford University Press, Inc., 1999, pp. 61–95.

[21] A. Peterlin, “Drawing and extrusion of semi-crystalline polymers,” *Journal of Colloid and Polymer Science*, vol. 265, no. 5, pp. 357–382, 1987.

[22] C. K. Haas and J. M. Torkelson, “Two-dimensional coarsening and phase separation in thin polymer solution films,” *American physical Society: Physical Review E*, vol. 55, no. 3, pp. 3191–3201, Mar. 1997.

[23] T. Young and L. Chen, “Pore formation mechanism of membranes from phase inversion process,” *Desalination*, vol. 103, no. 3, pp. 233–247, Dec. 1995.

Chapter 5

Advanced Pervaporation Membranes: Control of Skin-Layer

5 Advanced Pervaporation Membranes: Control of Skin Layer

The following is adapted from "*Unusual Trend of Increasing Selectivity and Decreasing Flux with Decreasing Thickness in Pervaporation Separation of Ethanol/Water Mixtures using Sodium Alginate Blend Membranes*". Journal of Colloid and Interface Science, Volume 370, Issue 1, 15 March 2012, Pages 176–182

Abstract

Pervaporation membranes were produced comprising a 4:1 sodium-alginate:poly(vinyl-alcohol) polymer blend selective layer with a plasticizing agent (glycerol). Membranes were supported on a poly(acrylonitrile) mesoporous support layer and non-woven fabric base. Pervaporation separation of ethanol/water mixtures was carefully followed as a function of film thickness and time. It was found, contrary to what might be expected from literature, that these films showed increased selectivity and decreased flux as film thickness was reduced. It is argued that the morphology and structure of the polymer blend changes with thickness and that these structural changes define the efficiency of the separation in these conditions.

5.1 Introduction

Pervaporation is a membrane separation technology used industrially for solvent dehydration and separation of organic mixtures and has a significant advantage over other separation methods in that it can be used to effectively separate azeotropic mixtures. Because of this, pervaporation may have considerable importance in water-ethanol separation and thus, allow low water content, fuel grade ethanol to be generated [1]. Sodium alginate (NaAlg), a naturally occurring polysaccharide, is a suitable choice of membrane for water/ethanol separation because it is partially soluble in water whilst it is insoluble in ethanol[2]. When exposed to a water-ethanol mixture the membrane will swell with water molecules, and in pervaporation, water will permeate through the membrane allowing separation. Because of the vacuum on the permeate side of the membrane, there will be a diffusion profile across it as shown in Figure 1. On the retentate side of the membrane, swelling will be almost complete and the glass transition temperature (T_g) of the of the polymer will be significantly lowered to a point where the feed side of the membrane is above the effective T_g ensuring that it is in a rubbery state. On the permeate side of the membrane, the water content is lower so that the temperature is below T_g and so in a glassy state. Between, the two sides of the membrane there will be a region where there is a transition between the two polymer states.

Whilst NaAlg has an almost ideal chemistry for this separation, it is mechanically unstable and thin membranes cast from solutions of pure NaAlg are brittle and prone to cracking [3], while pervaporation membranes suffer from a loss in performance over time due to *relaxation* [1], [4]. This limits the practicality of the use of these systems in industrial environments. Relaxation is the process by which residual stresses in a polymeric glass are released changing the polymer's physical and mechanical properties. These residual stresses are a result of non-equilibrium derived from changes in structure and mobility of the polymer chain matrix at the glass transition temperature (T_g)[5].

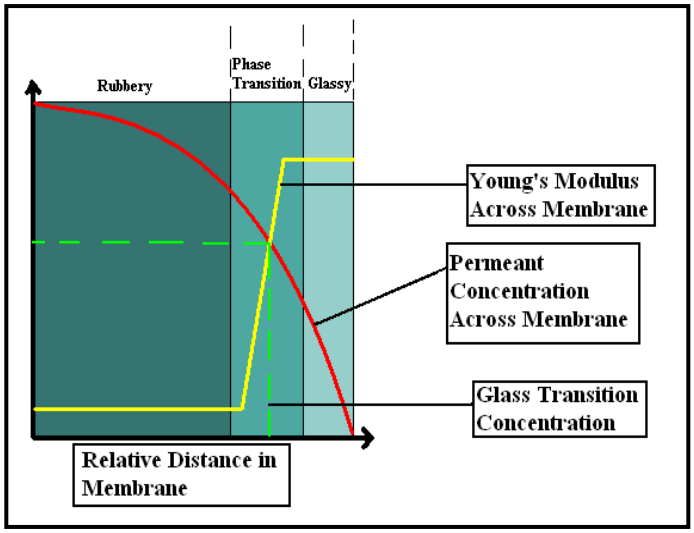


Figure 5.1: Schematic of a diffusion profile across a pervaporation membrane

As a polymer is cooled through the T_g the structural changes required to maintain thermodynamic equilibrium cannot occur in the time scale of cooling and residual stress is present. In a pervaporation process, the membranes are particularly prone to relaxation related damage because of the variation in the effective T_g and Young's modulus across the membrane. It is important to note that relaxation would occur almost instantly in the rubbery state and very slowly in the glass state resulting in stress variation across the membrane.

The focus of our work described here has been to reduce membrane thickness, thus minimising relaxation effects by limiting the thickness of the glassy phase. This should enable development of a membrane synthesis procedure whereby efficient separations can be achieved over long periods. The use of pristine sodium alginate was the experimental ideal, but initial testing proved that the mechanical and chemical stabilities of pristine sodium alginate membranes are too poor to permit long periods of testing required for the membrane system to reach equilibrium. This lack of stability becomes more of a problem as membrane selective layer thickness decreases. As such, in order to achieve suitably thin membrane layers it is necessary to use polymer blends and composition modifications as well as membrane supports to provide mechanical robustness (see chapter 2 section 2.1.2 for details). This means that the approach contrasts many academic studies of these systems but the methodology is applicable to use in commercial environments. In this chapter, it is demonstrated that this membrane type produces highly unexpected results, with high performance characteristics,

while expected trends in pervaporation performance and film thickness were not observed.

5.2 Experimental

See chapter 2 for details on all materials, apparatus and procedures.

5.3 Results and Discussion

The aspects of solution diffusion theory concerning diffusion in polymers have not been fully explained in literature due to the difficulties with calculation of diffusion coefficients in polymer membranes[4]. Observed decreases in flux with membrane thickness are normally explained by relaxation theory as outlined by Yeom[1]. As membrane thickness decreases, the relative increase in the glassy region results in a flux decrease. However, the results here need this model to be refined to provide understanding of the more complex variation in flux and selectivity with membrane thickness.

5.3.1 DSC

It is highly important for operation of pervaporation membranes that the T_g exceeds that of the operation temperature so that the combination of rubbery and glassy properties described above are maintained. The T_g of NaAlg is 119 ^oC whilst PVA is around 85 ^oC[7]. The T_g value of the selective membrane layers used here (i.e. NaAlg + PVA + plasticizer) was 96^oC as determined by DSC (see figure 2). This is significantly higher than the 60^oC operating temperature of pervaporation unit and should ensure that the membrane has the correct structure during use. However, the endotherm in the DSC is very broad and suggestive of considerable interactions or cross-linking between the various components. The endotherm at 240 ^oC can be assigned to a melting point. The value is significantly lower than that of NaAlg (>300 ^oC) but greater than that of PVA (180 – 190 ^oC)[8]. This also suggests that the systems are miscible with strong interactions or cross-linking between the components.

5.3.2 XRD:

Powder XRD studies of the 24 μm as cast membranes were also made (figure 5.2) and the data does suggest significant amounts of crystallization and possible cross-

linking have occurred confirming the DSC results. Three broad diffraction features are seen at about 11.5, 20.8 (and a higher angle shoulder that can just be resolved by fitting at about 23-25°) and 43.5 °2θ. Very similar broad features in positions and with peak shapes close to this have been seen previously for calcium ion cross-linked NaAlg-PVA membranes[9] as well as chemically cross-linked PVA-gelatine membranes and are generally typical of amorphous or very weakly crystalline samples[10]. Diols, dialdehydes and - particularly relevant - glycerol have all been used to crosslink similar systems[11]. Cross-linked PVA can also produce some very sharp features [9], [12] and the feature at 28 °2θ seen here suggest some highly crystalline cross-linked material is present. The value of these sharp features (~ 28 °2θ) are significantly higher than for PVA alone (~ 20 °2θ) and does suggest there has been structural modification by the NaAlg consistent with extensive cross-linking. In figure 5.2, the data with the higher concentration of glycerol also shows slightly narrower XRD features (since the peaks at 11.5 and 20.8 °2θ are better resolved) and this does support the suggestion that the glycerol is acting as a cross-linker. This is further confirmed in figure 5.3A where a 60 μm as cast film was studied to compare with the usual preparation (containing glycerol) and one in the absence of glycerol. It can be seen, that the presence of glycerol does very significantly enhance the crystalline features and discrete, sharp and well-resolved diffraction features are clearly observed.

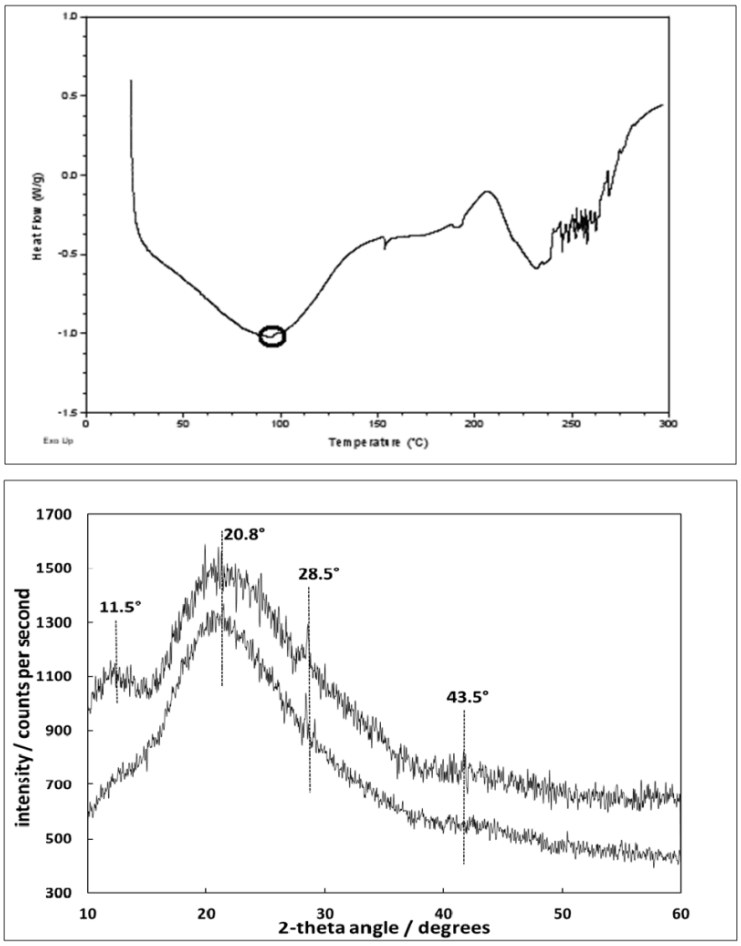


Figure 5.2: Upper image: DSC curve for the 4:1 ratio NaAlg:PVA selective membrane. Lower image: XRD curves for same membrane with additional glycerol; upper curve contains 5 g glycerol; lower curve contains 4 g (bottom)

Interestingly, there is a variation of crystallinity with film cast thickness. This is shown in figure 5.3B. Data was consistent for all samples studied but only cast thicknesses of 40, 100 and 600 μm are shown for illustration purposes. At 40 μm cast thickness, sharp diffraction features are very weak and almost undetectable. At 60 μm they become readily observed (figure 5.3A) but are much lower in intensity than the broad feature around 20 °2θ. At a cast thickness of 100 μm they are now around the same intensity as the broader feature at about 20 °2θ and this increasing contribution of crystalline features increases with cast thickness until a thickness of 600 μm when they dominate the diffraction profile and suggest a highly crystalline material is present.

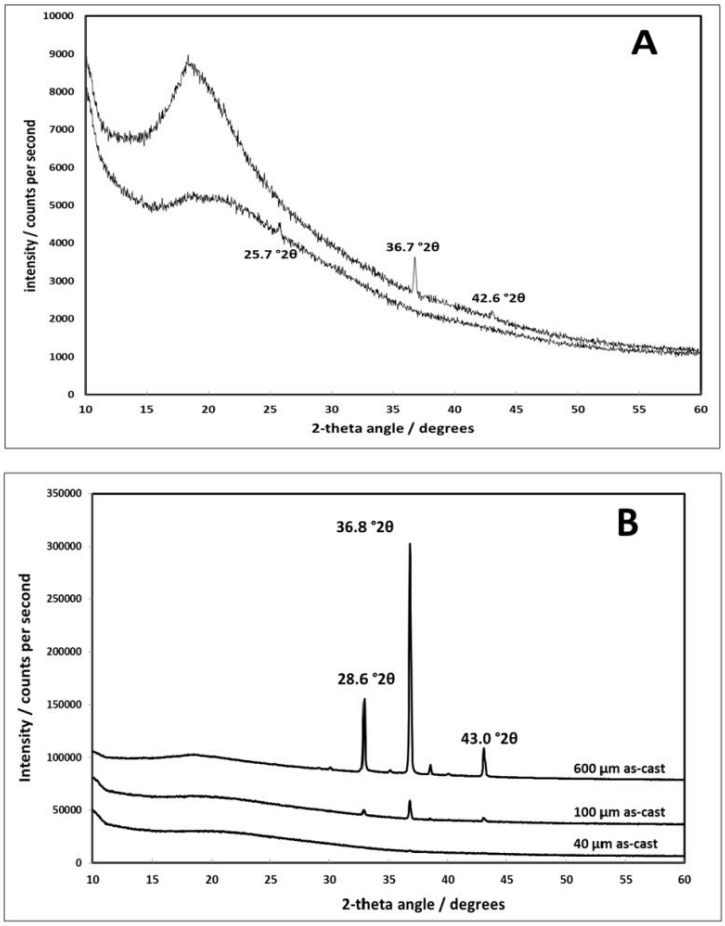


Figure 5.3: (A) XRD profiles of 60 um films with and without glycerol addition. (B) XRD profiles of membrane films (with PVA and glycerol) as a function of cast thickness as described in figure

This is corroborated by the flexibility data shown in appendix C; as the membrane selective layer thickness decreases, the membrane becomes more brittle, suggesting a greater crystallinity in the polymer (see appendix C, table C.2).

NaAlg and PVA polymers are hydrogel forming systems[12], [13]. It is generally accepted that these hydrogels consist of three components [12]; a porous matrix (which stores water molecules), amorphous polymer walls (highly swollen with water molecules) defining the porous structure, and crystalline cross-links that define the links between the amorphous walls. The links are dense and essentially not swollen due to the crystallinity and cross-linking present. NaAlg and PVA are relatively easily crosslinked[9], [14–16].

Cross-links increase hydrophobicity and consequently decrease water uptake[17][18]. Since the effectiveness of pervaporation membranes is related to the ability of molecules to pass through the polymer matrix, solvent parameters, which measure the surface cohesive energy and describe the chemical similarity

between molecules and their environment, are a useful method of understanding this phenomena[19]. Various solvent parameters for polymers and solvents are widely reported[8], [19]. If solvent parameters (δ) are similar, the materials will be soluble. In the case of polymers, the polymer will swell in that material. Hydrophobic systems have low values of δ and hydrophilic systems high values. The solvent parameters of water and ethanol are 48 and 26.2 $Mpa^{1/2}$ respectively. The solvent parameter of sodium alginate is difficult to measure but it appears to be at least 37 $Mpa^{1/2}$[20]. This explains why it is an effective pervaporation membrane material, as the value indicates a highly hydrophilic material. Although glycerol also has a high value of (36.2 $Mpa^{1/2}$), once it cross-links - removing hydroxyl groups - the δ value will decrease towards that of polyglycerolic acid which has a value of around 25 $Mpa^{1/2}$ making it closer to that of ethanol (26.2 $Mpa^{1/2}$). It would also be expected to reduce the δ value of the sodium alginate and PVA by removal of the hydroxyl groups on these. Thus, cross-linking in this system might be expected to decrease the hydrophilicity of the membranes as suggested above.

This relationship of cross-linking to hydrophobicity can be used to explain the rather unexpected trends in selectivity with cast film thickness seen in figure 5.7 below. It would be expected that a highly hydrophilic membrane would selectively swell and allow permeation of the most hydrophilic molecule (i.e. water) and, as observed, the permeate flux would largely be water. As membrane thickness increases it would be expected that the selectivity would also increase. However, as the Yiotas model shows, the thicker films show enhanced relaxation and densification because the solvent evaporation rate is slower[21]. If it is assumed that this slow evaporation and densification also leads to increased cross-linking and crystallization (as reaction time is increased) as shown in figure 5.3, it can be suggested that the films of greatest cast thickness are also the most hydrophobic. The solvent parameters of these hydrophobic films are considerably reduced towards that of ethanol and the permeation of this molecule becomes more probable, decreasing selectivity. In this way, selectivity increases with decreasing cast thickness. The decrease of selectivity for the 24 μm film is probably related to the small amount of material present which allows some ethanol penetration.

5.3.3 SEM:

Cross-sectional and top view SEM images of the as-prepared membranes are provided in figure 5.4 (400, 150, 100 and 80 μm) and figure 5.5 (60, 50, 40 and 24 μm). At the bottom of each cross-section, the porous PAN support can be seen as a disordered honeycomb type structure. The mottled film above it is the active NaAlg:PVA membrane. This sometimes appears detached from the support; this is believed to be a result of thermal shock on liquid nitrogen cooling in the CRISP method (outlined in chapter 2). The structure of the bulk of this membrane layer is reasonably consistent, composed of irregular and undulating strata or lamellae in a direction approximately parallel to the surface plane. The upper surface (top-down images) is not consistent and can vary from sample to sample and across the samples. The films generally appear to be crack-free and - where seen - are thought to result from sample preparation for microscopy studies. Some of the films appear to be somewhat porous but there was no evidence of this porosity in the cross-sections. When examined under higher magnification (e.g. 150 μm film, figure 5.4) they appear to be crater-like structures resulting from solvent pooling. It is, therefore, concluded that the surface is quite regular with little sign of penetrative pore structures and at the surface the polymer has a denser structure than in the bulk.

It is apparent from the cross-sectional data that the selective membrane thickness attained on drying is much lower than the as-cast thickness due to solvent removal during drying. However, a plot of selective layer thickness shows a well-resolved minimum in terms of selectivity; clearly the selective layer formation is more complex than expected. A simple formation process is expected to give a linear variation of cast to measured thickness as the ratio of the volume of polymer to the volume of solvent is constant. These data suggest that the selective membrane is becoming less dense on average as the film thickness decreases (see appendix C, table C.1). The distinct minimum in the selectivity figures (see figure 5.7) is due to decreasing density with film thickness (membrane films are thicker than expected) and an opposing trend that film thickness decreases with as-cast thickness. The relative density of the film (compared to a fully dense film) can be calculated from the measured volume of the film per cm^{-2} and the theoretical volume of polymer from the cast solution concentration. The variation of this

calculated relative density shows the 400µm film to be close to full density (~95%) but as thickness decreases, density progressively reduces to a minimum value of ~6.7 %. The variation in the density of the membrane film with thickness can be explained using the relaxation effects discussed above. Yiotis *et al* have described how polymer films cast from solution are strongly dependent on evaporation rate[21]. Relaxation effects should also be considered in these polymer film models and it is suggested that membranes formed immediately after casting are fully (solvent) swollen and the polymer chains are highly mobile and, hence, contain significant free volume from both chain mobility etc. as well as solvent inclusion. As solvent drying is limited by the surface area of the membrane thicker membrane films will dry more slowly, this allows the films to move towards equilibrium or relaxed structures, rendering them denser. For thinner films, drying will be much more rapid and these very open polymer chain arrangements will be 'frozen-in' forming highly non-equilibrium structures. These different selective membrane film structures will play an important role in determining pervaporation performance. What also might be expected to change membrane separation performance is the morphological variation observed in the SEM images (figures 5.3 and 5.4).

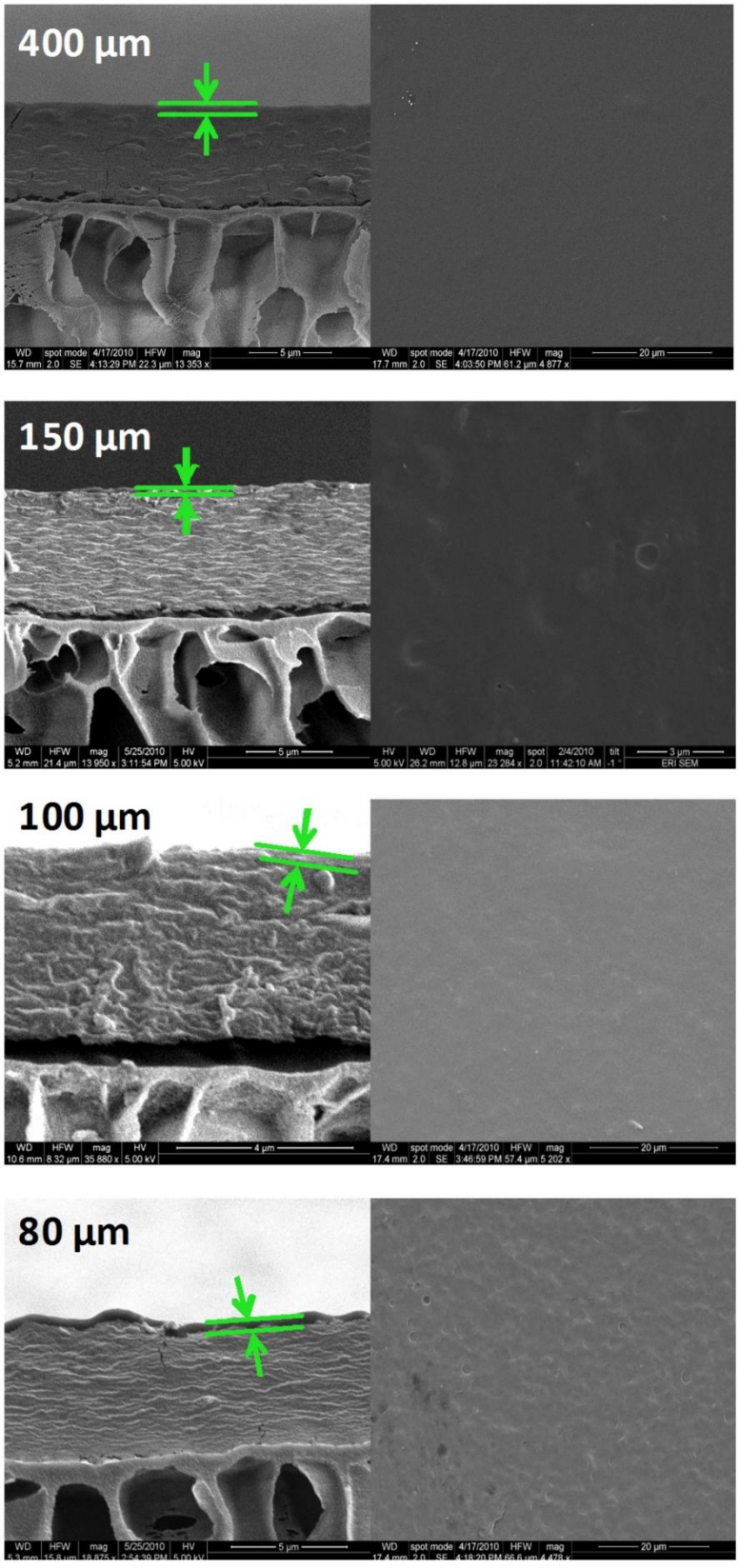


Figure 5.4: SEM images of membranes prepared: Left are cross-sectional images and right are top-down images. Thicknesses are shown in image. Magnifications as shown

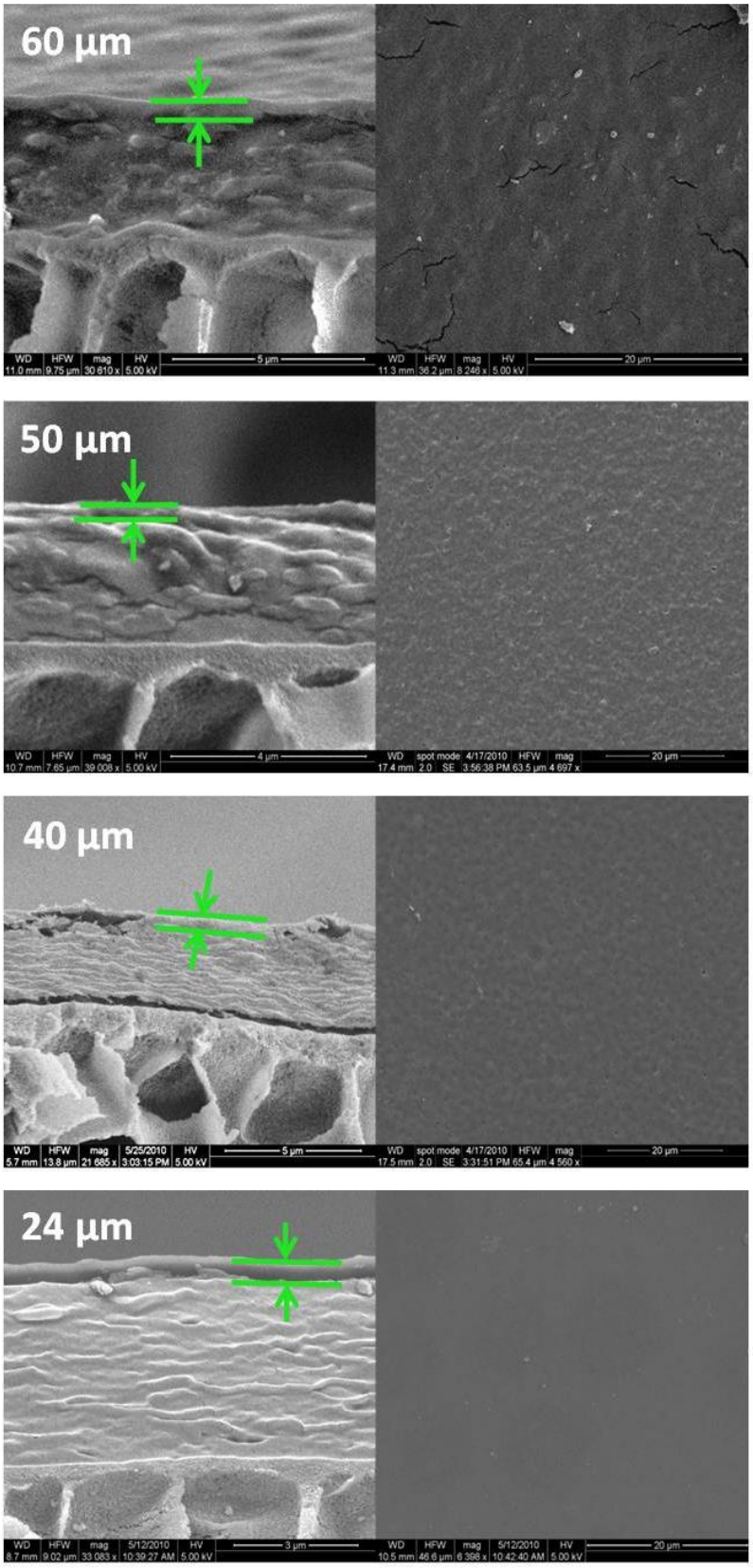


Figure 5.5: SEM images of membranes prepared: Left are cross-sectional images and right are top-down images. Thicknesses are shown in image. Magnifications as shown

Examining these images reveal that that the surfaces of the selective membranes have textures quite different from their bulk. In several of the cross-sections a well resolved surface 'skin' can be observed. These surface 'skins' are expected for polymer films cast from solution [21] and appear to be smooth and dense compared to the bulk. The thicknesses of the skin layers decreases with cast thickness until the thinnest membrane layers are produced. Increases in skin layer thickness for thin films is expected following models outlined by Yiotis et al [21] and are related to decreasing evaporation rates for thin films because of decreasing strain in the film, substrate-film interface effects and effects of cracks and other defects.

5.3.4 Pervaporation Results

All of these membranes were found to be highly selective for water permeation during pervaporation. The permeate flux was found to be a minimum of 95 mass% water (400 µm cast thickness after 5 h) and a maximum of 98.8 mass% water (40 µm cast thickness, 5 h). It is generally expected that these films will show a decrease in flux and an increase in selectivity as membrane thickness increases [15]. However, the variation in efficacy with cast film thickness could not be readily described in this simple manner. In order to provide an understanding of the fundamental properties (necessary to assess potential value of the membranes in commercial operation) a detailed study of performance for each selective membrane thickness was made.

The flux and selectivity results from membrane tests are described below. Figure 5.6 describes the variation of flux and selectivity for each membrane cast thickness. For each thickness studied, the pervaporation flux (figure 5.6A and 5.6B) shows a similar variation with time; an increase between 1 h and 2 h followed by a decrease before reaching an approximately consistent value at 5 h. The initial increase may be due to slow swelling processes with the slower loss of flux being due to polymer chain movement and densification of the selective membrane layers. The pervaporation selectivity results for all membranes show an improvement with time over the 5 h period. The thinnest and thickest membranes appear to show the smallest change with time (around 30 %) with the greatest

change with time occurring for the 60 µm cast film. These results might be rather simply explained in terms of the density, which has a profound effect on the selective passage of material through the polymer system. The rather low increase in selectivity with time for the 400 µm membrane thickness is probably related to the limited amount of free volume present and so there is a smaller change in measured density with time. The thinnest membrane, 24 µm, might also be expected to show limited changes in density because the volume of the polymer in the membrane is the lowest and changes in polymer structure will have a limited effect on free volume.

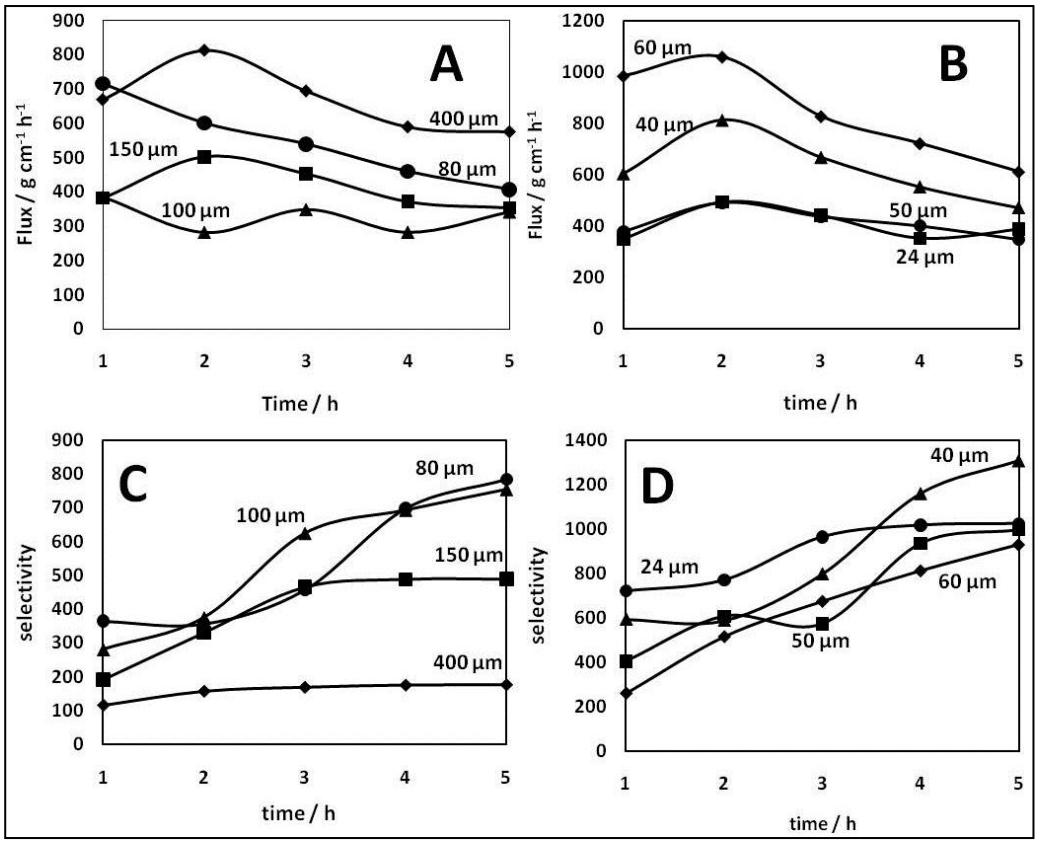


Figure 5.6: Plots of pervaporation performance indicators versus time. A and B are flux and C and D are selectivity. Various films were studied; the cast thickness is indicated in the figure. Estimated errors in measurements are around 5% of value

Data showing the variation in selectivity and flux after 5 h of testing (i.e. at or close to equilibrium) are described in figure 5.6 as a function of membrane selective layer thickness and cast thickness. Plots of selectivity and flux as a function of (measured) thickness shows little clear trend although it might be seen that a general increase in selectivity with decreasing membrane thickness is observed. Since flux is generally expected to decrease, and selectivity increase,

with thickness, it is clear that these membranes show considerable changes in structure and/or chemistry. As seen above, the density is changing with thickness and it might be expected that chemical changes are present because of the possibility of PVA-NaAlg-glycerol reactions and the possibility of crystallisation suggested by the XRD and DSC data.

The variation in flux with cast thickness does show more obvious trends as described in figure 5.7B. The thickest cast membrane film (400 µm) shows a relatively high flux (although the density is the highest) and this decreases until a distinct maximum is seen at lower film thicknesses until the lowest thickness (24 µm) where a strong decrease in flux is observed. There has been no systematic study of NaAlg – PVA chemistry as a function of cast thickness reported previously to our knowledge and these results are unusual. The data suggest (as outlined above) that the cross-linking of these selective membrane layers which affects their chemical nature changes as a function of thickness.

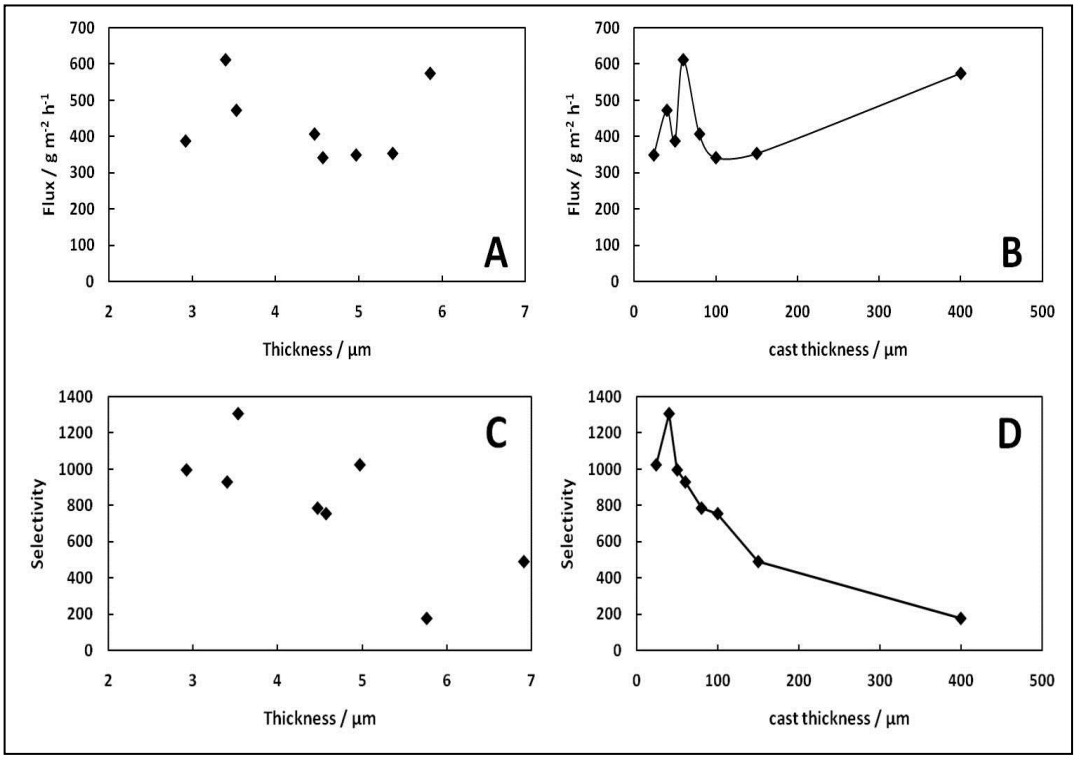


Figure 5.7: Plots of flux (A and B) and selectivity (C and D) against measured (A and C) and cast (B and D) thickness. Estimated errors in measurements are around 5 % of value

Where chemical changes are present, it might be expected that selectivity would also show an unusual dependence on cast film thickness. Indeed this is the case as described in figure 5.6D. Unexpectedly, considering the thickness and density

(since these offer a barrier to diffusion of molecules), the 400 µm membrane film shows the lowest selectivity. The selectivity then increases to a well-defined maximum before decreasing for the 24 µm membrane. As the films decrease in cast thickness, hydrophilicity increases and a hydrogel is formed, the interactions of water molecules with other water molecules through polar forces causes the permeation rate to decrease and so the flux decreases. At lower thicknesses, flux begins to increase again due to the thinness of the membrane structure. At the lowest thickness flux decreases. This might be due to the very well-defined skin layer formed (figure 5.4). The formation of skin layers for low polymer film thicknesses is well described by Yiotas[21]. These skin layers are dense and may decrease flux.

The relationship of flux and cast thickness is more difficult to understand. It is a complex variation as shown in figure 5.7 and may result from several factors. Firstly, for the thickest cast films, flux may be high because they are hydrophobic enough to not form a hydrogel and molecules pass through the polymer chains rather quickly.

The flux after 5 h (600 – 800 g cm^{-1} h^{-1}) and the selectivity after a similar period (800 – 1300) compare well with previous reports and are adequate for large scale separation[22], [23]. The key advantage is that these membranes are made using supports and processes to give membranes that would have physical properties to survive in industrial conditions. It is important to note that the pervaporation performance was measured after flux had stabilised (5 h) and survived periods of 14 h without compromising performance significantly. It is suggested that the systems have potential for further development and work is underway.

5.4 Conclusions

Studies of the pervaporation performance of supported NaAlg-PVA membranes have been made. These materials showed high selectivity (values) and flux (values) and potential for commercial development. The structure of the films was complex and density increased significantly as cast thickness was reduced. It is thought that this was due to relaxation phenomena related to the variation in the rate of solvent evaporation with cast thickness. It was observed that the pervaporation and flux depended strongly on the cast thickness. A hitherto unreported increase in the

selectivity of the membranes with decreasing membrane thickness was also observed. This can be explained by an increase in the polymer blend hydrophobicity as the membrane thickness increases due to decreasing porosity and longer periods during solvent evaporation allowing for extensive cross-linking to occur. The results suggest that very significant care must be taken when studying supported membrane systems where selective membrane film thicknesses can be small and structural-chemical changes significant.

5.5 Summary

As membrane thickness decreased selectivity increased

- This occurred down to a minimum thickness between 40 and 24µm

Previously unreported increase in the selectivity with decreasing membrane thickness observed

- Due to increase in the polymer blend hydrophobicity as membrane thickness increases
- Due to longer periods during solvent evaporation allowing for cross-linking to occur

References: Chapter 5

[1] C. K. Yeom, J. G. Jegal, and K. H. Lee, "Characterization of relaxation phenomena and permeation behaviors in sodium alginate membrane during pervaporation separation of ethanol-water mixture," *Journal of Applied Polymer Science*, vol. 62, no. 10, pp. 1561–1576, Dec. 1996.

[2] P. Shao and R. Huang, "Polymeric membrane pervaporation," *Journal of Membrane Science*, vol. 287, no. 2, pp. 162–179, Jan. 2007.

[3] R. Russo, M. Malinconico, L. Petti, and G. Romano, "Physical behavior of biodegradable alginate-poly(vinyl alcohol) blend films," *Journal of Polymer Science Part B: Polymer Physics*, vol. 43, no. 10, pp. 1205–1213, May 2005.

[4] R. W. Baker, *Membrane Technology and Applications*, 2nd ed. John Wiley and Sons, Ltd., 2007.

[5] M. P. Stevens, *Polymer Chemistry: An Introduction*, 1st ed. Oxford University Press, Inc., 1999.

[6] C. K. Yeom and K.-H. Lee, "Characterization of sodium alginate and poly(vinyl alcohol) blend membranes in pervaporation separation," *Journal of Applied Polymer Science*, vol. 67, no. 5, pp. 949–959, Jan. 1998.

[7] J. Brandrup, E. H. Immergut, and E. A. Grulke, *Polymer Handbook, 4th Edition*. John Wiley and Sons, New York, 2003.

[8] C. A. D. Charles E. Wilkes, James W. Summers, *PVC Handbook*. Hanser Gardener Publications, Inc., 2005.

[9] S. Hua, H. Ma, X. Li, H. Yang, and A. Wang, "pH-sensitive sodium alginate/poly(vinyl alcohol) hydrogel beads prepared by combined Ca2+ crosslinking and freeze-thawing cycles for controlled release of diclofenac sodium.," *International journal of biological macromolecules*, vol. 46, no. 5, pp. 517–23, Jun. 2010.

[10] K. Pal, A. K. Banthia, and D. K. Majumdar, "Preparation and characterization of polyvinyl alcohol-gelatin hydrogel membranes for biomedical applications.," *AAPS PharmSciTech*, vol. 8, no. 1, p. 21, Jan. 2007.

[11] K. Fujimoto, M. Minato, and Y. Ikada, "Chapter 20, Poly(vinyl alcohol) Hydrogels Prepared under Different Annealing Conditions and Their Interactions with Blood Components," in *Polymers of Biological and Biomedical Significance*, American Chemical Society, 1994, pp. 228–242.

[12] B. Liu, D. Qiu, and C. Z. Zhao, "Effect of Mixture of Plasticizer on the Thermoplastics Formability of Polyvinyl Alcohol (PVA)," *Key Engineering Materials*, vol. 447–448, no. 1, pp. 652–656, 2010.

[13] R. Ricciardi, F. Auriemma, C. De Rosa, and F. Lauprêtre, “X-ray Diffraction Analysis of Poly(vinyl alcohol) Hydrogels, Obtained by Freezing and Thawing Techniques,” *Macromolecules*, vol. 37, no. 5, pp. 1921–1927, Mar. 2004.

[14] S. Kalyani, B. Smitha, S. Sridhar, and a Krishnaiah, “Pervaporation separation of ethanol–water mixtures through sodium alginate membranes,” *Desalination*, vol. 229, no. 1–3, pp. 68–81, Sep. 2008.

[15] K. Y. Lee, J. A. Rowley, P. Eiselt, E. M. Moy, K. H. Bouhadir, and D. J. Mooney, “Controlling Mechanical and Swelling Properties of Alginate Hydrogels Independently by Cross-Linker Type and Cross-Linking Density,” *Macromolecules*, vol. 33, no. 11, pp. 4291–4294, 2000.

[16] A. R. Kulkarni, K. S. Soppimath, T. M. Aminabhavi, A. M. Dave, and M. H. Mehta, “Glutaraldehyde crosslinked sodium alginate beads containing liquid pesticide for soil application.,” *Journal of controlled release : official journal of the Controlled Release Society*, vol. 63, no. 1–2, pp. 97–105, Jan. 2000.

[17] E. E. Shafee and H. . Naguib, “Water sorption in cross-linked poly(vinyl alcohol) networks,” *Polymer*, vol. 44, no. 5, pp. 1647–1653, Mar. 2003.

[18] K. Pal, K. Banthia, and D. K. Majumdar, “Polymeric Hydrogels: Characterization and Biomedical Applications,” *Designed Monomers and Polymers*, vol. 12, no. 3, pp. 197–220, 2009.

[19] J. H. Hildebrand, “Solubility of non-electrolytes,” *Journal of the Society of Chemical Industry*, vol. 55, no. 34, p. 665, 1936.

[20] A. F. M. Barton, *CRC Handbook of Polymer-Liquid Interaction Parameters and Solubility Parameters*. CRC Press, 1990.

[21] A. G. Yiotis, I. N. Tsimpanogiannis, A. K. Stubos, and Y. C. Yortsos, “Pore-network study of the characteristic periods in the drying of porous materials.,” *Journal of colloid and interface science*, vol. 297, no. 2, pp. 738–48, May 2006.

[22] J. C. Richardson, P. W. Dettmar, F. C. Hampson, and C. D. Melia, “Oesophageal bioadhesion of sodium alginate suspensions: particle swelling and mucosal retention.,” *European journal of pharmaceutical sciences : official journal of the European Federation for Pharmaceutical Sciences*, vol. 23, no. 1, pp. 49–56, Sep. 2004.

[23] M. T. Bhat, D. Santoshkumar, Aminabhavi, “Pervaporation Separation Using Sodium Alginate and Its Modified Membranes - A Review,” *Separation and Purification Reviews*, vol. 36, no. 3, pp. 203–229, 2007.

Chapter 6

Advanced Later Flow Membranes: Control of Pore Structure

6 Advanced Lateral Flow Membranes: Control of Pore Structure

The following is adapted from "*Control of Pore Structure Formation in Cellulose Nitrate Polymer Membranes*". Advances in Chemical Science Vol. 2 Issue. 2, June 2013

Abstract

Porous cellulose based membranes are commonly used for filtration and controlled flow of fluid through the 3D pore network in the bulk (lateral flow). It has been shown that the performance of *cellulose nitrate* membranes in terms of capillary driven lateral flow of fluid through the system is inhibited by the formation of surface skin layers and bulk macrovoids. These 'defects' are created during phase inversion when the porous structure is formed using a water anti-solvent. The work carried out in this study shows that the incorporation of ethanol as a *meso-solvent* into the membrane casting solution for use in *vapour induced phase seaparation* (VIPS) produced lateral flow membranes, effectively prevents the formation of both skin layers and macrovoids while simultaneously increasing membrane porosity resulting in an improvement in lateral flow rates of the final membranes. It is shown that the improved performance is achieved through reduction of the rate of evaporation of solvent from the membrane surface/demixing front during membrane formation.

6.1 Introduction

Porous, lateral-flow, polymer membranes are the basis for the vast majority of immunological and diagnostic assays. Cellulose derived polymers are most commonly used for the production of lateral flow membranes. In particular, cellulose nitrate (CN, often referred to by the misnomer *nitrocellulose*) is very widely used[1–3]. However, despite widespread use, there has been relatively little investigation into the formation of cellulose nitrate lateral flow membranes in literature.

These porous membranes are formed through a process known as *phase inversion* which defines their internal pore structure[4–6]. This is a phenomenon whereby the phases of a liquid-liquid dispersion interchange such that the dispersed phase spontaneously inverts to become the continuous phase and vice versa under conditions determined by the system properties, volume ratio and energy input[7]. The phase inversion method utilised here is vapour induced phase inversion (VIPS)[8] wherein diffusion of water from atmospheric humidity into the polymer solution of CN in acetone induces demixing of the polymer from the solution to form the solid porous CN matrix of the final membrane. When a polymer solution is in a single phase the polymer is stable in the solvent. The addition of nonsolvent (water) decreases the thermodynamic stability of the solution as it's' concentration relative to the solvent (acetone) decreases. At a critical concentration (*cloud point*) of nonsolvent the solution becomes thermodynamically unstable and two liquid phases – a polymer rich phase, containing solvent and polymer, and a polymer lean phase containing the non-solvent – are formed. Upon drying, the polymer rich phase forms the rigid matrix of the membrane while the polymer lean phase forms the pores[9]. Evaporative loss of solvent precipitates the final membrane morphology[10]. Phase inversion is a sensitive process and can be affected by many parameters; solution concentration, viscosity, surface tension, density, temperature, humidity, container geometry, agitation and flow[11]. The sparse literature on CN membranes (and membranes produced by phase inversion in general) consistently shows the formation of skin layers [9], [12–15] and macrovoids [3], [16–18] in the membrane cross sections (see chapter 1, section 1.4 for detailed explanation of phase inversion and lateral flow theory).

While methods for preventing macrovoid formation during the phase inversion process have been documented and detailed studies exist [3], [14], prevention of the formation of skin layers has not. Skin layers and macrovoids inhibit and retard lateral flow in porous membranes respectively, limiting their properties and use. The work in this study shows how the formation of both skin layers and macrovoids can be successfully prevented through the use of an additional solvent that has solvating properties somewhere between those of the solvent and non-solvent used in preparation. This additional solvent (which is described here as the *meso-solvent*) is also partially miscible with both the solvent and the non-solvent. In this case ethanol is the meso-solvent to the basic phase inversion make-up of polymer (CN), solvent (acetone) and non-solvent (water). The use of ethanol as a meso-solvent increases the porosity of the membrane internal structures which also results in an increase in lateral flow rates through the membranes.

Ethanol has been used as a quencher in the casting of similar membranes,[19] but this role is distinct from the meso-solvent role and, in addition, was found to be inferior to methanol as a quencher. To the best of our knowledge, the use of ethanol as a meso-solvent in the production of membranes of the type herein has not been covered in the literature and we present it here for scientific posterity.

6.2 Experimental

See chapter 2 for details on all materials, apparatus and procedures not mentioned below.

6.2.1 Membrane Preparation

A series of membranes were produced from casting solutions. The content of these solutions can be seen in table 6.1 below. The solvent/meso-solvent/non-solvent mixture for each casting solution contained differing amounts of ethanol and acetone with a constant water content (prior to addition of extra non-solvent to bring solution near cloud point; for precise definition of what was considered "near" see chapter 2 and chapter 4), ranging from 25 wt% ethanol/70 wt% acetone/5 wt% water to 50 wt% ethanol/45 wt% acetone/5wt% water. Outside this composition range membranes were either highly irreproducible or had poor physical properties in terms of fragility, pore structure, porosity and skin formation.

Although it has previously been shown that near cloud-point compositions lead to instantaneous skin formation[20], the inclusion of ethanol as a meso-solvent negates this effect for reasons outlined below, allowing for casting and formation of membranes without skin layers. The membranes in this series are labelled MesoXCP; X denotes ethanol content, CP denotes cloud point and "Meso" denotes the use of a meso-solvent; ethanol (EtOH). These membranes were then compared with one produced using a simple solvent/non-solvent solution of 95 wt% acetone and 5 wt% water in which 17 g CN was dissolved to provide a membrane produced from a more typical phase inversion without a meso-solvent (development of this membrane outlined in chapter 4). 2.3 g of water were added to bring this solution near cloud point. The weight percentage composition can be seen in the final row of table 6.1. This control membrane was labelled BasMemBCP (see chapter 2, section 2.1.2 for label details). Final membranes were produced with backing supports of the 100 % polyester film by casting the near cloud point polymer solutions on to the support material using the automatic film coater. This cast layer underwent VIPS in the controlled glovebox atmosphere at 35 % humidity and ~24 ^{o}C and remained in this environment for 12 h. Finally, the resulting membrane was dried at 30 ^{o}C for approximately 4 h to remove excess solvent/meso-solvent/nonsolvent before characterization.

Table 6.1: Casting solution composition before/after cloud point

Mem.	Initial Phase Inversion Solution				Non-sol. (H_2O) for CP. (g)	Solution Near Cloud Point			
	Poly. (CN) wt%	Sol. (ace) wt%	Meso-Sol. (EtOH) wt%	Non-sol. (H_2O) wt%		Poly. (CN) wt%	Sol. (ace) wt%	Meso-Sol. (EtOH) wt%	Non-sol. (H_2O) wt%
MesoACP	17	58.10	20.75	4.15	5.30	13.030	44.534	15.902	26.533
MesoBCP	17	53.95	24.90	4.15	5.43	12.890	40.904	18.878	27.328
MesoCCP	17	49.80	29.05	4.15	5.55	12.800	37.499	21.872	27.828
MesoDCP	17	45.65	33.20	4.15	5.94	12.565	33.740	24.540	29.153
MesoECP	17	41.50	37.35	4.15	4.80	13.220	32.272	29.043	25.465
BasMemBCP	17	78.85	0	4.15	2.30	15.123	70.142	0	14.733

6.2.2 Lateral Flow Testing

The effect of gravity on the flow rate is constant for all membranes so the relative differences in flow between membranes serves to show improvement brought about through changes in membrane structure.

6.3 Results and Discussion

6.3.1 EtOH Content

Figure 6.1 shows a graph of the required additional non-solvent (water) to bring the casting solutions to near cloud-point versus their ethanol content. It can be seen from this that there is an increase in the amount of water required as ethanol content increases up to a maximum, beyond which the amount of water required decreases. The Hildebrand solubility parameters of acetone, ethanol and water are 19, 26.2 and 48 $Mpa^{1/2}$ respectively whilst CN is around 22 $Mpa^{1/2}$[22]. The maximum observed in figure one as the water required to achieve cloud point, can be explained on the basis of these. As ethanol concentration increases, hydrogen bonding with water reduces the anti-solvent properties of the water, thus, requiring increased water concentrations. At higher ethanol content, the reduced amount of acetone has a more pronounced effect and the solubility of the CN decreases (since acetone is an effective solvent for CN).

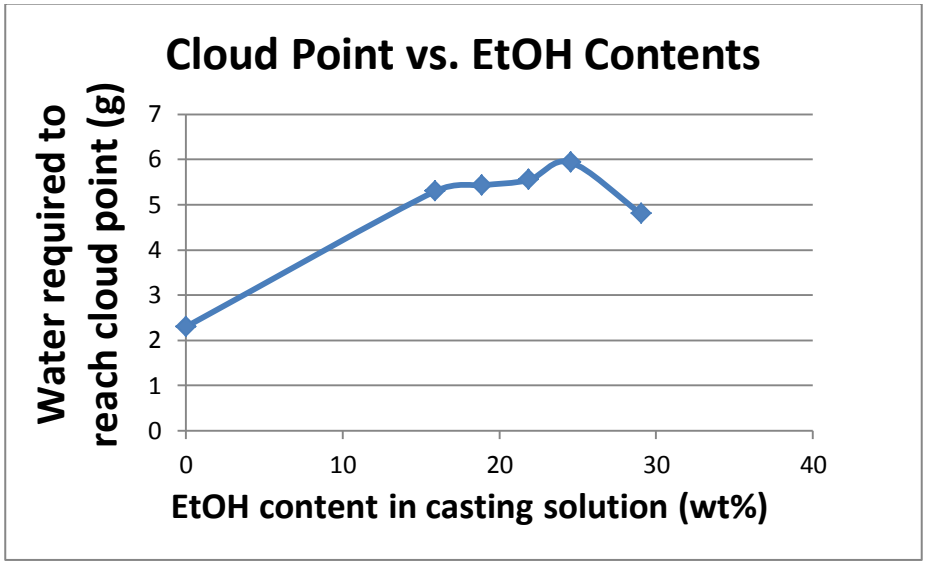


Figure 6.1: Plot of non-solvent (water) required to reach cloud point versus ethanol content in casting solution at cloud point

6.3.2 SEM

Figure 6.2, below, shows SEM image pairs of the membranes MesoACP to MesoECP in images A-E respectively while pair F shows BasMemBCP. Each pair is composed of a cross sectional membrane image (i) and an exposed membrane surface image (ii). Images 6.F(i) and 6.F(ii) show cross sectional and surface

images respectively of BasMemBCP, which has no ethanol in its casting solution. The cross section indicates some porosity but this is limited and there is little sign of pores extended in the direction normal to the membrane surface. What pores are visible appear to be largely 1D or 2D in nature and sandwiched between layers of CN. Although bringing solutions near to cloud-point prior to casting is thought to reduce skin layer formation by some,[18] (and refuted by others[20]) a well-formed skin layer is clearly visible in the top-down image shown in figure 6.2F(ii). There is little indication of open pores at the membrane surface although circular type features can be seen of either surface indentations or sub-surface structures. The observation of these is consistent with the formation of a closed 2D pore structure in the film. The layered nature of CN and the pore structure is suggested to be due to rapid solvent evaporation during casting as the solvent moves too rapidly through the membrane to allow 3D formation of pores[23].

Images figure 6.2A(i) and 6.2A(ii) show MesoACP which has the lowest meso-solvent (ethanol) content of 15.902 wt% in its casting solution (table 1). The cross sectional image, 6.2A(i), still indicates distinct layer formation consistent with a high rate of solvent evaporation. Again some inter-layer porosity is present. However, the presence of the ethanol has begun to evolve a new form of 3D pore structure that extends through the layers. This is largely seen as smaller pores of around 1 to 5µm in size. These are marked with rings and are visible in both cross-section and top-down images (through much larger pore openings). These small pores seen in the surface are highly distorted into elliptical shapes and indicate considerable strain at the surface during membrane formation. The surface image, 6.2A(ii), also shows a shows the formation of a 3D pore structure with very large pore openings of approximately 100 µm in diameter. We suggest the large surface morphologies are formed because of the same surface tension effects described above that are causing some of these pores to be deformed[24].

Images in figure 6.2B(i) and 6.2B(ii) show cross sectional and surface images respectively of MesoBCP, which has an ethanol content of ~18.9 wt% in its casting solution (~3 wt% more than MesoACP). The cross sectional image shows a similar structure to that observed in MesoACP, however, there is a less distinctive layered structure, void formation and interconnectivity between layers is increasing. This might suggest that the ethanol is decreasing the rate of membrane formation

(through reduction in the solvent evaporation rate) allowing more pore volume to be included.

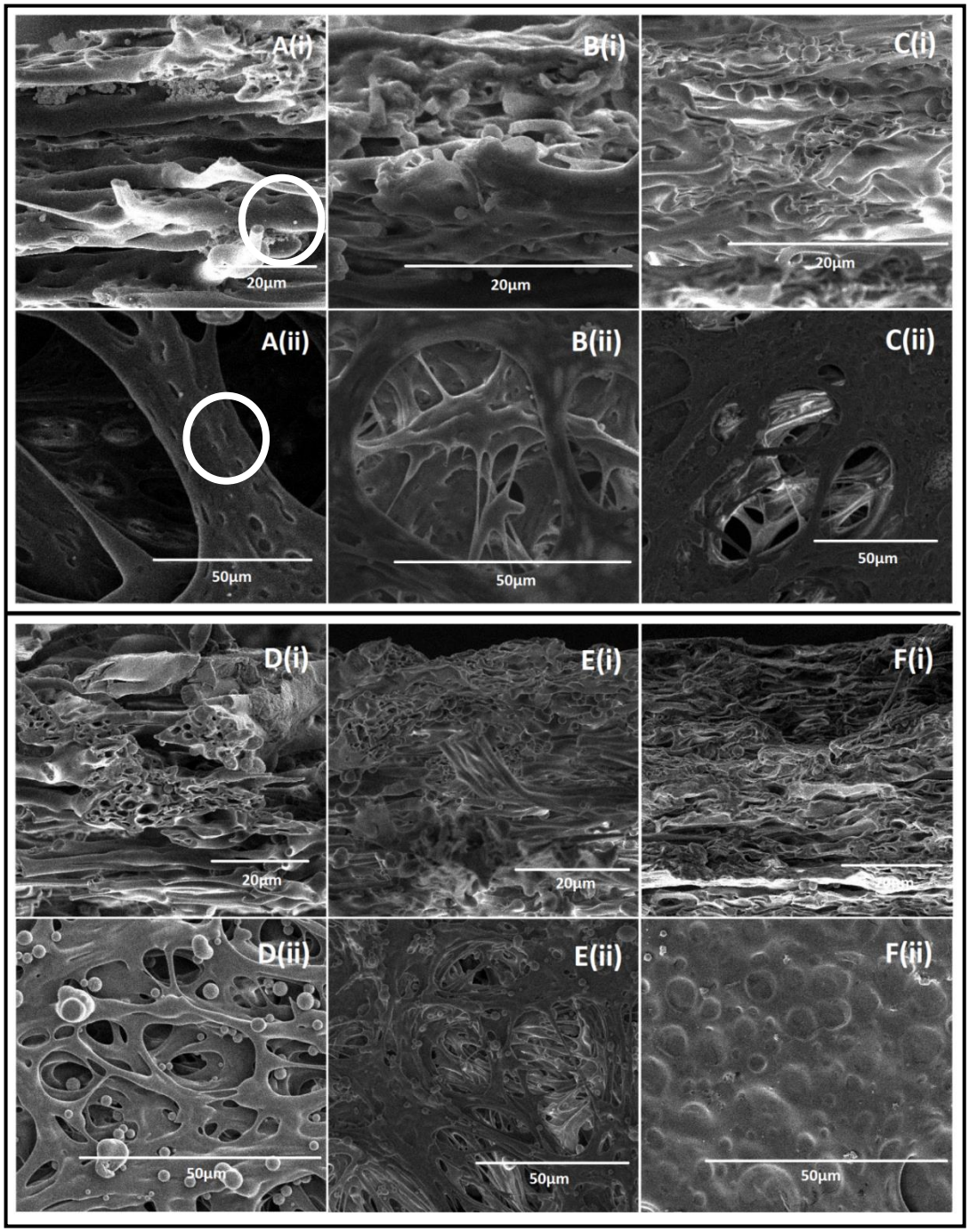


Figure 6.2: SEM images of the lateral flow membranes MesoACP – MesoCCP and BasMemBCP (lettering follows sample labels see table 6.1). Images with the (i) labels show membrane cross sectional morphology while those with label (ii) show membrane surface morphology

The interconnectivity of the layers and the progression of a 1D or 2D pore structure into a 3D pore arrangement can be clearly seen in the top-down surface image, in figure 6.2B(ii). Note that the size of the openings at the surface morphologies is

significantly reduced; about 60µm compared to similar features seen in MesoACP. This is consistent with lower evaporation rate which would allow some of the surface strain to be reduced during membrane formation. The smaller pores seen for MesoACP are also observed and are around the same size but, as might be expected, are significantly less strained and distorted at the surface.

Increasing the ethanol further to around 22 wt% (MesoCCP) continues the trend seen for membranes discussed so far. Images shown in figures 6.2C(i) and 6.2C(ii) show cross sectional and surface images respectively. The formation of a layered structure is barely observed and the pore volume is clearly increasing. It is clear that the films membranes form by this methodology will always have significant layered structure probably because of the way in which the solvent from moves through the film during drying. Noticeable also is the appearance of quite large spherical structures or nodules suggestive of some nucleation and growth which is consistent with lower rates of membrane formation. The smaller pores can be seen quite clearly in both top-down and cross-section images but it should be noted that at the surface the pores are largely undistorted, consistent with low strain resulting from lower rates of membrane formation.

Images figure 6.2D(i) and 6.2D(ii) show cross sectional and surface images respectively of MesoCCP, which has an ethanol content of about 25 wt% in its casting solution. The trends in morphologies observed in membranes MesoACP – MesoCCP continue in MesoCCP. The cross section, image figure 6.2D(i), still shows indications of layering but the layering appears to be very much 1D and filamental in form. This is because there are large pore opening in the layers as can be seen quite clearly in the corresponding top-down SEM (figure 6.2D(ii)). There is now quite clear void formation between the layers and the small pores of (1-5µm) can not only be seen as existing through the layers but within the material as well. It is apparent that this is the most porous of the membranes seen thus far. The top-down surface image, figure 6.2D(ii) reveals the 3D nature of the open porous structure formed although their size is reduced a little compared to MesoCCP to an approximate diameter of 25 µm. The size and shape is consistent with continued slower membrane formation and strain release. While no nodules are observed in cross section, they are present in the surface image.

Images in figure 6.2E(i) and 6.2E(ii) detail the morphology of MesoECP (about 29 wt% ethanol). The morphology of the membrane appears to be quite close to that of MesoDCP in all respects and is observed in both cross-section and top-down images. The only difference appears to be increased density and lower void volume. This can be particularly seen in the upper region of the membrane in figure 6.2E(i). The data, thus, suggest that MesoDCP is the most porous of those studied.

6.3.3 XRD

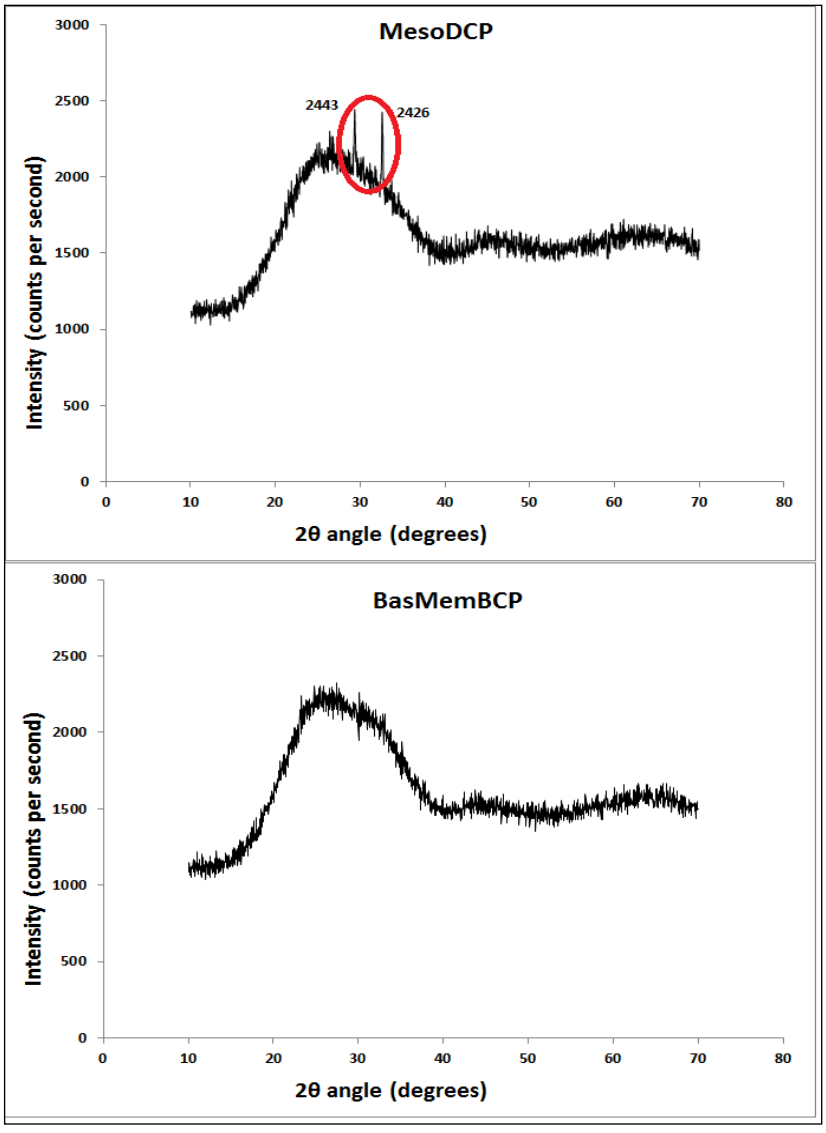


Figure 6.3: XRD profiles of MesoDCP and BasMemBCP (to see images superimposed see appendix D, section D.1, figure D.1). Both membranes show a large broad feature around 22-32 $^{o}2\theta$ and weaker features around 45 and 65 $^{o}2\theta$; consistent with a poorly ordered crystalline material. MesoDCP material also shows to sharp diffraction features at 29.34 $^{o}2\theta$ and 32.58 $^{o}2\theta$ (as highlighted)

In order to understand these changes in the membrane further, MesoDCP and BasMemBCP were studied to assess and compare the non-ethanol containing solvent and the most porous of the meso-solvent modified membranes. Figure 6.3 shows XRD data for the membranes. A large broad feature around 22-32 $^{o}2\theta$ and weaker features around 45 and 65 $^{o}2\theta$ are consistent with a poorly ordered crystalline material and the features are similar for both membranes[25]. However, the MesoDCP material also shows to sharp diffraction features at 29.34 $^{o}2\theta$ and 32.58 $^{o}2\theta$ (as highlighted in the figure). These are consistent with the presence of highly crystalline material as well as a majority of the poorly defined phase. These are likely due to the increased presence of nodules seen in the SEM images, as nodules are a crystalline morphology[26], [27]. The is evidence that increasing the membrane casting solution ethanol content increases the final membrane crystallinity and has a very direct effect on the kinetics of membrane formation. Increased crystallinity is consistent with longer membrane formation times which allow structural refinement during synthesis.

Flexibility data corroborates the XRD data showing that as the membrane EtOH content increased the brittleness increased; evidence of a more crystalline structure (see appendix D, section D.4, table D.2).

6.3.4 Mercury Porosimetry

To confirm the image analysis, mercury porosimetry data were recorded from MesoDCP and BasMemBCP and these are recorded in figure 6.4. BET testing was conducted using nitrogen and even argon gases. However, it was found that the membranes retain too much gas to give an accurate measurement, leaving mercury porosimetry as the only viable accurate means of obtaining porosity data. Figure 6.4A shows the cumulative intrusion of mercury in the membrane versus pressure and the data clearly show that MesoDCP has a greater overall internal volume that of BasMemBCP in agreement with the SEM analysis. Figure 6.4B shows the log differential of mercury intrusion into the membrane versus pore size diameter. The data shows that the ethanol meso-solvent increases the number of large pores (i.e. >10µm) within the membrane. The data also show a well-defined peak below 10µm which is consistent with the smaller pores seen in the SEM data from samples made

with ethanol included. Again all data are consistent with the analysis of the SEM images in figure 6.2.

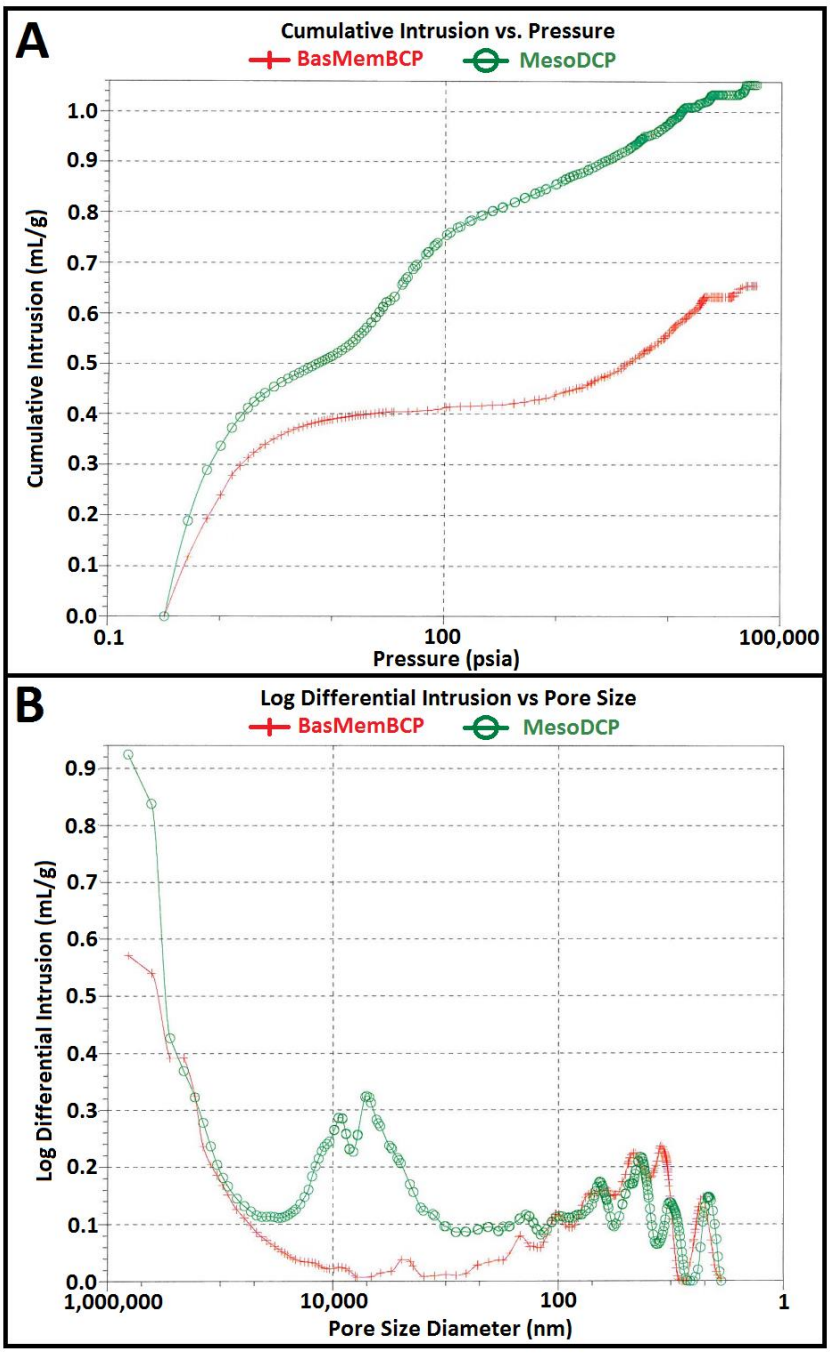


Figure 6.4: MesoDCP and BasMemBCP porosimetry. As labelled in diagram

6.3.5 Lateral-Flow Rate

The apparent changes in porosity with ethanol content should be reflected in the lateral flow rate measured following surfactant treatment. The lateral flow rates

were measured for each membrane and plotted in figure 6.5. The data points show the average flow rate calculated from ten samples at each membrane composition.

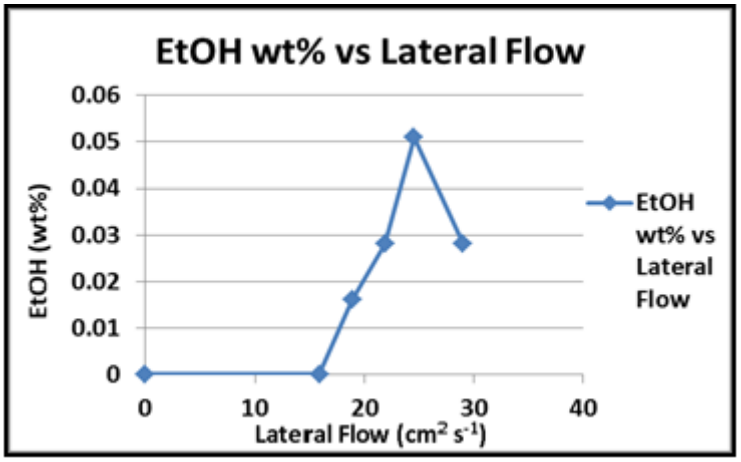


Figure 6.5: Lateral flow rate against the ethanol content for each of the membranes prepared here (for tabulated data see appendix D, section D.2, table D.1)

The BasMemBCP and MesoACP showed negligible flow rates in these measurements. However, as the ethanol content in the preparation lacquer increases the flow rate increases through MesoBCP (avg. 0.0165 $cm^2\ s^{-1}$ max. 0.018 $cm^2\ s^{-1}$ min. 0.015 $cm^2\ s^{-1}$), MesoCCP (avg. 0.0282 $cm^2\ s^{-1}$ max. 0.031 $cm^2\ s^{-1}$ min. 0.026 $cm^2\ s^{-1}$) to a maximum in MesoDCP (avg. 0.0508 $cm^2\ s^{-1}$ max. 0.054 $cm^2\ s^{-1}$ min. 0.048 $cm^2\ s^{-1}$) before decreasing with MesoECP (avg. 0.0276 $cm^2\ s^{-1}$ max. 0.030 $cm^2\ s^{-1}$ min. 0.025 $cm^2\ s^{-1}$). The trend in lateral flow rate reflects the changes seen in SEM images and the water needed for cloud point reported in figures 6.2 and 6.1 respectively. As might be expected, MesoDCP exhibits the highest lateral flow rate and the highest water content in the synthesis lacquer. The decrease in lateral flow seen between MesoDCP and MesoECP can be accounted for directly by the decreased total amount of water present which (as the porogen) reflects the total pore volume. However, although similar amounts of water are used in the formation of membranes MesoACP – MesoCCP, this is not reflected in the lateral flow and indicates that the pore morphology has a strong affect. This probably reflects the changes seen in the SEM images with a progression from 1D to a 3D pore network.

6.3.6 Discussion

There are three issues worthy of detailed discussion here. Firstly, the change in membrane structure observed; secondly, the role of ethanol in the membrane synthesis reaction and, finally, the origin of the nodules formed.

Briefly, in this type of phase inversion synthesis process, the membrane forms from a single phase, homogeneous solution which on addition of non-solvent becomes a dual phase consisting of a polymer rich region (i.e. polymer and solvent) and a polymer poor region (comprised of the non-solvent; water). The phase separation of these leads to pockets of non-solvent which will form the nascent pores of the final membrane structure, while the surrounding polymer rich phase, upon solvent loss, forms the polymer walls[28]. In this sort of phase inversion process, the membrane is precipitated by a combination of s*pinodal decomposition* (SD) and *nucleation and growth* (NG)[29–31]. The rate of evaporation is key to the morphology of the membrane. In general, precipitation occurs because evaporation leads to loss of solvent and de-stabilisation of the polymer rich phase[24]. If the solvent evaporation is rapid, the evaporation forces bring polymer molecules to the surface increasing their concentration and resulting in skin layers. Further, the "de-mixing" front passes down through the membrane from the air exposed surface. The rate of solvent evaporation decreases as the demixing front moves back from the air exposed surface and layers of polymer build up above it[32]. This would explain the appearance of the non-ethanol containing membrane. The formation of macrovoids is also a result of rapid solvent evaporation as explained by Kahre et al[16]. Briefly, the interface between the polymer rich and polymer poor phase undergoes motion due to solvent evaporation. Any macrovoid formed by an agglomeration of non-solvent undergoes a differential stress across the leading edge of the void and the trailing edge. This results in convection currents within the voids which in turn promote further non-solvent inclusion and void growth (see chapter 1, section 1.4.3, figure 1.14). Ahmad *et al* have argued that macrovoids inhibit lateral flow by increasing the bulk porosity of a membrane without increasing the actual number of pores[3]. It is also clear that, above a critical size, pores will not contribute to capillary flow. It is suggested that the synthesis of membranes not containing meso-solvent is a direct result of rapid solvent loss. The presence of a skin layer makes imaging macrovoids rather difficult but in membrane MesoACP (with the lowest ethanol content), macrovoids can be clearly seen (Figure 6.2A(i)). Further the direct effect of high evaporation rate related surface stress can be seen on both the macrovoid and microvoid shapes and size.

Using these models it is possible to explain the results observed here. Acetone has a low boiling point, 50.5 °C and a high evaporation rate from the polymer rich component. Although water and acetone are miscible (because of hydrogen bonding), the miscibility of the CN-acetone and water phases is limited. Thus, evaporative loss from the polymer rich phase will be high. This evaporation results in skin layer formation and production of relatively large macrovoids, as seen in BasMemBCP. Ethanol can exist in both the polymer rich and polymer deficient phases since the solubility parameter of ethanol and CN are similar. Ethanol and acetone mixtures are miscible with no known azeotrope[33], [34]. Thus, the boiling point of the solvent in the polymer rich phase will increase thereby decreasing evaporation rate. This then leads to formation of less and smaller sized macrovoids, decreased skin layer formation and reduced surface strain as seen in the SEM images. At the highest concentration of ethanol, the effect is reduced because the water content of the final mixture is reduced decreasing total porosity. Note also the effect of having ethanol in the non-solvent (water) dominated, polymer deficient phase. Ethanol forms an azeotrope with water. This leads to an increase the concentration of CN in this phase, reducing the concentration gradient across the phase front and so reducing layering and macrovoid formation.

Nodules: spherical morphologies that occur in membranes due to coarsening. The number of these nodules depends on the degree of crystallinity of the membranes. Coarsening occurs when the two separated phases in an *instantaneous* phase inversion build up energy at interfacial regions between the two phases, which makes the solution thermodynamically unstable. Stability is regained by dissipating this energy into coarsening; which is the formation of droplets of semi-crystalline polymer at the interfacial regions. From these droplets, nodules are formed[35]. Naturally, the further from instantaneous the phase inversion is, the less coarsening will occur; therefore, if the affinity of the solvent for the non-solvent is increased (as it is through the use of a meso-solvent here), the phase inversion will proceed more through the spinodal region of nucleation and growth [28] and reduce the degree of coarsening and so the eventual number of nodules.

The formation of nodules seen in the solutions result from an Ostwald ripening process occurring at the interface of a dispersed phase of the polymer rich and deficient phases[35], [36]. Given that nodules, like other polymer structures such as

epitaxials and spherulites, are crystalline,[26], [27] it is unsurprising that the appearance of the highly crystalline phase is only seen for ethanol containing preparations. It is suggested that the ethanol addition promotes these phases because the ethanol mediated interactions between the polymer rich and polymer poor phases results in higher concentrations of dispersed phases (since the ethanol could stabilise polymer rich phases in the non-solvent). In this way, decreased layering and nodule formation rates are closely related.

It is tempting, given the morphologies observed in the SEM images, to say that the effect of water upon on the final structure of the membranes is the dominant effect. However, the structure of BasMemBCP in which no ethanol was used - while the non-solvent treatment of the casting solution was maintained - shows conclusively that the incorporation of the meso-solvent ethanol is essential to yielding the structures that typify MesoDCP granting it greater lateral flow rate.

6.4 Conclusion:

The inclusion of ethanol in the membrane casting solution at cloud point of CN lateral flow membranes prepared by phase inversion effectively prevents the formation of both skin layers and macrovoids, as shown in SEM cross sectional and surface images and mercury porosimetry data. In addition to the prevention of these undesirable structural anomalies, the inclusion of ethanol also increases the porosity of the CN membrane internal structure; increasing lateral flow rates significantly. The inclusion of ethanol also increases the prevalence of nodules in membrane formation and these spherical polymer structures remain in the final membrane. Their increased numbers results in increased crystallinity of the polymer, as shown in XRD analysis of the final membranes. The overall conclusion of the work reported here is that all these controlled changes in membrane internal structure are achieved through a reduction in the rate of evaporation of solvent from the membrane air exposed surface/demixing front. The use of a meso-solvent to this end should be applicable to any membrane production process utilizing polymer VIPS and future work will be centred on such investigations.

6.5 Summary

Use of meso-sol. (EtOH) in casting lacquer: • Increases membrane porosity • Prevents skin layer formation (in conjunction with bringing lacquer to CP) • Increases lateral-flow rate
Use of meso-sol. Also increases occurrence of nodules • No discernible effect on membrane performance

References: Chapter 6

[1] M. Ulbricht, "Advanced functional polymer membranes," *Polymer*, vol. 47, no. 7, pp. 2217–2262, Mar. 2006.

[2] M. Lönnberg and J. Carlsson, "Chromatographic performance of a thin microporous bed of nitrocellulose.," *Journal of chromatography. B, Biomedical sciences and applications*, vol. 763, no. 1–2, pp. 107–20, Nov. 2001.

[3] A. L. Ahmad, S. Low, and S. Shukor, "Effects of membrane cast thickness on controlling the macrovoid structure in lateral flow nitrocellulose membrane and determination of its characteristics," *Scripta Materialia*, vol. 57, no. 8, pp. 743–746, Oct. 2007.

[4] Y. Yip and a Mchugh, "Modeling and simulation of nonsolvent vapor-induced phase separation," *Journal of Membrane Science*, vol. 271, no. 1–2, pp. 163–176, Mar. 2006.

[5] P. Vandewitte, P. Dijkstra, J. Vandenberg, and J. Feijen, "Phase separation processes in polymer solutions in relation to membrane formation," *Journal of Membrane Science*, vol. 117, no. 1–2, pp. 1–31, Aug. 1996.

[6] B. F. Barton, J. L. Reeve, and a. J. McHugh, "Observations on the dynamics of nonsolvent-induced phase inversion," *Journal of Polymer Science Part B: Polymer Physics*, vol. 35, no. 4, pp. 569–585, Mar. 1997.

[7] S. Arirachakaran, K. D. Oglesby, M. S. Malinowsky, O. Shoham, and J. P. Brill, "An Analysis of Oil/Water flow Phenomena in Horizontal Pipes," in *society of Petroleum Engineers, Oklahoma*, 1989.

[8] H. Chae, Y. Po, H. Yong, and Y. Soo, "Membrane formation by water vapor induced phase inversion," *Journal of Membrane Science*, vol. 156, pp. 169–178, 1999.

[9] Y.-S. Kang, H.-J. Kim, Y.-H. Kim, and W.-H. Jo, "The Mechanism of Assymetric Membrane Formation via Phase Inversion," *Polymer Society of Korea*, vol. 12, no. 3, pp. 279–287, 1988.

[10] J. P. Salamone, *Polymeric Materials Encyclopedia*, Vol. 6. CRC Press, 1996.

[11] B. Hu, L. Liu, O. Matar, P. Angeli, G. Hewitt, and E. Perezdeortiz, "Investigation of Phase Inversion of Liquid-Liquid Dispersions in Agitated Vessels*," *Tsinghua Science & Technology*, vol. 11, no. 2, pp. 202–206, Apr. 2006.

[12] A. L. Ahmad, M. Sarif, and S. Ismail, "Development of an integrally skinned ultrafiltration membrane for wastewater treatment : effect of different

formulations of PSf / NMP / PVP on flux and rejection," *Desalination*, vol. 179, no. November 2004, pp. 257–263, 2005.

[13] A. L. Ahmad, S. C. Low, S. R. A. Shukor, and A. Ismail, "Synthesis and Characterization of Polymeric Nitrocellulose Membranes : Influence of Additives and Pore Formers on the Membrane Morphology," *Journal of Applied Polymer Science*, vol. 108, no. 4, pp. 2550–2557, 2008.

[14] T.-H. Young and L.-W. Chen, "Pore formation mechanism of membranes from phase inversion process," *Desalination*, vol. 103, pp. 233–247, 1995.

[15] J. Kim and K. Lee, "Effect of PEG additive on membrane formation by phase inversion," *Rain*, vol. 138, pp. 153–163, 1998.

[16] V. P. Khare, A. R. Greenberg, J. Zartman, W. B. Krantz, and P. Todd, "Macrovoid growth during polymer membrane casting," *Desalination*, vol. 145, no. 1–3, pp. 17–23, 2002.

[17] C. A. Smolders, A. J. Reuvers, R. M. Boom, and I. M. Wienk, "Microstructures in phase-inversion membranes. Part 1. Formation of macrovoids," *Journal of Membrane Science*, vol. 73, no. 2–3, pp. 259–275, 1992.

[18] F. G. Paulsen, S. S. Shojaie, and W. B. Krantz, "Effect of evaporation step on macrovoid formation in wet-cast polymeric membranes," *Journal of Membrane Science*, vol. 91, no. 3, pp. 265–282, 1994.

[19] J. Hao and S. Wang, "Calculation of Alcohol-Acetone-Cellulose Acetate Ternary Phase Diagram and their Relevance to Membrane Formation," *Jounral of Applied Polymer Science*, vol. 80, pp. 1650–1657, 2001.

[20] S. C. Pesek and W. J. Koros, "Aqueous quenched asymmetric polysulfone membranes prepared by dry/wet phase separation," *Journal of Membrane Science*, vol. 81, no. 1–2, pp. 71–88, 1993.

[21] E. J. Flynn, D. Keane, J. D. Holmes, and M. A. Morris, "Unusual trend of increasing selectivity and decreasing flux with decreasing thickness in pervaporation separation of ethanol/water mixtures using sodium alginate blend membranes.," *Journal of Colloid and Interface Science*, vol. 370, no. 1, pp. 176–82, Mar. 2012.

[22] A. F. M. Barton, *CRC Handbook of Polymer-Liquid Interaction Parameters and Solubility Parameters*. CRC Press, 1990.

[23] A. G. Yiotis, I. N. Tsimpanogiannis, A. K. Stubos, and Y. C. Yortsos, "Pore-network study of the characteristic periods in the drying of porous materials.," *Journal of colloid and interface science*, vol. 297, no. 2, pp. 738–48, May 2006.

[24] L. Pauchard and C. Allain, “Buckling instability induced by polymer solution drying,” *Europhysics Letters*, vol. 62, no. 6, pp. 897–903, 2003.

[25] T. Thurn-Albrecht, R. Thomann, T. Heinzel, and S. Hugger, “Semicrystalline morphology in thin films of poly(3-hexylthiophene),” *Colloid & Polymer Science*, vol. 282, no. 8, pp. 932–938, Jun. 2004.

[26] M. P. Stevens, “Chapter 3: Chemical Structure and Polymer Morphology,” in *Polymer Chemistry: An Introduction*, Oxford University Press, Inc., 1999, pp. 61–95.

[27] P. Van-de-Witte, “Phase separation processes in polymer solutions in relation to membrane formation,” *Journal of Membrane Science*, vol. 117, no. 1–2, pp. 1–31, Aug. 1996.

[28] T. Young and L. Chen, “Pore formation mechanism of membranes from phase inversion process,” *Desalination*, vol. 103, no. 3, pp. 233–247, Dec. 1995.

[29] S. P. Nunes and T. Inoue, “Evidence for Spinodal Decomposition and Nucleation and Growth Mechanisms during Membrane Formation,” *Journal of Membrane Science*, vol. 111, no. 1, pp. 93–103, 1996.

[30] H. Chae Park, K. Yoon Po, K. Hwa Yong, and K. Yong Su, “Membrane formation by water vapor induced phase inversion,” *Journal of Membrane Science*, vol. 156, no. 2, pp. 169–178, Apr. 1999.

[31] I. Pinnau and W. J. Koros, “A qualitative skin layer formation mechanism for membranes made by dry/wet phase inversion,” *Journal of Polymer Science Part B: Polymer Physics*, vol. 31, no. 4, pp. 419–427, Mar. 1993.

[32] A. G. Yiotis, I. N. Tsimpanogiannis, A. K. Stubos, and Y. C. Yortsos, “Pore-network study of the characteristic periods in the drying of porous materials.,” *Journal of colloid and interface science*, vol. 297, no. 2, pp. 738–48, May 2006.

[33] J. Gmehling, J. Menke, J. Krafczyk, and K. Fischer, *Azeotropic Data, Volume 1*. Wiley-VCH, 2004.

[34] J. Gmehling, J. Menke, J. Krafczyk, and K. Fischer, *Azeotropic Data, Volume 2*. Wiley-VCH, 2004.

[35] C. K. Haas and J. M. Torkelson, “Two-dimensional coarsening and phase separation in thin polymer solution films,” *Physical Review E*, vol. 55, no. 3, pp. 3191–3201, 1997.

[36] I. Pinnau and W. J. Koros, “A qualitative skin layer formation mechanism for membranes made by dry/wet phase inversion,” *Journal of Polymer Science Part B: Polymer Physics*, vol. 31, no. 4, pp. 419–427, 1993.

Chapter 7

Advanced Pervaporation Membranes: Mixed Matrix Membranes

7 Pervaporation Mixed Matrix Membranes

The following is adapted from "*Pervaporation Performance Enhancement through the Incorporation of Mesoporous Silica Spheres into PVA membranes*". Separation and Purification Technology, Volume 118, 30 October 2013, Pages 73–80

Abstract

Spherical, discreet, size-monodisperse mesoporous silica particles of 1.8 – 2 µm diameter, with pore diameters of ~1.8 nm were incorporated into a poly(vinyl alcohol) [PVA] polymer to produce composite pervaporation membranes. The selective membrane layers were cast on polyacrylonitrile [PAN]/non-woven fabric supports. The inclusion of particulate silica had beneficial effects on pervaporation performance for the dehydration of ethanol, improving flux throughout the composition range studied, as well as increasing selectivity in all but the highest silica content samples. The unique pervaporation in mesoporous membranes is discussed in terms of polarity and solubility data.

7.1 Introduction

Pervaporation is a membrane separation technology primarily used to dehydrate and recover solvents and also to separate organic-organic mixtures[1–6]. It has significant advantage over other separation techniques in that it can be used to effectively 'break' azeotropes of mixtures without any of the typically associated physical difficulties and negative environmental impacts of techniques such as azeotropic distillation[7]. Consisting of a feed solution of solvent and water (or solvent and solvent) to be separated and a suitable polymer, inorganic, or composite material membrane that allows selective permeation of one of the feed molecules via absorption/diffusion through the polymer[1]. A partial vacuum is maintained on the permeate side, providing the driving force for diffusion by creating a vapour pressure difference across the membrane. The size, motion and permanence of gaps in the polymer chain matrix of the membrane define both the flux and selectivity[1]. These two parameters have an inverse relationship to one another; as flux increases selectivity decreases and vice versa (see chapter 1, section 1.2.1 for detailed explanation of pervaporation theory). One method of improving membrane flux without significantly compromising selectivity is by inclusion of porous particles into the polymer matrix, e.g. zeolites[8]. In porous ceramic-polymer membrane hybrids of this type the engineering of the particles, i.e. size, shape, monodispersivity, pore size and surface chemistry, is important.

Incorporating ceramic materials into membranes (*mixed matrix membranes* (MMM)) is a challenge of maintaining membrane mechanical integrity and controlling free volume (other than the designed ceramic pore volume). Additional free volume arises from polymer-particle interactions[9][10]. When a particle is incorporated into a polymer matrix, chain entanglement of the particle occurs. Since polymer chain segments are rigid and inflexible on the nanoscale [11], free volumes form between the particle and the polymer matrix. Further, as in all particulate systems, if the particles are not well-dispersed throughout the matrix, are not monodisperse or, have ill-defined shape, extra free volume is created[12]. These uncontrolled free volumes can significantly and unpredictably compromise selectivity. Particle agglomeration related free volume can also act as stress raisers and crack initiators, propagating defects quickly through the ceramic

particle/polymer network. For the sake of clarity in the data presented here and its' subsequent discussion, the distinction between the different volumes that can occur within the membrane should be carefully defined: *pore-volume* - the volume contributed to the membrane by the presence of pores within the particle, *free-volume* - the volume contribution from the space around particles created by polymer chain entanglement and *chain gaps* - the fluctuating gaps between polymer chains in the membrane matrix that allow for diffusion as described above.

Whilst microporous zeolitic composite membranes have been frequently studied, mesoporous systems with pore sizes greater than 2 nm have been less researched. The use of mesoporous silica for pervaporation application was first reported by Cot et al.[13] using homogeneous membranes prepared by alkyltrimethylammonium bromide templated silica. They carried out tests on a polar/non-polar binary, ethanol‑cyclohexane separation and observed a pervaporation effect. Mesoporous silica has also been used in mixed matrix membranes as a filler particulate in pervaporation and gas separation. Aminabhavi et al.[14] reported an increase in both flux and selectivity when MCM-41 particles were embedded in a cross-linked sodium alginate membrane for dewatering isopropanol by pervaporation. MCM-41 nanoparticles have also been used in polysulfone membranes for gas separation and have been found to increase gas permeability without a loss in selectivity[15], [16]. In mesoporous materials the pores are significantly larger than in zeolites but they are uni-directional and at dimensions which favour molecular movement. Further, the shape and size of the particles and the pores can be carefully engineered. Size/shape uniformity may afford considerable advantage in terms of regular particle distribution as well as membrane mechanical performance[17]. Further, they can be relatively easily functionalised to change the surface chemistry to promote molecular selectivity[18]. In this way, the particle synthesis methods used here afford many advantages over traditional ceramic particulates. The mesoporous particles used in this study are detailed in previous work by the group[17]. The process yields discreet, monodisperse non-agglomerated mesoporous silica particles. Incorporation of these particles into membranes results in high dispersion through polymer matrices. This allows for reduction of free volume to a minimum and, importantly, means the free volume created by their incorporation is approximately

the same for all membranes of common particle loading; something which has hitherto been unachievable[16], [19]. This article focuses on the incorporation of novel small-pore (1.8-2.0 nm diameter), spherical, monodispersive mesoporous silica microspheres into PVA (*poly(vinyl alcohol)*) membranes for use in pervaporation dehydration of azeotropic ethanol-water mixtures. PVA was chosen as the base polymer as it possesses a high strain at fracture [20] allowing for significant particle loadings without overly compromising mechanical stability. PVA pervaporation membranes require careful crosslinking for optimum performance[21]. This chapter does not centre on achieving the highest possible membrane efficacy but rather on assessing the potential of these mesoporous silica particles as enhancing agents in pervaporation membranes. A low selectivity polymer is best used to observe the effect of introducing these novel materials into a membrane matrix. With superselective membranes, where permeate water content typically exceeds 98 %, the relative enhancement of performance by incorporated particles constitutes a much lower percentage increase in selectivity. It becomes difficult to ascertain whether an increase in performance is statistically relevant, as small changes in retentate/permeate composition, permeate side vacuum, or feed solution flow-rate can have a similarly significant effect on flux/selectivity figures. However these effects can be random, irreproducible and unrelated to the particles incorporated. Thus, cross-linked PVA was chosen over highly selective materials like sodium alginate as the polymeric membrane matrix. Typical experimental results are shown below.

7.2 Experimental

See chapter 2 for details on all materials, apparatus and procedures not mentioned below.

7.2.1 Materials

Mesoporous silica particles were prepared using a modified Stöber process [17].

7.2.2 Membrane preparation

Membrane supports were prepared similar to a literature procedure[22]. Membranes were thermally crosslinked;[23–25] to provide the mechanical stability

required for assessing the potential of mesoporous materials as pervaporation enhancers.

7.2.3 Pervaporation

Pervaporation experiments conducted using Laboratory 6" Test Cell produced by Sulzer Chemtech. A detailed schematic diagram of this pervaporator can be found elsewhere[26], [27].

7.2.4 Characterization

All membrane samples were prepared for imaging by the Cryo-Rupturing Image Sample Preparation (CRISP) method[28].

7.3 Results and Discussion:

7.3.1 Characterisation

SEM and TEM of the silica particles are shown in figure 7.1 A and 7.1B. The images show the spherical morphology. It is clear from figure 7.1A that the particles have a highly monodisperse nature. The measured mean particle size was 1.8 - 2.0 µm. The porosity and pore structure has been characterized previously using X-ray diffraction (XRD), electron microscopy and nitrogen adsorption[17]. Figure 7.1B shows a TEM image of particles produced by the same process as those used in the membranes. Particles of smaller diameter are imaged here since larger particles are less electron-transparent and direct imaging of the pore structure is not readily achieved. However, the pore size of the particles is representative of the larger particles as little variation from particle-to-particle is observed.

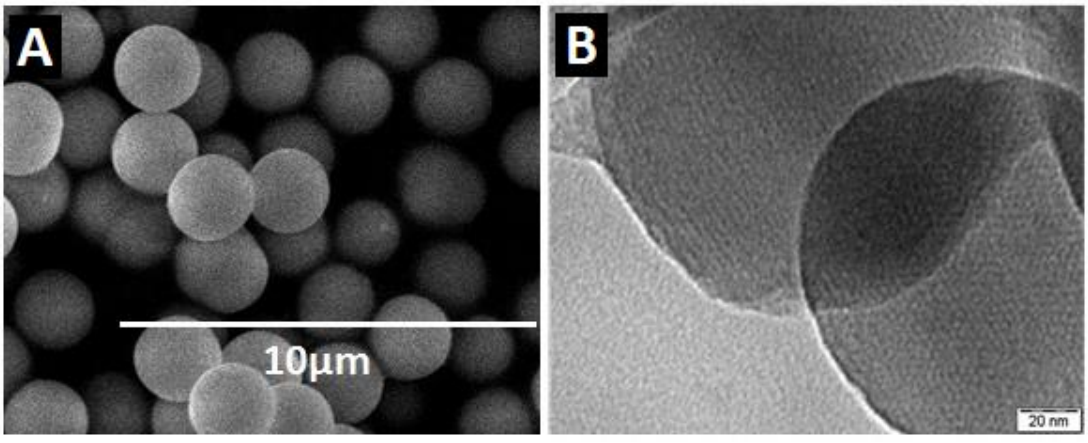


Figure 7.1: A) mesoporous silica particles SEM image B) TEM image of pores resulting from modified Stöber process

The pore structure of the particles is largely disordered as characterized by a broad low angle XRD peak[17]. However, the presence of areas with local order is also possible as shown by the channels visible in figure 7.1B. The average pore diameters were measured at about 1.8 nm with an average pore volume of approximately 0.45 cm^3 g^{-1} and the material had surface area of approximately 700 m^2 g^{-1} (from BET measurements reported previously[17]).

When these particles are placed in a solvent solution and subjected to sonication, they form dispersions that are stable for several hours due to their monodispersivity and small size. Particles of these dimensions and chemistry are expected to exhibit relatively slow aggregation kinetics and, hence, form stable dispersions[29–31]. Whilst the solvent mixtures used to prepare the membranes exhibit good dispersions, the degree of dispersion in the cast and dried membrane might not be the same due to aggregation effects during film formation and solvent loss. Below a 15 wt% loading, the particles are observed to be well-dispersed and very few areas of aggregated particles can be seen. However, at 15 wt% particle loading and above, aggregation is obvious and extensive phase separation of particles and polymer is clear. Illustrative SEM images are shown in figure 7.2. Figure 7.2A shows an image of a PVA membrane with 15 wt% loading of silica particles present. Particulate agglomeration can be observed (highlighted) as well as extensive segregation of particles to the film surface. In regions of aggregation, there appears to be a degree of close packing within the clusters. The cross-section image of the same membrane in figure 7.3G confirms the poor integration; not only is aggregation present but also extensive segregation to the surface is obvious. The poor binding of the silica to the polymer chains is evident from the close proximity and direct contact of silica particles to each other and also by surface segregation. Poor binding of PVA to small silica particles has been seen previously and has been explained by low PVA coverage at the nanoparticle surfaces and consequently phase separation due to depletion effects[32].

In comparison to the 15 wt% samples, figure 7.2B and 7.3F show the surface and cross section images respectively of a pervaporation membrane with 10 wt% particle loading (the optimum membrane produced in terms of pervaporation performance as described below). In contrast to the 15 wt% silica loaded materials,

the 10 wt% particles are very well dispersed through the membrane and there is no sign of aggregation or segregation of the particles to the surface in the cross section.

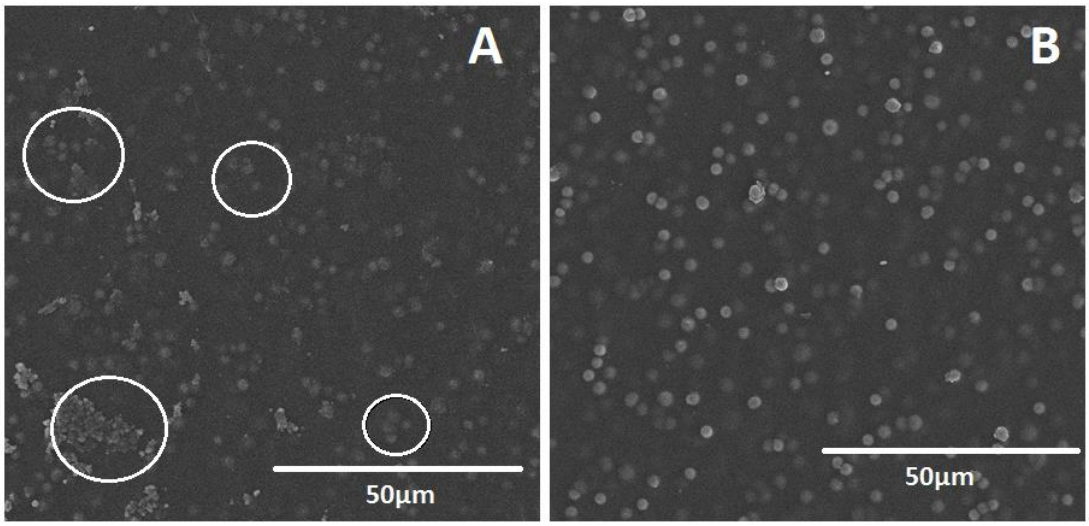


Figure 7.2: A) surface image of 15 wt% silica loaded PVA membrane B) surface image of 10 wt% silica loaded PVA membrane

It can be seen that the particles appear to exhibit direct polymer attachment and some particles appear to be in contact with the polymer over large areas of their surface: This is markedly different to higher loadings as can be seen above. It can be concluded from the data that at low silica content, the particles are well distributed through the membrane but at 15 wt% and above aggregation occurs: A maximum loading for good dispersion is present in this system. Similar aggregation of particles was observed by Aminabhavi *et al.* upon incorporation of nanoparticles into chitosan membranes[10].

A series of membranes of increasing silica content are shown in figure 7.3. In each case, cross-section images confirm the top-down image analysis. Further, these are consistent with good dispersion of particles at lower loadings. The unloaded sample (figure 7.3A and 7.3E) has a dense film structure (and is consequently much thinner than a membrane loaded particle) with no sign of porosity. It has a film thickness about 5 µm. The 10 wt% silica containing sample has a good film structure with little sign of segregation of particles to the surface (figure 7.3C and 7.3F). The 5 wt% sample (figure 7.3D) also exhibited similar dispersion of the added particles. The measured thicknesses are around 15 µm and 10 µm for the 10 wt% loaded and 5 wt% loaded membranes respectively, the

thickness increase being due to the material addition and the volume of the porous particles.

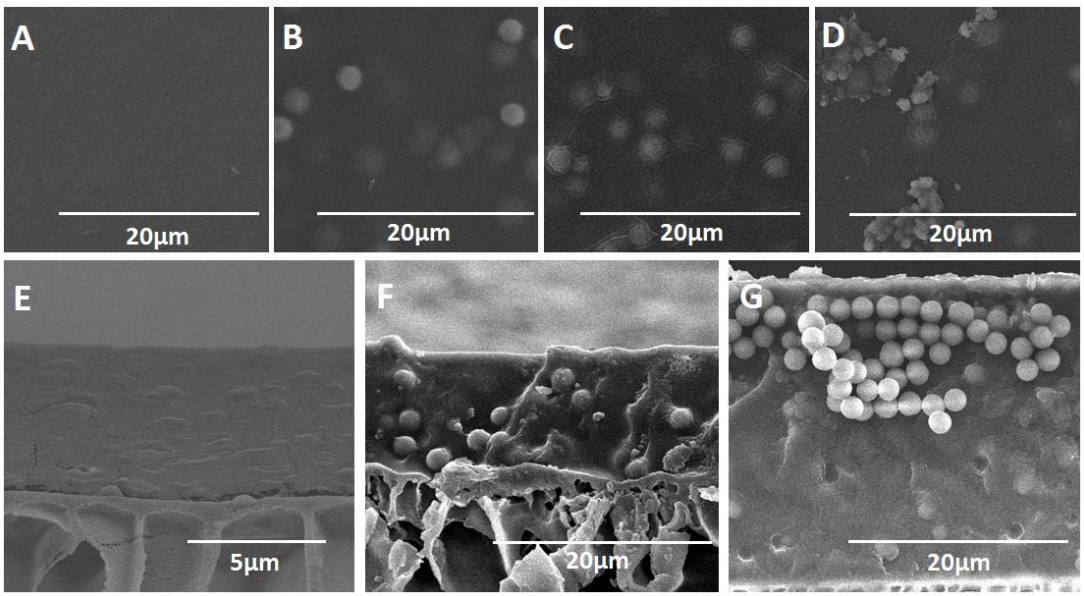


Figure 7.3: Images A, B, C and D show surface of pervaporation membranes with 0 wt%, 5 wt%, 10 wt% and 15 wt% silica loading respectively. Images E,F and G show cross section images of 0 wt%, 10 wt% and 15 wt% silica loaded membranes respectively

The measured film thickness of the 15 wt% silica sample was measured at about 25 µm, consistent with the trend observed. The increase in film thickness seen is consistent with the volume of particles added. PVA has a density of ~1.1 g cm^{-3}. Silica has a density of ~2.2 g cm^{-3} but these mesoporous particles have porosity of approximately 75 % by volume and, hence, a density around half that of the PVA. The pervaporation performance of these membranes was tested and details are provided below.

7.3.2 Membrane Absorption

The absorption data for a section of membrane selective layer (70 mm x 50 mm x 20 µm), shows that in a solution of 50 wt% water to 50 wt% ethanol the rate at which said solution is absorbed and the maximum absorption achieved before the membrane becomes so swollen that it dissolves. Incorporation of silica particles into the membrane polymer matrix results in increased rate and capacity, up to a defined maximum between 10 wt% and 15 wt% loading of silica particles.

This can be seen from the data in figure 7.4: At 0 wt% silica particle loading, the membrane dissolves after only 40 s in solution, at ~257 wt% of its original dry mass. The average rate of absorption was 3.91 wt% s^{-1}; the membrane showed little

deviation from this rate before eventually dissolving. Incorporating 5 wt% silica into the membrane matrix, figure 7.4 shows that the membrane dissolves after 50 s in solution with a mass ~327 wt% of the original dry mass of the membrane, suggesting an increase in the membrane matrix mechanical stability; a well-documented benefit of incorporation of silica particles[33–35]. The rate at which absorption occurs is increased to 4.51 wt% s^{-1}; an increase in hydrophilicity which is due to the hydrophilic silanol groups on the silica particle surfaces and the high surface area of the particles due to their porosity.

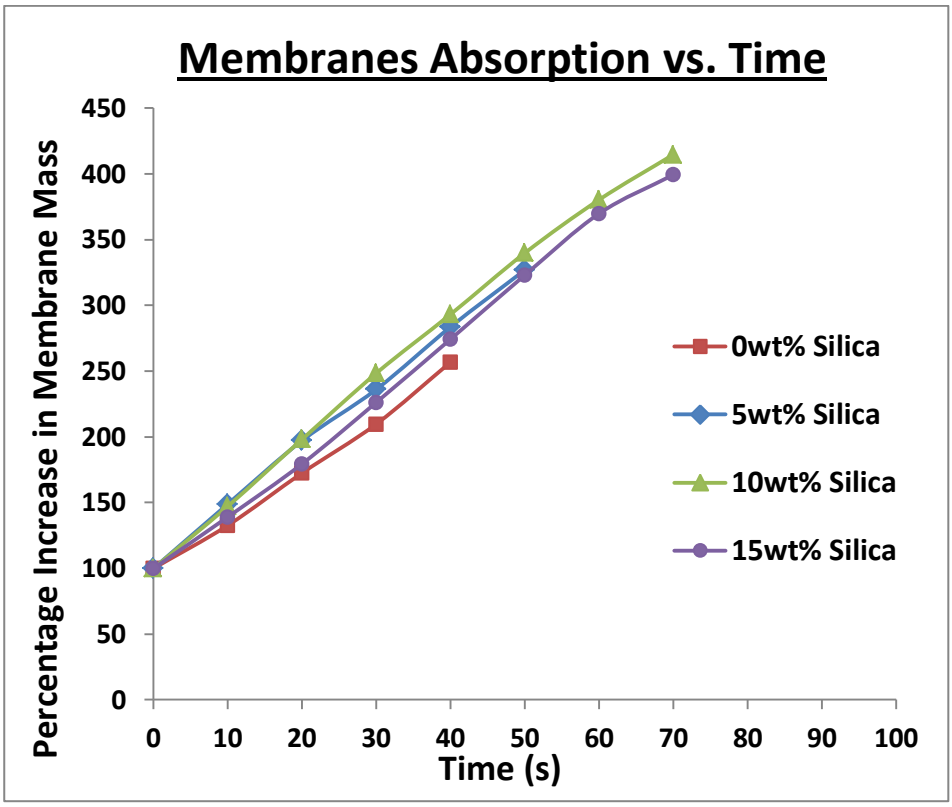


Figure 7.4: Membrane absorption vs. time; shows absorption of a solution of 50 wt% EtOH and 50 wt% water into selective membrane over time. Maxima represent point at which membrane becomes dissolute, i.e. loses membrane form and so becomes unusable. (See appendix E, table E.1 for tabulated data)

Increasing the particle loading to 10 wt% results in a further increase in the capacity of the membrane before dissolving in solution at ~415 wt% of its original dry mass over a period of 70s. The average rate of absorption of solution was 4.57 wt% s^{-1}. This data shows a positive trend in all parameters with the increase in silica loading for the same reasons highlighted for the 5 wt% loading.

Increasing the silica loading to 15 wt%, the absorption capacity of the membrane decreases to 399 wt% of its original dry mass over the same time period

as the 10 wt% silica loaded membrane. The rate at which the membrane absorbs the solution is also reduced from that of the 10 wt% loading, dropping to 4.44 wt% s^{-1}. Some of the hydrophilic nature of the particles has been lost compared to the expected increase based on the trend observed from 0 to 10 wt% loading. In addition, the lower absorption capacity shows the degree of the mechanical stabilization expected has been reduced. The reasons for this can be explained by looking again at the SEM images of figures 7.2 and 7.3. It can be seen clearly that in the 15 wt% silica loaded membrane, compared to the 10 wt% and 5 wt%, there is a greater degree of agglomeration of particles. This agglomeration increases particle-particle contact and so effectively reduces the available surface area as well as the number of silanol groups thus, reducing the potential increase in hydrophilicity. The reduction in mechanical stability is due to the increase in free volume around large agglomerates compared to the increase from much smaller, well dispersed single silica spheres at lower weight percentage loadings. This is due to the limited motion of polymer chain segments, an effect that is enhanced with larger, irregularly shaped particles, which is what the agglomerates formed at 15 wt% silica loading effectively are[11], [12]. It has been reported that after incorporation of filler particles membrane swelling *decreases* with loading [36], [37]. However in these instances the size and nature of the particles resulted in greater bonding with the polymer chain matrix and/or occupation of interstitial spaces within polymer matrix of the membrane.

7.3.3 Pervaporation

Pervaporation results are detailed in figure 7.5 which summarises flux and selectivity data from four membranes prepared containing different weight percentage loadings of silica ranging from 0 wt% to 15 wt%. Table 7.1 shows the average selectivity and flux attained for each membrane over the duration of a pervaporation test and the maximum selectivity and flux obtained during the test.

Table 7.1: Tabulated flux, selectivity, feed and permeate purity, and contact angle data for membranes at different wt% silica particle loadings

Mem: PVA Diameter: 0.158m Area: 0.0177m^2	Flux (g m^{-2} h^1)		Selectivity		Permeate H_2O purity (max)	Feed EtOH Purification (after 6 h)	Contact Angle
Silica (wt%)	Avg.	Max.	Avg.	Max.	(wt%)	(wt%)	degrees
0	409.3	427.3	20.8	22.8	87.5	0.8	~80
5	453.9	531.3	22.3	24.4	88.7	1.1	~76
10	855.1	945.5	42.3	48.4	93.2	2.0	~71
15	1193.4	1334.0	10.3	11.1	78.5	0.1	~68

Figure 7.5(A) describes the selectivity of the membranes as a function of time. The unloaded membrane shows an average selectivity of ~21 over the six hour measurement and varies little throughout this period.

Inclusion of 5 wt% silica brings about a small increase in selectivity over the unloaded membrane, with no significant change in flux. At 10 wt% loading, there is a dramatic increase in selectivity to an average value of ~42, twice that of the lower weight loading. The selectivity (and to some extent flux) appears to show a distinct peak with time, having lower values at the start and end of the run. However, the selectivity is always in excess of the non-silica containing PVA membrane. Such variation in selectivity can be ascribed to conditioning[22] and relaxation effects [20][24] which are particularly prevalent in PVA membranes. At a loading of 15 wt%, there is a significant decrease in selectivity to ~10.25, below that of the 0 wt% membrane. This is related to the poor dispersion and segregation of the mesoporous silica particles as seen in figure 7.3(D). The free-volume increase, described above, resulting from particulate agglomerates such as those seen at 15 wt% loading, results in facile, less selective diffusion of feed through the membrane. It is suggested that the 10 wt% membrane represents close to the maximum amount of silica that can be included without gross segregation and agglomeration effects occurring, this is corroborated by the SEM images of figures 7.2 and 7.3 and by the trends seen in the absorption data. The variation in selectivity observed is clearly shown in figure 7.5C where average values as a function of silica loading are plotted. The data suggest that the silica does have a beneficial effect on separation.

Whilst selectivities here were modest compared to other inorganic modified membranes, the corresponding fluxes are higher than might be expected. Compared with reported figures in which zeolites (the most commonly used and most effective material incorporated into MMMs industrially) are incorporated into a PVA

membrane, the membranes produced here showed a considerable increase in the average flux of the plain PVA membrane upon incorporation of 10 wt% loading of silica[19], [22], [38].

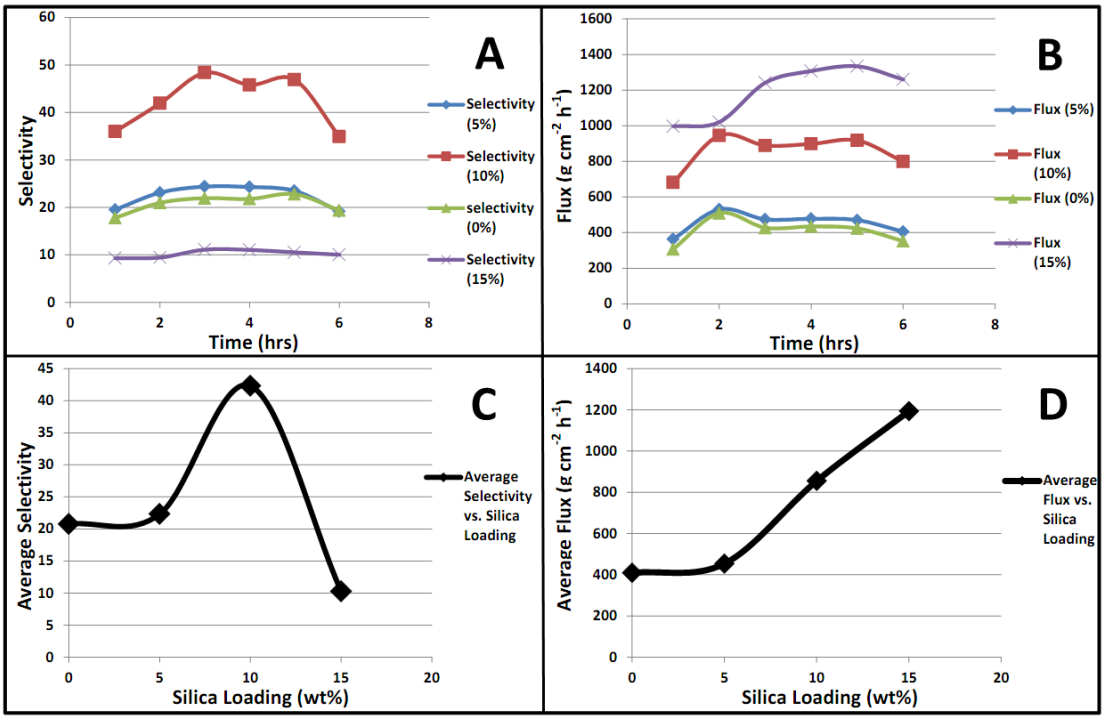


Figure 7.5: A: Selectivity vs. time for membranes of particle loading from 0 wt% to 15 wt% silica loading. B: Flux vs. time for membranes of particle loading from 0 wt% to 15 wt% silica loading. C: Average flux of membrane vs. membrane silica loading. D: Average selectivity of membrane vs. membrane silica loading

The flux measured from the PVA membrane is ~410 g $m^{-2}h^{-1}$. While selectivity values showed a distinct peak with loading amount, the flux shows a continual increase (figure 7.5D). The increase in flux seen on 5 wt% loading, like the selectivity, is limited with an average value of ~455 g $m^{2}h^{-1}$. This suggests that in the lower loaded sample that permeation through the PVA is dominant. At a loading of 10 wt% the rise in flux is significant at about 855 g $m^{-2}h^{-1}$ averaged over the 6 h test period. It, thus, appears that a 10 wt% loading of mesoporous silica particles increases both selectivity and flux considerably. The increase in flux seen could be due to molecules being transported more efficiently through the pores within the mesoporous silica matrix. At 15 wt% loading, the flux further increases to an average value of 1194 g m^{-2} h^{-1}. However, since this occurs in conjunction with a significant decrease in selectivity, the flux increase is also due in significant part to the free volume introduced by increased interface void volume around agglomerated particles which are not observed at lower particle loadings.

7.3.4 Discussion

The difference between the 10 and 15 wt% samples in terms of pervaporation performance and membrane morphology is marked and they are related. The morphological differences are significant, being well-dispersed and aggregated for the 10 and 15 wt% samples respectively. The aggregation in the film derives from particle-polymer interaction differences in the membrane formation process (since in dry dense membrane structures particle movement is severely restricted). A significant difference in the membrane synthesis solutions is the ionic strength and it is suggested here that this plays a significant role in determining the particle aggregation. The higher the silica content in PVA-SiO_2 suspensions, the higher the ionic strength is expected to be[39]. The bonding of PVA to silica surfaces has been well explored and it is generally accepted that the PVA is attached through hydrogen bonding and condensation with surface silanol groups[14], [40], [41]. However, the density of active silanol groups is related to the ionic strength and as ionic strength increases, the activity of the silanol sites decreases due to ionization of the –OH groups[39]. As a result the surface coverage of the polymer on the particles will lessen. The coverage of PVA is important in deciding the degree of aggregation[42], [43]. High molecular weight polymers attached to a surface form pendant chains, chain loops, etc. The osmotic pressure (resulting from the free volume between the polymer segments and various chain morphologies) acts as a repulsive force (since free volume is associated with higher energy states) to keep two approaching particles away from each other. In this way, as polymer coverage at the particle increases, the repulsive forces between particles and resistance to aggregation should also increase. Further, unsaturated surfaces, i.e. lower surface coverage, can promote bridging and flocculation[39], [42], [43]. In this way, as polymer is subjected to increased silica loadings, the PVA coverage will decrease and favour particle aggregation as observed here. Decreases in membrane free volume upon particle incorporation have been reported elsewhere,[37] contrary to what is observed above. This decrease has been attributed to an increase in membrane crosslink density due to the reinforcing effect of filler nanoparticles (size 282-290nm) occupying interstitial spaces within the polymer matrix[37]. However, the particles used in this study with mean size diameters of 1.8 – 2.0 µm are too large to occupy interstitial spaces between polymer chains[44].

Additionally, free volume increases in membranes have been observed upon incorporation of filler particles but this has been attributed to aggregation of the particles[10]. Given that polymer chain segments are rigid and inflexible on the nanoscale,[11] when incorporating larger scale particles, such as those used here – assuming they are discreet – polymer chains can conform more closely to the particle shape as the extent to which the polymer chains must bend to do so is within the limits of their flexibility. Thus the free volume formed from this is less per mass of filler particles that with smaller particles, minimising the loss in flux attributed to these free volumes. Further, with discreet particles the free volume increase is consistent from membrane to membrane as discussed previously. Also, this is achieved with minimal loss of active particle surface area suffered by the formation of agglomerates.

The data from figure 7.5 shows conclusively that the incorporation of around 10 wt% of novel mesoporous silica particles into a PVA pervaporation membrane matrix results in a considerable improvement in pervaporation performance in terms of both flux and selectivity. The improvement of both selectivity and flux simultaneously is relatively uncommon[36], [45]. The improvement in selectivity with loading can only be explained by concluding that the silica particles are themselves selective to diffusion of water molecules. Zeolite membranes and particles are active ethanol-water pervaporation materials because of their molecular sieving and adsorption properties[8]. Since the mesopore diameter here (1.8 - 2.0 nm) is considerably greater than the effective diameter of both ethanol (~0.40 nm) and water molecules (~0.28 nm), it can be concluded that there is little molecular sieving effect through these pores. In this respect, the selection of mesoporous materials in pervaporation is not theoretically obvious but still worthy of further comment and reasoning.

It has been proposed that the polar groups in the membrane matrix, responsible for the membrane hydrophilicity, act as the fixed carriers for mass transport in the membrane[46]. In the case of dehydration of organic solvents, it is believed that water transport in the membrane proceeds in a unique manner. Unlike the random path of the less polar species, the water molecule jumps from one polar site to another. The fixed-carrier theory implies that water and the less polar species in the liquid mixture take different paths while diffusing through the membrane.

Mesoporous silica systems are known to both adsorb and transport water molecules very efficiently[47].

Empirically, solubility and polarity data support this separation mechanism. The use of such data has previously been used in polymeric membrane material selection for pervaporation.[48] Water and ethanol have a Dimroth and Reichardt's solvent polarity ET(30) value of 264.01 kJ mol^{-1} and 217.15 kJ mol^{-1} respectively. The Hildebrand solvent parameter of silica is measured at between 28 - 38 $MPa^{1/2}$ [40] whilst water and ethanol are around 48 and 26 $MPa^{1/2}$ respectively[41]. Both sets of data suggest additional selectivity to water over ethanol. Furthermore, the solubility parameter of mesoporous silica is expected to be increased over bulk silica materials because of its very high reactivity to water[47].

The inclusion of the mesoporous component is also indicated by the increased hydrophilicity of the membranes. This can be seen directly from contact angle measurements made on the membrane (see table 7.1). These were 80, 76, 71 and 68 ° from 0 to 15 wt% loading respectively. It is thus suggested that the improved selectivity arises from the increased hydrophilicity/water adsorption properties of the membranes. This is consistent with previous arguments [14], [19]. The increased flux in these improved membranes is certainly due to the addition of the pore volume.

7.4 Conclusion

This work shows that the incorporation of engineered mesoporous particles into polymer pervaporation membranes can be highly beneficial and warrants extended study to optimise performance and assess the ideal structural parameters such as size, shape and pore dimensions. Results show that incorporation of spherical, discreet, size-monodisperse mesoporous silica particles of 1.8 – 2 µm diameter and with pore diameters of ~1.8 nm, when incorporated into a poly(vinyl alcohol) [PVA] polymer to produce composite pervaporation membranes, resulted in statistically significant increases in both flux and selectivity. Inexpensive mesoporous synthesis routes as well as chemical functionalization treatments are now available[18] and the cost should not be prohibitive. Unlike zeolitic systems, mesoporous solids can be very controllably engineered to give a wide range of pore

sizes and chemistries and may provide new generations of membranes for various pervaporation applications.

7.5 Summary

Incorporation 10 wt% of mesoporous silica particles results in improvement in flux & selectivity
Improvement of both selectivity & flux simultaneously uncommon
Improvement in selectivity leads to conclusion that silica particles are themselves selective to diffusion of water molecules
Improvement in performance achieved through particle polar surface silanol groups - add to membrane hydrophilicity – increase fixed carrier capability of membrane

References: Chapter 7

[1] R. W. Baker, *Membrane Technology and Applications*, 2nd ed. John Wiley and Sons, Ltd., 2007.

[2] A. Jonquières, "Industrial state-of-the-art of pervaporation and vapour permeation in the western countries," *Journal of Membrane Science*, vol. 206, no. 1–2, pp. 87–117, Aug. 2002.

[3] P. Van De Witte, J. W. A. Van Den Berg, and J. Feijen, "Phase separation processes in polymer solutions in relation to membrane formation," *Journal of Membrane Science*, vol. 117, pp. 1–31, 1996.

[4] S. Kalyani, B. Smitha, S. Sridhar, and a Krishnaiah, "Pervaporation separation of ethanol–water mixtures through sodium alginate membranes," *Desalination*, vol. 229, no. 1–3, pp. 68–81, Sep. 2008.

[5] R. Y. M. Huang, R. Pal, and G. Y. Moon, "Characteristics of sodium alginate membranes for the pervaporation dehydration of ethanol–water and isopropanol–water mixtures," *Journal of Membrane Science*, vol. 160, no. 1, pp. 101–113, Jul. 1999.

[6] S. Ray and S. K. Ray, "Separation of organic mixtures by pervaporation using crosslinked and filled rubber membranes," *Journal of Membrane Science*, vol. 285, no. 1–2, pp. 108–119, Nov. 2006.

[7] V. Van Hoof, L. Van den Abeele, A. Buekenhoudt, C. Dotremont, and R. Leysen, "Economic comparison between azeotropic distillation and different hybrid systems combining distillation with pervaporation for the dehydration of isopropanol," *Separation and Purification Technology*, vol. 37, no. 1, pp. 33–49, Jun. 2004.

[8] T. Bowen, R. Noble, and J. Falconer, "Fundamentals and applications of pervaporation through zeolite membranes," *Journal of Membrane Science*, vol. 245, no. 1–2, pp. 1–33, Dec. 2004.

[9] C.-L. Li, S.-H. Huang, W.-S. Hung, S.-T. Kao, D.-M. Wang, Y. C. Jean, K.-R. Lee, and J.-Y. Lai, "Study on the influence of the free volume of hybrid membrane on pervaporation performance by positron annihilation spectroscopy," *Journal of Membrane Science*, vol. 313, no. 1–2, pp. 68–74, Apr. 2008.

[10] V. T. Magalad, G. S. Gokavi, M. N. Nadagouda, and T. M. Aminabhavi, "Pervaporation Separation of Water - Ethanol Mixtures Using Organic - Inorganic Nanocomposite Membranes," *Journal of Physical Chemistry C*, vol. 115, no. 1, pp. 14731–14744, 2011.

[11] P. Winberg, M. Eldrup, and F. H. J. Maurer, “Nanoscopic properties of silica filled polydimethylsiloxane by means of positron annihilation lifetime spectroscopy,” *Polymer*, vol. 45, no. 24, pp. 8253–8264, 2004.

[12] D. J. Shaw, *Introduction to Colloid and Surface Chemistry: 4th Edition*. Butterworth - Heinemann, 1992.

[13] L. Cot, J. Durand, C. Guizard, N. Hovnanian, and A. Julbe, “Inorganic membranes and solid state sciences,” *Solid State Sciences*, vol. 2, no. 3, pp. 313 – 334, 2000.

[14] S. Bhat, B. Naidu, G. Shanbhag, S. Halligudi, M. Sairam, and T. Aminabhavi, “Mesoporous molecular sieve (MCM-41)-filled sodium alginate hybrid nanocomposite membranes for pervaporation separation of water – isopropanol mixtures,” *Separation and Purification Technology*, vol. 49, no. 1, pp. 56–63, Apr. 2006.

[15] S. Kim and E. Marand, “High permeability nano-composite membranes based on mesoporous MCM-41 nanoparticles in a polysulfone matrix,” *Microporous and Mesoporous Materials*, vol. 114, no. 1–3, pp. 129–136, Sep. 2008.

[16] B. D. Reid, F. A. Ruiz-trevino, I. H. Musselman, K. J. Balkus, and J. P. Ferraris, “Gas Permeability Properties of Polysulfone Membranes Containing the Mesoporous Molecular Sieve MCM-41,” *Chemistry of Materials*, vol. 13, no. 7, pp. 2366–2373, 2001.

[17] D. A. Keane, J. P. Hanrahan, M. P. Copley, J. D. Holmes, and M. A. Morris, “A modified Stöber process for the production of mesoporous Sub 2 micron silica microspheres; applications in HPLC,” *Journal of Porous Materials*, vol. 17, no. 2, pp. 145–152, Mar. 2009.

[18] A. M. Burke, J. P. Hanrahan, D. A. Healy, J. R. Sodeau, J. D. Holmes, and M. A. Morris, “Large pore bi-functionalised mesoporous silica for metal ion pollution treatment.,” *Journal of Hazardous Materials*, vol. 164, no. 1, pp. 229–34, May 2009.

[19] M. Patil, R. Veerapur, S. Patil, C. Madhusoodana, and T. Aminabhavi, “Preparation and characterization of filled matrix membranes of sodium alginate incorporated with aluminum-containing mesoporous silica for pervaporation dehydration of alcohols,” *Separation and Purification Technology*, vol. 54, no. 1, pp. 34–43, Mar. 2007.

[20] R. Russo, M. Malinconico, L. Petti, and G. Romano, “Physical behavior of biodegradable alginate-poly(vinyl alcohol) blend films,” *Journal of Polymer Science Part B: Polymer Physics*, vol. 43, no. 10, pp. 1205–1213, May 2005.

[21] T. Uragami, K. Okazaki, H. Matsugi, and T. Miyata, “Structure and Permeation Characteristics of an Aqueous Ethanol Solution of Organic-

Inorganic Hybrid Membranes Composed of Poly (vinyl alcohol) and Tetraethoxysilane," *Macromolecules*, vol. 35, no. 1, pp. 9156–9163, 2002.

[22] Z. Huang, Y. Shi, R. Wen, Y. Guo, J. Su, and T. Matsuura, "Multilayer poly(vinyl alcohol)–zeolite 4A composite membranes for ethanol dehydration by means of pervaporation," *Separation and Purification Technology*, vol. 51, no. 2, pp. 126–136, Sep. 2006.

[23] A. Svang-Ariyaskul, R. Y. M. Huang, P. L. Douglas, R. Pal, X. Feng, P. Chen, and L. Liu, "Blended chitosan and polyvinyl alcohol membranes for the pervaporation dehydration of isopropanol," *Journal of Membrane Science*, vol. 280, no. 1–2, pp. 815–823, Sep. 2006.

[24] A. S. E Otsuka, "Swelling Properties of Physically Cross-linked PVA Gels Prepared by a Cast-drying Method," *Progress in Colloid and Polymer Science*, vol. 136, no. 2, pp. 121–126, 2009.

[25] R. Y. M. Huang and C. K. Yeom, "Pervaporation separation of aqueous mixtures using crosslinked poly(vinyl alcohol)(pva). II. Permeation of ethanol-water mixtures," *Journal of Membrane Science*, vol. 51, no. 3, pp. 273–292, 1990.

[26] W. Kaminski, J. Marszalek, and A. Ciolkowska, "Renewable energy source—Dehydrated ethanol," *Chemical Engineering Journal*, vol. 135, no. 1–2, pp. 95–102, Jan. 2008.

[27] D. A. Keane, E. J. Flynn, and M. A. Morris, "Report Series No . 50 Preparation of Polymer-Based Membranes for Dehydration of Ethanol by Pervaporation," 2010.

[28] E. J. Flynn, D. Keane, J. D. Holmes, and M. A. Morris, "Unusual trend of increasing selectivity and decreasing flux with decreasing thickness in pervaporation separation of ethanol/water mixtures using sodium alginate blend membranes.," *Journal of Colloid and Interface Science*, vol. 370, no. 1, pp. 176–82, Mar. 2012.

[29] K. J. M. Bishop, C. E. Wilmer, S. Soh, and B. a Grzybowski, "Nanoscale forces and their uses in self-assembly," *Small (Weinheim an der Bergstrasse, Germany)*, vol. 5, no. 14, pp. 1600–30, Jul. 2009.

[30] P. Somasundaran, S. C. Mehta, X. Yu, and S. Krishnakumar, "Colloid Systems and Interfaces Stability and Surfactant Adsorption," in *Handbook of Surface and colloid Chemistry*, 2009, pp. 155 – 196.

[31] M. Kobayashi, F. Juillerat, P. Galletto, P. Bowen, and M. Borkovec, "Aggregation and charging of colloidal silica particles: effect of particle size.," *Langmuir : the ACS journal of surfaces and colloids*, vol. 21, no. 13, pp. 5761–9, Jun. 2005.

[32] L. Guyard, J. Persello, J. Boisvert, and B. Cabane, “Relationship Between the Polymer / Silica Interaction and Properties of Silica Composite Materials,” *Journal of Polymer Science Part B: Polymer Physics*, vol. 44, pp. 1134–1146, 2006.

[33] J. Li, J. Suo, and R. Deng, “Structure, Mechanical, and Swelling Behaviors of Poly(vinyl alcohol)/SiO2 Hybrid Membranes,” *Journal of Reinforced Plastics and Composites*, vol. 29, no. 4, pp. 618–629, Mar. 2009.

[34] P. D. Chapman, T. Oliveira, A. G. Livingston, and K. Li, “Membranes for the dehydration of solvents by pervaporation,” *Journal of Membrane Science*, vol. 318, no. 1–2, pp. 5–37, Jun. 2008.

[35] S. G. Adoor, L. S. Manjeshwar, S. D. Bhat, and T. M. Aminabhavi, “Aluminum-rich zeolite beta incorporated sodium alginate mixed matrix membranes for pervaporation dehydration and esterification of ethanol and acetic acid,” *Journal of Membrane Science*, vol. 318, no. 1–2, pp. 233–246, Jun. 2008.

[36] S. D. Bhat and T. M. Aminabhavi, “Novel sodium alginate composite membranes incorporated with SBA-15 molecular sieves for the pervaporation dehydration of aqueous mixtures of isopropanol and 1,4-dioxane at 30°C,” *Microporous and Mesoporous Materials*, vol. 91, no. 1–3, pp. 206–214, Apr. 2006.

[37] V. T. Magalad, G. S. Gokavi, C. Ranganathaiah, M. H. Burshe, C. Han, D. D. Dionysiou, M. N. Nadagouda, and T. M. Aminabhavi, “Polymeric blend nanocomposite membranes for ethanol dehydration—effect of morphology and membrane–solvent interactions,” *Journal of Membrane Science*, vol. 430, no. 1, pp. 321–329, Mar. 2013.

[38] Y. Ma, J. Wang, and T. Tsuru, “Pervaporation of water/ethanol mixtures through microporous silica membranes,” *Separation and Purification Technology*, vol. 66, no. 3, pp. 479–485, May 2009.

[39] J. Persello, J. Boisvert, A. Guyard, and B. Cabane, “Structure of Nanometric Silica Clusters in Polymeric Composite Materials,” *J. Phys. Chem. B*, vol. 108, no. 10, pp. 9678–9684, 2004.

[40] R. F. Grossman, *The Mixing of Rubber*. Chapman and Hall, 1997.

[41] A. F. M. Barton, *CRC Handbook of Polymer-Liquid Interaction Parameters and Solubility Parameters*. CRC Press, 1990.

[42] A. A. Zaman, “Effect of polyethylene oxide on the viscosity of dispersions of charged silica particles: interplay between rheology, adsorption, and surface charge,” *Colloid & Polymer Science*, vol. 278, no. 12, pp. 1187–1197, Dec. 2000.

[43] S. K. Pattanayek and V. a. Juvekar, “Prediction of Adsorption of Nonionic Polymers from Aqueous Solutions to Solid Surfaces,” *Macromolecules*, vol. 35, no. 25, pp. 9574–9585, Dec. 2002.

[44] M. Smit, H. V. Mulder, C. A. Smolders, H. Karrenbeld, J. Van Eerden, and D. Feil, “Modelling of the diffusion of carbon dioxide in polyimide matrices by computer simulation,” *Journal of Membrane Science*, vol. 73, no. 2, pp. 247–257, 1992.

[45] Z. Huang, H. Guan, W. Tan, X. Qiao, and S. Kulprathipanja, “Pervaporation study of aqueous ethanol solution through zeolite-incorporated multilayer poly(vinyl alcohol) membranes: Effect of zeolites,” *Journal of Membrane Science*, vol. 276, no. 1–2, pp. 260–271, May 2006.

[46] P. Shao and R. Huang, “Polymeric membrane pervaporation,” *Journal of Membrane Science*, vol. 287, no. 2, pp. 162–179, Jan. 2007.

[47] R. A. Farrell, K. Cherkaoui, N. Petkov, H. Amenitsch, J. D. Holmes, P. K. Hurley, and M. A. Morris, “Physical and electrical properties of low dielectric constant self-assembled mesoporous silica thin films,” *Microelectronics Reliability*, vol. 47, no. 4–5, pp. 759–763, Apr. 2007.

[48] A. Jonquières, D. Roizard, J. Cuny, and P. Lochon, “Solubility and polarity parameters for assessing pervaporation and sorption properties. A critical comparison for ternary systems alcohol/ether/polyurethaneimide,” *Journal of Membrane Science*, vol. 121, no. 1, pp. 117–133, 1996.

Chapter 8

Closing Remarks & Future Work

8 Closing Remarks & Future Work

Addressing pervaporation membranes first; this work has shown that sodium alginate is among the best, if not *the* best material for production of pervaporation membranes, possessing an unrivalled combination high flux and high selectivity. It is however, physically/mechanically unsuitable. As such it must be blended with a more physically durable polymer, such as poly(vinyl alcohol), and a plasticizing agent – glycerol. The results of the work in chapter 3 show that the optimum combination of these is a 4:1 mass ratio of sodium alginate to poly(vinyl alcohol) plus glycerol.

It was also established in chapter 3 that the use of a support is *essential* to produce a high flux membrane. The necessary thickness of an unsupported membrane is so great that it reduces diffusion time to an unfeasible degree, resulting in poor flux. Producing an unsupported membrane of a thickness similar to that of the selective layers of supported membranes is also unfeasible as the membrane thickness renders it physically fallible. Furthermore, the use of a support reduces the chance of catastrophic membrane failure when utilizing highly hydrophilic polymers such as sodium alginate. These polymers tend to swell to such a degree that they can break up within the pervaporation membrane cell if unsupported. While flexibility tests show that unsupported membranes are slightly more flexible than their supported equivalents; this slight increase in durability does not justify their use when one considers their inferior performance in all other aspects. All of these facts lead to the conclusion that pervaporation membranes must be supported at the industrial scale.

Chapter 5 took the optimum membrane described in chapter 3 and attempted to show how the effect of relaxation can be minimized by making the membrane selective layer thinner (down to a minimum, beyond which the effect is absent). This had the unanticipated benefit of increasing membrane selectivity without reducing flux; an effect which was due to changes in the density and thickness of the membrane skin layers. This was due to the rate at which solvent evaporated from the cast polymer solution during drying: Polymer density increases at the air exposed surface with increased rate of evaporation. This rate was increased by increasing the surface area to volume ratio of the membrane, i.e. reducing

membrane thickness. Understanding of skin layers has proven to be central to understanding the formation mechanics of both membrane types throughout the work. Chapter 5 and the work published from it represent our biggest cognitive leap in that understanding.

Chapter 7 deals with the incorporation of filler particles into a polymer membrane matrix to produce a mixed matrix membrane. In this instance the filler particles in question were mesoporous silica particles. A pristine poly(vinyl alcohol) membrane was used as it offered the most physically durable membrane type. The aim of the work was to assess the effect of the particles on pervaporation performance of the membrane, not to produce the best possible performing membrane. Results showed conclusively that the incorporation of engineered mesoporous silica particles into the poly(vinyl alcohol) membrane matrix conferred greater selectivity upon the membrane without sacrificing flux. This was due to the discreet and highly monodisperse nature of the silica particles. Particle discretion was only possible below 15 wt% loadings however. The nature of the particles does allow for a greater degree of reproducibility in the mixed matrix membranes produced from them, than previously seen due to how they increase membrane free volume.

Moving on to the other type of membrane studied: Chapter 4 established basic requirements for producing lateral-flow membranes; skin layer formation needs to be controlled and lacquers must be brought to near cloud-point before casting. While this chapter did not establish absolutely how to control skin-layer formation in lateral-flow membranes it did determine that their presence inhibits formation of the membrane pore network in the bulk membrane beneath. Also conclusively shown was that skin-layers inhibit and retard lateral-flow. It would take the application of the understanding of skin-layer formation established from the work in chapter 5 to achieve complete prevention of skin-layer formation.

The need to bring casting lacquers to near cloud-point was established as it not only reduces skin layer formation (partially, not entirely) but also improves pore network structure in the bulk membrane. This was due to the fact that having the casting lacquer near cloud-point renders the phase inversion of the uppermost parts of the membrane complete in a shorter time-frame, giving less time for skin layers to form. The formation of the skin layer earlier in the formation process reduces the

evaporation rate of solvent from the bulk membrane below it, therefore increasing the timeframe over which phase inversion occurs in the bulk membrane, thus allowing more time for nucleation and growth and so a more open pore network. The conclusion drawn here is that reducing the rate of loss of solvent from the lacquer would produce a more open pore structure and so a better lateral flow membrane, but this must be done without a skin layer.

This was achieved in the work of chapter 6 where the "meso-solvent" (ethanol) was introduced to the lacquer makeup. This had the effect of increasing the affinity of the polymer lean phase for the polymer rich phase during liquid-liquid demixing which reduced the rate of solvent evaporation from the casting lacquer, resulting in greater and more open pore network formation. This reduction in evaporation rate also inhibited the formation of macrovoids.

While the addition of ethanol on its own did not completely prevent the formation of skin-layers it did reduce them. Thus, when used in combination with bringing the lacquer to near cloud-point, as in chapter 4, skin-layer formation was completely prevented, as seen in membrane MesoDCP. The work of chapter 6 resulted in the production of a lateral flow membrane comparable with the top industrial equivalents.

Despite the obvious differences between the two membrane types; one produced from simple drying of polymer solutions (pervaporation), the other from a complex phase inversion process (lateral-flow); this project has served to highlight the parallels between the formation mechanics of the two and how these can be controlled. In particular, control of the formation of skin layers is applicable to both membrane formations. The principle methods of that control, determined in this thesis, could be applied to the formation of any other flat sheet polymer membranes produced from polymer solutions. This opens up many avenues of future membrane research; porous filtration membranes such as ultrafiltration, microfiltration and nanofiltration - where the desired isotropic structures are dependent on *not* forming skin layers; gas separation, reverse osmosis and ion-exchange membranes; where an anisotropic nature, such as that seen in pervaporation membranes, is of benefit to selectivity.

In the specific case of the lateral-flow membrane research, the ability to control pore structure of membranes formed via phase inversion of cast polymer solutions, through control of the cloud point of the solution and the use of meso-solvents could be applied to any system in which membranes are formed by phase inversion. This is the production method of almost all porous polymeric filtration membranes and so applicable to industrial research.

More specific future work will continue on from some of the results described here.

Chapter 4 offered a theory on the cause of skin layer formation at the support interface; that is was due to the greater affinity of the Melinex backing material for the solvent acetone than for the non-solvent water. In order to confirm that this is what is occurring future experiments would be conducted using an impermeable, non-polar support material which would, theoretically, eliminate the skin layers. This would be a costly – though simple - venture but, since the residue left by these skin layers on the support material has been cited as a problem industrially, it may be suitable for further investigation.

While the results of chapter 6 showed how skin layers can be prevented and pore network structure can be made more open; increasing lateral flow rate, the resolution of the flow front in such membranes is poor due to the uneven pore size distribution within the bulk lateral flow membrane. This requires refinement of the lacquer polymer/solvent/meso-solvent/non-solvent system. However success in this venture would be of interest to industry and results would be highly publishable given the dearth of academic information on the subject.

Further work on the protein binding abilities of the porous-lateral flow membranes is also desirable, as this is the obvious next step beyond refinement of the pore structures. These results are directly applicable to any research into porous, flat-sheet, polymeric membranes using polymers other than cellulose nitrate; most notably poly(methylmethacrylate) lateral-flow membrane research, as the meso-solvent principle applicable to any phase inversion system.

Given the equipment and expertise available within this research group, future pervaporation research should focus on two main avenues: Incorporation of novel filler particles into mixed matrix membranes and production of membranes for

other separations, in particular organic-organic separations. Future mixed matrix membrane research should begin with the incorporation of the silica particles utilized in chapter 7 into the optimum membrane produced in chapter 5. This is a highly publishable follow-up to the published work of chapter 7. Moving on from there, work should focus the use of novel filler particles such as synthetic zeolites which are more monodisperse than those obtained from natural sources. These have been produced within the group already which should facilitate the work. An initial feasibility study should be conducted incorporating the particles into a pristine PVA matrix as done in chapter 5. This work would be publishable for its novelty alone. Should it prove to have some significant benefit to performance then a second publication would be possible by incorporating the same particles into a high performance membrane matrix such as that refined in chapter 5. Different types of separations could be achieved through the use of novel polymers. Of particular interest would be the use of bio-polymers; polysaccharides from various natural sources.

Pervaporation research worldwide, due to the method's versatility, is moving in the direction of solvent reclamation; in particular, difficult organic-organic solvent separation through the use of polyamides in the membrane selective layer. The use of filler particles in organic-organic pervaporation separations is an area of great interest and functionalized silica could prove very effective. The laboratory is already set up to conduct such research without the need for new equipment.

Appendices

A. Chapter 3 Supporting Information

NOTE I: All average figures shown for pervaporation performance data below are calculated excluding data from the first hour of testing as the membrane has not reached equilibrium with the feed solution before this time.

NOTE II: The selectivity data for the pristine unsupported PVA membrane in table A.2 is the earliest pervaporation data obtained in the entire project and was determined using a different precision setting on the density meter than in later membrane tests, as such selectivity data is only given to one decimal place.

NOTE III: Data given for membranes that were physically capable of undergoing the full five hours of testing represents the averages of the data for five tests of each membrane type.

A.1 Pristine Unsupported Membrane Data

Table A.1: Pervaporation performance of unsupported pristine NaAlg membrane cast from 2 wt% solution of NaAlg in water. Cast at 400 μm thickness

Run (hr)	Mass of Flux (g)	Flux ($g\ m^{-2}\ h^{-1}$)	Retent. Density ($g\ cm^{-3}$)	Retentate (%)		Perm. Density ($g\ cm^{-3}$)	Permeate (%)		Select.
				Water X_i	Ethanol X_j		Water Y_i	Ethanol Y_j	
1	3.337	188.53	0.8187	6.96	93.04	0.9908	94.81	5.19	243.56
2	3.422	193.33	0.8177	6.68	93.32	0.9958	98.39	1.61	853.72
3	1.623	91.69	0.8172	6.55	93.45	0.9913	95.78	4.22	323.78
Average Flux and Selectivity Figures									
		142.51							588.75

Table A.2: Pervaporation performance of unsupported pristine PVA membrane cast from 10 wt% solution of PVA in water. Cast at 150 μm thickness

Run (hr)	Mass of Flux (g)	Flux ($g\ m^{-2}\ h^{-1}$)	Retent. Density ($g\ cm^{-3}$)	Retentate (%)		Perm. Density ($g\ cm^{-3}$)	Permeate (%)		Select.
				Water X_i	Ethanol X_j		Water Y_i	Ethanol Y_j	
1	5.067	286.3	0.8560	25.00	75.00	0.9667	79	21	11.3
2	9.358	528.7	0.8555	25.00	75.00	0.9315	76	24	9.5
3	7.817	441.6	0.8549	24.00	76.00	0.9358	70	30	7.4
4	8.594	485.5	0.8537	24.00	76.00	0.9625	76	24	10.0
5	8.270	467.2	0.8530	23.00	77.00	0.9540	70	30	7.8
Average Flux and Selectivity Figures									
		480.75							8.7

A.2 Pristine Supported Membrane Data

Table A.3: Pervaporation performance of supported pristine NaAlg membrane cast from 5 wt% solution of NaAlg in water. Cast at 100 μm thickness

Run (hr)	Mass of Flux (g)	Flux ($g\ m^{-2}\ h^{-1}$)	Retent. Density ($g\ cm^{-3}$)	Retentate (%)		Perm. Density ($g\ cm^{-3}$)	Permeate (%)		Select.
				Water X_i	Ethanol X_j		Water Y_i	Ethanol Y_j	
1	53.603	3028.470	0.8523	23.62	76.38	0.9173	51.56	48.44	3.442
2	21.930	1238.980	0.8492	22.34	77.66	0.9700	81.03	18.97	14.848
3	18.811	1062.770	0.8470	21.44	78.56	0.9749	88.22	11.78	27.440
4	17.145	968.644	0.8435	20.02	79.98	0.9818	89.95	10.05	35.756
5	14.760	833.898	0.8406	18.84	81.16	0.9831	90.87	9.13	42.876
Average Flux and Selectivity Figures									
		1026.073							30.23

Table A.4: Pervaporation performance of supported pristine PVA membrane cast from 10 wt% solution of PVA in water. Cast at 100 μm thickness

Run (hr)	Mass of Flux (g)	Flux ($g\ m^{-2}\ h^{-1}$)	Retent. Density ($g\ cm^{-3}$)	Retentate (%)		Perm. Density ($g\ cm^{-3}$)	Permeate (%)		Select.
				Water X_i	Ethanol X_j		Water Y_i	Ethanol Y_j	
1	25.79	1457.062	0.8540	24.32	75.68	0.9790	87.92	12.08	22.648
2	23.90	1350.282	0.8513	23.24	76.76	0.9780	87.17	12.83	22.441
3	23.54	1329.944	0.8509	23.02	76.98	0.9775	86.82	13.18	22.028
4	23.60	1333.333	0.8507	22.95	77.05	0.9764	85.95	14.05	20.538
5	23.23	1312.429	0.8505	22.87	77.13	0.9761	85.76	14.24	20.311
Average Flux and Selectivity Figures									
		1331.497							21.330

A.3 Blend Membrane Data

Table A.5: Pervaporation performance of supported pristine PVA membrane cast from 10 wt% solution of PVA in water. Cast at 100 μm thickness

Run (hr)	Mass of Flux (g)	Flux ($g\ m^{-2}\ h^{-1}$)	Retent. Density ($g\ cm^{-3}$)	Retentate (%)		Perm. Density ($g\ cm^{-3}$)	Permeate (%)		Select.
				Water X_i	Ethanol X_j		Water Y_i	Ethanol Y_j	
1	45.454	2568.023	0.8530	23.89	76.11	0.9622	75.34	24.66	9.73
2	52.600	2971.751	0.8525	23.68	76.32	0.9656	77.77	22.23	11.28
3	55.382	3128.927	0.8502	22.77	77.23	0.9660	78.06	21.94	12.06
4	52.330	2956.500	0.8486	22.09	77.91	0.9660	78.04	21.96	12.53
5	46.789	2643.446	0.8479	21.83	78.17	0.9546	70.44	29.56	8.53
Average Flux and Selectivity Figures									
		2925.156							11.1

Table A.6: Pervaporation performance of supported 4:1 NaAlg:PVA blend membrane cast from 5 wt% solution of polymer blend in water. Cast at 100 μm thickness

Run (hr)	Mass of Flux (g)	Flux ($g\ m^{-2}\ h^{-1}$)	Retent. Density ($g\ cm^{-3}$)	Retentate (%)		Perm. Density ($g\ cm^{-3}$)	Permeate (%)		Select.
				Water X_i	Ethanol X_j		Water Y_i	Ethanol Y_j	
1	58.475	3303.672	0.8537	2419	75.81	0.9598	73.73	26.27	8.796
2	72.856	4116.158	0.8531	23.95	76.05	0.9515	68.63	31.37	6.940
3	73.738	4165.989	0.8485	22.06	77.94	0.9515	68.63	31.37	7.729
4	70.891	4005.141	0.8483	21.97	78.03	0.9463	65.74	34.26	6.815
5	65.839	3719.718	0.8434	21.07	78.93	0.9434	60.19	39.81	5.664
Average Flux and Selectivity Figures									
		4001.752							6.787

Table A.7: Pervaporation performance of supported 7:3 NaAlg:PVA blend membrane cast from 5 wt% solution of polymer blend in water. Cast at 100 μm thickness

Run (hr)	Mass of Flux (g)	Flux ($g\ m^{-2}\ h^{-1}$)	Retent. Density ($g\ cm^{-3}$)	Retentate (%)		Perm. Density ($g\ cm^{-3}$)	Permeate (%)		Select.
				Water X_i	Ethanol X_j		Water Y_i	Ethanol Y_j	
1	11.826	668.1356	0.8162	9.34	90.66	0.9851	78.23	21.77	34.881
2	14.372	811.977	0.8138	9.12	90.88	0.9871	82.54	17.46	47.107
3	12.274	693.446	0.8117	8.88	91.12	0.9868	82.35	17.65	47.876
4	10.380	586.441	0.8098	8.69	91.31	0.9847	82.38	17.62	49.126
5	9.900	559.322	0.8080	8.49	91.51	0.9845	82.45	17.55	50.638
Average Flux and Selectivity Figures									
		662.797							48.687

A.4 Blend Membranes Utilising Glycerol Data

Table A.8: Pervaporation performance of supported 9:1 NaAlg:PVA blend membrane cast from solution of 5 g polymer blend + 5 g glycerol in 90 g water. Cast at 100 μm thickness

Run (hr)	Mass of Flux (g)	Flux ($g\ m^{-2}\ h^{-1}$)	Retent. Density ($g\ cm^{-3}$)	Retentate (%)		Perm. Density ($g\ cm^{-3}$)	Permeate (%)		Select.
				Water X_i	Ethanol X_j		Water Y_i	Ethanol Y_j	
1	10.326	583.390	0.8136	8.38	91.62	0.9858	92.70	7.30	138.836
2	10.277	580.621	0.8112	7.50	92.50	0.9907	95.79	4.21	280.620
3	8.615	486.723	0.8101	7.10	92.90	0.9915	96.27	3.73	337.707
4	6.306	356.441	0.8089	6.66	93.34	0.9903	95.55	4.45	300.929
5	6.913	390.565	0.8076	6.20	93.80	0.9930	97.14	2.86	513.858
Average Flux and Selectivity Figures									
		343.588							358.279

Table A.9: Pervaporation performance of supported 4:1 NaAlg:PVA blend membrane cast from solution of 5 g polymer blend + 5 g glycerol in 90 g water. Cast at 100 µm thickness

Run (hr)	Mass of Flux (g)	Flux ($g\ m^{-2}\ h^{-1}$)	Retent. Density ($g\ cm^{-3}$)	Retentate (%)		Perm. Density ($g\ cm^{-3}$)	Permeate (%)		Select.
				Water X_i	Ethanol X_j		Water Y_i	Ethanol Y_j	
1	19.728	1114.576	0.8159	9.23	90.77	0.9750	84.88	15.12	55.207
2	18.667	1054.632	0.8130	8.15	91.85	0.9786	87.62	12.38	79.850
3	15.374	868.588	0.8104	7.21	92.79	0.9767	86.19	13.81	80.321
4	13.000	734.463	0.8082	6.41	93.59	0.9734	83.64	16.36	74.645
5	12.668	715.706	0.8072	6.04	93.96	0.9760	85.65	14.35	92.850
Average Flux and Selectivity Figures									
		843.347							81.919

A.5 Flexibility Data

Table A.10: Results of flexibility tests (method outlined in chapter 2, section 2.3.2)

Membrane	Selective layer (µm) (approx.)		Support	PAN layer (µm) (approx.)		Cylinder radius (mm)
	Cast	Dry		Cast	Dry	
PVA	400	35	No	-	-	2.0
PVA	150	13	Yes	150	100	3.5
NaAlg	400	25	No	-	-	6.5
NaAlg	150	9	Yes	150	100	42.0
7:3	150	12	Yes	150	100	4.0
4:1	150	12	Yes	150	100	12.5
9:1	150	10	Yes	150	100	31.5
4:1 + Gly	150	12	Yes	150	100	9.5
9:1 + Gly	150	12	Yes	150	100	22.0

A.6 Absorption Data

Table A.11: Absorption data in solution of 50 wt% water/50 wt% ethanol for supported polymer blend membranes (designated by PVA:NaAlg ratio). Points at which mass data end represent points at which membranes dissolve

Time Absorbing (s)	Membrane					
	7:3		4:1		9:1	
	Mem. Mass (g)	Mem. Mass (%)	Mem. Mass (g)	Mem. Mass (%)	Mem. Mass (g)	Mem. Mass (%)
0	0.155	100	0.160	100	0.158	100
10	0.221	143	0.232	145	0.230	146
20	0.315	203	0.307	192	0.321	203
30	0.398	257	0.405	253	0.412	261
40	0.451	291	0.481	301	0.499	316
50	-	-	-	-	-	-
60	-	-	-	-	-	-

B. Chapter 4 Supporting Information

B.1 SEM

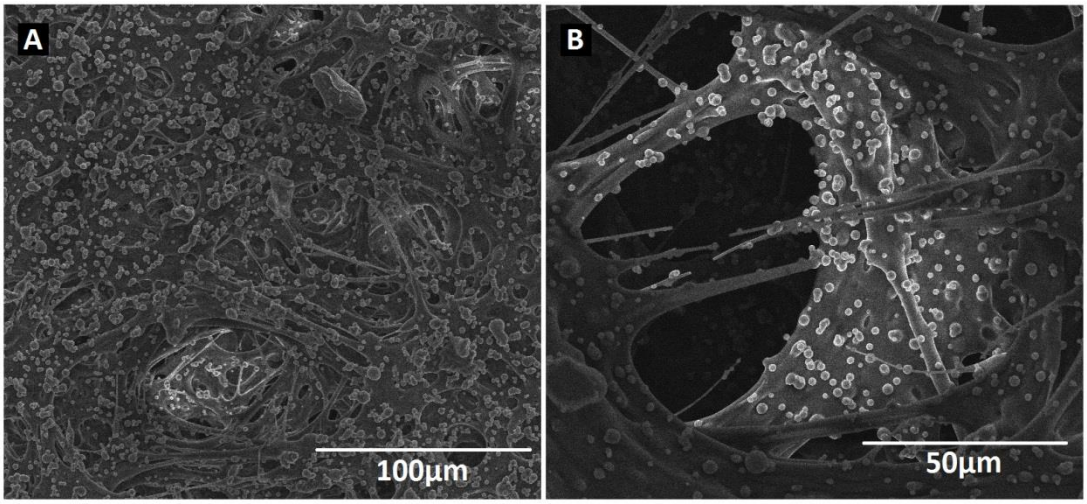


Figure B.1: SEM images of a lateral flow membrane after treatment with surfactant SDBS at 100 µm (image A) and 50 µm (image B)

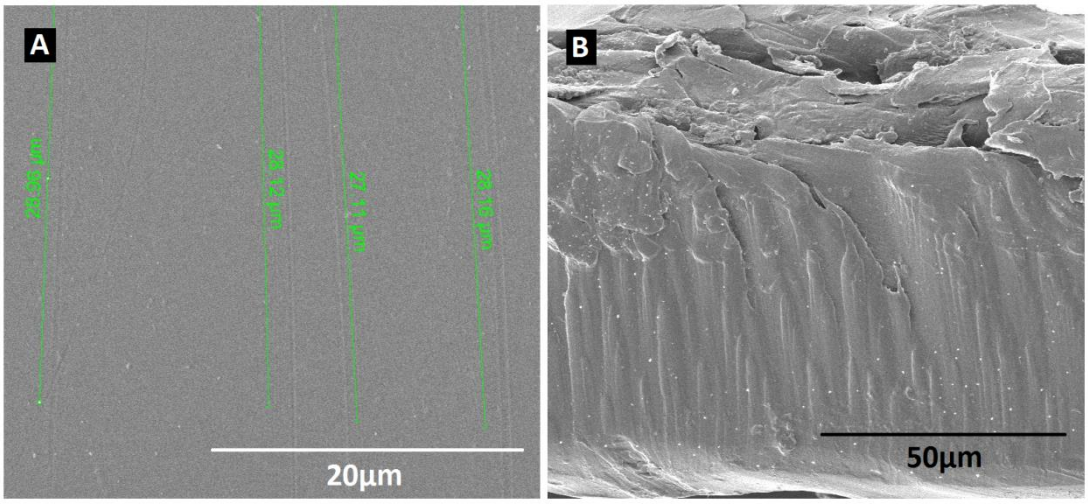


Figure B.2: SEM images of *Melinex* 100 % polyester backing material; surface in contact with membrane (image A) and cross section (image B)

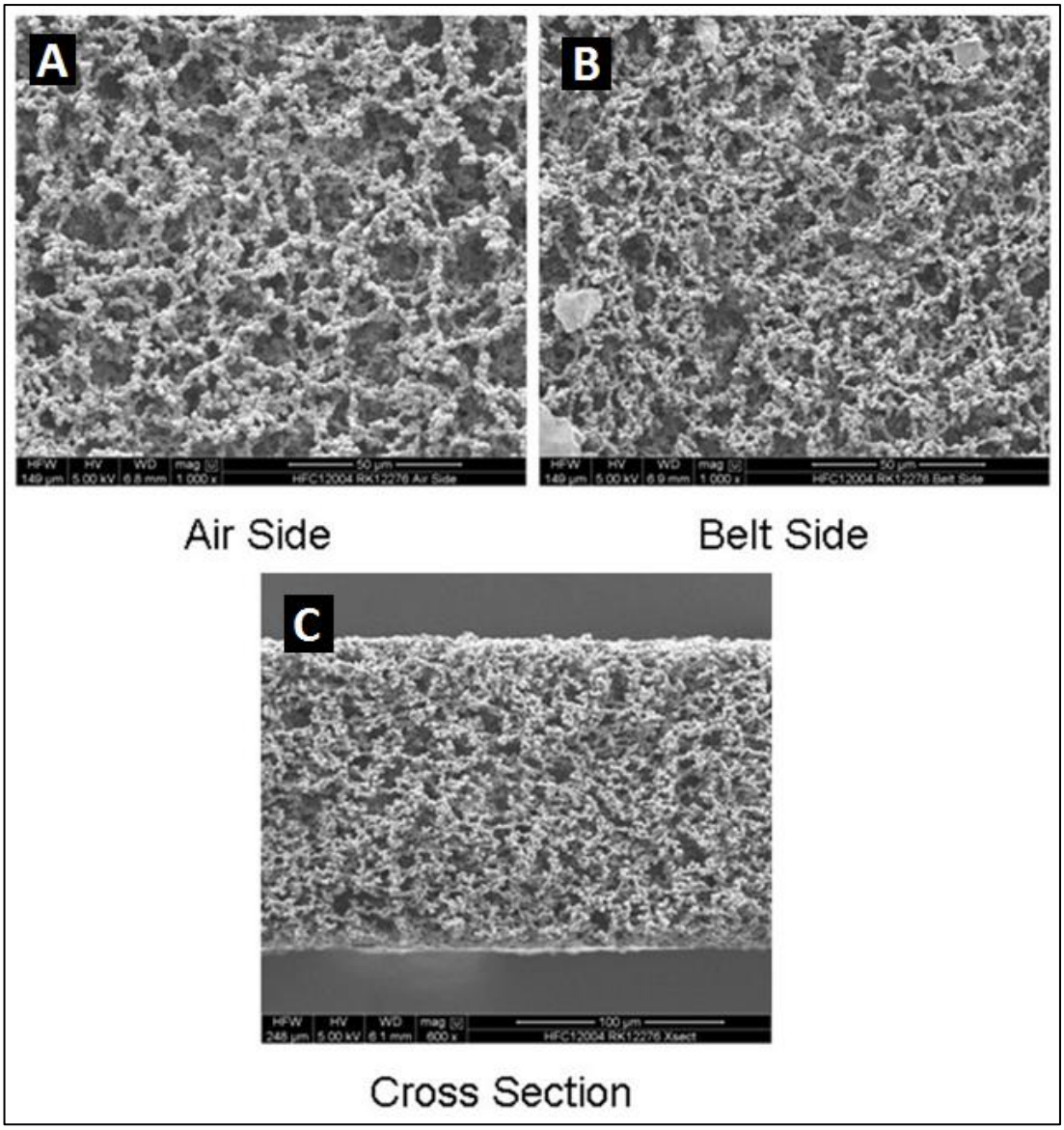


Figure B.3: SEM images of of Millipore HiFlow 120 lateral flow membrane; air surface (image A), blet surface (image B) and cross section (image C)

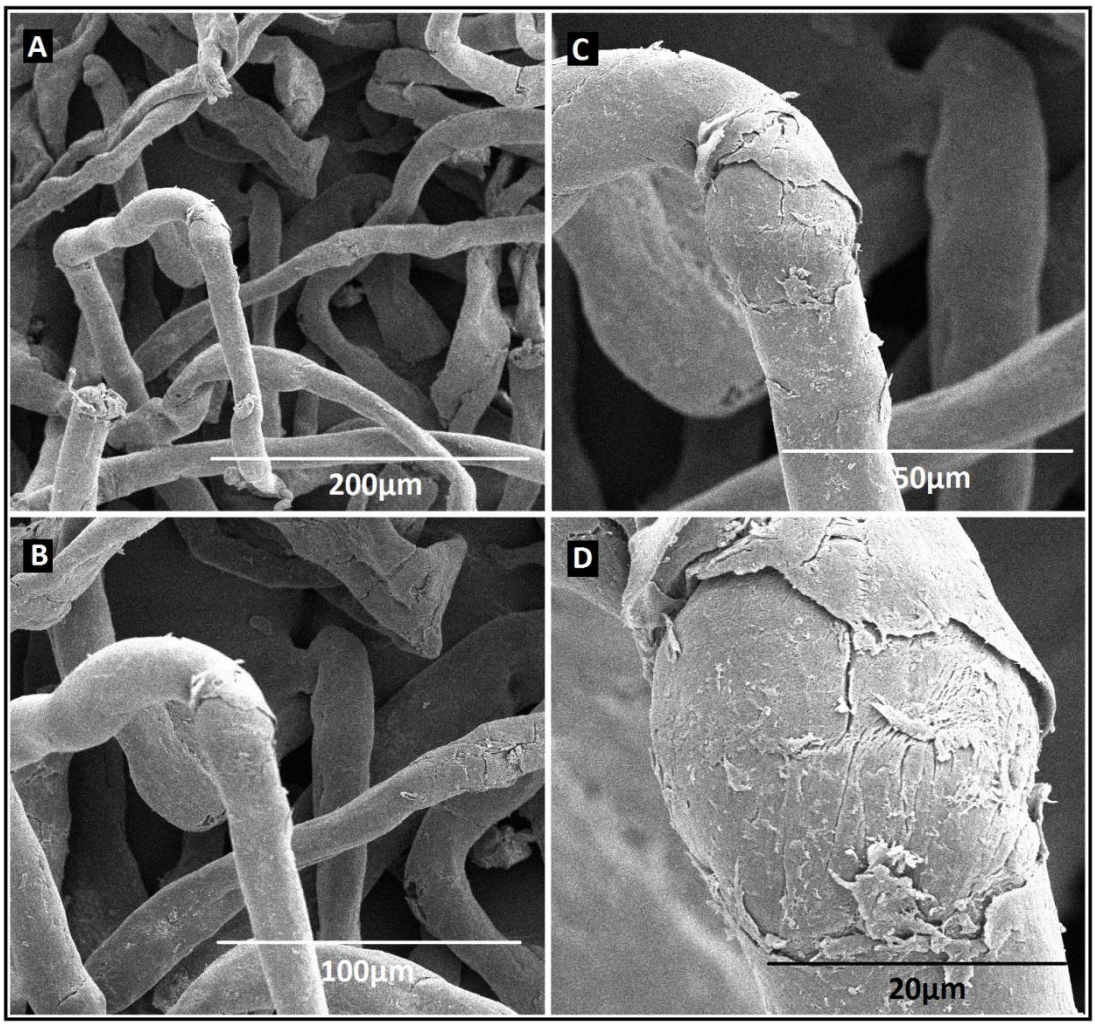


Figure B.4: SEM images of CN raw material at 200 µm (A), 100 µm (B), 50 µm (C) and 20 µm (D).

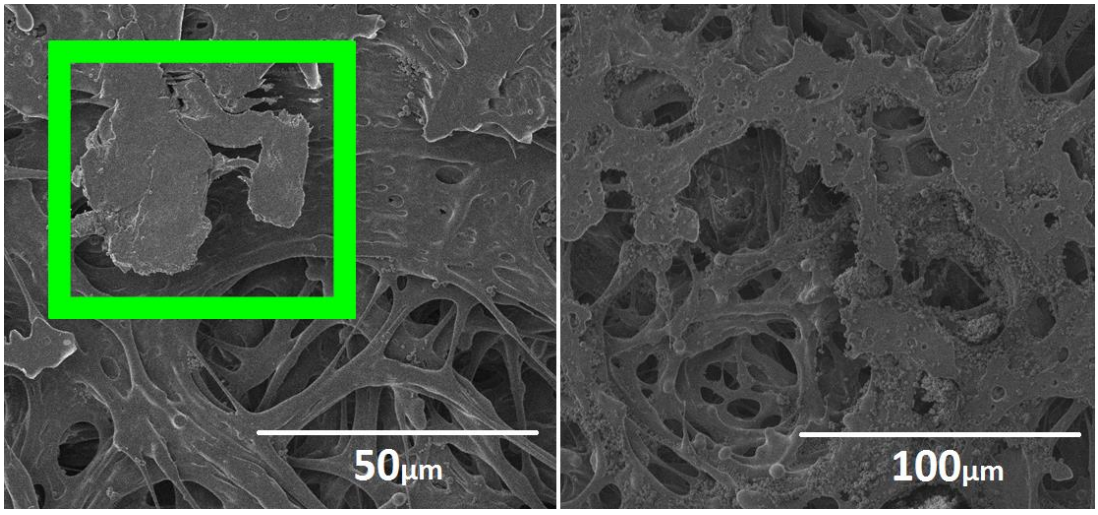


Figure B.5: Skin formation at membrane support interface

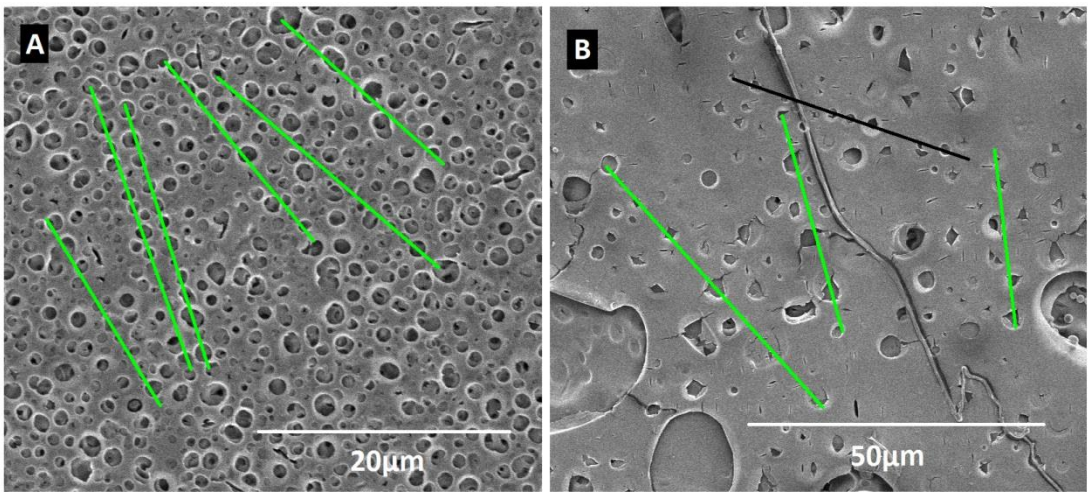


Figure B.6: SEM images of linear pore patterns at membrane support interface: Image A shows patterns in a membrane brought to cloud point with only acetone and water in the solvent mix. Image B shows patterns in a membrane cast from the same lacquer but *not* brought to cloud point

B.2 Flexibility Testing

Table B.1: Flexibility testing data of lateral flow membranes including industrial standard

Membrane	Selective layer (µm) (approx.)		Solvent Ratio Acetone(wt%):Water(wt%)	Cylinder radius (mm)
	Cast	Dry		
BasMemA	565	20	100:0	2.5
BasMemB	565	30	95:5	3.0
BasMemC	565	20	90:10	3.0
BasMemD	565	80	85:15	3.5
BasMemACP	-	-	100:0	-
BasMemBCP	565	20	95:5	3.5
BasMemCCP	565	40	90:10	5.0
BasMemDCP	565	100	85:15	10.0
HiFlow120	-	135	-	3.5

B.3 XRD

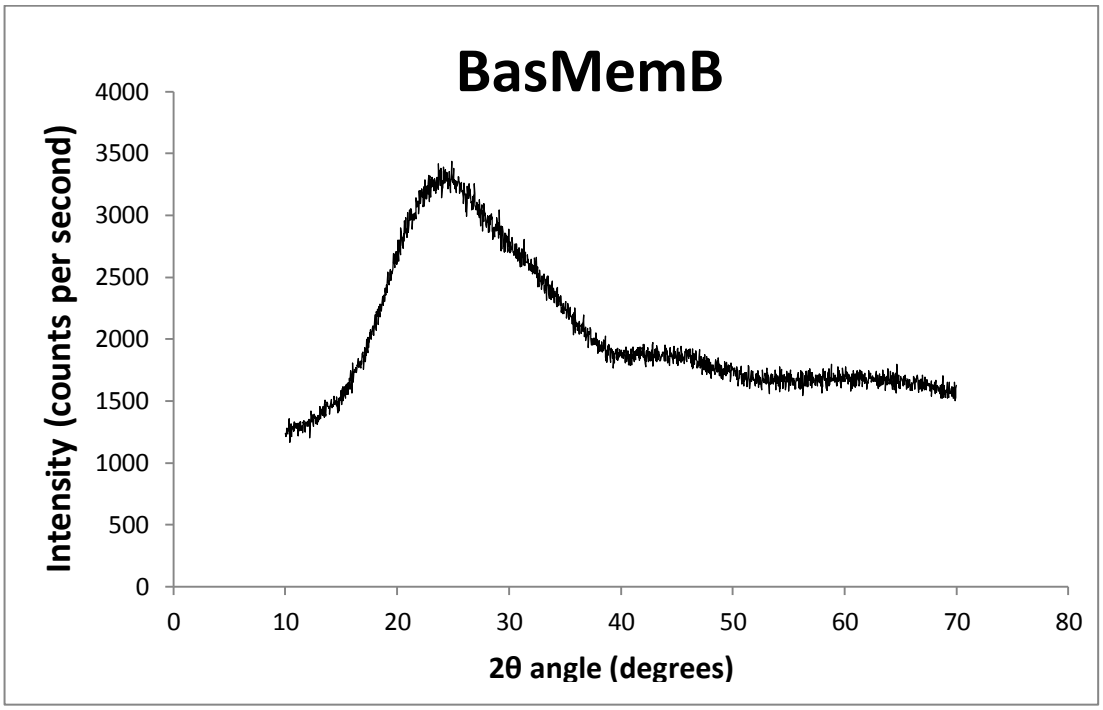


Figure B.7: XRD profile of BasMemD

B.4 AFM

Atomic force microscopy images were taken of the PET (Melinex) surfaces. Both 2 mm and 4 mm thick Melinex were scanned. 31 scans were taken on the 2 mm thick film surface and 25 scans of the 4 mm thick film were taken surface. The areas that were examined were taken at random across the films. The films were cut into ~1.5 cm x ~1.5 cm samples mounted on silicon wafer to prevent films from bending; disrupting measurement. Measurements of 10 x 10 μm were taken for the AFM images.

B.4.1 2 mm Melinex

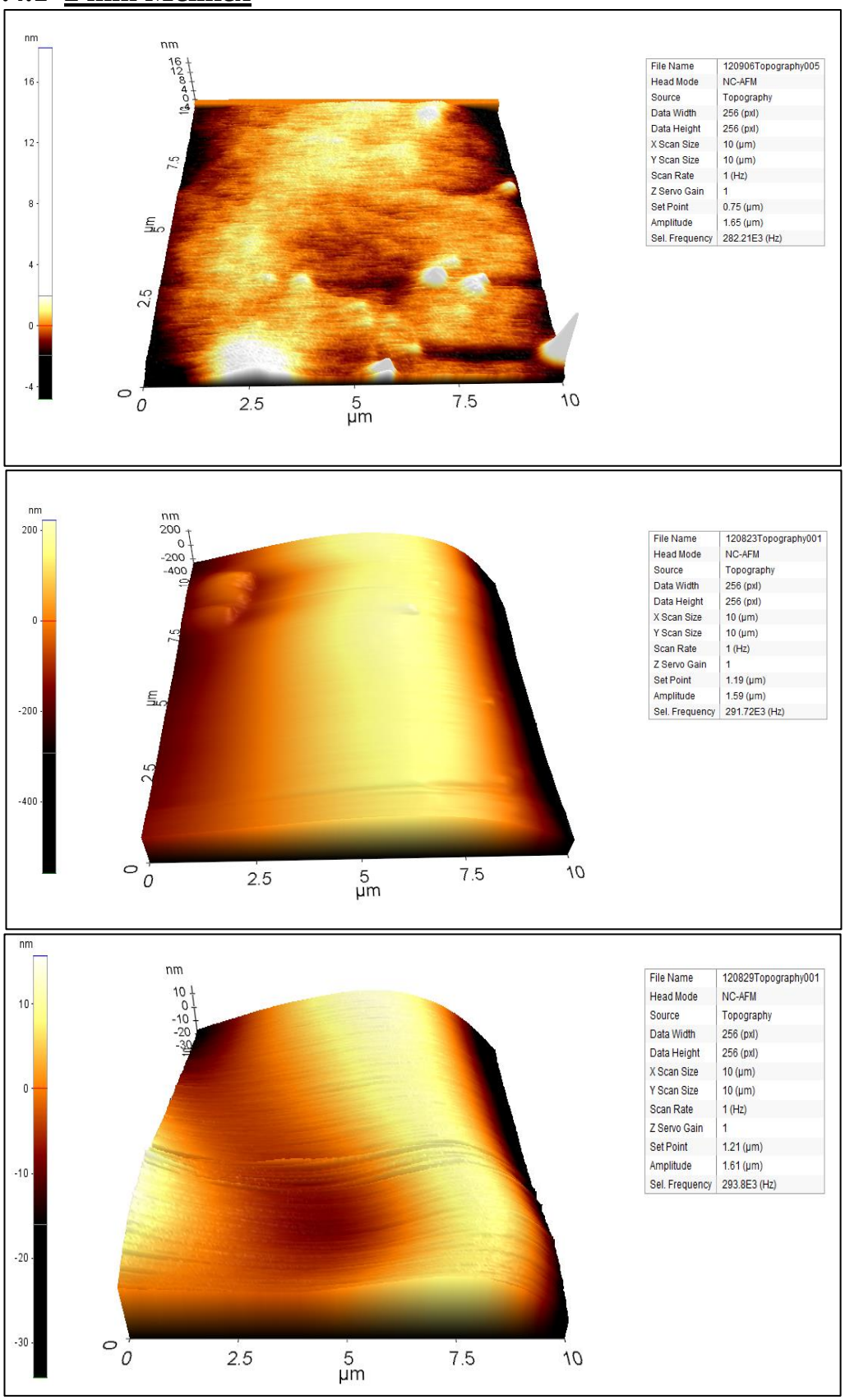


Figure B.8: AFM images of topography of three randomly chosen 10x10 µm sections of 2 mm thick Melinex film

B.4.1 4 mm Melinex

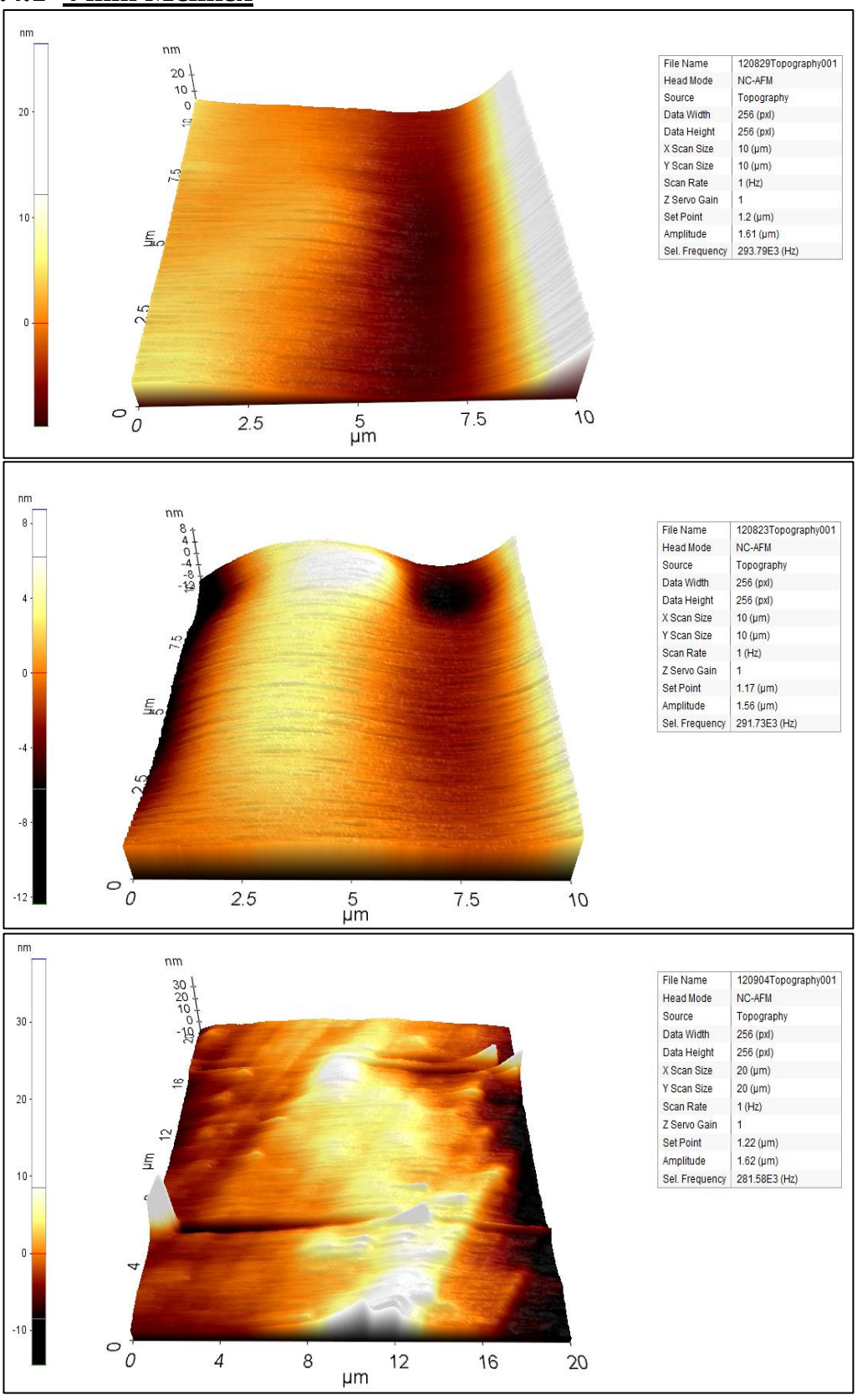


Figure B.9: AFM images of topography of three randomly chosen 10x10 µm sections of 4 mm thick Melinex film

B.5 Contact Angle Measurements

Melinex film of 2 mm and 4 mm thickness were analysed to find their hydrophobicity. Samples were ~2.5 cm^2. Droplet size was 10 µl. Each film sample was analysed with three drops. Results are as follows:

Table B.2: Contact angle data

2 mm Melinex		4 mm Melinex	
Left Angle of Droplet (degrees)	**Right Angle of Droplet (degrees)**	**Left Angle of Droplet (degrees)**	**Right Angle of Droplet (degrees)**
Water contact angle test			
Sample A			
90.9	89.9	86.7	85.0
86.1	87.5	74.7	76.0
83.3	85.5	79.4	80.3
Sample B			
76.3	77.8	80.3	79.3
73.3	74.4	79.4	78.3
61.6	63.2	84.0	85.6
Sample C			
77.3	80.2	79.7	89.3
71.3	76.7	83.1	80.6
80.3	79.5	81.0	81.0
Acetone contact angle test			
<15.0	<15.0	<15.0	<15.0

Acetone drop measurements were taken but were found to be under 15° which cannot be measured by equipment goniometer. Images of samples shown below for comparison:

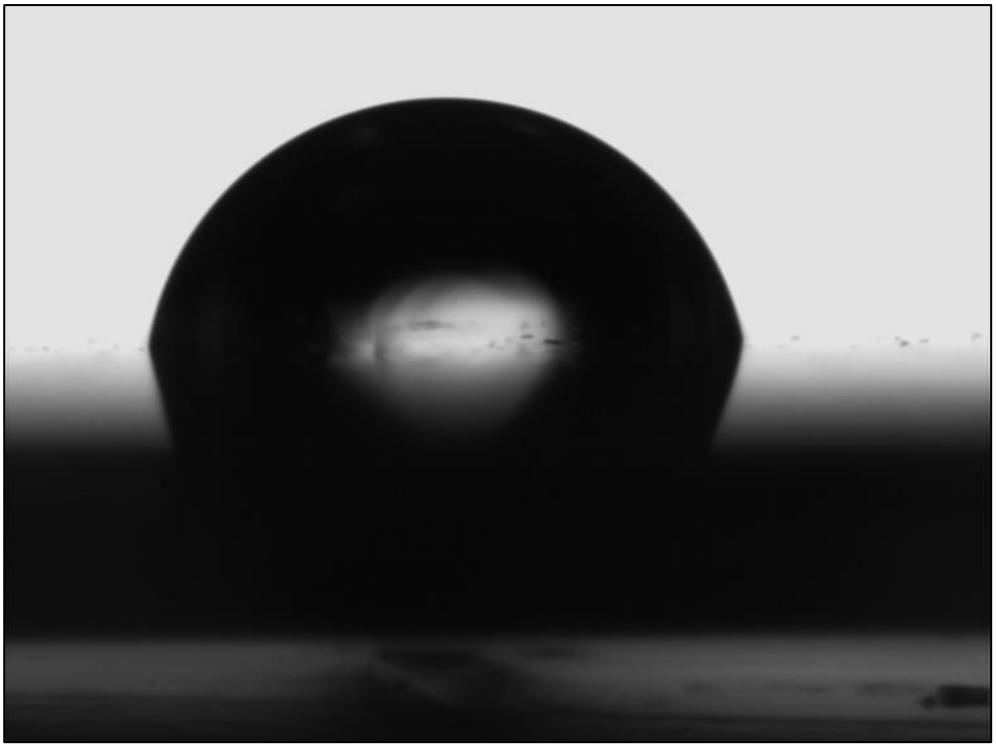


Figure B.10: Typical contact angle of water droplet on Melinex surface (specific image: 4 mm Melinex sample B)

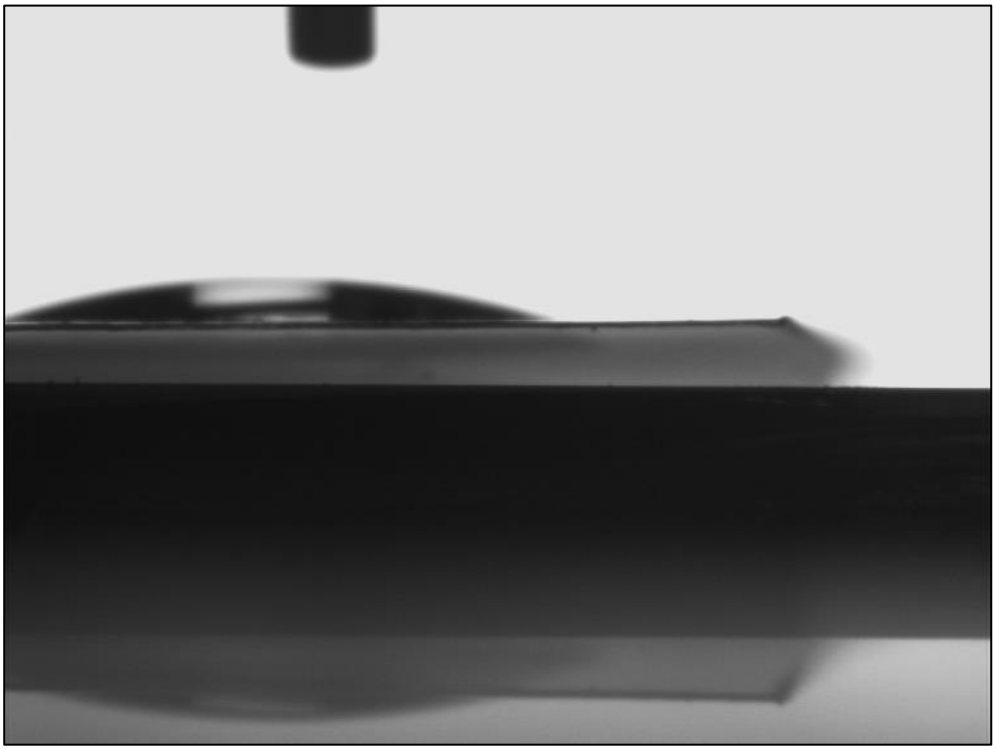


Figure B.11: Typical contact angle of acetone droplet on Melinex surface (specific image: 4 mm Melinex)

C. Chapter 5 Supporting Information

C.1 Membrane Selective Layer Data

Table C.1: Summary of SEM quantification and observations (P = partial, WD = well developed; describe nature of the skin layer at surface)

Film cast thickness (µm)	400	150	100	80	60	50	40	24
Apparent thickness (µm, +/- 0.5 µm)	5.86	5.41	4.57	4.47	3.4	2.92	3.53	4.97
Cast/apparent thickness ratio	68.3	28.1	21.9	17.9	17.6	17.1	11.3	4.8
Surface skin appearance	P	P	P	WD	WD	P	WD	WD
Surface skin thickness (µm, +/- 0.05µm)	0.41	0.37	0.31	0.32	0.29	0.25	0.275	0.485

Table C.2: Thickness and flexibility data

Selective layer	**Thickness (µm) (approx.)**		**Cylinder radius (mm)**
	Cast	**Dry**	
9:1 Gly	400	5.86	8.0
9:1 Gly	150	5.41	9.5
9:1 Gly	100	4.57	9.5
9:1 Gly	80	4.47	9.5
9:1 Gly	60	3.4	10.0
9:1 Gly	50	2.92	10.5
9:1 Gly	40	3.53	11.0
9:1 Gly	24	4.97	12.0

C.2 Pervaporation Data:

Table C.3: Flux, selectivity and permeate water content figures for NaAlg based membranes at 60 ^{o}C operating temperature and 90 wt% ethanol feed solution

Mem. (µm)	Time (hrs)	Flux (g $cm^{-1}h^{-1}$)	Selectivity	Mass % water
400	1	668.1356	115.218	89.87
	2	811.977	156.880	90.97
	3	693.446	168.744	91.77
	4	588.441	115.186	91.97
150	1	381.864	192.111	95.00
	2	502.09	330.894	96.74
	3	452.034	465.549	97.43
	4	371.243	488.389	97.44
100	1	383.898	281.083	96.27
	2	281.808	375.163	96.97
	3	348.079	624.077	98.00
	4	282.26	692.437	98.05
	5	341.265	753.657	98.05
80	1	716.271	14.803	59.09
	2	600.904	357.187	97.03
	3	539.605	457.842	97.49
	4	459.100	598.117	97.84
	5	406.836	784.138	98.16
60	1	984.350	260.615	96.33
	2	1058.588	515.104	97.94
	3	827.401	673.747	98.22
	4	722.090	810.843	98.33
	5	611.864	928.333	98.38
50	1	348.192	403.201	97.66
	2	493.842	605.682	98.33
	3	441.638	371.356	97.14
	4	351.525	933.706	98.22
	5	387.514	995.057	98.60
40	1	603.955	191.537	94.62
	2	812.316	586.372	97.94
	3	667.91	796.101	98.27
	4	553.399	1157.592	98.66
	5	472.26	1305.153	98.66
24	1	379.492	200.31	94.50
	2	491.695	770.03	98.38
	3	437.288	963.765	98.60
	4	401.073	1016.014	98.55
	5	348.757	1023.000	98.44

D. Chapter 6 Supporting Information

D.1 XRD

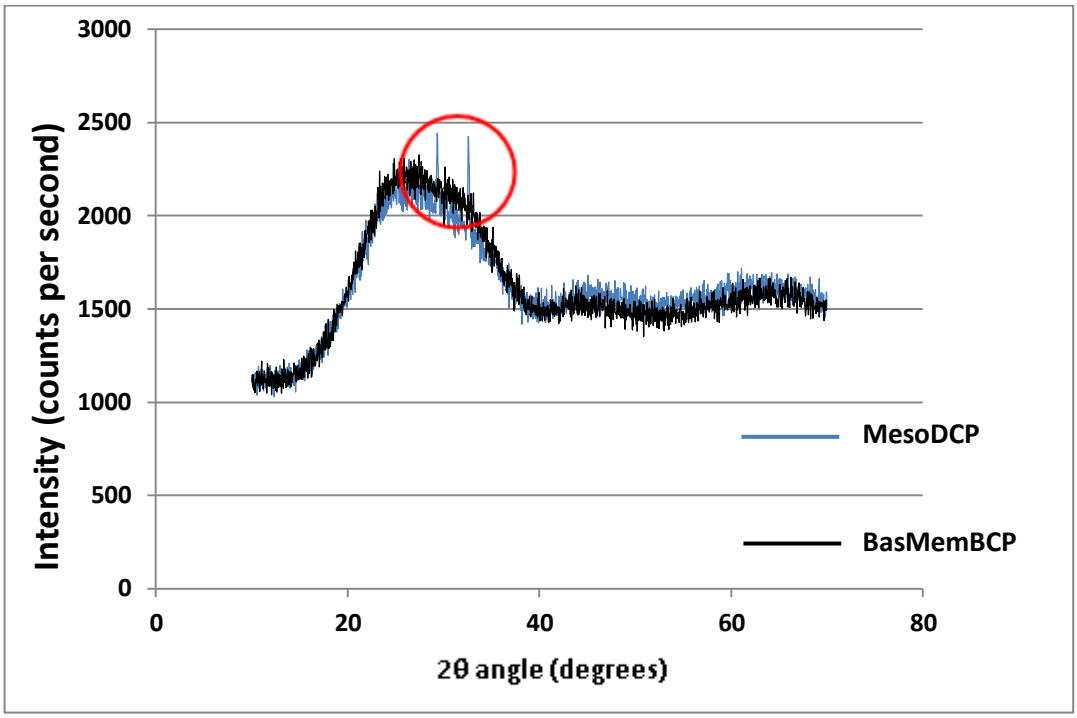


Figure D.1: XRD profiles of MesoDCP and BasMemBCP

D.2 Flow Rate Data

Table D.1: Lateral flow rates and ethanol content

Membrane	EtOH Content (wt%)	Lateral Flow (cm^2 s^{-1})
BasMemBCP	0	0
MesoACP	15.902	0
MesoBCP	18.878	0.016
MesoCCP	21.872	0.028
MesoDCP	24.540	0.051
MesoECP	29.043	0.028

D.3 SEM

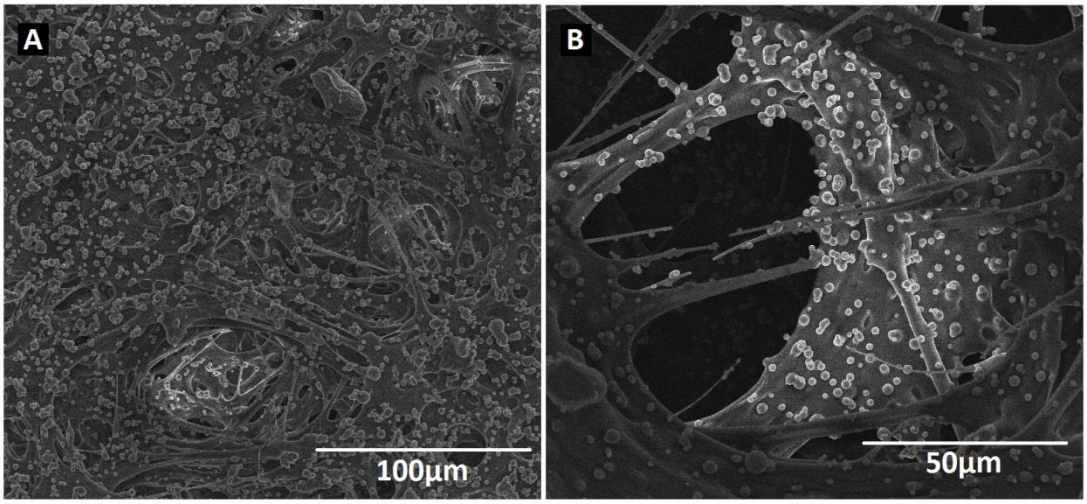


Figure D.2: SEM images of a lateral flow membrane after treatment with surfactant SDBS at 100 µm (image A) and 50 µm (image B)

D.4 Flexibility

Table D.2: Flexibility testing data of lateral flow membranes

Membrane	EtOH Content (wt%)	Cylinder radius (mm)
BasMemBCP	0	3.5
MesoACP	15.902	5.0
MesoBCP	18.878	5.0
MesoCCP	21.872	5.5
MesoDCP	24.540	6.0
MesoECP	29.043	7.0

E. Chapter 7 Supporting Information

E.1 Absorption Data

Table E.1: Absorption data in solution of 50 wt% water/50 wt% ethanol for MMMs. Tabulated data of figure 7.4 (see chapter 7). Points at which mass data end represent points at which membranes dissolve

Time Absorbing (s)	Membrane (expressed as wt% particle loading)							
	0wt%		5wt%		10wt%		15wt%	
	Mem. Mass (g)	Mem. Mass (%)	Mem. Mass (g)	Mem. Mass (%)	Mem. Mass (g)	Mem. Mass (%)	Mem. Mass (g)	Mem. Mass (%)
0	0.153	100	0.141	100	0.163	100	0.156	100
10	0.203	133	0.210	149	0.240	147	0.217	139
20	0.264	173	0.278	197	0.323	198	0.280	179
30	0.321	210	0.333	236	0.405	248	0.353	226
40	0.393	257	0.400	284	0.478	293	0.428	274
50	-	-	0.461	327	0.554	340	0.504	323
60	-	-	-	-	0.620	380	0.577	370
70	-	-	-	-	0.676	415	0.623	399
80	-	-	-	-	-	-	-	-

E.2 Flexibility Data

Table E.2: Results of flexibility tests (method outlined in chapter 2, section 2.3.2)

Membrane	Selective layer (µm) (approx.)		PAN layer (µm) (approx.)		Cylinder radius (mm)
	Cast	Dry	Cast	Dry	
0 wt%	150	~12	150	100	9.5
5 wt%	150	~14	150	100	11.5
10 wt%	150	~16	150	100	14.0
15 wt%	150	~16	150	100	20.0